ENERGY LABORATORY

MASSACHUSETTS INSTITUTE
OF TECHNOLOGY

A FOUR-EQUATION TWO-PHASE FLOW MODEL FOR SODIUM BOILING SIMULATION OF LMFBR FUEL ASSEMBLIES

by

A. L. SCHOR and N. E. TODREAS

MIT Energy Laboratory
Report No. MIT-EL-82-039
December 1982

A FOUR-EQUATION TWO-PHASE FLOW MODEL FOR SODIUM BOILING SIMULATION OF LMFBR FUEL ASSEMBLIES

by

A. L. SCHOR and N. E. TODREAS

Energy Laboratory and
Department of Nuclear Engineering
Massachusetts Institute of Technology
Cambridge, Massachusetts 02139

Topical Report of the MIT Sodium Boiling Project
Sponsored by the U.S. Department of Energy

Energy Laboratory Report No. MIT-EL-82-039

December 1982

A FOUR-EQUATION TWO-PHASE FLOW MODEL FOR SODIUM BOILING SIMULATION OF LMFBR FUEL ASSEMBLIES

by

ANDREI L. SCHOR

Submitted to the Department of Nuclear Engineering on November 12, 1982 in partial fulfillment of the requirements for the Degree of Doctor of Science in Nuclear Engineering

ABSTRACT

A three-dimensional numerical model for the simulation of sodium boiling transients has been developed. The model uses mixture mass and energy equations, while employing a separate momentum equation for each phase. Thermal equilibrium on the saturation line between coexisting phases is assumed.

The four governing equations are supplemented by a number of constitutive relations, addressing the interphase and intraphase exchanges, as well as the fluid-solid interactions. It should be noted that this four-equation two-phase flow model requires only one interfacial relation, i.e., the momentum exchange, compared to the six-equation model which needs two additional relations, describing the mass and energy exchanges. Consequently, the relatively high degree of uncertainty currently associated with the interfacial exchange phenomena is considerably reduced.

From a numerical point of view, the basic approach in this work is a semi-implicit method, in which pressure pulse propagation and local effects characterized by short characteristic times are treated implicitly, while convective transport and diffusion heat transfer phenomena, associated with longer time constants, are handled explicitly. The method remains tractable and efficient in multidimensional applications.

Simulation of a number of experiments has yielded very encouraging results. The numerical method and the constitutive relations have performed well, especially so in light of the extreme severity of the conditions involving sodium boiling.

Thesis Supervisor: Dr. Neil E. Todreas

Title: Professor of Nuclear Engineering

ACKNOWLEDGEMENTS

The authors gratefully acknowledge the support of this work by the United States Department of Energy. The additional support provided by the General Electric Corporation and the Hanford Engineering Development Laboratory in the early stages of this project is also appreciated.

The collective contribution of the co-workers in the MIT Sodium Boiling Project deserves special recognition. Their help, suggestions and readiness to share their experience and findings have proved invaluable.

The authors wish to express their appreciation to Dr. William Hinkle of the MIT Energy Laboratory for his efforts in the initial stages of the Sodium Boiling Project.

Thanks are due to Miss Cathy Lydon for her skill and patience while typing the manuscript.

The work described in this report is based on the thesis submitted by the first author for the Ph.D. degree in Nuclear Engineering at MIT.

TABLE OF CONTENTS

Table of Contents (cont'd)

Table of Contents (cont'd)

Table of Contents (cont'd)

Table of Contents (cont'd)

Table of Contents (cont'd)

Table of Contents (cont'd)

Table of Contents (cont'd)

Table of Contents (cont'd)

LIST OF FIGURES

List of Figures (cont'd)

List of Figures (cont'd)

List of Figures (cont'd)

LIST OF TABLES

NOMENCLATURE

A	flow area	m^2
c	specific heat	$T/(kg \cdot {}^oK)$
cf	contact fraction	-
D	diameter	m
e	internal energy per unit mass	J/kg
F	force	N
f	friction factor	-
G	mass flux, ρU	$kg(m^2 \cdot sec)$
g	gravitational acceleration	m/sec^2
h	enthalpy per unit mass	J/kg
h	heat transfer coefficient	$W/(m^2 \cdot {}^oK)$
I	identity matrix	-
K	friction coefficient	$N \cdot s/m^4$
k	thermal conductivity	$W/(m \cdot {}^oK)$
Nu	Nusselt number, hD/k	-
P	perimeter	m
p	pressure	Pa
Pr	Prandtl number, $\mu c_p/k$	-
Pe	Peclet number, $Re \cdot Pr$	-
Q	heat source	W
Re	Reynolds number, $\rho UD/\mu$	-
S	nucleate boiling suppression factor	-
T	temperature	${}^oK$
t	time	sec
U	velocity	m/sec
u	velocity	m/sec

NOMENCLATURE (continued)

V	fluid volume	m^3
w	mass flow rate	kg/sec
x	quality	-
x,y,z	spatial coordinates	m
α	void (vapor) fraction	-
α	thermal diffusivity, $k(\rho c_p)$	m^2/sec
Γ	phase change rate	$kg/m^3 \cdot sec)$
$\delta_{...}$	increment (or change) in ...	-
δ	liquid film thickness	m
Δt	time step size	sec
Δx, Δy, Δz	mesh spacings	m
ε	eddy diffusivity	m^2/sec
η	weighting factor for interfacial velocity	-
θ	angle of a Fourier component	-
λ	amplification factor	-
μ	viscosity	$N \cdot sec/m^2$
ρ	density	Kg/m^3
ρ	spectral radius	-
σ	superficial tension	N/m
τ	shear stress	Pa
ω	overrelaxation parameter	-

Subscripts

a	phase "a"
e	equivalent

NOMENCLATURE (continued)

i	interfacial
ℓ	liquid
p	at constant pressure
sat	saturation
v	vapor
w	wall
w	wetted

CHAPTER 1. INTRODUCTION

1.1 LMFBR Safety and Sodium Boiling

During the operation of a large liquid-metal-cooled fast breeder reactor (LMFBR), a substantial amount of radioactive material will be present within the reactor core. Of particular concern is the Pu fuel and the fission products generated within the fuel rods, since the accidental release to the environment of a large quantity of these materials could be a hazard to the public. LMFBR power plants will accordingly be designed, constructed and operated to assure that the public risk from such an occurrence will be acceptably low.

To provide this assurance, the U.S. Fast Breeder Reactor Safety Development Program is based on four levels of protection ([1]), aimed at reducing both probability and consequences of a postulated core disruptive accident (CDA). These levels of protection, referred to as lines of assurance (LOAs), have been defined as follows:

- LOA-1: Prevent Accidents;
- LOA-2: Limit Core Damage;
- LOA-3: Control Accident Progression;
- LOA-4: Attenuate Radiological Products.

Figure 1.1 illustrates the possible accident paths for a po-

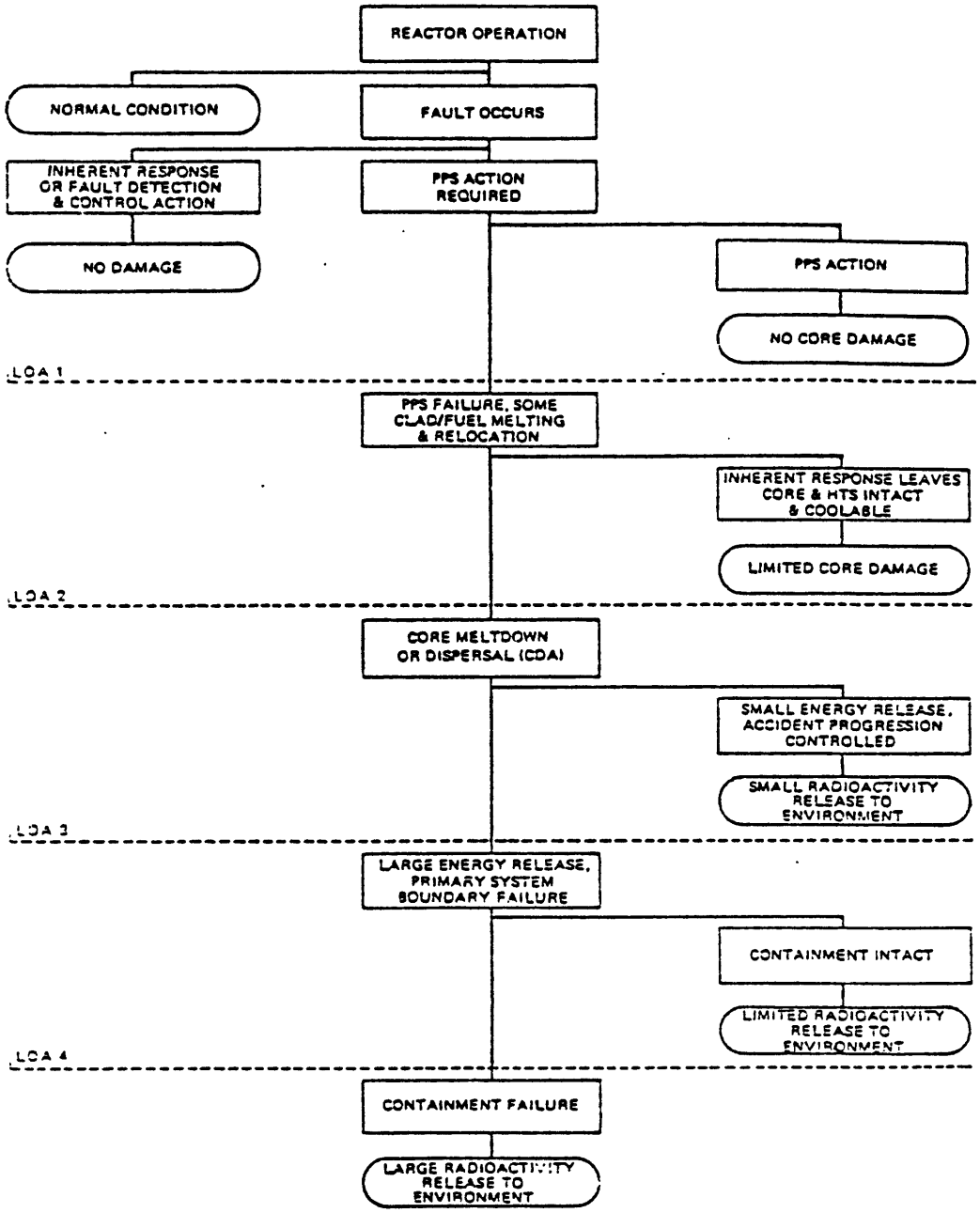

Figure 1.1 Possible Accident Paths and Lines of Assurance for a Potential CDA

tential CDA.

In the case of LOA-2, emphasis is placed on assuring that accidents, resulting from low probability but mechanistically possible events involving failure of LOA-1, can be terminated with only limited core damage. This is achieved by providing a reactor and plant design which inherently and predictably responds to such accidents in a way which reduces reactivity to subcriticality and maintains adequate core coolability with minimum damage.

There are five postulated accidents ([2]) that are currently considered in evaluating the effectiveness of LOA2. These accidents are:

1. Loss of flow without scram - loss of electrical power to motors driving the primary coolant pumps, resulting in pump rundown and loss of core flow while the reactor is operating at power--coupled with a simultaneous failure of the plant protection system to scram the reactor.

2. Loss of piping integrity - undetected defect or leak in a reactor coolant pipe, resulting in a double-eneded guillotine rupture at the inlet nozzle of the reactor vessel followed by rapid decrease in core flow and partial loss of liquid--with scram.

3. Transient overpower without scram - malfunction of plant reactivity control system or operator error, resulting in a sudden increase in core reactivity and power--coupled with a failure to scram.

4. Loss of shutdown heat removal system - loss of forced cooling to the core and failure of shutdown heat removal system--following shutdown.

5. Local subassembly fault - inlet flow blockage or internal subassembly fault resulting in cooling disturbance and potential for fuel failure propagation--with scram (once the condition is detected).

As a design goal, a failure probability of 10^{-2} or less has been set for LOA-2, for the above mentioned accidents ([3]). To meet this goal, R&D work relating to LOA-2 is focussed on developing a detailed understanding of phenomena controlling the progression of each of these accidents from inception to termination. In these accidents, the occurrence of sodium boiling assumes a major role in dictating the path, the rate of progression and the final consequences of the events taking place.

In large, commercial-sized LMFBR's, voiding due to sodium boiling could cause a reactivity and, hence, a power

increase. Under certain conditions, the boiling process could lead to dryout, to overheating of the fuel pins and eventually to pin failure. There are indications, however, that there are inherent rate limiting effects for specific accidents in the fuel assemblies and cores of the present designs, which when properly accounted for, will retard the onset of dryout and sustain longer cooling of the fuel. Thus, a better understanding of the sodium boiling behavior should help in developing favorable system designs that will terminate all previously mentioned postulated accidents with limited core damage, thus meeting the LOA-2 design goal.

1.2 Previous and Current Related Work

Among the effects related to sodium boiling, it is believed that the radial boiling incoherence is of considerable importance in some accident sequences. The rate at which sodium voids grow would be controlled by radial nonuniformity in sodium temperatures within fuel assemblies, sodium void reactivity feedback where boiling occurs and subcooled sodium diversion caused by hydraulic displacement and pressure drop changes in fuel assemblies containing boiling coolant ([2]). Clearly, there is a strong incentive to develop reliable multidimensional analytical

models for sodium boiling.

In the following, we shall briefly review previous and current works aimed at building two- or three-dimensional computational tools for sodium boiling simulation.

The HEV-2D code developed at Purdue University ([4], [5]) used an equilibrium, equal-velocity two-phase flow model, with constant liquid density. While reasonably successful in simulating some transients, it had inherent limitations due to its basic modeling assumptions. Nonetheless, it should be recognized as a pioneering effort in this area.

Senglaub ([6]) used an equilibrium drift-flux formulation in a two-dimensional geometry to model sodium voiding. Generally, the numerical scheme used in his work proved unreliable. It is difficult to assess the impact of his physical model choice on the overall solution method.

Granziera and Kazimi ([7]) developed a two-dimensional, two-fluid (six-equation) model for sodium boiling in fuel assemblies. It uses a more powerful semi-implicit numerical technique ([8]) similar to that employed by the THERMIT ([9]) and TRAC ([10]) codes. In spite of the unavoidable uncertainty associated with the required interfacial constitutive relations, the code, NATOF-2D, has been applied with encouraging results to a number of

sodium boiling experiments. More recently, Zielinski and Kazimi ([11]) have made a number of improvements of physical and numerical nature to the original NATOF-2D code, extending its range of application and increasing the reliability of its predictions.

COMMIX-2([12]) is the product of a large, ongoing effort at Argonne National Laboratory. The code uses a three-dimensional, two-fluid (six-equation) two-phase flow model, employing a fully implicit numerical scheme. The few reported results are quite good. Novertheless, like all other numerical methods currently used in sodium two-phase flow, it sometimes encounters difficulties in obtaining a converged solution.

Dearing ([13]) recently presented a simplified two-dimensional model for sodium boiling. It uses an equilibrium mixture model, with a vapor/liquid slip ratio provided by correlation. The bundle is modeled as two interconnected flow channels. To our knowledge, details of the code (THORAX) have not been published to date.

A new code, CAPRICORN ([14]) has just been released in a preliminary version by Hanford Engineering Development Laboratory. It employs a more implicit scheme than say, THERMIT or NATOF-2D. However, it is not at all certain at this point whether the significant increase in computational

work per time step and in storage requirements is balanced out by an ability to reliably run a calculation with time step sizes substantially greater than the convective transport time, such as to achieve a net decrease in overall computing effort.

A significant developmental effort aimed at obtaining reliable, multidimensional, analytical tools for sodium boiling modelling, has been carried out at M.I.T. over the last few years. The previously mentioned NATOF-2D code is one product of this effort. In parallel, the development of a three-dimensional capability has been pursued. Starting from the original THERMIT code ([9]) designed for water-cooled reactors, Wilson ([14]) carried out the initial effort of conversion to a sodium version, adding and modifying a number of physical models to reflect the specific geometry and operating conditions of a LMFBR fuel assembly. The development was then pursued through two approaches. The first,currently under way ([15]), employs a two-fluid, six-equation two-phase model. While we have been most aware of the potential of this model in terms of flexibility and range of applications, we also realize its major drawback; the current difficulty of providing a full set of validated constitutive relations. It was then concluded that an alternate approach using a simpler formula-

tion, based on thermal but not mechanical equilibrium could provide an adequate capability. The latter approach constitutes the object of this work, highlights of which are presented in the next section of this chapter.

So far, our review of related work has presented only domestic efforts in this area. For completeness, it is appropriate to mention some work being performed in other countries involved in LMFBR safety research.

The adaptation of the British code SABRE-2 ([16]) to sodium boiling is currently being pursued at Cadarache Research Center, in France. SABRE-2 is a single-phase, transient code for subchannel geometry. It uses a fully implicit scheme, SIMPLE ([17]), a variation of which is also used in COMMIX-2. Initial attempts to run it as a homogeneous equilibrium model have been unsuccessful ([18]). The inclusion of a slip ratio, provided as a constant "fine-tuned" by experiment, appears to provide an adequate calculational capability ([19]). (The modified SABRE-2 code is called THEBES).

At Grenoble Research Center, also in France, a new code--BACCUS--has been under development for the last few years. It started as a steady-state, homogeneous equilibrium model using a two-dimensional (r-z) geometry ([20]);

later it evolved into a transient, homogeneous non-equilibrium model, using a semi-implicit difference scheme ([21]).

The BACCUS code is being extended to a three-dimensional geometry, with a full two-fluid two-phase model, through work currently under way at Karlsruhe Institute for Reactor Development, in Germany ([22]). The numerical method being implemented is a semi-implicit scheme.

At the Winfrith Atomic Energy Establishment, in England, work is continuing on the development of the SABRE family of codes ([23]). Currently the SABRE-3C code is being used for sodium boiling simulation. Similarly to the THEBES code, it uses a correlated slip ratio, also assuming thermal equilibrium.

In Japan, a two-fluid, three-dimensional two-phase flow code, TOPFRES ([24]), is being developed. Either a fully implicit or a semi-implicit numerical scheme will be adopted, following some preliminary studies.

It is clear from this brief review that there exists a strong national and international interest in developing an analytical tool to help settle some still outstanding issues in the LMFBR safety research.

At the same time, one cannot help but notice the seemingly uncontained proliferation of models and methods. This clearly attests to the challenge (and frustration) that sodium

boiling modeling has constituted for many years.

1.3 Outline of Present Investigation

In developing an analytical tool, the choices shaping the approach to be taken are:

- Degree of Spatial Averaging;
- Dimensionality;
- Two-Phase Model;
- Numerical Method.

All practical numerical models for reactor analysis today are lumped parameter, porous body approaches; this is the approach used in our work. The general porous body approach can be formulated with a full three-dimensional transverse momentum balance and is structured to accommodate homogenization of arbitrary-sized regions of interest. This region size flexibility is very useful, but the attendant requirement to provide appropriate constitutive relations should not be underestimated.

We use a full three-dimensional model in x-y-z cartesian coordinates. Although in our simulations to date the configurations studied did not evince any azimuthal asymmetry, a full three-dimensional representation was deemed desirable in order to provide a capability for the analysis of strong power tilts and flow blockages, i.e., situations

for which the assumption of azimuthal uniformity would no longer be valid.

In any analytical study of two-phase flows a decision must be made on the type of representation of such flows from a physical and mathematical point of view. The model chosen must be capable of adequately describing the essential features of the flow without unwarranted complications. The two-fluid, six-equation model could provide in theory the maximum in capability and physical consistency. However, its very generality represents a major practical drawback: the presence of the interfacial exchange terms calls for a number of constitutive relations for which current understanding is rather incomplete. A "mixture" model (i.e., a less-than-six equation model) may then become appealing because:

- it theoretically needs fewer constitutive relations;
- it may be computationally more economic;
- in many applications, the specific nature of the physics of the two-phase interaction, combined with the type of information needed (or obtainable) from experiment or simulation may not warrant the detail and complexity of a six-equation model.

Based on this reasoning and with the objective of maximizing the range of applications and computational efficiency, a four-equation mixture model was selected.

The model uses mixture mass and energy equations, while employing a separate momentum equation for each phase. Thermal equilibrium on the saturation line between co-existing phases is assumed.

To complete the definition of the two-phase model a package of constitutive relations, addressing the interphase and intraphase exchanges as well as the fluid-solid interactions, has been assembled. Our effort was mainly directed towards a careful selection and implementation of models, with particular attention given to their efficiency and compatibility within our solution scheme. One should realize that the complexity of the flow geometry combined with the current inability to quantitatively describe two-phase flow patterns introduce a great deal of empiricism and hence, uncertainty. Consequently, while a great deal of thought went into the selection and implementation of the necessary constitutive relations, the ultimate justification for a specific choice lies in the capability of the overall model to simulate and display reasonable agreement with experiments.

From a numerical point of view, our basic approach is a semi-implicit method, in which pressure pulse propagation and local effects characterized by short characteristic times are treated implicitly, while convective transport

and diffusion heat transfer phenomena, associated with longer time constants, are handled explicitly. The method remains tractable and efficient in multidimensional applications. The temporal and spatial discretization process generates a set of non-linear equations, solved by Newton's method, in its regular form or in one of its related versions, the secant and the parallel-chord schemes, which under some circumstances may become more advantageous. The fluid-to-heat source coupling is handled in a highly implicit manner, avoiding stability problems related to some of the rather short time constants involved. A large flexibility is provided in regard to the choice of boundary conditions.

The particular discretization and linearization scheme chosen leads to a large system of linear equations for pressures. Indeed this is a key feature of our method and is characteristic of many currently used numerical schemes. The pressure field incorporates both the spatial coupling (due to fluxes of mass, momentum and energy) and, through a reduction process, the local coupling. After its solution, the pressure is used to infer all the other relevant quantities. Consequently, the efficient and accurate solution of the pressure field is fundamental to our method. A number of solution schemes, both direct and iterative, have been investigated.

A method allowing the specification of the total inlet mass flow rate was devised. Noteworthy the fact that the method is perfectly integrated into the pressure field solution, does not call for another layer of iterations and, therefore, does not add significantly to the total computational work and storage requirement.

A detailed stability and characteristic analysis has been performed. The main conclusion of the stability analysis was that stable solution may be obtained even for apparently ill-posed problems. However, we showed that while the very short and the very long wavelength components are stabilized by the donor cell differencing and the damping terms respectively, the intermediate wavelength components may be limiting from a stability point of view.

The characteristic analysis confirmed the existence of complex characteristics for a wide range of two-phase flow conditions. We found that an approximate (analytical) analysis assuming incompressible phases was in very good agreement with the exact (numerical) analysis, except very near the limits of the void fraction range. Another interesting and somewhat surprising finding was that apparently there are differential constitutive relations which do not affect the characteristics.

Simulation of a number of experiments has yielded

very encouraging results. The numerical method and the constitutive relations have performed quite well, especially so in light of the extreme severity of transients involving sodium boiling. To further assess the predictive ability of our model we strongly recommend that a systematic sensitivity analysis be undertaken. Such study would greatly increase our confidence in the model's predictions and at the same time would clearly point those areas in which further work would be most beneficial.

1.4 Organization of Report

Chapter 2 of this thesis presents the derivation and the selection of the two-phase flow model. Chapter 3 describes the state functions and the constitutive relations supplementing the basic governing equations. Chapter 4 contains a very detailed description of the numerical techniques selected and investigated in this work. The solution of the pressure field, a key feature of our method constitutes the object of Chapter 5. Chapter 6 elaborates on some stability considerations and describes the results of the characteristics analysis performed for our two-phase flow mathematical model. Chapter 7 presents the results of our simulations of various experiments. Finally, Chapter 8 lists the major conclusions

of this work and recommends a number of areas for further study.

The computer code, THERMIT-4E, in which the two phase flow model described in this study has been implemented, is fully operational. Complete information regarding its structure, features and use is provided in a companion report ([25]).

1.5 REFERENCES

1. W.H. Hannum, J.D. Griffith, A.C. Millunzi, "Reactors--Safe at Any Speed," Trans. Am. Nuc. Soc., 22, (1975).

2. W.D. Hinkle, ed., "LMFBR Safety and Sodium Boiling--A State of the Art Report," U.S. DOE (June 1978).

3. W.D. Hinkle, P.M. Tschamper, M.H. Fontana, R.T. Henry and A. Padilla, "LMFBR Safety and Sodium Boiling", ENS/ANS International Topical Meeting on Nuclear Reactor Safety, Brussels, Belgium (1978).

4. T.G. Theofanous, et al, "Multiphase Transients with Coolant and Core Materials inLMFBR Core Disruptive Accidents Evaluations," NUREG/CR-0224, (1978).

5. C. Miao and T.G. Theofanous, "Transient Two-Dimensional Sodium Boiling in LMFBR Subassemblies. The HEV-2D Code," Purdue University Report No. PNE-78-130 (1978).

6. M.E. Senglaub , "Low Heat Flux Sodium Voiding Using the Drift Flux Formulation," Ph.D. Thesis, Northwestern University (1979).

7. M.R. Granziera, M.S. Kazimi, "A Two-Dimensional, Two-Fluid Model for Sodium Boiling in LMFBR Fuel Assemblies," MIT Energy Laboratory Report No. MIT-EL-80-011, (1980).

8. D.R. Liles and W.H. Reed, "A Semi-implicit Method for Two-Phase Fluid Dynamics", J. Comp. Physics, 26, (1978).

9. J. Loomis, W.H. Reed, A. Schor, H.B. Stewart, L. Wolf, "THERMIT: A Computer Program for Three-Dimensional Thermal-Hydraulic Analysis of Light Water Reactor Cores," EPRI Report No. NP-2032, (1981) (first released in 1978 as a MIT Department of Nucl. Engineering internal report).

10. "TRAC-P1: An Advanced Best Estimate Computer Program for PWR LOCA Analysis," LASL Report No. LA-7279-MS (1978).

11. R.G. Zielinski and M.S. Kazimi, "Development of Models for the Two-Dimensional, Two-Fluid Code for Sodium Boiling NATOF-2D," MIT Energy Laboratory Report No. MIT-EL-81-030 (1981).

12. H.M. Domanus, W.T. Sha, V.L. Shah, T.G. Bartzis, J.L. Krazinski, C.C. Miao and R.C. Schmitt, "COMMIX-2: A Steady/Unsteady Single-Phase/ Two-Phase Three-Dimensional Computer Program for Thermal-Hydraulic Analysis of Reactor Components," ANL Report NO. ANL-81-10 (also issued as NUREG/CR-1807), (1981).

13. J.F. Dearing, "Two-Dimensional Computational Modeling of Sodium Boiling in Simulated LMFBR Fuel Pin Bundles," Trans. Am. Nucl. Soc., 38, (1981).

14. G.J. Wilson and M.S. Kazimi, "Development of Models for the Sodium Version of the Two-Phase Three-Dimensional Thermal Hydraulics Code THERMIT," MIT Energy Laboratory Report No. MIT-EL-80-010, (1980).

15. H.C. No, "Simulation of Sodium Boiling by the Two-Fluid Model," Ph.D. Thesis, Nuclear Engineering Department, in preparation.

16. T.D. Macdougall, "SABRE 2--A Computer Program for the Calculation of Transient Three-Dimensional Flows in Rod Clusters," AEEW-R 1104, (1978).

17. S.V. Patankar, "Numerical Heat Transfer and Fluid Flow," p. 113-134, Hemisphere Publ. Corp., McGraw-Hill (1980).

18. F. Camous, private communication (Dec. 1981).

19. F. Camous and P. Berns, "Transient Boiling Calculations in Rod Bundles Using the THEBES Code," Trans. Am. Nucl. Soc., 38, (1981).

20. G. Basque, D. Grand, B. Menant, "Theoretical Analysis and Experimental Evidence of Three Types of Thermohydraulic Incoherency in Undisturbed Cluster Geometry," IAEA Specialists' Meeting on Thermodynamics of Fast Breeder Reactor Fuel Sub -Assemblies under Nominal and Non-Nominal Operating Conditions, Karlsruhe, Germany (1979).

21. G. Basque, P. Mercier, D. Grand, "Recent Development in the Calculation of Boiling in a Subassembly with the BACCHUS Code and its One-Dimensional Version, MANDRIN," to be presented at the Tenth LMBWG* Meeting in Karlsruhe, Oct. 1982.

22. M. Bottoni, B. Dorr, Ch. Homann, D. Struwe, "Development of the Three-Dimensional Two-Phase Flow Version of the BACCUS Computer Programme," to be presented at the Tenth LMBWG meeting in Karlsruhe, Oct. 1982.

23. T.D. Macdougall, "Recent Developments of the SABRE Code and its Application to the Calculation of Boiling Propagation in Loss of Flow and Over-power Transients in Single Channels and Rod Clusters," to be presented at the Tenth LMBWG meeting in Karlsruhe, Oct. 1982.

24. H. Ninokata, S. Tamura, "Analytical Studies of Loss of Flow Experiments by ASFRE/TOPFRES Codes," to be presented at the Tenth LMBWG meeting in Karlsruhe, Oct. 1982.

25. A.L. Schor and N.E. Todreas, "THERMIT-4E: A Computer Code for Sodium Boiling Simulation in LMFBR Fuel Assemblies," MIT Energy Laboratory Report (to be published).

---

*Liquid Metal Boiling Working Group.

CHAPTER 2. THE TWO-PHASE FLOW MODEL

2.1 Introduction

In any analytical study of two-phase flows a decision must be made on the type of representation of such flows from a physical and mathematical point of view. The model chosen must be capable of adequately describing the essential features of the flow without unwarranted complications.

The two-fluid, six-equation model could provide in theory the maximum in capability and physical consistency among the two-phase flow models. However, it is in its very generality and complexity that its major drawback lies. The presence of the interfacial exchange terms calls for a number of constitutive relations for which current understanding is rather incomplete.

A "mixture" model (which is how any less-than-six equation models will be referred to from now on) may then become appealing because:

- it theoretically needs fewer constitutive relations,
- it may be computationally more economic,
- in many applications, the specific nature of the physics of the two-phase interaction, combined with the type of information needed

(or obtainable) from experiment or simulation may not warrant the detail and complexity of a six-equation model.

Based on this reasoning we decided on a mixture model, selected such as to maximize its range of applications and computational efficiency. The remainder of this chapter will describe the selection process and the derivation of the model.

2.2 The Six-Equation Model

Appendix A contains a detailed derivation of the volume-averaged two-phase flow equations. After arriving at this exact set of governing equations, the following assumptions are made to obtain an initial "working" set:

- equal bulk phase pressures,
- uniform spatial distribution for all dependent variables,
- temporal or statistical fluctuations are accounted for through an enhancement of some already derived transport terms.

This set of conservation equations is given below. All the dependent variables in the following equations are understood to be space and time (or ensemble) averaged.

Vapor mass equation

$$\frac{\partial}{\partial t}(\alpha\rho_v) + \nabla\cdot(\alpha\rho_v\vec{U}_v) = \Gamma \qquad (2.1a)$$

Liquid mass equation

$$\frac{\partial}{\partial t}[(1-\alpha)\rho_\ell] + \nabla\cdot[(1-\alpha)\rho_\ell\vec{U}_\ell] = -\Gamma \qquad (2.1b)$$

Vapor momentum equation

$$\frac{\partial}{\partial t}(\alpha\rho_v\vec{U}_v) + \nabla\cdot(\alpha\rho_v\vec{U}_v\vec{U}_v) + \alpha\nabla p - \nabla\cdot(\alpha\bar{\bar{\tau}}_v) - \alpha\rho_v\vec{F}$$

$$= -\vec{F}_{wv} - \vec{F}_i \qquad (2.1c)$$

Liquid momentum equation

$$\frac{\partial}{\partial t}[(1-\alpha)\rho_\ell\vec{U}_\ell] + \nabla\cdot[(1-\alpha)\rho_\ell\vec{U}_\ell\vec{U}_\ell] + (1-\alpha)\nabla p$$

$$-\nabla\cdot[(1-\alpha)\bar{\bar{\tau}}_\ell] - (1-\alpha)\rho_\ell\vec{F} = -\vec{F}_{w\ell} + \vec{F}_i \qquad (2.1d)$$

Vapor total energy equation

$$\frac{\partial}{\partial t}\left[\alpha\rho_v\left(e_v + U_v^2/2\right)\right] + \nabla\cdot\left[\alpha\rho_v\left(e_v + U_v^2/2\right)\vec{U}_v\right]$$

$$+ \nabla\cdot\left(\alpha\vec{q}_v\right) + p\frac{\partial\alpha}{\partial t} + \nabla\cdot\left(\alpha p\vec{U}_v\right) - \nabla\cdot\left(\alpha\bar{\bar{\tau}}_v\cdot\vec{U}_v\right)$$

$$- \alpha\rho_v\vec{F}\cdot\vec{U}_v = Q_{wv} + Q_i \qquad (2.1e)$$

Liquid total energy equation

$$\frac{\partial}{\partial t}\left[(1-\alpha)\,\rho_\ell\left(e_\ell + U_\ell^2/2\right)\right] + \nabla\cdot\left[(1-\alpha)\,\rho_\ell\left(e_\ell + U_\ell^2/2\right)\vec{U}_\ell\right]$$

$$+ \nabla\cdot\left[(1-\alpha)\,\vec{q}_\ell\right] - p\,\frac{\partial\alpha}{\partial t} + \nabla\cdot\left[(1-\alpha)\,p\vec{U}_\ell\right]$$

$$- \nabla\cdot\left[(1-\alpha)\bar{\bar{\tau}}_\ell\cdot\vec{U}_\ell\right] - (1-\alpha)\rho_\ell\vec{F}\cdot\vec{U}_\ell = Q_{w\ell} - Q_i$$

(2.1f)

The notations in these equations are given in the Nomenclature.

It is more convenient, from a numerical point of view, to use equations for the internal energies instead of total energy equations. In the following the derivation of the vapor internal energy equation will be presented.

First an equation for the kinetic energy will be obtained. The procedure parallels that used by Bird, et al [1] for single-phase flow. Using the continuity equation (2.1a), the vapor momentum equation (2.1c) may be cast into the non-conservative form:

$$\alpha\rho_v \frac{D_v\vec{U}_v}{Dt} + \alpha\nabla p - \nabla\cdot(\alpha\bar{\bar{\tau}}_v) - \alpha\rho_v\vec{F}$$

$$= -\Gamma\vec{U}_v - \vec{F}_{wv} - \vec{F}_i \qquad (2.2)$$

using the definition of the the substantial derivative with respect to the vapor velocity:

$$\frac{D_v}{Dt} = \frac{\partial}{\partial t} + \vec{U}_v\cdot\nabla$$

Form the scalar product of the equation of motion (2.2) and the vapor velocity $\vec{U}_v$:

$$\alpha\rho_v \frac{D_v}{Dt} (U_v^2/2) + \alpha\vec{U}_v \cdot \nabla p - \vec{U}_v \cdot \nabla \cdot (\alpha\bar{\bar{\tau}}_v) - \alpha\rho_v \vec{F} \cdot \vec{U}_v$$

$$= - \Gamma U_v^2 - (\vec{F}_{wv} + \vec{F}_i) \cdot \vec{U}_v \qquad (2.3)$$

Using the substantial derivative, the vapor continuity equation may be written as

$$\frac{D_v}{Dt} (\alpha\rho_v) + \alpha\rho_v \nabla \cdot \vec{U}_v = \Gamma \cdot \qquad (2.4)$$

Multiplying Eq. (2.4) by $U_v^2/2$, adding it to Eq. (2.3) and noting that

$$\frac{D_v}{Dt} (\alpha\rho_v U_v^2/2) + (\alpha\rho_v U_v^2/2) \nabla \cdot \vec{U}_v$$

$$= \frac{\partial}{\partial t} (\alpha\rho_v U_v^2/2) + \nabla \cdot [(\alpha\rho_v U_v^2/2) \vec{U}_v]$$

gives the vapor kinetic (or mechanical) energy equation:

$$\frac{\partial}{\partial t} (\alpha\rho_v U_v^2/2) + \nabla \cdot [(\alpha\rho_v U_v^2/2) \vec{U}_v] + \alpha\vec{U}_v \cdot \nabla p$$

$$- \vec{U}_v \cdot \nabla \cdot (\alpha\bar{\bar{\tau}}_v) - \alpha\rho_v \vec{F} \cdot \vec{U}_v$$

$$= - \Gamma U_v^2/2 - (\vec{F}_{wv} + \vec{F}_i) \cdot \vec{U}_v \qquad (2.5)$$

Then by subtracting this equation from Eq. (2.1e) the vapor internal energy equation is obtained:

$$\frac{\partial}{\partial t}(\alpha\rho_v e_v) + \nabla\cdot(\alpha\rho_v e_v \vec{U}_v) + \nabla\cdot(\alpha\vec{q}_v) + p\frac{\partial\alpha}{\partial t}$$

$$+ p\nabla\cdot(\alpha\vec{U}_v) - \alpha\bar{\bar{\tau}}_v:\nabla\vec{U}_v = Q_{wv} + Q_i$$

$$+ \Gamma U_v^2/2 + (\vec{F}_{wv} + \vec{F}_i)\cdot\vec{U}_v \qquad (2.6)$$

The liquid internal energy equation is obtained in an entirely similar manner.

An additional assumption is made to further simplify the momentum and energy equations. Given the large number of fluid-solid interfaces in our applications it is reasonable to assume that the wall drag will dominate the intrafluid viscous effects. Thus, we shall neglect the terms $\nabla\cdot(\alpha\bar{\bar{\tau}}_v)$ and $\nabla\cdot[(1-\alpha)\bar{\bar{\tau}}_\ell]$ in the momentum equations and the dissipation functions, $\alpha\bar{\bar{\tau}}_v:\nabla\vec{U}_v$ and $(1-\alpha)\bar{\bar{\tau}}_\ell:\nabla\vec{U}_\ell$, in the energy equations.

Clearly, this assumptions would not be suitable in other applications such as flow in large plena. In such situations, the contribution of the above mentioned terms becomes essential and must be included in the model.

We shall consider gravity the only body force and denote $\vec{F} = -\vec{g}$ in the momentum equations.

The final working six-equation model, as used in this work, is given below:

Vapor mass equation

$$\frac{\partial}{\partial t}(\alpha\rho_v) + \nabla\cdot(\alpha\rho_v\vec{U}_v) = \Gamma \tag{2.7a}$$

Liquid mass equation

$$\frac{\partial}{\partial t}[(1-\alpha)\rho_\ell] + \nabla\cdot[(1-\alpha)\rho_\ell\vec{U}_\ell] = -\Gamma \tag{2.7b}$$

Vapor momentum equation

$$\alpha\rho_v\frac{\partial\vec{U}_v}{\partial t} + \alpha\rho_v\vec{U}_v\cdot\nabla\vec{U}_v + \alpha\nabla p = -\vec{F}_{wv} - \vec{F}_{iv} - \alpha\rho_v\vec{g} \tag{2.7c}$$

Liquid momentum equation

$$(1-\alpha)\rho_\ell\frac{\partial\vec{U}_\ell}{\partial t} + (1-\alpha)\rho_\ell\vec{U}_\ell\cdot\nabla\vec{U}_\ell + (1-\alpha)\nabla p = -\vec{F}_{w\ell} - \vec{F}_{i\ell} - (1-\alpha)\rho_\ell\vec{g} \tag{2.7d}$$

Vapor internal energy equation

$$\frac{\partial}{\partial t}(\alpha\rho_v e_v) + \nabla\cdot(\alpha\rho_v e_v\vec{U}_v) + p\nabla\cdot(\alpha\vec{U}_v) + p\frac{\partial\alpha}{\partial t} = Q'_{wv} + Q_{iv} + Q_{kv} \tag{2.7e}$$

Liquid internal energy equation

$$\frac{\partial}{\partial t}\left[(1-\alpha)\rho_\ell e_\ell\right] + \nabla\cdot\left[(1-\alpha)\rho_\ell e_\ell \vec{U}_\ell\right) + p\nabla\cdot\left[(1-\alpha)\vec{U}_\ell\right]$$

$$- p\frac{\partial\alpha}{\partial t} = Q'_{w\ell} + Q_{i\ell} + Q_{k\ell} \qquad (2.7f)$$

where

$$\vec{F}_{iv} = \vec{F}_i + \Gamma\vec{U}_v \qquad (2.8a)$$

$$-\vec{F}_{i\ell} = \vec{F}_i + \Gamma\vec{U}_\ell \qquad (2.8b)$$

$$Q'_{wv} = Q_{wv} + \vec{F}_{wv}\cdot\vec{U}_v \qquad (2.8c)$$

$$Q'_{w\ell} = Q_{w\ell} + \vec{F}_{w\ell}\cdot\vec{U}_\ell \qquad (2.8d)$$

$$Q_{iv} = \Gamma U_v^2/2 + \vec{F}_i\cdot\vec{U}_v + Q_i \qquad (2.8e)$$

$$-Q_{i\ell} = \Gamma U_\ell^2/2 + \vec{F}_i\cdot\vec{U}_\ell + Q_i \qquad (2.8f)$$

$$Q_{kv} = -\nabla\cdot(\alpha\vec{q}_v) \qquad (2.8g)$$

$$Q_{k\ell} = -\nabla\cdot\left[(1-\alpha)\vec{q}_\ell\right] \qquad (2.8h)$$

A few remarks may be made with regard to Eq.(2.7). The momentum equation (2.7c,d) are written in a non-conservative form, which is particularly convenient for the numerical solution. One notes that in this form the interfacial momentum terms, $\vec{F}_{iv}$ and $\vec{F}_i$, do not add up to zero, unless either $\Gamma = 0$ or $\vec{U}_v = \vec{U}_\ell$. This is so because only in a conservative form can the interfacial terms satisfy the jump condition, thus cancelling out in a mixture (i.e., sum) equation.

Regarding the internal energy equations, it should be pointed out that, unlike the equations for total energy (Eqs. (2.1e,f)), they are not conservation equations. Again this particular form of the energy equations is chosen for numerical convenience. One notes the presence of some work terms in both the wall and interfacial heat sources, Eqs. (2.8c - f). As before, we also note that the interfacial heat terms, Q_{iv} and $Q_{i\ell}$, do not add up to zero unless $\vec{U}_v = \vec{U}_\ell$.

There are twelve unknowns appearing in Eqs. (2.7): the void fraction α, the pressure p, the densities ρ_v and ρ_ℓ, the specific energies e_v and e_ℓ and the three components of $\vec{U}_v$ and $\vec{U}_\ell$. The wall and interfacial exchange terms, as well as the effective fluid conduction heat sources (Eqs. (2.8g, h)) are assumed to depend, via constitutive relations, upon these variables and the phase temperatures T_v and T_ℓ. Thus, we have a total of fourteen unknowns. Noting that Eqs. (2.7) represent a total of ten equations, we must supply four additional relationships for closure. They are the equations of state, in the form:

$$\rho_v = \rho_v\ (p, T_v) \tag{2.9a}$$

$$\rho_\ell = \rho_\ell\ (p, T_\ell) \tag{2.9b}$$

$$e_v = e_v\ (p, T_v) \tag{2.9c}$$

$$e_\ell = e_\ell\ (p, T_\ell) \tag{2.9d}$$

A natural subset of variables (which may be viewed as "the main variables") can then be chosen as p,α,T_v, T_ℓ and the phase vector velocities, $\vec{U}_v$ and $\vec{U}_\ell$, i.e., ten "main" unknowns, from which any other variables may be inferred via known functional dependencies.

The six-equation model presented herein constitutes the starting point for developing mixture models, described in the next section.

2.3 Mixture Model Selection

2.3.1 Mixture Models

As previously defined, a mixture model uses fewer conservation equations than the six-equation model to describe the two-phase flow. While it is generally true that a mixture model requires fewer constitutive equations, it is also evident that less information can be obtained from the particular set of equations used. Therefore, the lost information must be provided in an alternate form by imposing restrictions on the two-phase flow evolution. To place the above considerations in perspective, Table 2.1 summarizes the main features of the two-phase flow models that can be constructed by using three to six conservation equations. The suggested nomenclature is of the form: nCmT

TABLE 2.1

Two-Phase Flow Models

(General assumption: $p_\ell = p_v$)

Two-Phase-Flow Model (suggested nomenclature)	Conservation Equations				Imposed Restrictions			Required Constitutive Relations					
								External		Interfacial			Total
	M	E	K	Total	T_a	U_r	Total	Q_w	F_w	Γ	Q_i	F_i	
3 C	1	1	1	3	2	1	3	1	1	0	0	0	2
4 C 2 M	2	1	1	4	1	1	2	1	1	1	0	0	3
4 C 2 E	1	2	1	4	1	1	2	2	1	1*	1	0	5
4 C 2 K	1	1	2	4	2	0	2	1	2	1*	0	1	5
5 C 1 K	2	2	1	5	0	1	1	2	1	1	1	0	5
5 C 1 E	2	1	2	5	1	0	1	1	2	1	0	1	5
5 C 1 M	1	2	2	5	1	0	1	2	2	1*	1	1	7
6 C	2	2	2	6	0	0	0	2	2	1	1	1	7

Legend: M = Conservation of Mass
E = Conservation of Energy
K = Conservation of Momentum
T_a = Phase "a" temperature; a = v or ℓ
U_r = Relative velocity = $U_v - U_\ell$

*note that the interface mass exchange, Γ, is needed whenever Q_i and/or F_i are needed.

where:

n is the number of conservation ("C") equations,

m is 1 or 2, representing the number of conservation equations of a given type ("T")

T = M, E or K, representing mass, energy and momentum, respectively.

An insightful discussion on obtaining consistent two-phase flow models is given by Boure in [2].

An examination of Table 2.1 indicates that, as expected, a decreased number of conservation equations comes at the expense of an increased number of restrictions. (Indeed, it can be seen that the sum of the number of conservation equations and the number of imposed restrictions is always six). On the other hand, the number of required constitutive relationships clearly increases with the number of conservation equations.

The three-equation model requires constitutive relations only for the wall exchange terms, as applied to the mixture as a whole. The three mixture conservations equations are supplemented by three constraints:

- both phase temperatures are related to the saturation temperature (and hence to pressure), usually by the assumption of thermal equilibrium, $T_v = T_\ell = T_{sat}(p)$.

- a constraint on the relative phase motion; if no slip is assumed, we have the equilibrium homogeneous model, while if a correlation for the relative velocity is used, the model may be called equilibrium drift flux.

The four-equation models present a wider variety, depending on the quantity for which two conservation equations are used. The first such model, 4C2M in our table is the traditional (non-equilibrium) drift flux model, where the use of two mass equations allows the departure from saturation of one phase. In addition to the mixture-wall exchange terms, the interfacial mass exchange rate, Γ, must be provided. The other four-equation models require more constitutive relations, as the use of two momentum or two energy equations raises the need for more wall exchange terms. We also note the need to provide the rate of mass exchange Γ whenever the energy (Q_i) or the momentum (F_i) exchange rate is required. This is obviously a consequence of the fact that one mechanism for energy and momentum transfer is the mass transport. Fortunately, the mass conservation equation for one of the phases may be used to determine the mass exchange rate, thus obviating the need for an extraneous correlation. There is no

incentive to use the 4C2E model, as it provides the same information as 4C2M, while requiring more constitutive equations. On the other hand, the 4C2K model may be used to advantage in situations characterized by virtual thermal equilibrium, but inadequately described by a drift flux-type formulation.

The five-equation models represent the next level of refinement, achieved at the cost of requiring additional constitutive relations compared to the previous category. The first model, 5C1K might be of interest in situations where thermal non-equilibrium (i.e., departure from saturation) for both phases might be expected, while the relative motion may be adequately treated as a constraint on the relative velocity. The next model, 5C1E, is quite appealing, since setting one phase to saturation, an assumption quite plausible in many applications, provides the necessary single constraint. There is no particular incentive to use the last model in this category, 5C1M, as it provides the same information as the previous one (5C1E), while requiring more constitutive equations. The comment regarding the need for the mass exchange rate, made in connection with the four-equation models 4C2E and 4C2K, applies here too.

Finally, the six-equation model removes the need for any (more or less artificial) constraints, at the price of requiring the largest number of (non-degenerate) constitutive relations. It should be noted that through appropriately modified constitutive relations, the six-equation model can be made to simulate a lower level model. For instance, a very high interfacial momentum exchange leads to a virtual equal velocity model. Similar artifices may be used to obtain thermal equilibrium of one or both phases. This demonstrates the flexibility of the six-equation model. However, if the applications of interest clearly do not warrant the full potential of this model, its use as a computational tool may be uneconomical.

2.3.2 Selection of a Mixture Model for This Work

For our particular applications using liquid sodium as a coolant, it was felt that the assumption of thermal equilibrium, at saturation, between coexisting phases is quite reasonable. Indeed the very high thermal conductivity of liquid sodium will preclude any significant temperature gradients in the vicinity of the liquid-vapor interface. We should mention that after complete dryout, with vapor directly heated by the wall, a large temperature gradient may exist in the vapor due to its low conductivity. Thus, while entrained liquid droplets are still at saturation, the vapor may be superheated. For our work we are not interested in calculations at relatively late times following boiling

inception and, therefore, chose to ignore this regime. Actually, an additional comment must be made here. As our numerical treatment is a lumped parameter approach, the implied spatial averaging leads to an inherent loss of information in as far as the temperature distribution within such a "lump" (i.e., control volume) is concerned. Under hypothetical accident conditions, fairly steep temperature gradients may develop in the assembly. Since assuming thermal equilibrium is equivalent to bulk boiling in the control volume of interest, this control volume (i.e., mesh size) should not be too large. While in principle a thermal non-equilibrium model might be able to simulate more "localized" phenomena within a relatively larger control volume, in practice this potential advantage is of limited value, as any assumption of a temperature distribution within an extremely complex three-dimensional flow field would raise grave doubts as to its validity. Consequently, the remark made above regarding the size of the control volumes applies generally to all two-phase flow models.

While thermal equilibrium appears a reasonable assumption, mechanical equilibrium does not. The enormous liquid-to-vapor density ratio for sodium at near atmospheric pressures together with the low flow conditions under consideration lead to very substantial slip ratios. In one-dimensional configurations, an adaptation of a drift-

flux type formulation might be possible, however, its use for a predominantly annular flow regime would be somewhat questionable. As our applications deal with multi-dimensional flows, in complicated geometries, defining adequate drift-flux like parameters becomes a hopeless exercise. It is worth mentioning that a persistent complication in multi-dimensional flows is the current inability to quantify flow regimes.

In light of the above, it was concluded that the use of separate momentum equations for each phase becomes a necessity. Such a formulation provides a suitable framework for a much needed development of the interfacial momentum exchange.

The consequence of all these considerations was the adoption of a four-equation model, using two momentum equations and assuming thermal equilibrium on the saturation line between coexisting phases. Using the nomenclature of Table 2.1, our four-equation model is 4C2K.

2.4 The Four-Equation Model

Any mixture model can be obtained in a consistent manner from the six-equation model previously described. To obtain our four-equation model, the phase mass and energy equations are summed up to yield a mixture mass and a mixture energy equation, respectively. The resulting governing equations are:

Mixture mass equation

$$\frac{\partial}{\partial t}\rho_m + \nabla\cdot[\alpha\rho_v\vec{U}_v + (1-\alpha)\rho_\ell\vec{U}_\ell] = 0 \qquad (2.10a)$$

Momentum equations

(identical to the six-equation model, e.g., (2.7c,d)) (2.10b,c)

Mixture internal energy equation

$$\frac{\partial}{\partial t}(\rho_m e_m) + \nabla\cdot[\alpha\rho_v e_v\vec{U}_v + (1-\alpha)\rho_\ell e_\ell\vec{U}_\ell] + p\nabla\cdot[\alpha\vec{U}_v + (1-\alpha)\vec{U}_\ell] = Q_w + Q_{im} + Q_k \qquad (2.10d)$$

where $\rho_m = \alpha\rho_v + (1-\alpha)\rho_\ell$ (2.11a)

$$e_m = [\alpha\rho_v e_v + (1-\alpha)\rho_\ell e_\ell]/\rho_m \qquad (2.11b)$$

Q_w = mixture wall heat source

$= Q'_{wv} + Q'_{w\ell}$

Q_{im} = mixture heat source due to interfacial effects

$= Q_{iv} + Q_{i\ell}$

Q_k = mixture conduction heat transfer rate

$= Q_{kv} + Q_{k\ell}$

To the fourteen unknowns we counted for the six-equation model we added two new ones, the mixture density, ρ_m and the specific mixture internal energy, e_m. Equations (2.10) and the definitions (2.11) represent a total of ten equations. We need six additional relationships. Four of them are again provided by the equations of state (2.9). The other two are implied by the assumption of thermal equilibrium on the saturation line:

$$T_v = T_\ell = T_{sat}(p) \tag{2.12}$$

A particularly advantageous set of main variables is p, e_m and the phase vector velocities, $\vec{U}_v$ and $\vec{U}_\ell$, i.e., eight "main" unknowns, from which all the others can be determined. Note that e_m applies equally to single-phase flows (sensible heat) and to two-phase flows (latent heat), thus no switch in variables is needed. This is especially important in as far as the numerical treatment is concerned. We shall see in the next chapter that through the use of the four equations of state (2.9), the two definitions (2.11) and the two constraints (2.12) one can calculate the following eight quantities: α, T_v, T_ℓ, ρ_m, ρ_v, ρ_ℓ, e_v, e_ℓ, for any given p and e_m. Consequently, we have the equivalent of eight equations of state, which supplement the eight governing equations (2.10) to balance the previously identified sixteen unknowns.

Some further simplifying assumptions, widely used, will be made. First the contribution of interfacial effects to the mixture heat source will be neglected. While the work terms due to the interfacial momentum exchange, i.e., $\vec{F}_i \cdot \vec{U}_v$ and $\vec{F}_i \cdot \vec{U}_\ell$ are always very small, there is some recent evidence ([3]) that in some circumstances, the kinetic energy transport via interfacial mass exchange, i.e., $\Gamma \vec{U}_v^2/2$ and $\Gamma \vec{U}_\ell^2/2$, while still small, may represent one or two percent of the total heat source; nonetheless, we chose to neglect this term in this work, thus $Q_{im} = 0$. We shall also neglect the pseudowork terms due to wall forces, i.e., $\vec{F}_{wv} \cdot \vec{U}_v$ and $\vec{F}_{w\ell} \cdot \vec{U}_\ell$, in the wall heat source, since they never exceed a fraction of one percent.

To conclude, we now have a two-phase flow model, whose governing "conservation" equations, supplemented by appropriate equations of state and constitutive relations, form a complete set, i.e., formally effect closure.

2.5 REFERENCES

1. R.B. Bird, W.E. Stewart and E.N. Lightfoot, "Transport Phenomena", p. 81-82 and 314-316, John Wiley & Sons, 1960.

2. J.A. Boure, "Mathematical Modeling and Two-Phase Flow Constitutive Equations", European Two-Phase Flow Meeting, Haifa, Israel, 1975.

3. K.Y. Huh, "Simulation of Sodium Boiling Experiments with THERMIT Sodium Version," M.S. Thesis, Nuclear Engineering Department, M.I.T., May 1982. (Also issued as Energy Laboratory Report No. MIT-EL 82-023, May 1982).

CHAPTER 3. STATE FUNCTIONS AND CONSTITUTIVE EQUATIONS

3.1 Introduction

The previous chapter has presented the selection and derivation of a two-phase flow model. Our choice, a four-equation model containing two momentum equations, requires additional relations to effect closure. These additional relations are provided by the appropriate equations of state and constitutive equations.

The thermal equilibrium assumption, requiring that co-existing phase temperatures be equal to the saturation temperature corresponding to the local pressure, leads to a functional relationship, directly relating the mixture density to the pressure and mixture internal energy. We will present the derivation of this important relation.

Regarding the constitutive equations, our effort was mainly directed towards a careful selection and implementation of models, with particular attention given to their efficiency and compatibility within our solution scheme.

3.2 State Functions

We recall from Chapter 2 that our four-equation model calls for four equations of state, relating each phase density and internal energy to the (common) pressure and to the respective phase temperature. They

are supplemented by two constraints, requiring that when both phases coexist they be at saturation, corresponding to the local pressure. We have:

$$\rho_v = \rho_v\ (p,\ T_v) \tag{3.1a}$$

$$\rho_\ell = \rho_\ell\ (p,\ T_\ell) \tag{3.1b}$$

$$e_v = e_v\ (p,\ T_v) \tag{3.1c}$$

$$e_\ell = e_\ell\ (p,\ T_\ell) \tag{3.1d}$$

$$T_{sat} = T_{sat}\ (p) \tag{3.1e}$$

and

$$T_v = T_\ell = T_{sat} \tag{3.2}$$

The fits used for Eqs. (3.1) are given in Appendix B. We also recall the definitions of the mixture density and internal energy:

$$\rho_m = \alpha\rho_v + (1 - \alpha)\rho_\ell \tag{3.3a}$$

$$e_m = [\alpha\rho_v e_v + (1 - \alpha)\rho_\ell e_\ell]/\rho_m \tag{3.3b}$$

Equations (3.1 - 3.3) may be used to generate a virtual equation of state, relating the mixture density to pressure and mixture internal energy in both single-phase (liquid or vapor) and two-phase flow situations.

Let us start with the two-phase flow situation.

The void fraction, α, can be eliminated between Eqs. (3.3) to yield

$$\rho_m = \frac{\rho_\ell \rho_v \ (e_v - e_\ell)}{\rho_\ell \ (e_m - e_\ell) + \rho_v (e_v - e_m)} \tag{3.4}$$

The assumption of thermal equilibrium at saturation implies that ρ_v, ρ_ℓ, e_v and e_ℓ are all functions of pressure only (e.g., $\rho_v = \rho_v \ (p, \ T_{sat}(p)) = \rho_v(p)$). Therefore, Eq. (3.4) represents a functional dependence of the form:

$$\rho_m \ = \rho_m \ (p, \ e_m) \tag{3.5}$$

Knowing ρ_m, one can immediately determine the void fraction from Eq. (3.3a) re-arranged as:

$$\alpha = (\rho_\ell - \rho_m)/(\rho_\ell - \rho_v) \tag{3.6}$$

It can be seen that ρ_m given by Eq. (3.4) correctly reduces to ρ_ℓ for $e_m = e_\ell$ and to ρ_v for $e_m = e_v$. We note that Eq. (3.4), with ρ_v, ρ_ℓ, e_v and e_ℓ evaluated at saturation, implies a certain interphase mass exchange, namely that which ensures thermal equilibrium at saturation. In other words, when both phases coexist, the thermal energy can be absorbed or released only as latent heat.

The logic employed to recognize a single- or two-phase flow condition is shown in Fig. 3.1.

We have already seen how we can determine all the necessary thermodynamic properties for a two-phase mixture. In single-phase situations, the calculational sequence is as follows:

- given p and e_m, set $e_{single\text{-}phase} = e_m$;
- from Eq. (3.1c or d) determine the temperature (see Appendix B);
- from Eq. (3.1a or b) determine the density.

This section would not be complete without discussing the derivatives of the state functions. It will be seen in the next chapter that the numerical solution is built around a linearization requiring the derivatives of mixture density and temperature with respect to pressure and mixture internal energy (here mixture refers to the fluid generically, regardless of its condition). The single-phase situations do not raise any special difficulty. In two-phase flow conditions the density derivatives are more complicated, a reflection of the functional dependence embodied in Eq. (3.4). After some algebraic work the following expressions can be obtained:

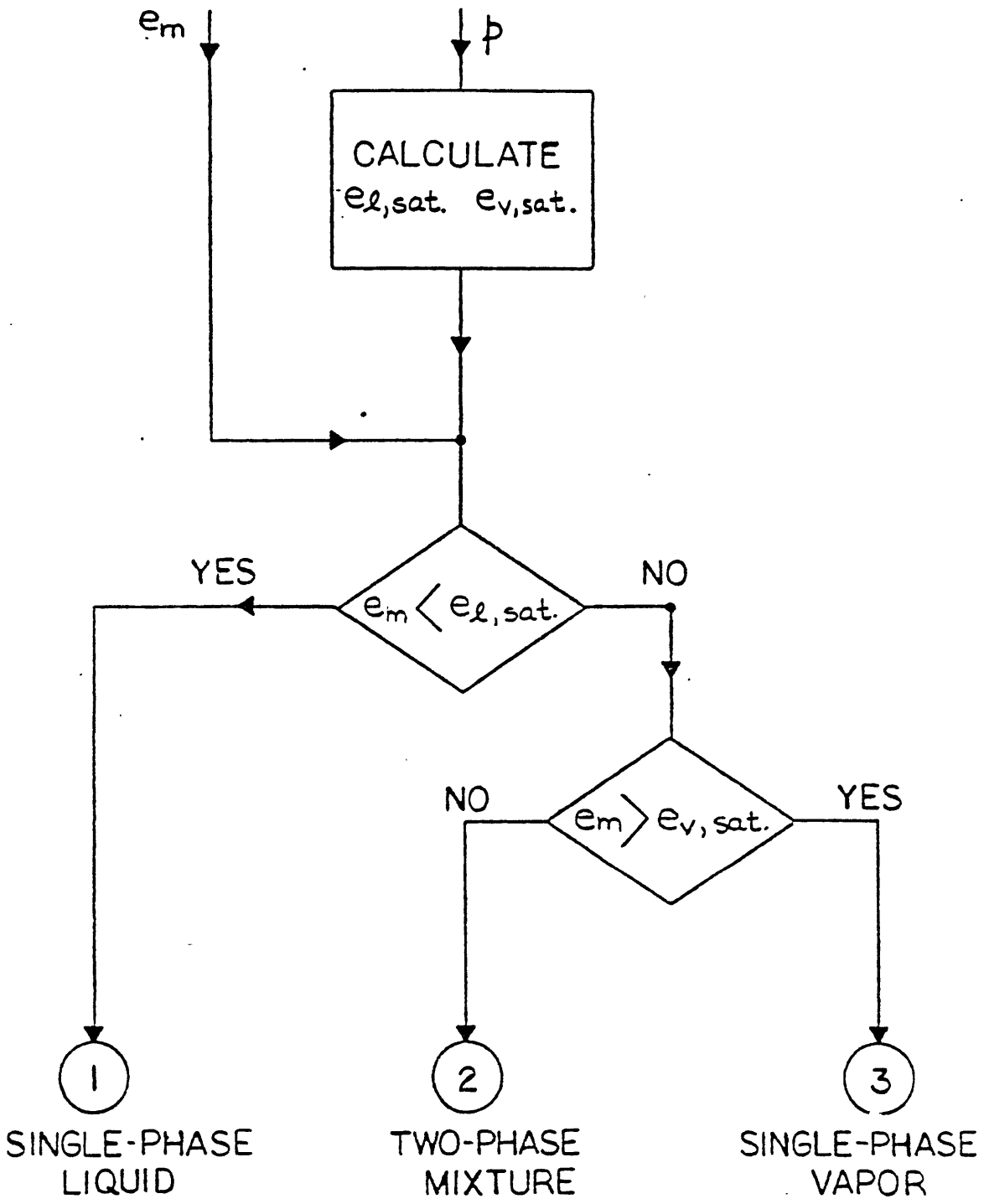

Figure 3.1 Equation of State Selection Logic

$$\frac{\partial \rho_m}{\partial p} = \frac{\partial \rho_m}{\partial \rho_v} \cdot \frac{d\rho_v}{dp} + \frac{\partial \rho_m}{\partial \rho_\ell} \cdot \frac{d\rho_\ell}{dp} + \frac{\partial \rho_m}{\partial e_\ell} \cdot \frac{de_\ell}{dp} + \frac{\partial \rho_m}{\partial e_v} \cdot \frac{de_v}{dp} \tag{3.7}$$

$$\frac{\partial \rho_m}{\partial \rho_v} = \frac{\rho_\ell^{\,2} (e_v - e_\ell)(e_m - e_\ell)}{(\text{denom})^2} \tag{3.8a}$$

$$\frac{\partial \rho_m}{\partial \rho_\ell} = \frac{\rho_v^{\,2} (e_v - e_\ell)(e_v - e_m)}{(\text{denom})^2} \tag{3.8b}$$

$$\frac{\partial \rho_m}{\partial e_v} = \frac{\rho_v \rho_\ell (\rho_\ell - \rho_v)(e_m - e_\ell)}{(\text{denom})^2} \tag{3.8c}$$

$$\frac{\partial \rho_m}{\partial e_\ell} = \frac{\rho_v \rho_\ell (\rho_\ell - \rho_v)(e_v - e_m)}{(\text{denom})^2} \tag{3.8d}$$

$$\frac{\partial \rho_m}{\partial e_m} = - \frac{\rho_v \rho_\ell (e_v - e_\ell)(\rho_\ell - \rho_v)}{(\text{denom})^2} \tag{3.9}$$

where denom = $\rho_\ell (e_m - e_\ell) + \rho_v (e_v - e_m)$.

The appearance of the total derivatives of ρ_v, ρ_ℓ, e_v and e_ℓ signifies their dependence on pressure only (directly, and indirectly via temperature). For example:

$$\frac{d\rho_v}{dp} = \left(\frac{\partial \rho_v}{\partial p}\right)_{T_v} + \left(\frac{\partial \rho_v}{\partial T_v}\right)_p \frac{dT_{sat}}{dp}$$

with $T_v = T_{sat}$.

It can be easily verified that while the density is continuous, its derivatives change abruptly between the single- and two-phase domains. The variation of density with pressure and internal energy is illustrated in Figs. 3.2 and 3.3. As it can be seen, the discontinuity in slope is particularly dramatic at the liquid/two-phase transition point. It is thus conceivable that a secant-like approximation to the derivatives might be a better representation of the behavior of the function in the vicinity of this point (see Fig. 3.4). In a sense, a "smoothing" effect is obtained.

There is no unique prescription as to how to construct these secant approximations to the function $\rho_m\ (p,e_m)$. A simple approximation of $(\partial\rho_m/\partial e_m)_p$ for example may be

$$\left(\frac{\partial \rho_m}{\partial e_m}\right)_p \cong \frac{\rho_m(p,e_m + \delta e_1) - \delta_m(p,e_m - \delta e_2)}{\delta e_1 + \delta e_2} \qquad (3.10)$$

where δe_1 and δe_2 are "suitably" chosen increments. A more refined approach would consider perturbations in both variables in an attempt to provide a better approximation of the function around the point of interest. Basically one resorts to a two-dimensional interpolation.

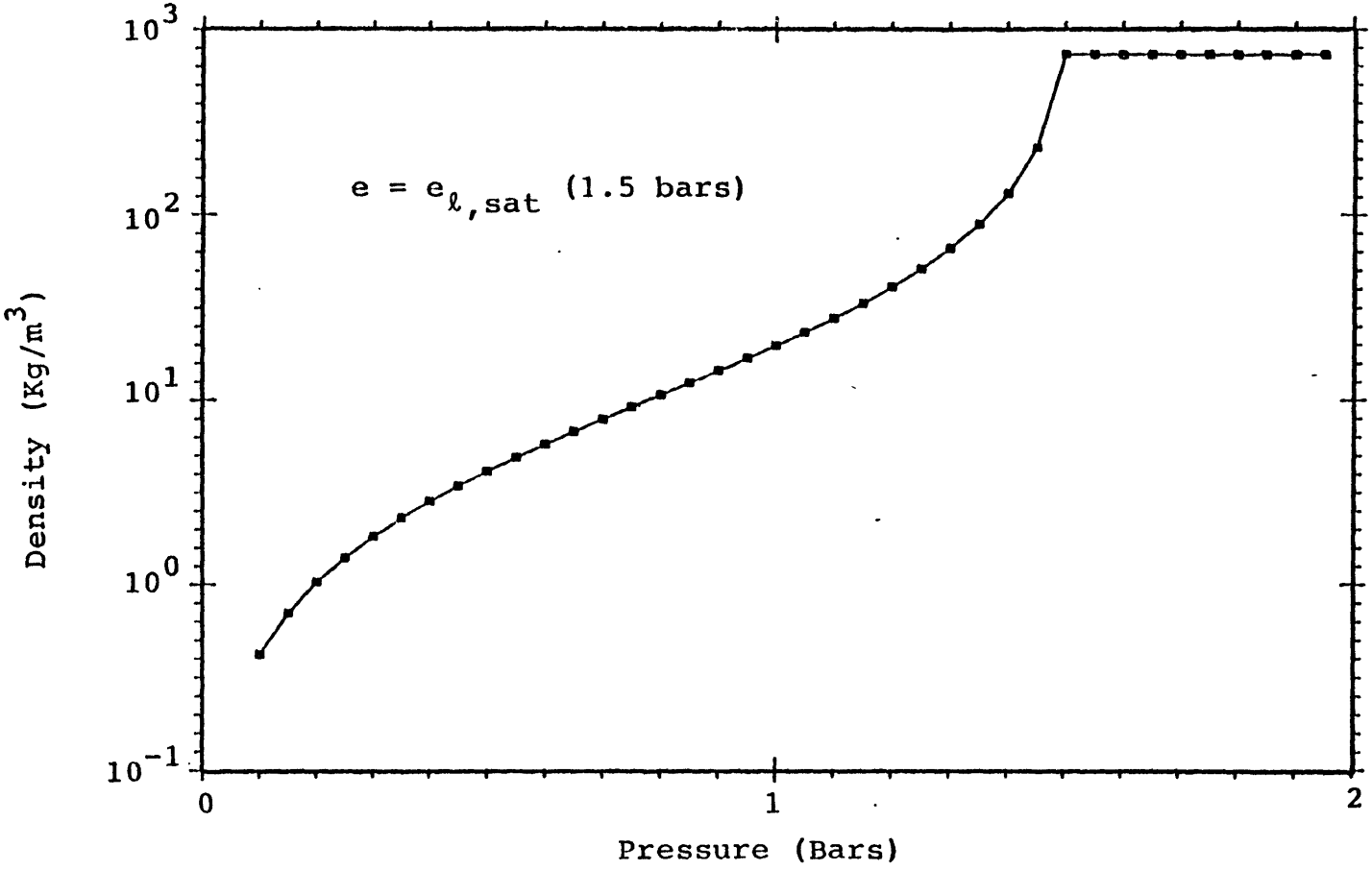

Figure 3.2 Sodium Density versus Pressure

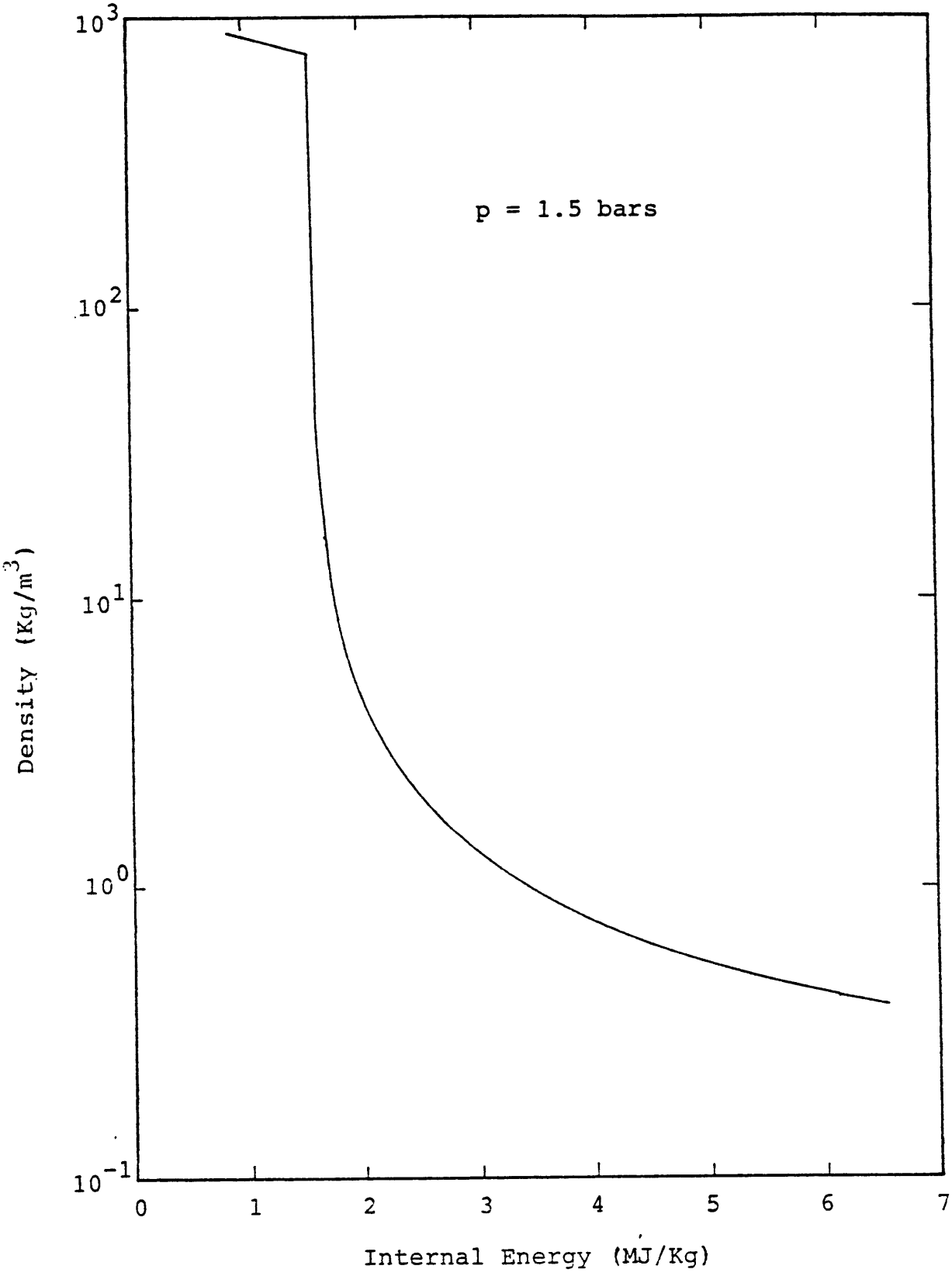

Figure 3.3 Sodium Density versus Internal Energy

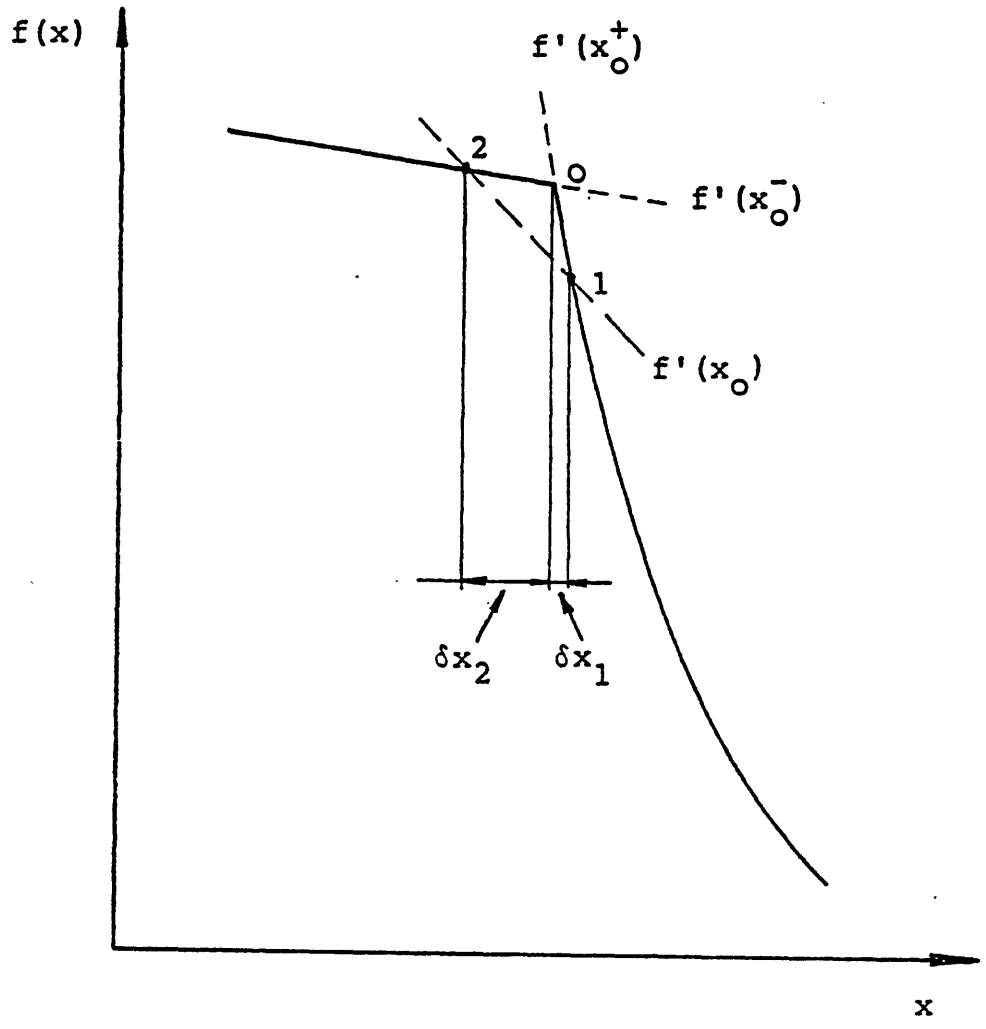

Figure 3.4 Secant Approximation of the First Derivative

The simplest scheme in this context is the bilinear interpolation (see for example, [1]). Consider a rectangle whose vertices are:

$$\rho_{m,1} = \rho_m\ (p + \delta p_1,\ e_m + \delta e_1)$$

$$\rho_{m,2} = \rho_m\ (p - \delta p_2,\ e_m + \delta e_1)$$

$$\rho_{m,2} = \rho_m\ (p + \delta p_1,\ e_m - \delta e_2)$$

$$\rho_{m,4} = \rho_m\ (p - \delta p_2,\ e_m - \delta e_2)$$

The following approximation for ρ_m in the neighborhood of the point $(p,\ e_m)$ can then be constructed:

$$\rho_m\ (p', e_m') \cong \sum_{i=1}^{i=4} \eta_i \rho_{m,i} \qquad (3.11)$$

where: $\eta_1 = (1+2x)(1+2y)/4$, $\eta_2 = (1-2x)(1+2y)/4$

$\eta_3 = (1+2x)(1-2y)/4$, $\eta_4 = (1-2x)(1+2y)/4$

$$x = \frac{e_m' - e_m^*}{\delta e_1 + \delta e_2}\ , \qquad y = \frac{p' - p^*}{\delta p_1 + \delta p_2}\ ,$$

$$e_m^* = e_m + (\delta e_1 - \delta e_2)/2$$

$$p^* = p + (\delta p_1 - \delta p_2)/2$$

Note that p^* and e_m^* are the coordinates of the center of the above mentioned rectangle. One can now obtain the desired derivatives at any point inside this rectangle. Let us evaluate $(\partial\rho_m/\partial e_m)_p$ at (p^*, e_m^*), for example:

$$\left(\frac{\partial\rho_m}{\partial e_m}\right)_p \cong \frac{1}{2(\delta e_1 + \delta e_2)} \left(\rho_{m,1} + \rho_{m,2} - \rho_{m,3} - \rho_{m,4}\right) \tag{3.12}$$

Even more complicated interpolation schemes may be considered, making use of the function (i.e., density) evaluated at more points. The computational penalty increases substantially and it is justifiable only if the convergence of the non-linear iterations is significantly improved.

3.3 Constitutive Equations

In the process of obtaining a tractable mathematical model, a great deal of informaton is lost. Spatial and temporal (or statistical) averaging renders such a model unable to represent the details of interfacial interactions and of intraphase distributions. The role of the constitutive equations is to provide this lost information thus rendering the model solvable. Clearly the complexity of the flow geometry combined with the current

inability to quantitatively describe two-phase flow regimes introduce a great deal of empiricism and hence, uncertainty. Consequently, while a great deal of thought went into the selection and implementation of the necessary constitutive relations, the ultimate justification for a specific choice lies in the capability of the overall model to simulate and display reasonable agreement with experiments.

3.3.1 Wall Friction

3.3.1.1 General Framework

The effect of the solid-fluid interfaces leads to the appearance of momentum sink terms through the volume-averaging process presented in Appendix A. These terms ($\vec{F}_{wv}$ and $\vec{F}_{w\ell}$ in Eqs. (2.7)) have the dimension of a force per unit volume. (The reader should note that the volume referred to is that occupied by the two-phase mixture). Let us consider a one-dimensional situation and let τ_{wa} and A_{wa} be the average wall shear and the "wetted" area for phase "a", respectively. We then have

$$F_{wa} = (A_{wa}/V)\tau_{wa} \tag{3.13}$$

By analogy with single-phase flow, τ_{wa} can be related to the kinetic energy of phase a through a Darcy-type relation:

$$\tau_{wa} = \frac{1}{8} f_{wa} \rho_a |U_a| U_a \tag{3.14}$$

where

f_{wa} = friction factor for phase a.

This formulation has also been used in [2] and we adopted it because it provides a consistent framework for modeling and presentation.

The wetted area per unit volume, for phase a, can also be written as

$$\frac{A_{wa}}{V} = \frac{P_{wa} L}{AL} = \frac{P_w}{A} cf_a = \frac{4}{D_e} cf_a \tag{3.15}$$

where:

p_{wa} = wetted perimeter for phase a

L = "length" of control volume

A = total flow area

P_w = total wetted perimeter

D_e = equivalent hydraulic diameter

$= 4A/P_w$

cf_a = contact fraction of phase a =

P_{wa}/P_w

Substituting Eqs. (3.14 and 3.15) into Eq. (3.13), we obtain the final forms of the wall friction force per unit

volume, for phase a:

$$F_{wa} = \frac{cf_a}{2D_e} f_{wa} \rho_a |U_a| U_a \tag{3.16a}$$

$$= K_{wa} U_a \tag{3.16b}$$

We shall call K_{wa} the wall friction coefficient for phase a. Equation (3.16b) represents a linearized form of the wall friction force, which will be used in the numerical solution scheme.

According to Eq. (3.16a), we must supply two pieces of information to fully define the wall friction force, for each phase, i.e., cf_a and f_{wa}.

In single-phase flow situations, the contact fractions are obviously 1.0 for the present phase and 0.0 for the other phase. Thus, we have to provide only one wall friction factor.

In two-phase flow situations, the flow regime that is likely to exist must be given some consideration. It is not easy to quantitatively identify two-phase flow regimes even in simple configurations, say a straight tube. It is probably hopeless to attempt it for the extremely complicated bundle geometry. Consequently, a simplified approach is taken. The assumption is made that whenever

two-phase flow exists, an annular flow regime prevails, with liquid coating the solid surfaces. In light of the enormous liquid-to-vapor density ratio for sodium at low pressure, annular flow at low qualities is probably an adequate assumption. Also an extensive body of test data has demonstrated the retention of a thin liquid film on the solid surfaces as the flow regime passed into the annular zone. At very high void fractions, some vapor to wall contact is allowed, thus providing a transition to single-phase vapor flow. The contact fractions are defined such as to represent the conditions just described:

$$cf_\ell = \begin{cases} 1.0, & \alpha < 0.89 \\ 10\ (0.99-\alpha), & 0.89 \leq \alpha \leq 0.99 \\ 0.0, & \alpha > 0.99 \end{cases} \qquad (3.17)$$

and

$$cf_v = 1 - cf_\ell$$

We will now postulate that the wall friction factor for phase a, f_{wa}, can be calculated from single-phase correlations of the form

$$f_{wa} = C/Re_a^n \qquad (3.18)$$

modified to take into account the actual flow area of phase a. This modification is accomplished by the following definition of a Reynolds number for the phase:

$$Re_a = \rho_a U_a D_{e,a} / \mu_a \tag{3.19}$$

where

$$D_{e,a} = \frac{4A_a}{P_w} = \frac{4\alpha_a A}{P_w} = \alpha_a D_e \tag{3.20}$$

This ad-hoc definition of the equivalent hydraulic diameter for a phase implicitly assumes that the phase is in full contact with the wall. A potential refinement would be the consideration of an effective wetted perimeter, P_{wa}, and hence of a contact fraction in the definition of $D_{e,a}$. Since verification of this concept is currently lacking, we have not pursued it. It is interesting to note that the same definition of the phase Reynolds number, i.e.,

$$Re_a = \alpha_a \rho_a U_a D_e / \mu_a \tag{3.19'}$$

can be obtained by considering that phase flowing alone. Indeed, observing that $\alpha_a \rho_a U_a = G_a$, Eq. (3.19') can be written as

$$Re_a = G_a D_e / \mu_a \qquad (3.19")$$

which is, according to Collier ([3]), just the Reynolds number of phase a flowing alone.

Finally, we made the common (albeit questionable) extrapolation of this formalism to a multidimensional flow. In other words, Eq. (3.16b) becomes:

$$\vec{F}_{wa} = \bar{\bar{K}}_{wa} \cdot \vec{U}_a \qquad (3.21)$$

where $\bar{\bar{K}}_{wa}$ is a diagonal tensor. We should mention at this point some recent work ([4]) which suggests how this formulation (Eq. (3.21)) may be generalized to consider a full tensor $\bar{\bar{K}}_{wa}$. This work is still in progress, awaiting additional experimental data.

3.3.1.2 Axial Flow

We adopted the following set of correlations, suggested by Wilson in [5], which are specific forms of Eq. (3.18):

$$(f_{wa})_{Laminar} = \frac{32}{\sqrt{H}} \left(\frac{P}{D}\right)^{1.5} \frac{1}{Re_a} \text{ , for } Re_a \leq 400 \qquad (3.22a)$$

$$(f_{wa})_{Turbulent} = \frac{0.316M}{Re_a^{0.25}}, \text{ for } Re_a \geq 2600 \quad (3.22b)$$

$$(f_{wa})_{Transition} = (f_{w,a})_{Turbulent}\sqrt{\psi} + (f_{w,a})_{Laminar}\sqrt{1-\psi}, \text{ for } 400<Re_a<2600 \quad (3.22c)$$

where

$$M = \left[\frac{1.034}{(P/D)^{0.124}} + \frac{29.7(P/D)^{6.94}Re_a^{0.086}}{(H/D)^{2.239}}\right]^{0.885}$$

$$\psi = (Re_a - 400)/2200$$

H = wire wrap lead length (meters)

P/D = pitch-to-diameter rato

The laminar flow correlation, Eq. (3.22a) was proposed by Engel et al, in [6]. Based on results presented in that reference, a cutoff is imposed to avoid an unrealistic situation for bare rods (i.e., $H \to \infty$) by requiring $f_{Laminar} \cdot Re \geq 60$. The correlation used in turbulent flow, Eq. (3.22c), is a slightly modified version of a correlation due to Novendstern ([7]).

In recent years, work performed at M.I.T. (see [8], [9], [10]) has generated various correlations for pressure drops in bundles. If used strictly for the intended

geometry (i.e., subchannel representation), these correlations would most likely provide a better model. However, in the context of our porous body representation, the error in their application has not been assessed. In fact, these remarks are equally applicable to the correlations of Engel, et al, and Novendstern. A very significant effort of adaptation would be required to exploit the potential for increased accuracy of the MIT-developed correlations. In light of the above, we considered there was no incentive to shift from Wilson's work for our applications.

We note that while most test results used in producing the correlations for $f_{w,a}$ were obtained for liquids, some experiments were performed with air (see [6]), therefore it appears reasonable to apply the same correlations to single-phase vapor flow.

We make a final remark regarding the calculation of the equivalent hydraulic diameter, D_e. In principle one could determine it from the local flow areas and wetted perimeters. However, we advice against this approach, as it would be inconsistent with the bundle "average" behavior implied in the correlations (3.22). We recommend simply that D_e be calculated as:

$$D_e = 4xA\ (\text{bundle})/P_w\ (\text{rods + duct}) \qquad (3.23)$$

3.3.1.3 Transverse Flow

To our knowledge, there is no correlation addressing the flow across wire-wrapped rods. Therefore, a correlation applicable to flow across tubes without wire wrap spacers (such as used in various industrial heat exchangers) had to be adopted and adapted to our applications.

The correlation selected for this work is that of Gunter and Shaw ([11]), developed for single-phase flow. We have:

$$(f_{wa})_{\text{Laminar}} = \frac{180}{Re_a}\ , \text{ for } Re_a \leq 202.5 \qquad (3.24a)$$

$$(f_{wa})_{\text{Turbulent}} = \frac{1.92}{Re_a^{0.145}}, \text{ for } Re_a > 202.5 \qquad (3.24b)$$

where Re_a has been defined by Eqs. (3.19, 3.20).
A number of remarks are in order concerning Eqs. (3.24). First, the crossover value for the Reynolds number assures continuity in the friction factor. Second, the velocity used in evaluating the Reynolds number, as well as in Eq. (3.16), is the transverse velocity at the

point of maximum constriction between rods. Finally, the equivalent hydraulic diameter appearing in Eq. (3.19) is defined as:

$$D_e = \frac{4 \times \text{Net fluid volume in tube bank}}{\text{Wetted surface}} \qquad (3.25)$$

Clearly, in view of Eq. (3.15), the "volumetric" hydraulic diameter defined above is identical to that defined in (3.23). This is why we have not used a different notation for D_e in Eq. (3.25).

It should be pointed out that these correlations apply strictly to bare rod banks. Further refinement must wait for additional analytical and especially experimental investigations.

3.3.2 Wall Heat Transfer

There are two types of solid surfaces exchanging heat with the fluid: the fuel or heater rods and the "passive" hex can surrounding the bundle. Actually, in transients any distinction between them is purely artificial insofar as the fluid is concerned. This is so because during cooling down periods in transients, the hex can behaves just like a heat source, due to its stored energy.

Nontheless, we shall treat the heat transfer correlations for the two solid structures separately mainly due to their geometrical representation in our applications.

3.3.2.1 Fuel or Heater Rods

The objective is to obtain a consistent set of correlations, covering adequately all the heat transfer regimes expected to occur. The heat transfer regime selection logic is presented in Fig. 3.5.

The correlation adopted for single-phase liquid convection is due to Schad [12]. This correlation, based on an exhaustive compilation of available experimental data on paralled liquid-metal flow through triangular-arrayed rod bundles, is given below:

$$\begin{aligned} Nu &= Nu_o \, (Pe/150)^{0.3} \qquad Pe > 150 \\ Nu &= Nu_o \qquad\qquad\qquad\quad Pe \leq 150 \end{aligned} \tag{3.26}$$

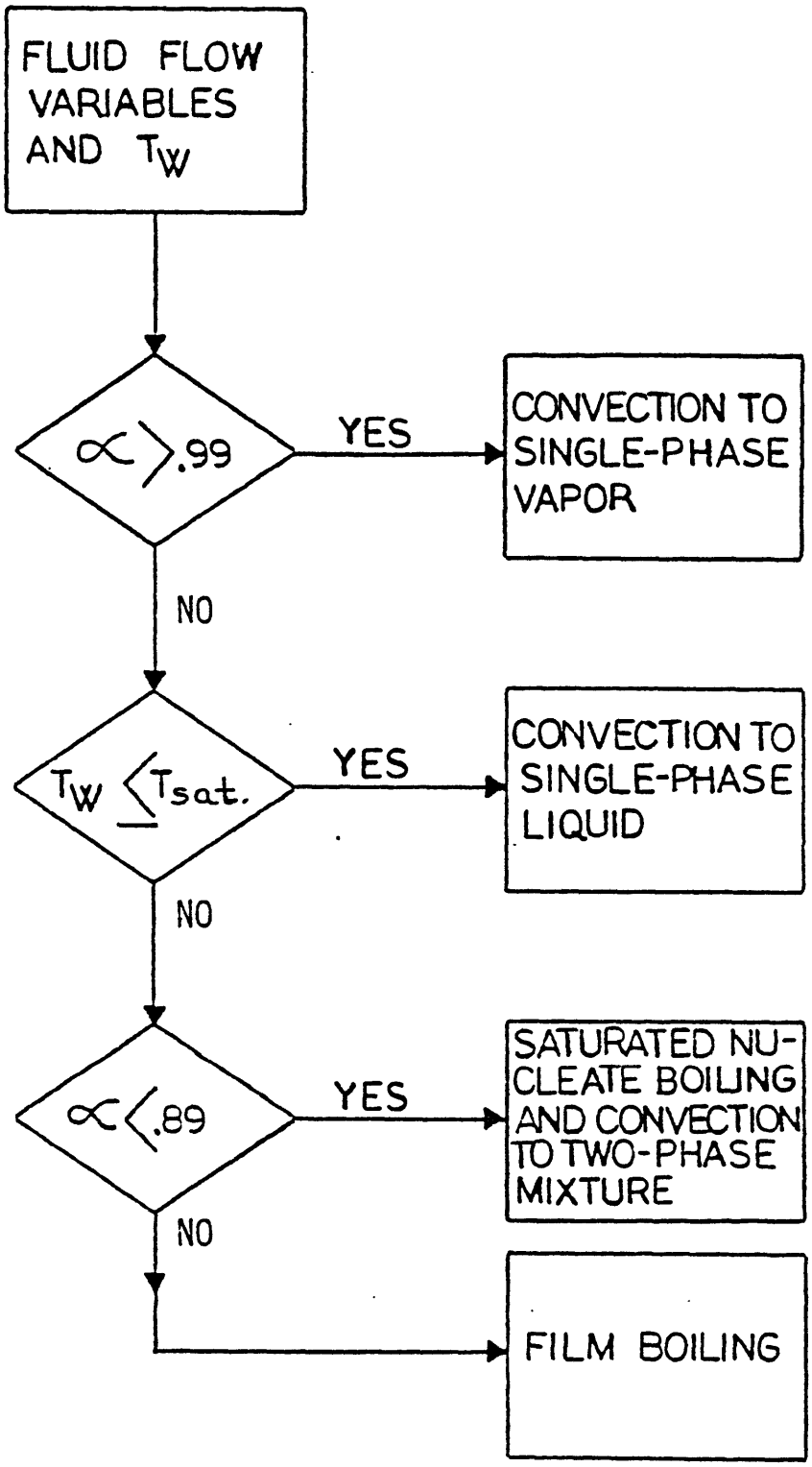

Figure 3.5 Heat Transfer Regime Selection Logic

where:

$$Nu_o = 4.5\ [-16.15 + 24.96\ (P/D) - 8.55\ (P/D)^2]$$

Experimental evidence indicates that in the lower Peclet number range, even under supposedly well-controlled test conditions, the presence of gas plus a less-than-perfect wetting can occur, thereby causing a relatively low heat transfer coefficient.

The choice for single-phase vapor convection is the well-known Dittus-Boelter's correlation:

$$Nu = 0.023\ Re^{0.8}\ Pr^{0.4} \qquad (3.27)$$

No "off-the-shelf" heat transfer correlation for convective two-phase flow in LMFBR rod bundles is currently available. Therefore, an existing correlation had to be modified to adapt it to our applications. Chen's correlation ([3], [13]) was selected as a starting point. This widely used correlation covers both the saturated nucleate boiling regime and the two-phase forced convection regime. The correlation postulates the existence of two separate heat transfer mechanisms. One such mechanism is associated with the overall flow and represents the convective component, h_c, of the total heat transfer coefficient, h_{TP}. The other mode of heat transfer is associated with the phenomenon of bubble growth in the liquid film in contact with the wall. This latter mechanism, admittedly of lesser importance for sodium, given its

high conduction and hence small temperature gradient in the film, is referred to as the nucleate boiling component, h_{NB}. Thus, the total heat transfer coefficient for two-phase flow boiling with no liquid deficiency is given by

$$h_{TP} = h_c + h_{NB} \tag{3.28}$$

As suggested by Manahan ([14]), the convective component, h_c, could be represented by the Schad's correlation, in which the Peclet number for two-phase (Pe_{TP}) is calculated as

$$Pe_{TP} = Re_{TP}\ Pr_{\ell} \tag{3.29}$$

where the two-phase Reynolds number (Re_{TP}) is obtained through the factor F defined as

$$F = (Re_{TP}/Re_{\ell})^{0.8}. \tag{3.30}$$

F has been determined experimentally as a function of the Martinelli's parameter, X_{tt}, a good approximation of which is given by ([3]):

$$X_{tt} \cong \left(\frac{1-x}{x}\right)^{0.9} \left(\frac{\rho_v}{\rho_{\ell}}\right)^{0.5} \left(\frac{\mu_{\ell}}{\mu_v}\right)^{0.1} \tag{3.31}$$

The liquid Reynolds number (Re_ℓ) has already been defined in Eq. (3.19).

For the nucleate boiling component, h_{NB}, the Forster-Zuber's analysis ([15]) is assumed to remain valid, as suggested by Chen ([16)], based on some evidence presented in [17]. The heat transfer correlation for this component is:

$$h_{NB} = 0.00122 \left[\frac{k_\ell^{0.79} C_{p\ell}^{0.45} \rho_\ell^{0.49}}{\sigma^{0.5} \mu_\ell^{0.29} h_{fg}^{0.24} \rho_\ell^{0.24}}\right] \Delta T_{sat}^{0.24} \Delta P_{sat}^{0.75} S \tag{3.32}$$

where ΔT_{sat} = wall superheat,

ΔP_{sat} = pressure difference corresponding to ΔT_{sat},

S = nucleate boiling suppression factor

$= (\Delta T_{sat,e}/\Delta T_{sat})^{0.99}$,

$\Delta T_{sat,e}$ = effective wall superheat.

Chen ([13]) correlated S against Re_{TP}, the latter being defined via F in Eq. (3.30). Butterworth (as reported in [18]) developed the following fits for F and S:

$$F = \begin{cases} 1.0, & X_{tt}^{-1} \leq 0.10 \\ 2.35\ (X_{tt}^{-1} + 0.213)^{0.736}, & X_{tt}^{-1} > 0.10 \end{cases} \tag{3.33}$$

$$S = \begin{cases} [1.0 + 0.12\ (Re'_{TP})^{1.14}]^{-1}, & Re'_{TP} < 32.5 \\ [1.0 + 0.42(Re'_{TP})^{0.78}]^{-1}, & 32.5 \leq Re'_{TP} \leq 70.0 \\ 0.1, & Re'_{TP} \geq 70.0 \end{cases} \quad (3.34)$$

where $Re'_{TP} = Re_{TP} \cdot (10^{-4})$

At high void fractions, vapor starts to blanket the surface, with the ensuing decrease in heat transfer. Currently, we treat this regime by interpolating between the two-phase forced convection and the single-phase vapor convection as follows:

$$h_{film} = \psi^2 h_{TP,c} + (1-\psi^2) h_{vapor} \quad (3.35)$$

where $\psi = 10(0.99 - \alpha)$

This pseudo film boiling regime is assumed to prevail in the range $0.89 < \alpha < 0.99$. We note that this particular treatment is advantageous also from a numerical point of view, providing a smooth transition. The square of the interpolating factor ψ is used to provide a faster de-

crease in the heat transfer coefficient.

3.3.2.2 Hex Can

It is important to provide a capability of representing the hexagonal can surrounding the fuel assembly because:

i) in some experiments, the heat losses to the surroundings are significant and must be accounted for if a correct energy balance is to be achieved, and

ii) during transients, this additional structure plays the role of a heat source or sink, affecting the fluid heat up and cool down behavior.

We chose a simplified yet entirely adequate model, adopted with only minor modifications from Wilson's work ([5]).

Most current applications deal with single-assembly simulations, for which no significant azimuthal variation in the surrounding temperature is expected. Therefore, azimuthal symmetry is assumed and the hex can is treated as an equivalent cylindrical shell, of equal circumferential perimeter and thickness. When using a grid layout for the numerical solution, there are a number of peripheral cells in direct contact with the

can. The sodium in these cells is combined and formed into an imaginary annulus adjacent to the can. Physical properties are volume-averaged. The actual and the equivalent geometrical representations just described are depicted in Fig. 3.6. Dwyer ([19]) developed a Nusselt number correlation for liquid sodium flowing in an annulus, transferring heat only through its outer boundary:

$$Nu = A + CPe^{\beta} \tag{3.36}$$

where:

$$A = 5.54 + 0.023\ (r_2/r_1)$$

$$C = 0.0189 + 0.316x10^{-2}(r_2/r_1) + 0.867 \times 10^{-4}(r_2/r_1)^2$$

$$\beta = 0.758\ (r_2/r_1)^{-0.0204}$$

r_2, r_1 = outer and inner radia.

For simplicity, the heat transfer to and from any fluid cell in which boiling has occurred is neglected. Such cells are not counted in the averaging process, as well as in the apportioning of the heat flux to the can to each adjacent cell. This apportioning is made based on the perimeter of contact of each of these cells.

If warranted, the hex can representation can be refined, treating each cell individually and also provid-

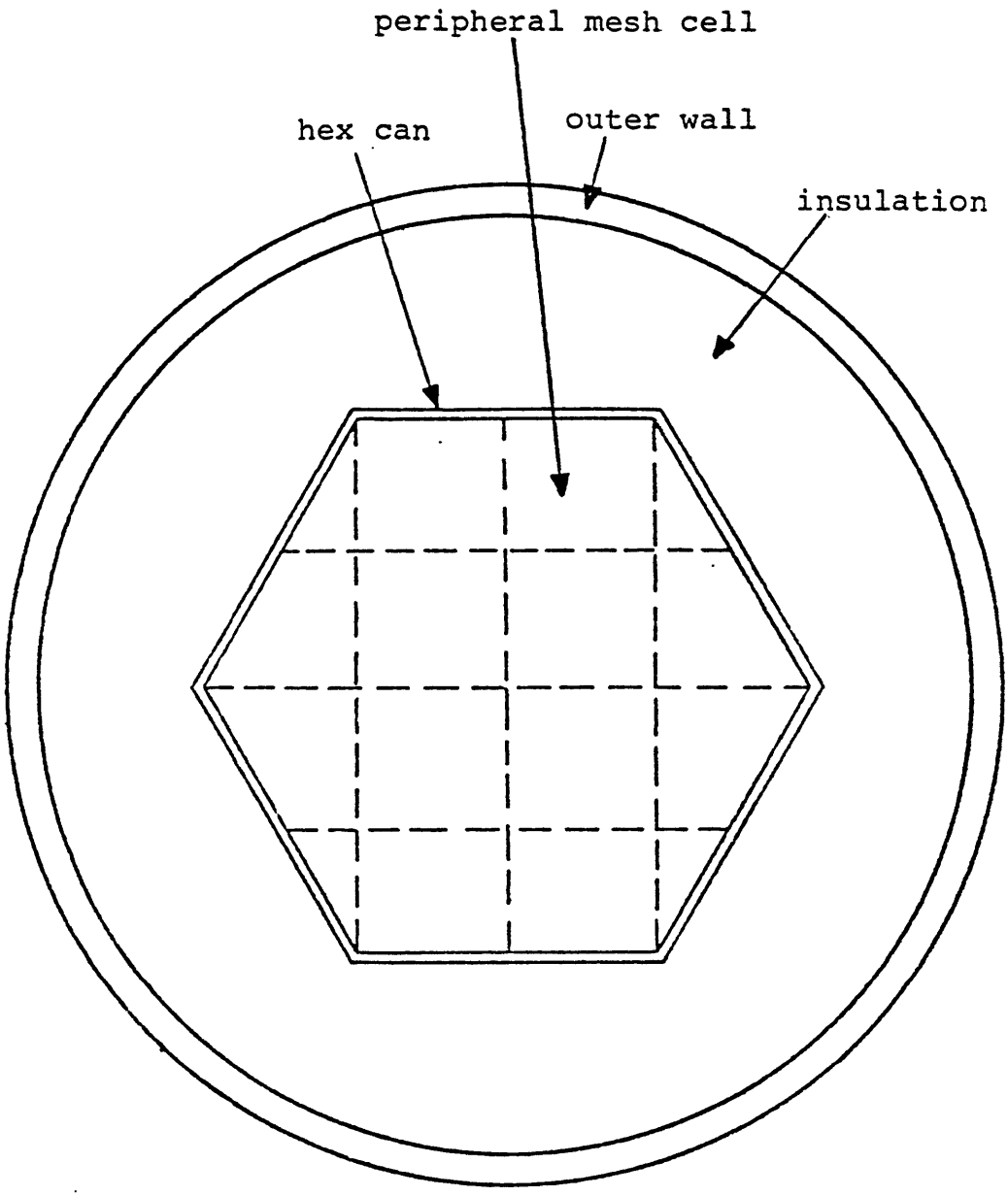

Figure 3.6 Hex Can with Associated Structure.
(a) Actual Representation.

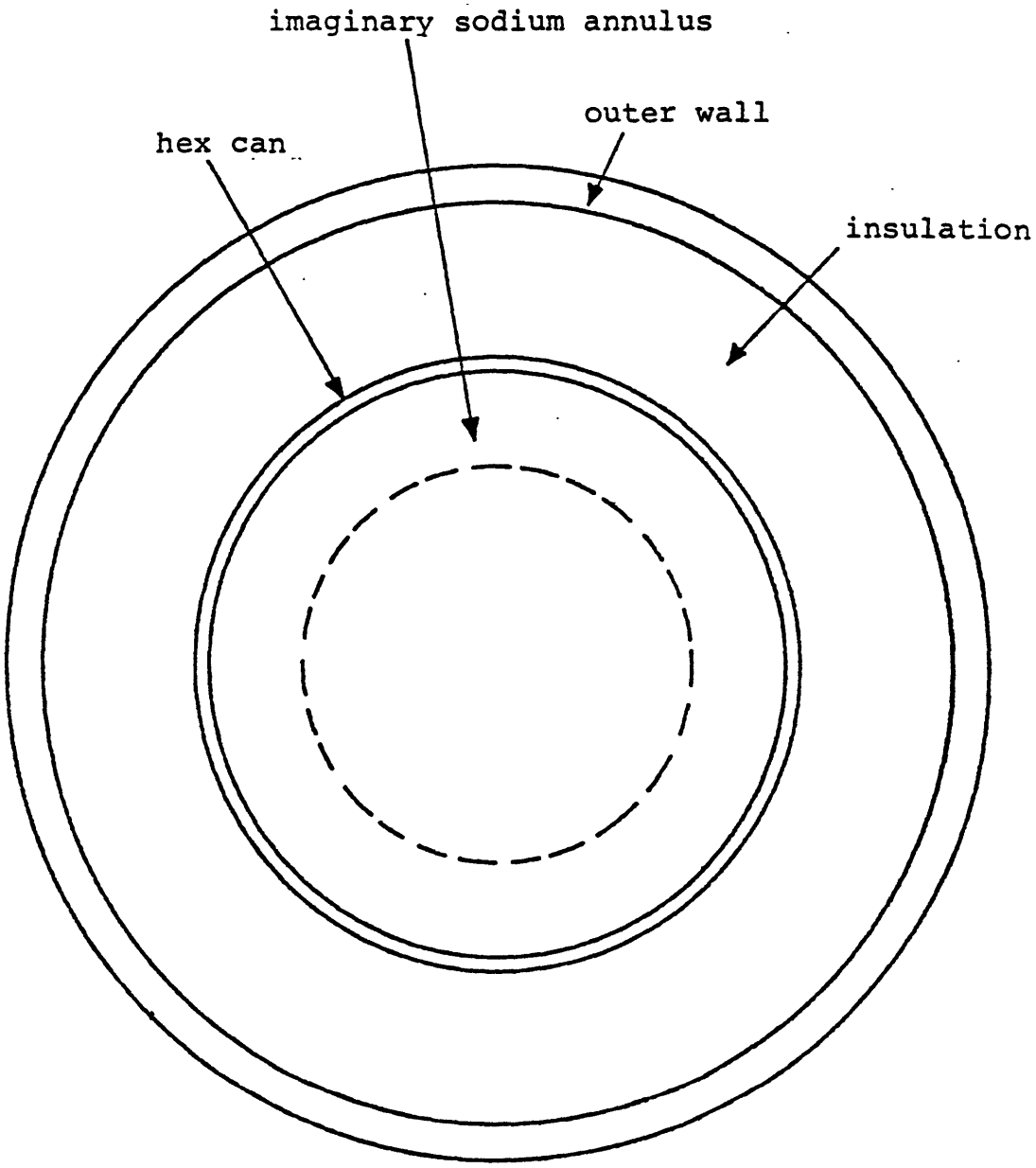

Figure 3.6 Hex Can with Associated Structure.
(b) Equivalent Representation.

ing for other heat transfer regimes, as it is done for the fuel/heater rod.

3.3.3 Interfacial Momentum Exchange

The use of two momentum equations, one for each phase, require an interphase constitutive relation, namely the interphase momentum exchange.

The terms we are about to discuss are $\vec{F}_{iv}$ and $\vec{F}_{i\ell}$, introduced in the previous chapter, and repeated here for convenience:

$$\vec{F}_{iv} = \vec{F}_i + \Gamma\vec{U}_v \tag{2.8a}$$

$$\vec{F}_{i\ell} = -\vec{F}_i - \Gamma\vec{U}_\ell \tag{2.8b}$$

The reader should recall that the second term in the right-hand-side of these equations appears because of the non-conservative form used for the momentum equations.

The interfacial momentum exchange, $\vec{F}_i$, was shown in Appendix A to be made up of two components, one due to interfacial mass exchange, the other due to form and shear drag at the interface. Considering the interfacially averaged phase velocities, $\vec{U}_v|_i$ and $\vec{U}_\ell|_i$, we have:

$$\begin{aligned} \vec{F}_i &= -\Gamma\vec{U}_v|_i + \vec{F}^d_{iv} \\ &= -(\Gamma\vec{U}_\ell|_i + \vec{F}^d_{i\ell}) \end{aligned} \tag{3.37}$$

The complexity of the flow near the interface leads to a great deal of simplification in the treatment of $\vec{F}_i$. First a relatively plausible assumption: the tangential components of the phase velocities at the interface are equal, i.e.,

$$\vec{U}_v^t\Big|_i = \vec{U}_\ell^t\Big|_i = \vec{U}_i \tag{3.38}$$

Clearly, unless the interface is parallel to the flow direction (a highly idealized situation), the normal components will contribute to the momentum exchange.

As it is customarily done, we shall neglect this effect, which is equivalent to assuming the equality of the normal components as well.

Therefore, we have:

$$\vec{U}_v\big|_i = \vec{U}_\ell\big|_i = \vec{U}_i \tag{3.39}$$

This interfacial velocity must be related to the bulk phase velocities. A "reasonable" expression is

$$\vec{U}_i = \eta\vec{U}_\ell + (1 - \eta)\,\vec{U}_v\,, \quad 0\leq\eta\leq 1 \tag{3.40}$$

where η is a weighting factor, discussed below.

There is no unique way, at present, to specify η. Wallis [20] recommends $\eta = 1/2$ based on entropy production considerations. A different approach, argued for by many investigators and chosen for this work, employes a donor-like formulation:

$$\eta = 1, \text{ if } \Gamma > 0 \text{ (evaporation)}$$
$$\eta = 0, \text{ if } \Gamma < 0 \text{ (condensation)} \tag{3.41}$$

that is, $\vec{U}_i = \vec{U}_\ell$ during evaporation, whereas $\vec{U}_i = \vec{U}_v$ when condensation occurs. This formulation has an additional advantage (a further argument for its selection) in that it always renders the momentum exchange equivalent to a retarding (damping) force, a fact of crucial importance for the stability of the numerical scheme.

Regarding the drag component, we shall assume that the total interfacial drag onto one phase applies with equal magnitude but in opposite direction to the other component. We note that this is purely a simplify-

ing assumption (widely used in this field) and not at all a reflection of any physical law. This assumption becomes equivalent to the momentum jump condition (i.e., conservation of momentum at the interface) only in the absence of mass exchange.

With these considerations, the interfacial momentum exchange can be written as

$$\vec{F}_i = - \Gamma \vec{U}_i + \vec{F}_i^d \tag{3.42}$$

Therefore, Eq. (2.8) can be re-written as:

$$\vec{F}_{iv} = \Gamma (\vec{U}_v - \vec{U}_i) + \vec{F}_i^d$$

$$\vec{F}_{i\ell} = \Gamma (\vec{U}_i - \vec{U}_\ell) - \vec{F}_i^d \tag{3.43}$$

or, after substituting Eq. (3.40)

$$\vec{F}_{iv} = \eta \Gamma (\vec{U}_v - \vec{U}_\ell) + \vec{F}_i^d$$

$$\vec{F}_{i\ell} = (1 - \eta)\, \Gamma (\vec{U}_v - \vec{U}_\ell) - \vec{F}_i^d \tag{3.44}$$

We now postulate the following expression for the drag term, F_i^d:

$$\vec{F}_i^d = K_i \ (\vec{U}_v - \vec{U}_\ell) \tag{3.45}$$

The origin of this expression will become clear later in this subsection. For now we shall consider K_i non-negative. Substituting Eq. (3.45) into (3.44) yields:

$$\begin{aligned} \vec{F}_{iv} &= K_{iv} \ (\vec{U}_v - \vec{U}_\ell) \\ \vec{F}_{i\ell} &= K_{i\ell} \ (\vec{U}_v - \vec{U}_\ell) \end{aligned} \tag{3.46}$$

where:

$$\begin{aligned} K_{iv} &= \eta\Gamma + K_i \\ K_{i\ell} &= (1 - \eta) \ \Gamma - K_i \end{aligned} \tag{3.47}$$

We now need two pieces of information, Γ and K_i, to define the momentum exchange coefficients, K_{iv} and $K_{i\ell}$. As already mentioned in the previous chapter, defining the mass exchange for a thermal equilibrium two-phase flow model does not present any difficulty. It is determined from the mass conservation equation for one of the phases, say vapor:

$$\Gamma = \frac{\partial}{\partial t} \ (\alpha\rho_v) + \nabla\cdot(\alpha\rho_v\vec{U}_v) \tag{3.48}$$

Indeed, in the code we use a finite difference counterpart of this equation.

It remains to define the coefficient K_i. Once again we make a major simplification with regard to the flow regime, assuming again that an annular flow regime prevails, with vapor the continuous phase. Let us consider a tube geometry, with the understanding that it is only for obtaining essentially correct (but of qualitative value) functional relationships. The force exerted on the vapor by the interfacial drag per unit volume is:

$$F_i^d = \tau_i \ (A_i/V) \tag{3.49}$$

where τ_i = interfacial shear stress,

(A_i/V) = interfacial area per unit volume.

It can be easily shown that

$$(A_i/V) = (P_i/A) = 4(P_i/P)/D_e = 4\sqrt{\alpha}/D_e \tag{3.50}$$

where D_e is the tube's diameter, or in general the equivalent diameter of the flow area under consideration.

For the shear stress we assume a Darcy-type form

$$\tau_i = \frac{1}{8} f_i \rho_v |U_r| U_r \tag{3.51}$$

where

f_i = friction coefficient,

U_r = relative velocity = $U_v - U_\ell$

For annular flow, Wallis' correlation ([20] or [21]), has been and still is widely used

$$f_i = 0.02 \ (1 + 300 \frac{\delta}{D_e}) \tag{3.52}$$

where δ = liquid film thickness

Noting that $\delta/D_e = (1 - \sqrt{\alpha})/2$, Eq. (3.52) can be written as

$$f_i = 0.02 \ [1 + 150(1 - \sqrt{\alpha})] \tag{3.53}$$

In [21], Wallis showed that this equation for vapor flowing over a wavy annular liquid film is equivalent to the equation used for turbulent flow in rough pipes.

Using Eqs. (3.50), (3.51) and (3.53) into (3.49) gives the following expression for the interfacial drag:

$$(F_i^d)_{\text{Turbulent}} = \frac{0.01}{D_e} \sqrt{\alpha} \ [1 + 150 \ (1-\sqrt{\alpha})] \cdot \rho_v |U_r| U_r \tag{3.54}$$

Thus, in turbulent flow, the interfacial drag coefficient, K_i is given by:

$$(K_i)_{\text{Turbulent}} = \frac{0.01}{D_e} \sqrt{\alpha} \ [1 + 150 \ (1 - \sqrt{\alpha})] \rho_v |U_r| \tag{3.55}$$

This expression would clearly yield too low values when $|U_r|$ is small. For such situations, we provide a "pseudo-laminar" formulation:

$$f_i = 64/Re_{v,i} \tag{3.56}$$

where:

$$Re_{v,i} = \frac{\rho_v |U_r| D_i}{\mu_v}$$

Noting that $D_i = D_e - 2\delta = D_e\sqrt{\alpha}$, Eq. (3.56) becomes:

$$f_i = \frac{64\mu_v}{\rho_v |U_r| D_e \sqrt{\alpha}} \tag{3.58}$$

Combing Eqs. (3.49), (3.50), (3.51) and (3.58) yields:

$$(F_i^d)_{Laminar} = \frac{32\mu_v}{D_e^2} U_r \tag{3.59}$$

and consequently

$$(K_i)_{Laminar} = \frac{32\mu_v}{D_e^2} \tag{3.60}$$

To insure continuity, the interfacial drag coefficient is taken as the greater of the values given by Eqs. (3.55) and (3.60).

A final remark, regarding the single-phase/two-phase transitions, should be made. It is reasonable to assume that the just appearing or disappearing phase will move at essentially the same velocity as the other phase. To obtain this behavior, the following formulation is used:

$$K_i^{actual} = \psi^3 K_i^{\infty} + (1-\psi^3) K_i \tag{3.61}$$

where:

$$K_i^{\infty} = 10^{10} \quad \text{(note that a very large interfacial drag coefficient will render the phase velocities virtually equal)}$$

$$\begin{aligned} \psi &= 100\,(0.01 - \alpha) && \alpha < 0.01 \\ \psi &= 0.0 && 0.01 \leq \alpha \leq 0.99 \\ \psi &= 100\,(\alpha - 0.99), && \alpha > 0.99 \end{aligned} \tag{3.62}$$

The cube of the interpolating parameter ψ is used to accentuate the rapid increase (or decrease) of the interfacial drag coefficient.

3.3.4 Fluid Conduction

The previous constitutive equations dealt with interfacial exchages between each phase and the wall as well as between the phases. As shown in Appendix A these constitutive equations are a direct consequence of the averaging process. Unlike them, the intraphase heat transfer requires a constitutive relation even for the local instantaneous energy conservation equation. The high conductivity of liquid sodium makes this phenomenon a significant mode of energy transport. In addition, the specific configuration of LMFBR fuel assemblies using wire-wrapped rods plays an important role in this context. The wires wrapped around the rods, all "in phase", serve both as rod spacers and as promoters for coolant mixing. This mixing greatly enhances the energy diffusion.

Consider two adjacent mesh cells, "i" and "j", and let A_{ij} be the intercell area. The heat transfer rate between these cells can be written:

$$Q_{ij} = A_{ij} h_{ij} (T_i - T_j) \tag{3.63}$$

where h_{ij} is an effective heat transfer coefficient, to be defined. Conservation of energy requires the heat flux to the interface between cells be equal to that from the

interface. In other words, denoting the interface temperature T_{int}:

$$h_i (T_i - T_{int}) = h_{i+1} (T_{int} - T_j) \tag{3.64}$$

Clearly, the heat flux between cells must also equal the heat fluxes above. Thus, we may write

$$h_{ij} (T_i - T_j) = h_i (T_i - T_{int}) \tag{3.65}$$

Eliminating T_{int}, the following expression for h_{ij} is obtained:

$$h_{ij} = \frac{h_i h_j}{h_i + h_j} \tag{3.66}$$

We must now define the intracell heat transfer coefficients, h_i and h_j. With d_i being the distance between the cell center and its edge, h_i is simply given by

$$h_i = k_i^{eff}/d_i \tag{3.67}$$

where k_i^{eff} is the effective conduction of cell i. A somewhat better representation for d_i in the porous body approach is through an equivalent conduction radius defined as

$$d_i = R^c_{e,i} = D^c_{e,i}/2 = 2V_i/\Sigma_j A_{ij} \qquad (3.68)$$

where V_i is the net cell fluid volume and A_{ij} (already introduced) is the net intercell fluid flow area. One should note that Eq. (3.68) is obtained based on a reasoning analogous to that used in Eq. (3.15). h_j is defined in a similar manner.

In our applications, it can be safely assumed that the axial conduction is negligible. It is easy to show that

$$\frac{\text{convection heat transfer}}{\text{conduction heat transfer}} = \frac{A\rho U_A c_p \Delta T}{A(k/\Delta z)\Delta T}$$

$$= Pe_D \frac{\Delta Z}{D_e} \qquad (3.69)$$

where

Pe_D = Peclet number based on the equivalent diameter D_e.

ΔZ = typical axial mesh length.

As the wire wraps promote mixing in the radial direction but not in the axial one, even at relatively low flows the Peclet number will be considerably greater than one. In addition, in most practical cases ΔZ is substantially larger than D_e, thus further reducing the relative importance of

the axial diffusion as a heat transport mechanism.

In two-phase flows, the existence of various flow regimes leads to a bewildering number of possibilities for vapor-liquid configurations, especially so in the complex geometry under consideration. For this work, we adopted a simplified approach. Given the fact that the vapor conductivity is much smaller than that of the liquid and that in an annular flow pattern the vapor becomes the continuous phase, it appears reasonable to neglect the conduction to and from voided cells.

It remains to define the effective conduction for single-phase liquid cells. This effective conduction must include the molecular conduction plus the enhanced eddy diffusivity, the latter mostly due to the flow sweeping induced by wire spacers. Let us define a Nusselt number relating the effective conduction to the molecular conduction:

$$Nu = \frac{k^{eff}}{k} \tag{3.70}$$

or, using the thermal diffusivity, $\alpha = k/\rho c_p$, and the (enhanced) eddy diffusivity, ε_H:

$$Nu = \frac{\alpha^{eff}}{\alpha} = \frac{\alpha+\varepsilon_H}{\alpha} = 1 + \frac{\varepsilon_H}{\alpha} \tag{3.71}$$

Given the extremely complicated flow pattern, ε_H must be

determined experimentally. (We note that the major contributor to the enhanced diffusion, i.e., ε_H, is not the turbulence-induced exchange but the wire spacer-induced flow sweep; in a sense, therefore, the mechanism of this enhancement is deterministic).

Once again, there is a substantial body of knowledge in this area (see [8], [9], [10] for work performed at MIT in recent years). The stumbling block in tapping and applying these (and other) sources of information is the geometrical representation. To our knowledge, all the work in this area deals with subchannel (or subchannel-like) configuration. It is by no means trivial to convert or extend this work to an arbitrary porous body treatment.

Nonetheless, we shall use some of the existing formulations in a mostly qualitative fashion. Following [10], let us use dimensionless diffusivities. Eq. (3.71) becomes

$$Nu = 1 + \varepsilon^*/\alpha^* \tag{3.71'}$$

where:

$$\varepsilon^* = \varepsilon_H/U_A D_e \tag{3.72a}$$

$$\alpha^* = \alpha/U_A D_e \tag{3.72b}$$

U_A = bundle average axial velocity

D_e = bundle equivalent diameter (Eq. 3.23)

(Note that in [10] the inner region's equivalent diameter, $D_{e,1}$, is used; for our purposes we will assume $D_{e,1}/D_e \cong 1$.)

In most applications, the flow split parameter (i.e., ratio of the axial velocity in a subchannel of a given type to the bundle average axial velocity) is not too far from unity; for simplicity we shall assume the flow split parameter approximately equal to unity.

With these simplifying assumptions, it can be shown ([10]) that the dimensionless subchannel eddy diffusivity, ε_1^*, is related to the "continuum" parameter ε^* through a strictly geometrical parameter:

$$\varepsilon_1^* \approx (\lambda_A/\lambda_L)\varepsilon^* \tag{3.73}$$

where:

(λ_A/λ_L) = ratio of axial to lateral porosities

It turns out that for wide range of Reynolds numbers, ε_1^* is independent of Re, being only a function of bundle geometry, i.e., pitch-to-diameter and wire wrap lead-to-diameter ratios.

Let us return to Eq. (3.71'). The dimensionless molecular diffusivity α^* can be expressed as

$$\alpha^* = \frac{\alpha}{U_A D_e} = \frac{k}{\rho c_p U_A D_e} = \frac{kP_w}{4Wc_p} \tag{3.74}$$

where

$$W = \text{mass flow rate} = \rho U_A A$$

(Note that the equivalent diameter's definition, $D_e = 4A/P_w$, was used above.)

Finally, the Nusselt number can be expressed as follows:

$$Nu = 1 + \frac{4\varepsilon^* c_p}{kP_w} W \tag{3.75}$$

Thus, the enhancement of diffusion due to mixing follows a linear variation with the flow rate. In Chapter 7, we will present some results in support of this hypothesis.

We make a final remark with regard to the flow pattern induced in wire wrapped rod bundle. In the interior region of the assembly, the wire-induced sweeping flows are periodically directed in opposing directions, thus justifying its modeling by an enhanced eddy diffusivity. In the region adjacent to the hexagonal can wall, however, a totally different flow pattern is observed. The diversion cross-flow induced by wires is always in the direction of the wire-wrap, thus generating a swirl flow. This is clearly an azimuthal convection-like mechanism, unlike the diffusion

process previously postulated for the interior region.

The work previously mentioned in connection with the flow mixing has generated a number of correlations enabling the determination and utilization of a "swirl" parameter in the context of the subchannel approach. Again, we face the difficulty of translating this work into a form applicable to a general porous body representation. At this point no clear answer can be provided. Some of our calculations were set up in a two-dimensional (r-z) geometry which implicitly assumes azimuthal symmetry, in which case the swirl flow does not have any effect. In three-dimensional (x-y-z) representations, the mesh cells adjacent to the wall actually straddle both the interior and the outer (wall) region. In our simulations to date, the configurations analyzed did not evince any azimuthal asymmetry, such as power skew or flow blockages. In light of these considerations, we decided not to account for this swirl flow. However, we emphasize the need for further investigation for applications in which the above assumptions may not be valid.

3.4 REFERENCES

1. T.J. Chung, "Finite Analysis in Fluid Dynamics," McGraw-Hill (1978).

2. E.D. Hughes, R.W. Lyczkowski, T.H. McFadden and G.F. Niederauer, "An Evaluation of State-of-the Art Two-Velocity Two-Phase Flow Models and Their Applicability to Nuclear Reactor Transient Analysis," EPRI Report No. NP-143 (1976).

3. J.G. Collier, "Convective Boiling and Condensation," McGraw-Hill (1972).

4. Y. Coëffé and N.E. Todreas, "Formulation of the Fluid-Solid Interaction Force for Multi-Dimensional, Two-Phase Flow within Tube Arrays, "Nuclear Engineering and Design, 58, (1980).

5. G.J. Wilson, "Development of Models for the Sodium Version of the Two-phase Three Dimensional Thermal Hydraulic Code-THERMIT," M.S. Thesis, Nuclear Engineering Department, MIT, May 1980 (Also issued as Energy Laboratory Report No. MIT-EL-80-010).

6. F.C. Engel, R.A. Markley and A.A. Bishop, "Laminar, Transition, and Turbulent Parallel Flow Pressure Drop Across Wire-Wrap-Spaced Rod Bundles," Nuclear Science and Engineerng, 69,(1979).

7. E.H. Novendstern, "Turbulent Flow Pressure Drop Model for Fuel Rod Assemblies Utilizing a Helical Wire-Wrap Spacer System", Nuclear Engineering and Design, 22, (1972).

8. C. Chiu, J.T. Hawley, W.M. Rohsenow, and N.E. Todreas, "Parameters for Laminar, Transition and Turbulent Longitudinal Flows in Wire Wrap Spaced Hexagonal Arrays," Topical Meeting on Nuclear Reactor Thermal Hydraulics, Saratoga, NY, October 1980.

9. S.F. Wang and N.E. Todreas, "Computer Model for MIT Correlations for Friction Factors, Flow Splits and Mixing Parameters in LMFBR Wire-Wrapped Rod Assemblies," DOE/ET/37240-87TR (1981).

10. J.T. Hawley, Y.N. Chan and N.E. Todreas, "Input Parameters to Codes which Analyze LMFBR Wire Wrapped Bundles," COO-2245-17TR, (Revision II),(1980).

11. A.Y. Gunter and W.A. Shaw, "A General Correlation of Friction Factors for Various Types of Surfaces in Crossflow," ASME Transactions, 67,(1945).

12. Y.S. Tang, R.D. Coffield and R.A. Markley, "Thermal Analysis of Liquid Metal Fast Breeder Reactors," American Nuclear Society (1978).

13. J.C. Chen, "A Correlation for Boiling Heat Transfer to Saturated Fluids in Convective Flow," ASME Paper 63-HT-34,(1963).

14. W. Hinkle, ed., "Development of Computer Code Models for Analysis of Subassembly Voiding in the LMFBR," MIT Energy Laboratory Report No. MIT-EL-80-005, (1980).

15. H.K. Forster and N. Zuber, "Dynamics of Vapor Bubbles and Boiling Heat Transfer," AIChE Journal 1 (4), (1955).

16. J.C. Chen, "A Proposed Mechanism and Method of Correlation for Convective Boiling Heat Transfer with Liquid Metals," Brookhaven National Laboratory Report BNL-7319 (1963).

17. W.G. Camack and H.K. Forster, "Test of a Heat Transfer Correlation for Boiling Liquid Metals," Jet Propulsion, 27,(1957).

18. T.A. Bjonard and P. Griffith, "PWR Blowdown Heat Transfer," in "Thermal and Hydraulic Aspects of Nuclear Reactor Safety-Vol. 1," O.C. Jones and S.G. Bankoff, Eds., ASME,(1977).

19. O.E. Dwyer, "On the Transfer of Heat to Fluids Flowing Through Pipes, Annuli and Parallel Plates," Nuclear Science and Engineering, 17,(1963).

20. G.B. Wallis, "One-Dimensional Two-Phase Flow", McGraw-Hill,(1969).

21. G.B. Wallis, "Annular Two-Phase Flow-Part 1: A Simple Theory," ASME Paper 69-FE-45 (1969).

CHAPTER 4. THE NUMERICAL METHODS

4.1 Introduction

The conservation equations for mass, energy and momentum, combined with the appropriate state equations and the constitutive relations required for closure, constitute a complete two-phase flow model. Needless to say, the complexity of the equations and relations involved rules out any attempt to an analytical solution.

The numerical modeling of two-phase flow has been the object of intense research over the last decade. To place our work in perspective it would be appropriate to present a review of some of the methods used in this area. We do not attempt to be exhaustive in this review, but our intention is rather to present the more representative methods that in some way can be considered milestones in this field, spawning new research or constituting the backbone of some of the major computer codes currently in use. Appendix C is devoted to this review.

In this chapter we will describe in detail the numerical schemes adopted for the treatment of the fluid dynamics equations and of the associated heat sources, i.e., the fuel or heater rods and the hex can. Starting with the introduction of the "base" scheme, we shall introduce thereafter a few variations to it, brought about by our investigations. It should be said that a good deal of hindsight has been used in presenting the material, as we

believe that a pure chronological account of our work might have been quite confusing.

4.2 The Numerical Method for Fluid Dynamics

In this major section, we shall provide a detailed discussion of the numerical treatment of the fluid dynamics equations chosen to describe our two-phase flow model.

4.2.1 Choice of Implicit and Explicit Treatments

When having to decide on a numerical representation of some differential equation(s), the first task confronting the numerical analyst is choosing from a spectrum of schemes, ranging from fully explicit to fully implicit ones. Whatever the choice, stability and consistency must be ascertained in order to guarantee convergence [1] for a properly posed initial boundary value problem (Lax Equivalence Theorem). While this theorem applies strictly to linear problems, it is reasonable to assume that the aforementioned conditions for convergence must be at least necessary in the case of non-linear problems.

A fully explicit scheme would be the cheapest per time step, however, its severe stability restriction would impose a very short time step which in most transients of interest would lead to an impractically large total computing effort. At the opposite end of the spectrum, one finds the fully implicit schemes, which

in principle offer unconditional stability, the only time step restriction being dictated by accuracy requirements. For our partial differential equations, a fully implicit method, especially in three-dimensions, would lead to a very large and complicated system of highly non-linear equations, whose solution might be very difficult and expensive. In this respect it is worth mentioning a somewhat subtler point related to the non-linear character of the equations. To start a non-linear iteration, a guess must be provided. In a time-dependent problem, a natural choice for such a guess for the new time solution is obviously the old time solution. Now for a non-linear iterative process, the better the initial guess, the faster the convergence to the solution will be. In fact, in some circumstances, convergence can be guaranteed only if the guess is "close enough" to the solution. Obviously, the shorter the time step, the closer the guess is to the solution (assuming a continuous dependence on time). Thus, a large time step can lead to very slow convergence, with the consequent increase in computational effort.

Clearly, an optimum scheme would allow acceptable time steps (on the scale of the transients under consideration) and would not lead to a prohibitively complex (possibly unreliable as a result) and expensive algorithm. Thus, it is important to realize that the phenomena

represented by our equations are associated with different time scales. We have:

i) local phenomena (couplings); here we should mention the interphase momentum exchange and the fluid-wall interaction. Generally the implied time constants could vary widely, from very short to moderate;

ii) sonic propagation; the very high sound speed in liquid makes the transient time for a pressure pulse quite small (10^{-6}-10^{-5} sec), for the grid size of interest in our applications;

iii) transport by convection; as long as the phase convective velocities are well below their sonic counterparts, the time constants involved will be considerably longer than above;

iv) transport by diffusion; in our applications, the time constant of this phenomenon is of the same order of magnitude as that associated with convection.

In light of the above, we seek a numerical method that treats the first two types of phenomena in a fully or highly implicit manner, while describing explicitly the two transport mechanisms (later, we shall bring up again the treatment of energy diffusion).

Before turning to our discretized equations, we feel it may be interesting to show how sonic propagation terms can be identified in a simpler situation, that of a one-dimensional flow of a compressible, inviscid, non-conducting fluid. As in [2], we shall consider that the fluid is originally at rest. A pressure perturbation then leads to a velocity perturbation about the reference. Considering now u=0, the terms containing the velocity in a multiplicative fashion will vanish, leaving however those involving the velocity derivatives. The governing conservation equations become:

$$\frac{\partial \rho}{\partial t} + \rho \frac{\partial u}{\partial x} = 0 \qquad (4.1.a)$$

$$\frac{\partial u}{\partial t} + \frac{1}{\rho} \frac{\partial p}{\partial x} = 0 \qquad (4.1.b)$$

$$\frac{\partial e}{\partial t} - \frac{p}{\rho^2} \frac{\partial \rho}{\partial t} = Q \qquad (4.1.c)$$

where the velocity divergence in the energy equation was eliminated through the use of the mass equation. The conclusion is that the spatial derivatives of velocity and pressure must be treated implicity.

4.2.2 Difference Equations

The discrete analogs of the partial differential equations describing our two phase model will now be

presented. The spatial discretization is based on the widely used staggered-mesh approach (see, for example, [3] or [4]). All unknowns, except the velocities, are associated with the mesh cell centers. The velocity components are associated with the mesh cell faces to which they are normal. A typical mesh cell indicating the placement of the unknowns is depicted in Figure 4.1. A superscript n or n+1 refers to the time level at which the dependent variables are evaluated. In the mass and energy equations, the areas A and the volumes V refer to net flow areas and net fluid volumes. Alternatively, one could have considered the full areas and volumes associated with the three-dimensional Cartesian grid and use the concept of porosity and permeability [5], to account for the presence of structure. The two approaches are absolutely equivalent insofar as the scalar conservation equations are concerned. Regarding the momentum equations, some additional considerations related to volume averaging in the context of a porous medium approach are addressed in Appendix D.

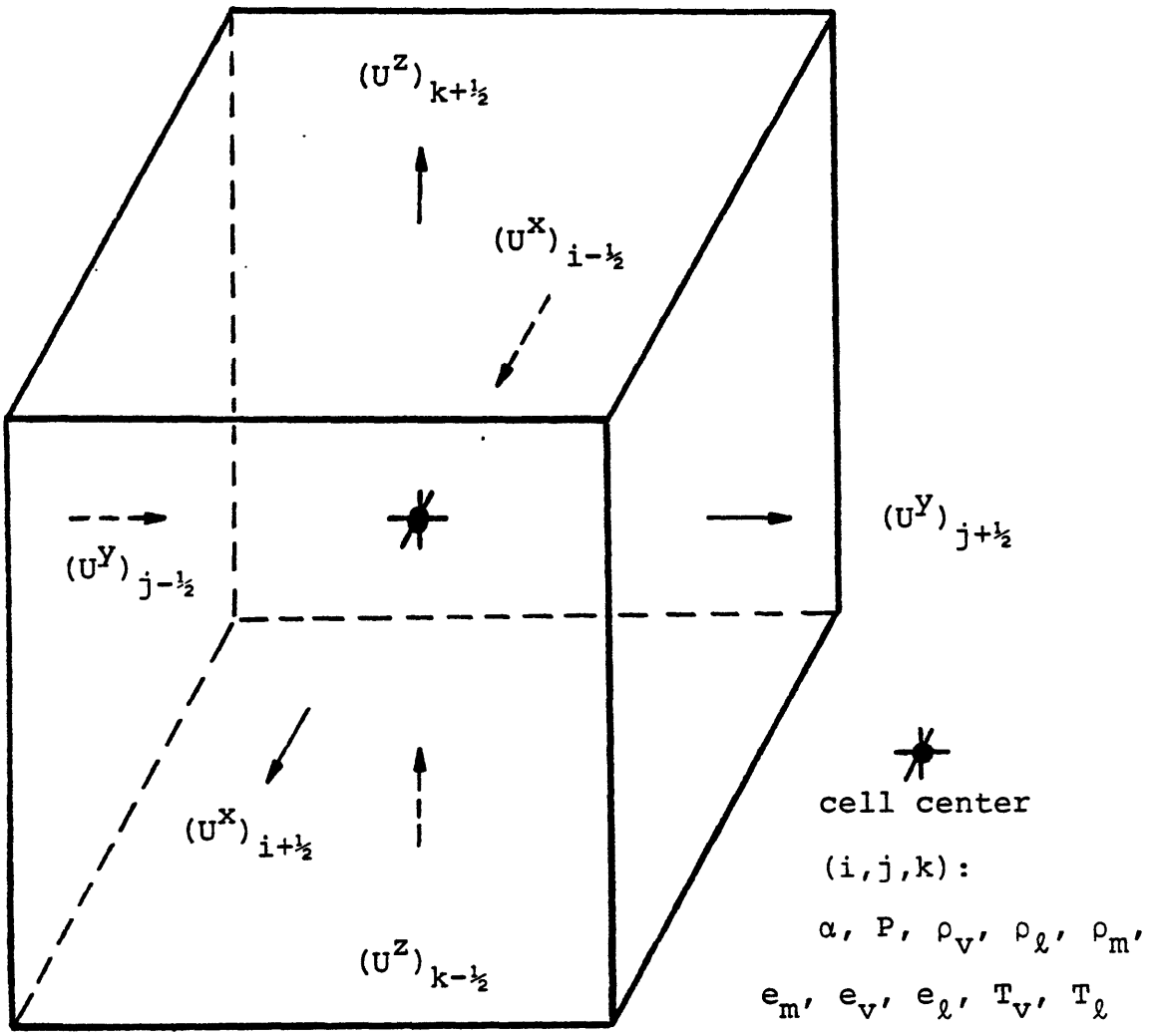

Figure 4.1 A Typical Fluid Mesh Cell Showing Location of Variables and Subscripting Conventions

4.2.2.1 The Mixture Mass Equation

$$
\begin{aligned}
& V(\rho_m^{n+1} - \rho_m^n)/\Delta t \\
& + \{A[(\alpha\rho_v)^n (U_v^x)^{n+1} + ((1-\alpha)\rho_\ell)^n (U_\ell^x)^{n+1}]\}_{i+1/2} \\
& - \{A[(\alpha\rho_v)^n (U_v^x)^{n+1} + ((1-\alpha)\rho_\ell)^n (U_\ell^x)^{n+1}]\}_{i-1/2} \\
& + \{A[(\alpha\rho_v)^n (U_v^y)^{n+1} + ((1-\alpha)\rho_\ell)^n (U_\ell^y)^{n+1}]\}_{j+1/2} \\
& - \{A[(\alpha\rho_v)^n (U_v^y)^{n+1} + ((1-\alpha)\rho_\ell)^n (U_\ell^y)^{n+1}]\}_{j-1/2} \\
& + \{A[(\alpha\rho_v)^n (U_v^z)^{n+1} + ((1-\alpha)\rho_\ell)^n (U_\ell^z)^{n+1}]\}_{k+1/2} \\
& - \{A[(\alpha\rho_v)^n (U_v^z)^{n+1} + ((1-\alpha)\rho_\ell)^n (U_\ell^z)^{n+1}]\}_{k-1/2} = 0
\end{aligned}
\tag{4.2}
$$

In the above equation, the convected quantities are needed at cell faces, where the fluxes are defined. A relationship defining the unknowns at locations other than their basic placement must be provided. There are various choices, but in light of its superior stability characteristics, a full donor-cell differencing has been selected. Let C stand for any cell-centered

quantity (see Fig.4.1) and consider the face $(i + 1/2)$, normal to the x-direction. The quantity $C_{i+1/2}$ is then determined as

$$C_{i+1/2} = \begin{cases} C_i, \text{ if } (U^x)_{i+1/2} \geq 0 \\ C_{i+1}, \text{ if } (U^x)_{i+1/2} < 0 \end{cases}$$

It is important to note that donor-cell decisions are made only with regard to quantities at time level n, using velocities at the same time level. As a result no difficulty arises even if a velocity sign change occurs during a time step. An important advantage with regard to the linearization process will later become apparent.

4.2.2.2 The Mixture Energy Equation

A number of variants for the finite difference energy equation have been examined. The reasons behind each variation of a basic scheme will be given in this subsection and later in this chapter. The remarks made in connection with the mass equation are also valid here.

4.2.2.2.1 Conservative/Semi-implicit Convection (CSIC)

$$V[(\rho_m e_m)^{n+1} - (\rho_m e_m)^n]/\Delta t$$

$$+[p^n+(\rho_v e_v)^n_{i+1/2}][A\alpha^n(U_v^x)^{n+1}]_{i+1/2}$$

$$+ [p^n+(\rho_\ell e_\ell)^n_{i+1/2}][A(1-\alpha)^n(U_\ell^x)^{n+1}]_{i+1/2}$$

$$-[p^n+(\rho_v e_v)^n_{i-1/2}][A\alpha^n(U_v^x)^{n+1}]_{i-1/2}$$

$$- [p^n+(\rho_\ell e_\ell)^n_{i-1/2}][A(1-\alpha)^n(U_\ell^x)^{n+1}]_{i-1/2}$$

$$+[p^n+(\rho_v e_v)^n_{j+1/2}][A\alpha^n(U_v^y)^{n+1}]_{j+1/2}$$

$$+ [p^n+(\rho_\ell e_\ell)^n_{j+1/2}][A(1-\alpha)^n(U_\ell^y)^{n+1}]_{j+1/2}$$

$$-[p^n+(\rho_v e_v)^n_{j-1/2}][A\alpha^n(U_v^y)^{n+1}]_{j-1/2}$$

$$- [p^n+(\rho_\ell e_\ell)^n_{j-1/2}][A(1-\alpha)^n(U_\ell^y)^{n+1}]_{j-1/2}$$

$$+[p^n+(\rho_v e_v)^n_{k+1/2}][A\alpha^n(U_v^z)^{n+1}]_{k+1/2}$$

$$+ [p^n+(\rho_\ell e_\ell)^n_{k+1/2}][A(1-\alpha)^n(U_\ell^z)^{n+1}]_{k+1/2}$$

$$-[p^n+(\rho_v e_v)^n_{k-1/2}][A\alpha^n(U_v^z)^{n+1}]_{k-1/2}$$

$$- [p^n+(\rho_\ell e_\ell)^n_{k-1/2}][A(1-\alpha)^n(U_\ell^z)^{n+1}]_{k-1/2}$$

$$= Q_w^{n+1/2} + Q_k^{n+1/2} \qquad (4.3)$$

Here the heat sources appear with superscript n+1/2, indicating a combination of implicit/explicit components, to be later discussed. We note that this difference form of the energy equation together with the discrete mass equation are a strict adaptation of the scheme used in [2] for a six-equation model to a four-equation "mixture" model. For single-phase, either liquid or vapor, the two schemes are equivalent. In two-phase flow, however, the four-equation rendition suffers of a subtle flaw, namely the lack of monotonicity of the mixture internal energy density ($\rho_m e_m$) with respect to e_m. This aspect, of great importance to the non-linear solution, will be addressed again later in this section.

4.2.2.2.2 Non-Conservative/Semi-Implicit Convection (NCSIC)

To avoid the problem raised by the product $\rho_m e_m$, we have decided to use a non-conservative form of the energy equation. To this end, the mass equation is multiplied by e_m and then subtracted from the conservative form of the energy equation. The resulting difference equation is

$$V(\rho_m)^n[(e_m)^{n+1}-(e_m)^n]/\Delta t + [conv_e - e_m\, conv_m]^{n+1/2} = (Q_w+Q_k)^{n+1/2} \qquad (4.4)$$

where $conv_m^{n+1/2}$ and $conv_e^{n+1/2}$ stand for the semi-implicit convective terms in the mass and energy equations, respectively. While a conservative form of the energy equation is generally desirable, it is not a major factor in deciding on a particular scheme. Certainly, in our case the overriding concern is the reliability of the non-linear solution. In fact a non-conservative energy equation has often been used ([6], [7], for example).

4.2.2.2.3 Non-Conservative/Explicit Convection (NCEC)

A further modification of the numerical scheme can be obtained by treating the convective terms in the energy equation fully explicitly. The equation will look just like Eq. (4.4), but with the superscript n used for the convective terms. The reason behind the use of the energy equation in this form will become apparent when the process through which the pressure problem is obtained will be discussed. The reader will see then that advantageous matrix properties can be obtained if this treatment of the energy equation is adopted.

4.2.2.2.4 Conservative, Fully Explicit (CFE)

Finally, one could treat the energy equation, in its conservative form, in a fully explicit manner, just as in [3] and in many related schemes. As the advance-

ment in time is performed explicitly, the problem related to ρe does not arise and at the same time the advantageous matrix properties alluded above can also be achieved. The equation can easily be obtained from Eq. (4.3), written with all the terms evaluated at time level n. (Obviously, the n+1st time level will appear only in the discretized temporal derivative).

4.2.2.3 The Phasic Momentum Equations

4.2.2.3.1 The Difference Scheme

The momentum equations are used in a non-conservative form, particularly convenient to our method. Unlike the mass and energy equations, each momentum equation is differenced about the face of a mesh cell, using the center of the face as reference point. In other words, the control volume for which the momentum equation is written is offset with respect to that used for the scalar quantities. To illustrate the concepts, consider the momentum equation for the vapor phase, in the x-direction, for the face with the center at (i+1/2,j,k):

$$(\alpha\rho_v)^n_{i+1/2} \frac{[(U^x_v)^{n+1} - (U^x_v)^n]_{i+1/2}}{\Delta t} + (\alpha\rho_v)^n_{i+1/2} [(U^x_v)_{i+1/2} (\frac{\Delta_x U^x_v}{\Delta x})_{i+1/2}$$

$$+ (U_v^y)_{i+1/2} \left(\frac{\Delta_y U_v^x}{\Delta y}\right)_{i+1/2} + (U_v^z)_{i+1/2} \left(\frac{\Delta_z U_v^x}{\Delta z}\right)_{i+1/2}\Big]^n$$

$$+ \alpha^n_{i+1/2} \frac{(P_{i+1} - P_i)^{n+1}}{\Delta x_{i+1/2}}$$

$$= - (F^x_{wv})^{n+1/2}_{i+1/2} - (F^x_{iv})^{n+1/2}_{i+1/2} \qquad (4.5)$$

In the above equation $\left(\frac{\Delta_x U_v^x}{\Delta x}\right)_{i+1/2}$ represents a difference approximation for the spatial derivative $\partial U_v^x / \partial x$ evaluated at the point i+1/2. Similar expressions have been used for the y and z directions. The precise manner in which the various terms involved are evaluated will be discussed below. Once again, we are faced with the problem of variables appearing at locations other than those at which they were originally defined. We observe that the cell centered quantities $\alpha, \rho_v, \rho_\ell$ now needed at the face enter as multipliers of the derivatives rather than in the derivatives themselves. From a linear stability point of view, they will be only coefficients and as such they will not affect the stability (see also Chapter 6). Consequently, their definition is not crucial from this point of view. One could use again a donor-cell logic or, alternately, some weighted average between values at the centers of the adjacent cells. The first choice would appear quite reasonable, being consistent with

the donor-cell differencing used in the mass and energy equations. In single-phase liquid or, generally when the properties in the adjacent cells are not greatly different, there is little to say about favoring one choice over the other. Things are different, however, once the face in question separates a liquid cell from a two-phase cell. In this case the mixture density (mainly through α) may vary by as much as two orders of magnitude. In such a situation a change in the sign of the velocity(ies) at the face, for the donor-cell scheme, would lead to very large changes in the terms of the momentum equations, which in turn could generate large pressure spikes and even ruin the solution, by imposing impractically short time steps. We have indeed noted this undesirable behavior in some of our numerical tests. This finding lead to the adoption of the weighted average scheme, through which the value of any cell-centered quantity C can be specified at the face between two mesh cells as:

$$C_{i+1/2} = (C_i \Delta x_i + C_{i+1} \Delta x_{i+1})/(\Delta x_i + \Delta x_{i+1}) \quad (4.6)$$

To avoid ambiguity, we define each such quantity individually and then form their product, such as

$$(\alpha\rho_v)_{i+1/2} = \alpha_{i+1/2}(\rho_v)_{i+1/2} \quad (4.7)$$

Now let us consider the velocities appearing in Eq. (4.5). For the velocities multiplying the velocity gradients, additional averaging is required. We define:

$$(U_v^y)_{i+1/2} = \frac{1}{4}[(U_v^y)_{j-1/2} + (U_v^y)_{j+1/2} + (U_v^y)_{i+1,j+1/2} + (U_v^y)_{i+1,j-1/2}] \tag{4.8a}$$

$$(U_v^z)_{i+1/2} = \frac{1}{4}[(U_v^z)_{k-1/2} + (U_v^z)_{k+1/2} + (U_v^z)_{i+1,k+1/2} + (U_v^z)_{i+1,k-1/2}] \tag{4.8b}$$

Then the difference approximations of the convective derivatives are defined through a donor-cell logic:

$$\left(\frac{\Delta_x U_v^x}{\Delta x}\right)_{i+1/2} = \begin{cases} \dfrac{(U_v^x)_{i+3/2} - (U_v^x)_{i+1/2}}{\Delta x_{i+1}} & \text{if } (U_v^x)_{i+1/2} < 0 \\ \dfrac{(U_v^x)_{i+1/2} - (U_v^x)_{i-1/2}}{\Delta x_i} & \text{if } (U_v^x)_{i+1/2} \geq 0, \end{cases} \tag{4.9a}$$

$$\left(\frac{\Delta_y U_v^x}{\Delta y}\right)_{i+1/2} = \begin{cases} \dfrac{(U_v^x)_{i+1/2,j+1} - (U_v^x)_{i+1/2}}{(\Delta y)_{j+1/2}} & \text{if } (U_v^y)_{i+1/2} < 0 \\ \dfrac{(U_v^x)_{i+1/2} - (U_v^x)_{i+1/2,j-1}}{(\Delta y)_{j-1/2}} & \text{if } (U_v^y)_{i+1/2} \geq 0 \end{cases} \tag{4.9b}$$

$$\left(\frac{\Delta_z U_v^x}{\Delta z}\right)_{i+1/2} = \begin{cases} \dfrac{(U_v^x)_{i+1/2,k+1} - (U_v^x)_{i+1/2}}{(\Delta z)_{k+1/2}} & \text{if } (U_v^z)_{i+1/2} < 0 \\ \dfrac{(U_v^x)_{i+1/2} - (U_v^x)_{i+1/2,k-1}}{(\Delta z)_{k-1/2}} & \text{if } (U_v^z)_{i+1/2} \geq 0 \end{cases} \tag{4.9c}$$

The mesh spacings $(\Delta y)_{j+1/2}$ and $(\Delta z)_{k+1/2}$ appearing in the above expressions are evaluated as:

$$(\Delta y)_{j+1/2} = (\Delta y_j + \Delta y_{j+1})/2 \tag{4.10a}$$

$$(\Delta z)_{k+1/2} = (\Delta z_k + \Delta z_{k+1})/2 \tag{4.10b}$$

Finally, the mesh spacing $(\Delta x)_{i+1/2}$ needed in the pressure gradient is given by:

$$(\Delta x)_{i+1/2} = (\Delta x_i + \Delta x_{i+1})/2 \qquad (4.10c)$$

Before going to the next subsection, a few comments regarding the exchange terms are in order. Both the wall-phase and the interphase interaction terms (i.e., F_{wk} and F_{ik}, with k = v or ℓ) must be cast as linear functions in terms of new time velocities at the cell face under consideration. That is

$$(F^x_{wk})^{n+1/2}_{i+1/2} = (K^x_{wk})^{n}_{i+1/2} \, (U^x_k)^{n+1}_{i+1/2} \qquad (4.11)$$

$$(F^x_{ik})^{n+1/2}_{i+1/2} = (K^x_{ik})^{n}_{i+1/2} \, (U^x_v - U^x_\ell)^{n+1}_{i+1/2} \qquad (4.12)$$

and similarly for all the other mesh cell faces. Here the coefficients K_{wk} and K_{ik} can be complex functions of any variables, the only requirement being its evaluation using old time quantities. From the material on constitutive equations one can immediately infer the expressions for K_{wk} and K_{ik}.

One further refinement is possible if these coefficients prove to be strong functions of the velocity itself. Specifically a more formal linearization about

the old time step can be done. We shall exemplify this approach on the wall friction term. Generally, one can write:

$$F_w = fU^2 \tag{4.13}$$

where f is a friction coefficient. Let us now express $F_w^{n+1/2}$ in terms of F_w^n via a truncated Taylor's series:

$$F_w^{n+1/2} = F_w^n + \left(\frac{dF_w}{dU}\right)^n (U^{n+1} - U^n) \tag{4.14}$$

or, after a few simple algebraic steps:

$$F_w^{n+1/2} = 2fU^nU^{n+1} - fU^nU^n \tag{4.15}$$

For additional generality, one can write:

$$F_w^{n+1/2} = (1-\theta)fU^nU^{n+1} + \theta fU^nU^n$$

where $-1 \leq \theta \leq +1$. For $\theta = +1$, the treatment of wall friction becomes fully explicit; $\theta = 0$ corresponds to our ad-hoc linearization, Eq. (4.11); $\theta = -1$ yields the rigorously linearized form, Eq. (4.15).

This linearization procedure can also be readily applied to the interfacial momentum exchange. In instances

in which K_{ik} depends strongly on the relative velocity between phases, this approach will generally give better results, avoiding or mitigating the possibility of oscillation because of K_{ik} evaluation lag.

In our applications, Eqs. (4.11 and 4.12) proved, however, entirely adequate and were implemented in our scheme.

4.2.2.3.2 New Time Phase Velocities as a Function of New Time Pressures

The specific choice of implicitness in the momentum equations previously described enables one to obtain linear expressions relating the new phase velocities to the applicable new time pressure gradient. In the following, we shall show how this is accomplished.

Let us look at the pair of momentum equations written at some cell face. For simplicity of notation we drop the spatial subscripts, keeping in mind all the conventions and definitions previously introduced. Also let *conv* stand for the convective terms in the momentum equation. Then we have:

$$[\alpha\rho_v]^n \frac{U_v^{n+1}-U_v^n}{\Delta t} + [\alpha\rho_v]^n conv_v^n + (\alpha)^n \frac{\Delta p}{\Delta x}^{n+1}$$

$$= -K_{iv}^n(U_v^{n+1}-U_\ell^{n+1}) - K_{wv}^n U_v^{n+1} + [\alpha\rho_v]^n g \tag{4.16a}$$

$$[(1-\alpha)\rho_\ell]^n \frac{U_\ell^{n+1}-U_\ell^n}{\Delta t} + [(1-\alpha)\rho_\ell]^n conv_\ell^n + (1-\alpha)^n \frac{\Delta p}{\Delta x}^{n+1}$$

$$= -K_{i\ell}^n(U_\ell^{n+1} - U_v^{n+1}) - K_{w\ell}^n U_\ell^{n+1} + [(1-\alpha)\rho_\ell]^n g \tag{4.16b}$$

These two linear equations are coupled through the momentum exchange terms. However, the system can be solved for the new time velocities as functions of the new time pressure gradient and other quantities evaluated at the old time. The result of this reduction process is:

$$U_v^{n+1} = a_v \Delta p^{n+1} + b_v$$

$$U_\ell^{n+1} = a_\ell \Delta p^{n+1} + b_\ell \tag{4.17}$$

where:

$$a_v = - \frac{\Delta t}{\Delta x} [\alpha e_2 + \Delta t K_{iv}(1-\alpha)]/d \tag{4.18a}$$

$$a_\ell = - \frac{\Delta t}{\Delta x} [(1-\alpha)e_1 + \Delta t K_{i\ell}\alpha]/d \tag{4.18b}$$

$$b_v = (f_1 e_2 + \Delta t K_{iv} f_2)/d \tag{4.18c}$$

$$b_\ell = (f_2 e_1 + \Delta t K_{i\ell} f_1)/d \tag{4.18d}$$

$$e_1 = \alpha\rho_v + \Delta t(K_{wv} + K_{iv}) \tag{4.19a}$$

$$e_2 = (1-\alpha)\rho_\ell + \Delta t(K_{w\ell} + K_{i\ell}) \tag{4.19b}$$

$$f_1 = \alpha\rho_v [U_v - \Delta t(conv_v - g)] \tag{4.19c}$$

$$f_2 = (1-\alpha)\rho_\ell [U_\ell - \Delta t(conv_\ell - g)] \tag{4.19d}$$

$$d = e_1 e_2 - (\Delta t)^2 K_{iv} K_{i\ell} \tag{4.19e}$$

In Eqs. (4.18) and (4.19) above, the time level superscript was dropped, with the understanding that everything is evaluated at the old time. Consequently, the coefficients a's and b's in Eqs. (4.17) can be calculated only once at the beginning of the current time step and stored.

It is interesting to note what happens in the limit of K_{iv} and $K_{i\ell}$ becoming very large and equal. In this case all the terms not containing K_{iv} or $K_{i\ell}$ can be dropped and it can be easily verified that

$$\lim_{\substack{k_{iv}\to\infty \\ k_{i\ell}\to\infty}} a_v = \lim_{\substack{k_{iv}\to\infty \\ k_{i\ell}\to\infty}} a_\ell = -\frac{\Delta t}{\Delta x}\left[\rho_m + \Delta t(K_{wv}+K_{w\ell})\right]^{-1} \tag{4.20a}$$

and

$$\lim_{\substack{k_{iv}\to\infty \\ k_{i\ell}\to\infty}} b_v = \lim_{\substack{k_{iv}\to\infty \\ k_{i\ell}\to\infty}} b_\ell = \frac{\rho_m U_m - \Delta t(\rho conv)_m + \Delta t \rho_m g}{\rho_m + \Delta t(K_{wv} + K_{w\ell})} \tag{4.20b}$$

where

$$\begin{aligned} \rho_m &= \alpha\rho_v + (1-\alpha)\rho_\ell \\ U_m &= [\alpha\rho_v U_v + (1-\alpha)\rho_\ell U_\ell]/\rho_m \\ (\rho conv_m) &= \alpha\rho_v\, conv_v + (1-\alpha)\rho_\ell conv_\ell \end{aligned} \tag{4.21}$$

Thus, Eqs. (4.17) yield the equal velocity model without any additional assumptions.

4.2.3 Solution Scheme

The finite difference equations previously described combined with the appropriate equations of state form a large system of non-linear equations with the

following new time variables as unknowns:

$$\rho_m^{n+1},\ p^{n+1},\ e_m^{n+1},\ T_\ell^{n+1},\ T_v^{n+1},\ U_v^{n+1} \text{ and } U_\ell^{n+1},$$

for all cells in the domain of the problem. (While not shown explicitly up to now in our equations, the new time temperatures are needed in our semi-implicit treatment of the heat sources). The sources of non-linearity in our discretized equations are the state equations as well as the appearance of fundamental variables in products, i.e., $(\rho_m e_m)^{n+1}$.

In this subsection, the overall solution scheme will be presented in detail, with special emphasis on the treatment of nonlinearities.

4.2.3.1 General Remarks on the Solution of Non-Linear Equations

With few exceptions, non-linear equations must be solved via an iterative technique. An extensive review and analysis of such methods is given by Ortega and Rheinboldt [8]. The method chosen in our application is Newton's iteration, with the possibility of using its variants, the secant and the parallel-chord methods.

The reasons behind our choice are:

- convergence is guaranteed, if the guess is close enough to the solution; it will be seen that a reduction in time step size in

principle assures a better guess (more on this will be discussed in Chapter 5);

- the method exhibits a relatively high rate of convergence;
- the evaluation of the necessary derivatives is not overly costly from a computational viewpoint;
- if only one non-linear iteration is performed, the method is equivalent to a linearization about the old time values for the main variables; this latter technique of linearization has been and still is widely employed for the numerical solution of fluid dynamics equations.

The essential aspects of Newton's method will be presented below.

Consider a system of n nonlinear equations in n unknowns:

$$
\begin{aligned}
&f_1(x_1,x_2,\ldots,x_j,\ldots,x_n) = 0\\
&f_2(x_1,x_2,\ldots,x_j,\ldots,x_n) = 0\\
&\vdots\\
&f_i(x_1,x_2,\ldots,x_j,\ldots,x_n) = 0\\
&\vdots\\
&f_n(x_1,x_2,\ldots,x_j,\ldots,x_n) = 0
\end{aligned}
\qquad (4.22)
$$

or, in compact vector notation

$$\bar{f}(\bar{x}) = 0$$

where

$$\bar{f} = (f_1, f_2, \ldots, f_n)^T$$
$$\bar{x} = (x_1, x_2, \ldots, x_n)^T$$

Then, in the neighborhood of a point defined by the vector $\bar{x}^o$, a linear approximation for the function $\bar{f}$ may be used:

$$\bar{f}(\bar{x}) \cong \bar{f}(\bar{x}^o) + J(\bar{x}^o)(\bar{x}-\bar{x}^o) \tag{4.23}$$

Considering $\bar{x}^o$ as a guess and $\bar{x}$ as the solution, i.e., $\bar{f}(\bar{x}) = 0$, the following iterative scheme can be constructed:

$$J(\bar{x}^k)(\bar{x}^{k+1} - \bar{x}^k) = -\bar{f}(\bar{x}^k) \tag{4.24}$$

In Eqs. (4.23) and (4.24) $J(\bar{x})$ stands for the Jacobian matrix associated with $\bar{f}(\bar{x})$. Its entries are

$$J_{ij} = \frac{\partial f_i}{\partial x_j} \tag{4.25}$$

Equation (4.24) defines the Newton's method. Denoting

$$\delta\bar{x}^{k+1} = \bar{x}^{k+1} - \bar{x}^k$$

eq. (4.24) can be written as

$$J(\bar{x}^k)\ \delta\bar{x}^{k+1} = -\bar{f}(\bar{x}^k). \qquad (4.26)$$

Equation (4.26) represents a system of n linear algebraic equations, which must be solved at every iteration. Sometimes two natural modifications to the scheme (4.24) or (4.26) can be used to advantage.

The first involves the evaluation of the partial derivatives (4.25). Generally, these partial derivatives can be replaced by some finite difference approximation. The incentive in many instances lies in the fact that the analytical partial derivatives have complicated expressions, the evaluation of which being possibly more expensive computationally than the evaluation of the functions themselves. However, in our application, the computational efforts required for the evaluation of the partial derivatives and of the functions proper are quite comparable. The potential benefit of using the secant method in our case is of a totally different nature. As it was shown in Chapter 3, the state functions, especially the mixture density, exhibit very large discontinuities in the first derivative, while the function itself is still continuous. In such a situation a finite difference representation for the partial derivatives achieves a "smoothing effect", defining an approximation for such

a derivative even when theoretically such a derivative does not exist. The manner in which these "secant" approximations to the derivatives of the state functions are constructed was presented in Chapter 3.

The other modification to the Newton's method is reevaluating the Jacobian matrix only periodically during the iteration cycle. Rather substantial computational savings are achieved when this modification, called the parallel-chord method, is used. Not only is the evaluation of the Jacobian entries less frequent, but also the average time spent on solving the system of Eqs. (4.26) is drastically reduced. As both direct and iterative methods are used to solve this system (see Chapter 5), a few additional comments are in order. When a direct solution is used, the relatively expensive LU factorization is performed only when the Jacobian is updated, while the computationally much cheaper back-substitution is all that is needed between updates. In the case of an iterative method, such as the successive overrelaxation, the optimum (or near optimum) relaxation parameter, determined when the Jacobian matrix is re-evaluated, is used unchanged (or as an estimate in a continuing refining process) between updates, since the matrix with which it is associated remains the same. Moreover, if a block iterative method (of the type to

be described in Chapter 5) is used for the solution of the system (4.26), the remarks made above in connection with a direct method extend to the inversion of the "blocks" involved.

Before closing this subsection, we would like to mention an important fact related to our choice of main variables, with consequences on the overall numerical scheme. We recall that in the energy conservation equation, the "conserved" quantity is the internal energy density, i.e., the group $\rho_m e_m$. In our investigations, we have discovered a subtle peculiarity in the behavior of $\rho_m e_m$ in the case of sodium two-phase flow. It turns out that the mixture internal energy density is not monotonic with respect to the mixture specific energy. This is illustrated in Fig. 4.2. Actually, this same behavior is exhibited by water at low pressures, while at high pressures, ρe becomes monotonic (see Fig. 4.3). The reason for this behavior is clearly the very large decrease of the mixture density for a relatively small increase in specific energy, when changing from single-phase liquid to a two-phase mixture. It is well known that if an extremum point exists between the guess and the solution, the convergence of the Newton-type methods is generally destroyed.

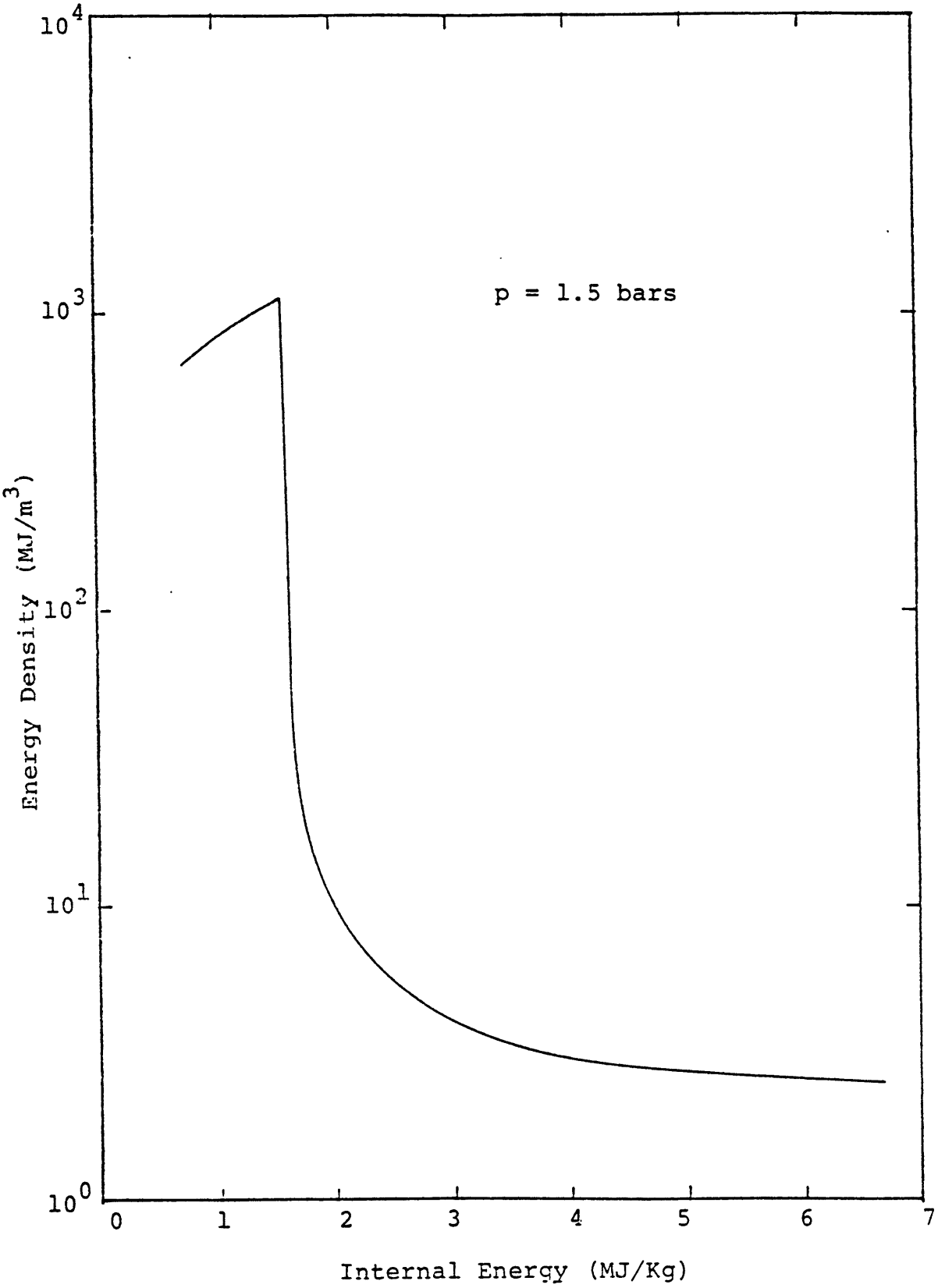

Fig. 4.2 Sodium Internal Energy per Unit Volume versus Internal Energy.

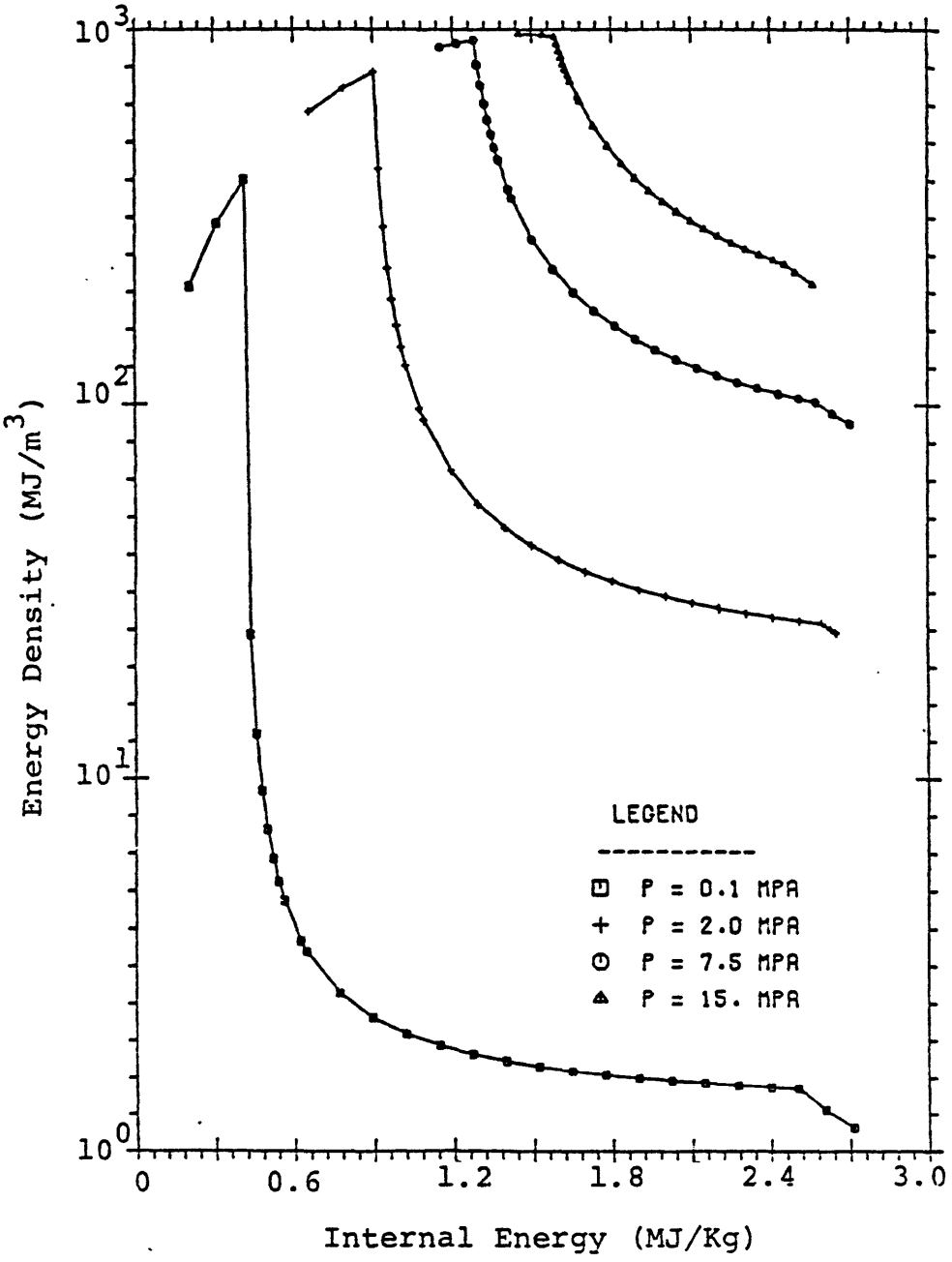

Fig. 4.3 Water Internal Energy per Unit Volume versus Internal Energy.

This undesirable feature of the group ρe lead to our decision to use a non-conservative form of the energy equation, in which a "splitting" of this group occurs, that is, instead of

$$[(\rho_m e_m)^{n+1} - (\rho_m e_m)^n]/\Delta t$$

we will have

$$\rho_m^n (e_m^{n+1} - e_m^n)/\Delta t.$$

Avoiding the presence of the group ρe in the non-linear stage of the solution can also be accomplished by explicitly advancing the energy equation. In this way, the only non-linearity arises due to the dependence of density on pressure, but fortunately this is always monotonic. Later in this section, we shall provide additional comments on this latter scheme (mentioned in 4.2.2).

4.2.3.2 The Jacobian Matrix

As it has just been explained, the linearization of our non-linear system of equations involves the construction of the Jacobian matrix for this system. In the following we shall describe in detail how this is accomplished.

We recall that the difference approximation of the momentum equations yielded a set of expressions, linearly relating each new time phase velocity at a cell face to the advanced pressures in the abutting mesh cells. Consequently, all advanced velocities can be eliminated in favor of the relevant pressures. This major simplification is made possible by the specific discretization scheme chosen for our method.

For each cell, we now have two equations, namely the mass and the energy equations, with velocities expressed in terms of pressure as mentioned above. Let R_m and R_e stand for the mass and energy equations, respectively; also assign the subscript "c" to the cell under consideration and the subscript "a" to any of its up to six neighboring cells. It is apparent from our difference equations that the spatial coupling between cells, at the new time, is due solely to the convective terms via the face-centered velocities, which are now replaced by the appropriate pressures. As a result each mass or energy equation will contain as main unknowns not only the local pressure and mixture internal energy but also the up to six neighboring pressures.

Therefore, the non-zero entries of the Jacobian, for cell "c", are:

$$\frac{\partial R_{m,c}}{\partial p_c} \; ; \quad \frac{\partial R_{m,c}}{\partial e_{m,c}} \; ; \quad \frac{\partial R_{e,c}}{\partial p_c} \; ; \quad \frac{\partial R_{e,c}}{\partial e_{m,c}} \; ;$$

$$\frac{\partial R_{m,c}}{\partial p_a} \quad \text{(up to six such entries)}$$

$$\frac{\partial R_{e,c}}{\partial p_a} \quad \text{(up to six such entries)}$$

that is a total of up to 16 entries per cell. The actual expressions of these partial derivatives will obviously depend upon the particular scheme chosen. We give the detailed expressions for the basic scheme, i.e., the semi-implicit treatment of the energy equation in conservative form, as the other schemes can be viewed (and obtained) as special cases. Recalling Eqs. (4.2) and (4.3), we have:

$$\frac{\partial R_{m,c}}{\partial p_c} = \frac{V_c}{\Delta t} \left(\frac{\partial \rho_{m,c}}{\partial p_c}\right) e_{m,c} + \frac{\partial conv_{m,c}}{\partial p_c} \tag{4.27a}$$

$$\frac{\partial R_{m,c}}{\partial e_{m,c}} = \frac{V_c}{\Delta t} e_{m,c} \left(\frac{\partial \rho_{m,c}}{\partial e_{m,c}}\right)_{p_c} \tag{4.27b}$$

$$\frac{\partial R_{e,c}}{\partial p_c} = \frac{V_c}{\Delta t} e_{m,c} \left(\frac{\partial \rho_{m,c}}{\partial p_c}\right) e_{m,c} + \frac{\partial conv_{e,c}}{\partial p_c} - \frac{\partial Q_{w,c}}{\partial p_c} - \frac{\partial Q_{k,c}}{\partial p_c} \quad (4.27c)$$

$$\frac{\partial R_{e,c}}{\partial e_{m,c}} = \frac{V_c}{\Delta t} \left[e_{m,c} \left(\frac{\partial \rho_{m,c}}{\partial e_{m,c}}\right)_{p_c} + \rho_{m,c}\right] - \frac{\partial Q_{w,c}}{\partial e_{m,c}} - \frac{\partial Q_{k,c}}{\partial e_{m,c}} \quad (4.27d)$$

$$\frac{\partial R_{m,c}}{\partial p_a} = \frac{\partial conv_{m,c}}{\partial p_a} \quad (4.27e)$$

$$\frac{\partial R_{e,c}}{\partial p_a} = \frac{\partial conv_{e,c}}{\partial p_a} \quad (4.27f)$$

The actual expressions for the heat sources will be given in the relevant sections of this chapter. Here we illustrate how a partial derivative of the mass convective term is formed:

$$\frac{\partial\, conv_{m,c}}{\partial\, p_a} = \frac{\partial\, conv_{m,c}}{\partial\, U_v^{c,a}} \cdot \frac{\partial\, U_v^{c,a}}{\partial\, p_a} + \frac{\partial\, conv_{m,c}}{\partial\, U_\ell^{c,a}} \cdot \frac{\partial\, U_\ell^{c,a}}{\partial\, p_a}$$

$$= A^{c,a}\left[(\alpha\rho_v a_v)^n + ((1-\alpha)\rho_\ell a_\ell)^n\right]^{c,a} \qquad (4.28)$$

Above, we used the superscript group c,a to denote the face between cells "c" and "a". The partial derivatives of the velocities with respect to pressure were obtained from Eqs. (4.17). A similar expression is easily obtained for the energy convective term.

We observe that the partial derivative of a convective term with respect to the local pressure contains contributions from all the (up to six) cell faces. In light of Eqs. (4.17), each such contribution will then be equal (but opposite in sign) to the partial derivative of the same convective term with respect to the appropriate neighboring pressure. Thus:

$$\frac{\partial\, conv_{m(e),c}}{\partial\, p_c} = -\sum_{\text{all a's}} \frac{\partial\, conv_{m(e),c}}{\partial\, p_a} \qquad (4.29)$$

It is worth noting that the derivatives of the convective terms involve only quantities evaluated at the old time. Therefore, they can be calculated only once, at the

beginning of the time step, stored and used during the non-linear iterative process. Thus, at the cost of some additional storage, a significant saving in computational work can be achieved. This and some other computation-saving features related to the construction of the Jacobian matrix and of the right-hand-side in Eq. (4.26) merit some further comments.

In general a mass or energy difference equation will contain linear and non-linear terms involving the main variables. In particular, we note that the non-linear terms, which have to be updated during the iteration cycle, are "local", i.e., not involved in spatial coupling.

We can write:

$$R(x) = G(x) + Ax + c = 0 \tag{4.30}$$

where $R(x)$ = vector representing the mass and energy equations;

$G(x)$ = non-linear terms;

A = matrix representing the linear dependencies;

C = vector containing constant terms;

x = vector representing the main unknowns.

Using the superscript ℓ as the non-linear iteration counter, the Newton's method (Eq. (4.36)) applied to Eq. (4.30) yields:

$$\left(\frac{\partial R}{\partial x}\right)_{x^{\ell}} \delta x^{\ell+1} = - R(x^{\ell}) \tag{4.31}$$

or

$$\left[\left(\frac{\partial G}{\partial x}\right)_{x^{\ell}} + A\right]\delta x^{\ell+1} = - [G(x^{\ell} + Ax^{\ell} + c] \tag{4.31a}$$

Clearly A and c can be calculated only once and used afterwards unchanged during iterations. We have implemented these computation-saving features in our numerical scheme. However, in computational environments where the storage is at a premium, A and c can be reconstructed at every iteration.

We make an additional remark regarding the fully explicit treatment of the energy equation. Once the energy advancement is performed, the mixture internal energy becomes known. Consequently, only the mass equation will have to be linearized, and moreover only with respect to presures. Clearly, the only nonlinear term in the mass equation is that involving the local pressure. In this situation, a certain computational advantage of the one-dimensional secant method [8] may be used. Specifically, the mixture density derivative can be evaluated from:

$$\left(\frac{\partial \rho_{m,c}}{\partial p_c}\right)^{\ell} \approx \frac{(\rho_{m,c}^{\ell} - \rho_{m,c}^{\ell-1})}{(p_c^{\ell} - p_c^{\ell-1})} \tag{4.32}$$

Note that one does not have to store the old ρ_m iterate, since as soon as the difference quotient is evaluted, the new ρ_m replaces the old one, component by component. The denominator is easily recognized as the "c"-component of the vector δp^{ℓ}, for which our method already requires separate storage.

The application of the secant method in the manner just described saves on the evaluation of the density derivative (with respect to pressure) from a rather complicated equation of state.

4.2.3.3 The Pressure Problem

So far we have seen how our discretized equations are linearized via Newton's method, leading to a system of linear algebraic equations (Eqs. (4.26) or (4.31)). For N mesh cells, the order of this system is obviously 2N. We shall see below that the special structure of the Jacobian matrix (which, in turn is a consequence of the particular differencing scheme employed) makes possible a further simplification, of great importance to the efficiency of the overall numerical method.

At this point, let us collect the results of the previous subsection, examining the above mentioned system of equations. Let us look first at the two equations corresponding to cell "c". They can be written as:

$$\begin{vmatrix} x & x \\ x & x \end{vmatrix} \begin{vmatrix} \delta p_c \\ \delta e_{m,c} \end{vmatrix} + \begin{vmatrix} x & x & x & x & x & x \\ x & x & x & x & x & x \end{vmatrix} \begin{vmatrix} \delta p_{a,1} \\ \delta p_{a,2} \\ \delta p_{a,3} \\ \delta p_{a,4} \\ \delta p_{a,5} \\ \delta p_{a,6} \end{vmatrix} = - \begin{vmatrix} R_{m,c} \\ R_{e,c} \end{vmatrix} \qquad (4.33)$$

where subscripts a,1 through a,6 correspond to the (up to) six neighboring cells. The 2x2 matrix represents the "local"

coupling, its entries being given by Eqs. (4.27a-d). The 2x6 matrix, whose entries are given by Eqs. (4.27e,f) represents the "spatial" coupling. It is immediately apparent that the spatial coupling is accomplished only through pressures, while the neighboring energies are not involved. It is worth reiterating that this is a direct consequence of the particular discretization selected. Thus, from any one of the two equations (4.33), if the pressure corrections in the cell under consideration and in the neighboring cells are known, the energy correction in cell "c", $\delta e_{m,c}$, can be readily obtained. This finding indicates that the energy correction can be eliminated from one of these equations in favor of the relevant pressures, thus obtaining an equation for pressures only. Mathematically, the procedure just mentioned amounts to inverting the 2x2 matrix, i.e., solving the system of two equations for δp_c and $\delta e_{m,c}$:

$$\begin{vmatrix} 1 & 0 \\ 0 & 1 \end{vmatrix} \begin{vmatrix} \delta p_c \\ \delta e_{m,c} \end{vmatrix} + \begin{vmatrix} x' & x' & x' & x' & x' & x' \\ x' & x' & x' & x' & x' & x' \end{vmatrix} \begin{vmatrix} \vdots \\ \delta p_{a,i} \\ \vdots \end{vmatrix} = - \begin{vmatrix} R'_{m,c} \\ R'_{e,c} \end{vmatrix} \tag{4.34}$$

Above the (') indicates an alteration resulting from the aforementioned manipulation. This procedure is applied to all cells, the result being a system of N equations for

the pressure corrections.

To ascertain the properties of the associated NxN matrix, the implications of this reduction process will be further examined. Let us re-arrange the order of the equations and of the unknowns as follows:

- place the N mass equations one after the other, followed by the N energy equations;
- in the vector for the unknowns, use the pressure corrections as the first N components, followed by the N energy corrections.

This reordering of both equations and unknowns is accomplished by row and column interchanges. The original system of 2N equations in 2N unknowns takes on the following structure:

$$\begin{vmatrix} A_1 & D_1 \\ A_2 & D_2 \end{vmatrix} \begin{vmatrix} \delta_p \\ \delta e_m \end{vmatrix} = - \begin{vmatrix} R_m \\ R_e \end{vmatrix} \qquad (4.35)$$

where:

A_1 and A_2 are banded matrices, containing up to 7 stripes (in three-dimensional problems); these

two matrices contain the coefficients of the pressure corrections in both the mass and the energy equations;

D_1 and D_2 are diagonal matrices; their entries are the coefficients of the energy corrections;

$$\delta p = (\delta p_1, \ldots, \delta p_c, \ldots, \delta p_N)^T$$

$$\delta e_m = (\delta e_{m,1}, \ldots, \delta e_{m,c}, \ldots, \delta e_{m,N})^T$$

$$R_m = (R_{m,1}, \ldots, R_{m,c}, \ldots, R_{m,N})^T$$

$$R_e = (R_{e,1}, \ldots, R_{e,c}, \ldots, R_{e,N})^T$$

We shall note a number of favorable properties that matrices A_1 and A_2 possess. Later in this chapter we will see that the partial derivatives of the heat sources with respect to pressure and internal energy are negative. A look at the coefficients a_v and a_ℓ in Eqs. (4.17) and at their defining relationships, Eqs. (4.18) and (4.19), reveals the fact that they are always negative, therefore, the partial derivatives of the convective terms with respect to the neighboring pressures, Eq. (4.28), are also always negative. Consequenty the off-diagonal

entries in both A_1 and A_2 are negative, while the diagonal elements, defined by Equations (4.27a) and (4.27c), are always positive. It is also obvious from Eq. (4.28) that

$$\frac{\partial\, conv_{m,c}}{\partial p_a} = \frac{\partial\, conv_{m,a}}{\partial p_c}$$

thus A_1 is symmetric. In contrast, because of the term $p\nabla\vec{U}$ in the internal energy equation, A_2 is not symmetric. On the other hand, since $(\partial\rho_m/\partial p)_{em} \geq 0$, both matrices are diagonally dominant. In particular, even with constant heat sources, i.e., $(\partial Q/\partial p)_{e_m} = 0$, and for an incompressible fluid, i.e., $(\partial\rho_m/\partial_p)_{e_m} = 0$, the boundary conditions (see next chapter) will provide the strict diagonal dominance required for irreducibility.

To summarize, A_1 and A_2 are:

- symmetric and not symmetric, respectively,
- irreducibly diagonally dominant,

and have

-positive diagonal entries,

-non-positive (i.e., negative or zero) off-diagonal entries.

Matrices such as A_1 are also positive definite and are called Stieltjes matrices, while matrices such as A_2 are called M-matrices [9].

We turn now to the D-matrices. The entries of D_1,

corresponding to the mass equation and defined by Eq. (4.27b) are always negative, since $(\partial \rho_m / \partial e_m)_p < 0$. (Obviously, they are zero if the incompressible fluid assumption is used). The situation is more complicated for the entries of D_2, Eq. (4.27d). While the heat source contributions are always positive, the derivative $(\partial \rho_m e_m)/\partial e_m)_p$ is not, as our earlier comments on the group $(\rho_m e_m)$ indicated. If the non-conservative form of the energy equation is used, then the expression in the brackets in (4.27d) becomes $\rho^n_{m,c}$, therefore, the elements of D_2 become always positive. But in this case, A_2 may not be diagonally dominant.

At this point, we can examine the procedure through which the energy correction is eliminated in favor of the pressure corrections, leading to a system of equations for the latter. Let us re-write Eq. (4.35) as

$$A_1 \, \delta p + D_1 \, \delta e_m = - R_m$$

$$A_2 \, \delta p + D_2 \, \delta e_m = - R_e \qquad (4.36)$$

Multiplying the first Equation in (4.36) by D_2, the second by D_1 and subtracting the two modified equations (say the second from the first) results in:

$$(D_2 A_1 - D_1 A_2) \delta p = -(D_2 R_m - D_1 R_e) \qquad (4.37)$$

or,

$$A_R \, \delta p = - R_R$$

(with obvious definitions for A_R and R_R). Note that unless D_1 and D_2 are of the form $C_1 I$ and $C_2 I$, respectively and the compression work term, $p\nabla\vec{U}$, in the energy equation is neglected, A_R will not be symmetric. Moreover, the diagonal dominance will, in some instances, be lost. The analysis of this second aspect requires a great deal of algebraic manipulation and is provided in Appendix E.

Diagonal dominance is needed for both direct and iterative solutions of (4.37), avoiding a possibly algorithmically singular matrix for the former and a diverging situation for the latter. Fortunately, diagonal dominance can be regained by a reduction of the time step. That this is so can be easily seen from the expressions of the off-diagonal terms which vanish in the limit of $\Delta t \to 0$. Thus, there will always be such a time step size as to ensure the diagonal dominance. The problem is that sometimes the required time step reduction may be significant.

We shall perform one additional manipulation in Eq. (4.37), the purpose of which will be readily apparent. Let $A_i = A_i^d + A_i^\sigma$, $i = 1,2$, where A_i^d is the diagonal of A_i and A_i^σ contains the off-diagonal entries. Then we rewrite Eq. (4.37) as:

$$[(D_2A_1^d - D_1A_2^d) + (D_2A_1^\sigma - D_1A_2^\sigma)]\delta p$$

$$= - (D_2R_m - D_1R_e) \qquad (4.38)$$

Let $B = D_2A_1^d - D_1A_2^d$. Since B is obviously a diagonal matrix, its inversion is trivial (we shall show in Appendix E that B is never singular). Multiplying Eq. (4.38) by B^{-1} we finally get:

$$[I + B^{-1}(D_2A_1^\sigma - D_1A_2^\sigma)]\delta p$$

$$= - B^{-1}(D_2R_m - D_1R_e) \qquad (4.39)$$

This is exactly equivalent to the system obtained by taking the first equation in (4.34), for all cells.

Before closing this subsection, we will briefly examine the implications of an explicit treatment of the convective terms in the energy equation upon the resulting pressure problem.

First consider the fully explicit advancement of the energy equation. In this case, this equation does not contribute directly to the construction of the pressure problem, which then becomes simply:

$$A_1 \, \delta p = - R_m \tag{4.40}$$

Clearly, no concerns regarding the diagonal dominance or the symmetry of the matrix in the equation above are raised.

Let us look now at the scheme treating explicitly not the entire energy equation but only its convective terms. In this situation, the matrix A_2 becomes diagonal, as only the local terms in the energy equation are treated implicitly. As the spatial coupling is provided now only by A_1, the symmetry of the matrix A_R is preserved. While not obvious at this point, we shall show in Appendix E that unconditional diagonal dominance is maintained.

4.2.4 Boundary Conditions

A combination of physical considerations and a characteristic analysis is generally used to establish the necessary and permissible boundary conditions. A conceptual problem arises because our system of differential equations is not always hyperbolic, i.e., not all the characteristics are distinct and real, when the phase velocities are not equal. Nevertheless, in the vast majority of our applications, the in-flow is single-phase and as we shall see, it is the in-flow boundary condition that raises potential questions. What we basically seek in the

context of our numerical method is to completely specify the problem avoiding obvious or subtle over- or under-determination.

The simplest boundary condition is the zero normal flow condition, applied on the sides of the three-dimensional problem domain. This condition reflects the existance of the hexagonal can around the assembly. Because in this case no information is transferred across such a cell face, the fluid properties on either side of the face are irrelevant to forming the corresponding flux terms. Thus, the specification of a null velocity completely defines such a situation. Note also that a momentum equation need not be written for such a cell face.

For the top and bottom of the assembly two types of boundary conditions are provided, namely prescribed pressure and prescibed velocity. If a pressure boundary condition is applied, then the velocity at the appropriate face will be determined from the solution. A velocity boundary condition implies the specification of the velocity during the transient. In this latter case, insofar as the solution is concerned, a momentum equation is not needed at the cell face located on the boundary. We, however, form the appropriate momentum equation even in this situation, solely for the purpose of updating the

pressure on the boundary. This update is necessary if at some point during a transient a switch from a velocity to a pressure boundary condition is desired.

For both types of boundary conditions, if the flow is inward, fluid properties at the boundary must be specified to characterize the incoming fluid. In particular, the internal energy must be provided. In the case of the pressure boundary condition everything is completely determined, as one obtains the fluid density at the boundary via the equation of state, from the appropriate known pressure and internal energy. In the case of the velocity boundary condition, the pressure on the boundary becomes theoretically non-essential information. In fact to specify it independently of the prescribed velocity constitutes overdetermination. Nonetheless, we need the pressure to define the fluid properties. Given the very weak dependency on pressure of the liquid density and the fact that in a vast majority of applications the entering fluid is single-phase liquid, the independent specification of pressure does not appear to cause any problems. Nevertheless, a more consistent approach would establish a relationship between the pressure and the velocity at the inflow boundary. Such a relationship is automatically accomplished in the formulation of another "velocity-type" boundary condition, the total inlet flow

rate condition, which will be described in detail in Chapter 5, in the context of the pressure field solution. Briefly, this latter boundary condition uses the momentum equations at the boundary to obtain an equation for the boundary pressure such as to obtain a prescribed total inlet mass flow rate. This option correctly treats even the case of an incoming two-phase mixture with (generally) unequal phase velocities.

If the flow is outward, no extraneous fluid properties are needed. Usually the outlet pressure is specified as a boundary condition, the imposition of a velocity at the exit being extremely unlikely.

An additional remark regarding the formation of the momentum equations at an inflow boundary is in order. The reader will recall that a donor-cell formulation is used to define the velocity gradients. When writing the axial velocity gradient in the z-direction (i.e., $\Delta U_z/\Delta z$) at the inflow boundary, one immediately notes the need for a velocity outside the problem domain. A number of choices are availble, the two most common being:

a. zero outside velocity (this situation may be viewed as attempting to simulate the existence of a large plenum at the inlet), or

b. zero gradient, that is, the outside velocity is equal to the velocity at the boundary.

We have adopted the second approach, based on the reasoning that in many instances of interest in our applications, the pressure is given (i.e., measured) not necessarily in a plenum upstream of the test section but at a location already inside the test section, near its inlet.

In any case, changing from one option to the other would involve only very minor modifications.

4.3 The Numerical Method for Fuel (Heater) Rod Conduction

In this section, we shall describe the numerical treatment of the conduction in the fuel or heater rod. Of particular interest in our applications, the strong coupling to the fluid energy equation will receive special attention.

4.3.1 Choice of Treatment

The radial heat conduction in the fuel/heater pin is described by

$$\rho c \frac{\partial T}{\partial t} - \frac{1}{r} \frac{\partial}{\partial r} \left(rk \frac{\partial T}{\partial r} \right) = \dot{q}''' \qquad (4.41)$$

where

ρ = material density

c = specific heat

k = thermal conductivity

$\dot{q}'''$ = volumetric heat generation rate

While it is true that ρ, c and k are all functions of temperature, their dependence is relatively weak, justifying an explicit treatment of the properties. In other words, ρ, c and k are evaluated as a function of the old time temperature. Therefore, Eq. (4.41) becomes a linear partial differential equation insofar as its solution over a time step is concerned.

It remains to decide on the numerical treatment of the rod conduction equation proper. For typical properties and radial mesh sizes encountered in our applications, a standard stability analysis for a fully explicit scheme yields an upper limit for the allowable time step which is generally more lenient than the time step limitations imposed by the fluid dynamics solution. Nevertheless we selected a fully implicit scheme and we will now explain the reasoning behind our choice.

Since the fluid dynamics is treated semi-implicitly, a steady-state calculation is performed as an unperturbed transient. At the same time, the generally large thermal inertia of the fuel (or heater) rods requires a rather long time to elapse before reaching a steady state. Because of the limitation on time step size dictated by the fluid flow solution, a large number of time steps would then be needed, rendering such calculations unnecessarily expensive. An implicit treatment of the rod conduction

makes possible the removal of the temporal derivative in such calculations, which is equivalent to setting to zero the thermal capacity (i.e., the product ρc) of the rod material. With this option, no heat storage occurs in the rod, the amount of heat generated being entirely and instantaneously transferred to the fluid, thereby signifying shortening the time required to reach steady state. As the fully implicit conduction gives rise to a tridiagonal matrix, with a very efficient solution, the increase in computational work per time step is insignificant.

In addition, we will see that an implicit scheme allows a very useful modification regarding the coupling to the fluid energy equation.

4.3.2 Difference Equations

The finite difference approximation is obtained by dividing the fuel/heater rod into an arbitrary number of mesh cells. The temperatures are calculated at the edges of the cells, denoted by the subscript i, while the material properties are associated with the centers of the mesh cells, i + 1/2 (see Fig. 4.4).

To generate a spatial difference analog, Eq. (4.41) is integrated between the centers of two adjacent mesh cells, i.e., from $r_{i-1/2}$ to $r_{i+1/2}$. Considering now an implicit time differencing scheme yields the difference equation for the interior points in the rod:

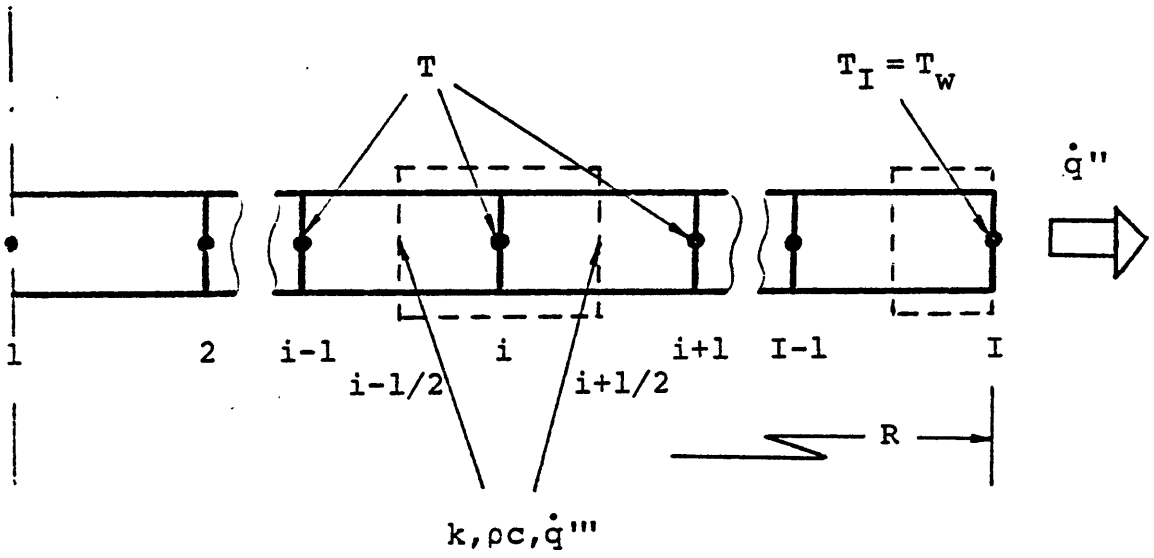

Figure 4.4 Discretized rod conduction

$$\frac{1}{2}[(r_i^2 - r_{i-1/2}^2)\ (\rho c)^n_{i-1/2} + (r_{i+1/2}^2 - r_i^2)(\rho c)^n_{i+1/2}]\ \frac{T_i^{n+1} - T_i^n}{\Delta t}$$

$$= -(\frac{rk^n}{\Delta r})_{i-1/2}\ (T_i^{n+1} - T_{i-1}^{n+1}) + (\frac{rk^n}{\Delta r})_{i+1/2}(T_{i+1}^{n+1} - T_i^{n+1})$$

$$+\frac{1}{2}[(r_i^2 - r_{i-1/2}^2)(\dot{q}'')^{n+1/2}_{i-1/2} + (r_{i+1/2}^2 - r_i^2)\ (q'')^{n+1/2}_{i+1/2}\ ] \qquad (4.42)$$

where $(\Delta r)_{i_{(\pm)1/2}} = r_{\substack{i+1 \\ (i)}} - r_{\substack{i \\ (i-1)}}$

At the center of the pin, this equation is modified by setting $r_1 = r_{1/2} = 0$, which is equivalent to integrating over the half cell extending from r = 0 to $r = r_{3/2}$. A modification is also required at the clad surface, i.e., for the last half cell of the rod. Setting $r_{I+1/2} = r_I = R$ (where R is the rod outer radius and I-1 is the number of mess cells) and adding to the right hand side the surface heat flux, $\dot{q}''$, Eq. (4.42) becomes:

$$\frac{1}{2}(r_I^2 - r_{I-1/2}^2)(\rho c)_{I-1/2}^n \frac{T_I^{n+1} - T_I^n}{\Delta t}$$

$$= -\left(\frac{rk^n}{\Delta r}\right)_{I-1/2} (T_I^{n+1} - T_{I-1}^{n+1})$$

$$-\dot{q}''R + \frac{1}{2}(r_I^2 - r_{I-1/2}^2)(\dot{q}''')_{I-1/2}^{n+1/2} \qquad (4.43)$$

The surface heat flux is a function of both the wall temperature ($T_w = T_I$) and the fluid temperature (T_f):

$$\dot{q}'' = h(T_w - T_f) \qquad (4.44)$$

where h = heat transfer coefficient. If the fluid temperature is known at this point and the heat transfer coefficient is evaluated explicitly, then the wall temperature may be treated either explicitly, i.e.,

$$(\dot{q}'')^n = h^n(T_w^n - T_f^n) \qquad (4.45a)$$

or implicitly, i.e.,

$$(\dot{q}'')^{n+1/2} = h^n(T_w^{n+1} - T_f^n) \qquad (4.45b)$$

In either case, the discrete conduction problem can be cast in matrix form:

$$\bar{\bar{A}}\ \bar{T}^{n+1} = \bar{b} \tag{4.46}$$

where: $\bar{\bar{A}}$ is a tridiagonal matrix,

$\bar{T} = (T_1, \ldots, T_i, \ldots, T_w)^T$, and

$\bar{b}$ contains contributions from the volumetric heat source, the old time temperatures and the surface heat flux.

The solution of (4.46) is easily accomplished by a direct forward elimination--backward substitution procedure. The reader should note that for steady-state conduction one must use the boundary heat flux in the form (4.45b), otherwise matrix $\bar{\bar{A}}$ would be singular. Physically, under steady-state conditions, the heat generation rate and the surface heat flux cannot be independently specified. By treating it implicitly, the wall temperature will always adjust to render the surface heat flux consistent with the internal source.

4.3.3 Implicit Coupling to the Fluid Energy Equation

The explicit or semi-implicit treatment of the wall heat flux may give rise to instabilities under some circumstances, characterized by a high heat transfer coefficient and/or a low heat capacity of the clad or the fluid. This undesirable behavior can be corrected by a reduction in time step size. In some applications,

this additional limitation on the time step size would significantly increase the computational cost. Fortunately, a method described in [2] eliminates this restriction by providing an implicit coupling between the wall and the fluid. This method, adapted to our thermal equilibrium two-phase flow model, will be presented below.

In the following discussion, an explicit evaluation of the heat transfer coefficient is assumed. An implicit treatment of the surface heat flux

$$(\dot{q}")^{n+1} = h^n \, (T_w^{n+1} - T_f^{n+1}) \tag{4.47}$$

allows us to re-write Eq. (4.43) as:

$$a_{I,I-1} \, T_{I-1}^{n+1} + a_{I,I} \, T_w^{n+1} = h^n T_f^{n+1} + \ldots \tag{4.48}$$

where the expressions for the coefficients a's can be readily inferred by comparision with Eq. (4.43). Eq. (4.48) is just the last equation in the system of equations (4.46). Following the forward elimination, Eq. (4.48) becomes:

$$a'_{I,I} \, T_w^{n+1} = h^n T_f^{n+1} + \ldots \tag{4.49}$$

Clearly this is a linear equation, relating the wall surface temperature to the temperature of the fluid at that particular axial level.

Formally, at this stage, we can eliminate the wall temperature in favor of the fluid temperature and proceed to the solution of the fluid dynamics equations. Once the new fluid temperature is obtained, the new wall temperature is calculated and then the backward substitution is performed to get the remaining new rod temperatures (at the interior points).

In this method, the surface heat flux is, therefore, a function only of the fluid temperature, directly and indirectly via the wall temperature. With this observation in mind we can now show in detail the expressions for the derivatives of the heat flux, needed in the fluid dynamics solution (see Eqs. (4.27c) and (4.27d)). Denoting wall heat transfer area by A_w, the wall heat source is simply:

$$Q_w = A_w \dot{q}'' \tag{4.50}$$

Its derivatives with respect to the main fluid dynamics variables, p and e_m are:

$$\frac{\partial Q_w}{\partial p} = \left(\frac{\partial Q_w}{\partial T_f} + \frac{\partial Q_w}{\partial T_w} \cdot \frac{dT_w}{dT_f}\right) \left(\frac{\partial T_f}{\partial p}\right)_{e_m} \tag{4.51a}$$

$$\frac{\partial Q_w}{\partial e_m} = \left(\frac{\partial Q_w}{\partial T_f} + \frac{\partial Q_w}{\partial T_w} \cdot \frac{dT_w}{dT_f}\right) \left(\frac{\partial T_f}{\partial e_m}\right)_p \tag{4.51b}$$

where, from Eqs. (4.47) and (4.50)

$$\frac{\partial Q_w}{\partial T_f} = - A_w h^n = - \frac{\partial Q_w}{\partial T_w} \tag{4.52a}$$

and from Eq. (4.49)

$$\frac{dT_w}{dT_f} = \frac{h^n}{a'_{I,I}} \tag{4.52b}$$

The derivative dT_w/dT_f provides the feedback effect of a change in T_f^{n+1} on T_w^{n+1}. It can be easily verified that for steady-state conduction, the wall heat source derivatives correctly reduce to zero.

The only penalty of the method is the necessity to provide extra storage space to hold the intermediate results of the rod conduction problem following the forward elimination stage. For practical applications, this represents only a very modestincrease in the overall storage requirements.

A further refinement is possible with only a slight increase in complexity. Namely, if h is a strong function of T_w and/or T_f, the method can be modified to treat h implicitly too.

4.4 The Numerical Method for Hexagonal Can Conduction

In this section we shall describe the numerical treat-

ment of the conduction in the can surrounding the fuel assembly. Most of the discussion in the previous section also pertains to the material herein, therefore, we will limit ourselves to presenting only those aspects which are different.

4.4.1 Choice of Treatment

Recalling the model description (Chapter 3), we consider only the radial conduction, with no internal heat sources:

$$\rho c \frac{\partial T}{\partial t} - \frac{1}{r} \frac{\partial}{\partial r} (rk \frac{\partial T}{\partial r}) = 0 \qquad (4.53)$$

where all the quantities have already been defined in connection with Eq. (4.41).

Once again a fully implicit treatment is selected for reasons already elaborated on in Section 4.3.1.

4.4.2 Difference Equations

The finite difference equation for the internal nodes is identical to that derived in Section 4.3.2, (Eq. (4.42), with no heat source. At the surface of the can exposed to the environment an equation analogous to Eq. (4.43) is obtained. We have to write a similar equation for the inner can surface, exposed to the coolant. Such an equation is obtained by integrating over the half cell extending from r_1 = inner radius to $r = r_{3/2}$:

$$\frac{1}{2}\,(r_{3/2}^2 - r_1^2)\,(\rho c)_{3/2}^n\,\frac{T_1^{n+1} - T_1^n}{\Delta t}$$

$$= + \left(\frac{rk^n}{\Delta r}\right)_{3/2} (T_2^{n+1} - T_1^{n+1})$$

$$-(\dot{q}''\ R)_{inner} \qquad (4.54)$$

A few comments on the surface heat flux treatment are in order. For the outer surface, the environment temperature (T_{env}) is given and an expression similar to Equation (4.45b) is used:

$$(\dot{q}'')_{outer}^{n+1} = h_{w,outer}^n\ (T_{w,outer}^{n+1} - T_{env}) \qquad (4.55)$$

For the inner surface we use an average sodium temperature, obtained by volume weighting the sodium temperatures in the cells adjacent to the hex can. An implicit treatment of this average sodium temperature would couple the above mentioned cells through the new time temperatures. Our numerical scheme for the fluid dynamics equations provides, however, for spatial coupling at the new time via pressures only. Consequently, the fluid temperature in the inner face heat flux is evaluated at the old time, i.e.,

$$(\dot{q}")^{n+1/2}_{inner} = h^{n}_{inner} (T^{n+1}_{w,inner} - T^{n}_{f}) \qquad (4.56)$$

Note that because of the explicit treatment of the fluid temperature, there will be no contribution to the Jacobian matrix. We have found this approach entirely adequate in all our applications.

4.5 The Numerical Method for Fluid Conduction

In this section we shall describe the numerical treatment of the cell-to-cell fluid conduction.

4.5.1 Choice of Treatment

The net rate of heat flow into a given fluid cell "i" due to diffusion effects is expressed as the sum of equivalent heat fluxes evaluated at the cell faces. Let us consider the face between cell "i" and its neighbor "j". The effective conduction heat flux at the face "ij" is

$$q_{ij} = A_{ij}\, h_{ij}\, (T_j - T_i) \qquad (4.57)$$

where

A_{ij} = open ("flow") area between cells "i" and "j"

h_{ij} = effective heat transfer coefficient (defined in Chapter 3).

Then the total heat flow into cell "i" (using the subscript k for "conduction") is:

$$Q_{k,i} = \sum_{j \neq i} A_{ij} h_{ij} (T_j - T_i) \qquad (4.58)$$

A fully implicit treatment would spatially couple the mesh cells through the temperature field. But as our numerical scheme for the fluid dynamics allows for spatial coupling at the new time via the pressure field only, this treatment cannot be applied. Therefore, we selected the other extreme, a fully explicit treatment for the effective conduction heat transfer. When the molecular conduction is greatly enhanced by turbulent mixing and the mesh cell size is small (true in our applications especially in the radial direction), this type of treatment may give rise to time step limitations more severe than the convective time step constraints. This is especially true for single-phase, relatively low flow conditions. To reduce the computational expenses in such situations, we provided a semi-implicit option, which displays unconditional stability. We will further discuss these aspects in the next section.

4.5.2 Difference Equations

The explicit treatment of the conduction heat flux leads simply, for a cell "i" to

$$Q^n_{k,i} = \sum_{j \neq i} A_{ij} h^n_{ij} (T^n_j - T^n_i) \qquad (4.59)$$

Obviously, there will be no contribution to the Jacobian matrix. Note also that this scheme assures strict conservation for the energy transferred by this mechanism, i.e.,

$$q_{ij}^{n} = - q_{ji}^{n} \tag{4.60}$$

This approach has an inherent stability limitation. Specifically, considering the conduction only in the transverse directions and assuming equal mesh spacings ($\Delta x = \Delta y$), the stability criterion which must be satisfied by the time step is:

$$\Delta t < \frac{(\Delta x)^2}{4\alpha} \tag{4.61}$$

where α = effective thermal diffusivity.

To circumvent this time step limitation within the framework of our numerical scheme, a semi-implicit formulation was also developed. Equation (4.59) is modified into a locally implicit form:

$$Q_{k,i}^{n+1/2} = \sum_{j \neq i} A_{ij} \, h_{ij}^{n} \, (T_j^{n} - T_i^{n+1}) \tag{4.62}$$

A stability analysis (see Chapter 6) indicates indeed unconditional stability. However, there is a penalty assoc-

iated with this formulation. Unlike the explicit one, the semi-implicit scheme does not conserve the energy transferred between adjacent cells. Indeed

$$q_{ij}^{n+1/2} = h_{ij}^{n} \, (T_j^n - T_i^{n+1}) \neq - h_{ij}^{n} \, (T_i^n - T_j^{n+1})$$

$$= - q_{ji}^{n+1/2} \qquad (4.63)$$

Obviously, the equality will be satisfied only when a steady-state is reached, i.e., $T_i^{n+1} = T_i^n$ for all i's. Therefore, the use of this scheme is recommended only for steady-state calculations. Actually, one might attempt its use in a very slow transient, but in this case the degree of energy conservation must be kept track of. In Chapter 6, we will provide some additional comments on this scheme.

The semi-implicit formulation provides a contribution to the jacobian matrix. First, re-write Eq. (4.62) as:

$$Q_{k,i}^{n+1/2} = - \Big(\sum_{j \neq i} A_{ij} \, h_{ij}^{n} \Big) T_i^{n+1}$$

$$+ \sum_{j \neq i} A_{ij} \, h_{ij}^{n} \, T_j^{n} \qquad (4.64)$$

Then, the derivatives of the conduction heat source with

respect to p and e_m are:

$$\frac{\partial Q_{k,i}}{\partial p} = - (Ah)_{k,i} \left(\frac{\partial T}{\partial p}\right)_{e_m} \tag{4.65a}$$

and

$$\frac{\partial Q_{k,i}}{\partial e_m} = - (Ah)_{k,i} \left(\frac{\partial T}{\partial e_m}\right)_{p} \tag{4.65b}$$

where $$(Ah)_{k,i} = \sum_{j \neq i} A_{ij} \, h^n_{ij} \tag{4.65b}$$

To avoid its repetitive calculation during the Newton iterations, the quantity $(Ah)_{k,i}$ is calculated and stored at the start of a new time step. The impact of the semi-implicit conduction formulation on the computational work per time step is insignificant.

4.6 Time Step Control

The description of the numerical methods would be incomplete without presenting the time step control strategy we have implemented in our computer code. Indeed, automatically determining the proper time step size constitutes an important consideration in our applications.

For our partially implicit method, two aspects are taken into account. First, the explicit treatment of

the convective and diffusive transport immediately imposes a stability condition. As shown in Chapter 6, the explicit convection leads to the following limitation:

$$\Delta t < \Delta t_{conv} = \min \left(\frac{1}{\Delta t_x} + \frac{1}{\Delta t_y} + \frac{1}{\Delta t_z}\right)^{-1} \qquad (4.66)$$

where the minimum is taken over the entire domain and

$$\Delta t_x = \frac{\Delta x}{|U_x|} \; ; \; \Delta t_y = \frac{\Delta y}{|U_y|} \; ; \; \Delta t_z = \frac{\Delta z}{|U_z|} \; .$$

For computing convenience and an additional margin of conservatism we actually calculate the minimum of each "directional" time steps, i.e., $\Delta t_x^{min} = \min(\Delta x/|U_x|)$ and similarly for Δt_y^{min} and Δt_z^{min}. Therefore,

$$\Delta t_{conv} = \left(\frac{1}{\Delta t_x^{min}} + \frac{1}{\Delta t_x^{min}} + \frac{1}{\Delta t_z^{min}}\right)^{-1} \qquad (4.67)$$

The reader should note that this limitation is more restrictive than the often used

$$\Delta t_{conv} = \min(\Delta t_x^{min}, \Delta t_y^{min}, \Delta t_z^{min}) \qquad (4.68)$$

Actually, this latter expression is incorrect when a multidimensional stability anaysis is performed. The two

expressions yield practically the same result if one directional limitation is much more severe than the others, for example $\Delta t_z << \Delta t_x$ and $\Delta t_z << \Delta t_y$. This situation is usually encountered in single-phase flow in a rod bundle, without blockages. However, when blockages are present or the flow becomes two-phase, the radial velocities are significant and in combination with the rather small radial mesh spacings may give rise to time step limitations comparable to or even more restrictive than that due to the axial flow. In such situations, clearly one must use Eq. (4.66) or (4.67).

The explicit treatment of energy diffusion places another restriction on the time step, as already mentioned. While it is perfectly feasible to calculte this time step size limit using the actual local properties, we decided to save some computational work by having a user-prescribed upper limit on the time step size, Δt^{max}, with the understanding that the diffusion-imposed restriction would be accounted for. This course of action is justified by the fact that currently only liquid conduction is considered and the rather weak variations of liquid properties (density, specific heat, conductivity) easily allow finding an appropriate upper bound. Consequently,

$$\Delta t = \min (\Delta t_{conv}, \Delta t^{max}) \tag{4.69}$$

The other aspect, often neglected, in time step control is accuracy. This consideration should be of major concern because

- our numerical scheme is only first order in time, and
- in two-phase flows, especially at low pressures, the main variables may change greatly over a time step whose size satisfies the stability criteria.

Consequently, it appears quite reasonable to place limits on changes in major variables over a time step. One should also note that limiting changes in velocities has a beneficial effect on stability. Indeed the time step limitation due to convection is determined based on old time velocities. If velocities change greatly over a time step an instability may result which will eventually destroy the solution (in fact, to further guard against such an occurrence, we apply a less-than-unity multiplier to Δt_{conv} obtained in (4.67)). Consider a quantity X whose changes over a time step are to be monitored. The actual relative changes are defined as

$$\Delta X_{actual} = (X^{n+1} - X^{n})/X^{n} \qquad (4.70)$$

Then imposing a maximum allowable change $\Delta X_{allowable}$, one can estimate the required time step from

$$\Delta t^{new} = (\Delta X_{allowable}/\Delta X_{actual})\ \Delta t^{old} \qquad (4.71)$$

This type of time step size adjustment may be applied in two ways:

a) at the end of the time step the actual relative changes are calculated and if found to exceed the allowable limits, then the advancement is repeated with the new time step given by (4.71);

b) similar to a), except that the advancement is not repeated but the adjustment given by (4.71) is used as an additional constraint on the time step size, in conjunction with Eq. (4.69), i.e.,

$$\Delta t = \min\ [\Delta t \text{ from } (4.69),\ \Delta t \text{ from } (4.71)]$$

Procedure (a) may be quite expensive as the severe non-linearities require at times numerous repetitions of the advancement. Procedure (b) is obviously cheaper by not actually enforcing the limits on changes but only attempting to. Both procedures have been implemented. The

quantities currently checked for maximum changes are pressure, mixture density and mixture internal energy.

Finally, an additional time step control is provided to remedy various error conditions that may be encountered. When an error condition occurs, the time step size is repeatedly halved until either the error disappears or a minimum (user supplied) time step size is reached. In this latter case, the calculation is stopped.

4.7 REFERENCES

1. R.D. Richtmayer and K.W. Morton, Difference Methods for Initial Value Problems, Interscience-Wiley (1967).

2. J. Loomis, W.H. Reed, A. Schor, H.B. Stewart, L. Wolf, THERMIT: A Computer Program for Three-Dimensional Thermal Hydraulic Analysis of Light Water Reactor Cores, EPRI NP-2032 (1981).

3. F.H. Harlow and A.A. Amsden, A Numerical Fluid Dynamics Calculation Method for All Flow Speeds, J. Comp. Phys.,8 (1971).

4. S. Patankar, Numerical Heat Transfer and Fluid Flow, Hemisphere (1980).

5. W.T. Sha·and B.T. Chao, Conservation Equations for Finite Control Volume Containing Simple-Phase Fluid with Fixed, Dispersed Heat Generating (or Absorbing) Solids, ANL-CT-79-42 (1979).

6. T.D. Ramshaw and J.A. Trapp, A Numerical Technique for Low-Speed Homogeneous Two-Phase Flow with Sharp Interfaces, J. Comp. Phys., 21 (1976).

7. L.D. Cloutman, C.W. Hirt, N.C. Romero, SOLA-ICE: A Numerical Solution Algorithm for Transient Compressible Fluid Flows, LA-6236 (1976).

8. T. Ortega and W. Rheinboldt, Iterative Solution of Nonlinear Equations in Several Variables, Academic Press (1970).

9. R. Varga, Matrix Iterative Analysis, Prentice-Hall (1962).

CHAPTER 5. THE PRESSURE FIELD SOLUTION

5.1 Introduction

In the previous chapter we have described a class of numerical methods for the solution of the fluid dynamics equations. A key feature of the methods (or variations thereof) is the obtaining of a pressure field problem. Indeed this pressure problem is characteristic of many currently used numerical schemes. The pressure field incorporates both the spatial coupling (due to fluxes of mass, momentum and energy) and, through a reduction process (described in the previous chapter), the local coupling. After its solution, the pressure is then used to infer all the other relevant quantities. When it is part of a nonlinear solution scheme (such as ours) the pressure field has to be determined repeatedly within each time step.

Thus it becomes quite clear that the efficient and accurate solution of the pressure field is fundamental to our method. In this chapter we will present a number of schemes that were investigated. Additional aspects relevant to our numerical method will be examined. Finally the implementation of various boundary conditions will be discussed.

5.2 Derivation of the Differential Pressure Field Equations from the Mass and Momentum Conservation Equations.

When the pressure field problem was derived, the reader will recall that basically we manipulated a sequence of finite difference equations. That derivation may have obscured the actual origin of the pressure problem. In the following we would like to show that the discrete pressure problem is actually the analog of a partial differential equation.

For simplicity let us consider the case of a one-dimensional, barotropic flow. The appropriate equations are:

$$\partial\rho/\partial t + \partial(\rho u)/\partial x = 0 \tag{5.1}$$

$$\partial(\rho u)/\partial t + \partial(\rho uu)/\partial x + \partial p/\partial x = F \tag{5.2}$$

$$\rho = \rho(p) \tag{5.3}$$

Differentiating eq.(5.1) with respect to time, taking into account the commutativity of the temporal and spatial differentiation and substituting eq.(5.2) yields

$$\partial^2\rho/\partial t^2 - \partial^2 p/\partial x^2 = \partial^2(\rho uu)/\partial x^2 - \partial F/\partial x \tag{5.4}$$

Let $c^2 = \partial\rho/\partial\rho$. Then eq.(5.4) may be written as

$$c^{-2}\partial^2 p/\partial t^2 - \partial^2 p/\partial x^2 = \partial^2(\rho uu)/\partial x^2 - \partial F/\partial x \qquad (5.5)$$

If the right-hand-side of eq.(5.5) were known, the above would be simply a hyperbolic equation for pressure.

One could use eq.(5.4) or (5.5) to derive a finite difference analog. What we will show is the correspondence between the pressure equation obtained as a result of our differentiation scheme and the differential equation (5.4 or 5.5) obtained above. Consider our familiar staggered mesh arrangement (Fig. 5.1). Let $G = \rho U$ and $conv = \partial(\rho UU)/\partial x$. Then the finite difference analogs of the mass and momentum equations are (in our scheme):

$$\frac{1}{\Delta t}(\rho_i^{n+1} - \rho_i^n) + \frac{1}{\Delta x}(G_+^{n+1} - G_-^{n+1}) = 0 \qquad (5.6)$$

$$\underset{(-)}{\frac{1}{\Delta t}}(\underset{(-)}{G_+^{n+1}} - \underset{(-)}{G_+^n}) + \underset{(-)}{conv_+^n} + \underset{(i)}{\frac{1}{\Delta x}}(\underset{(i)}{p_{i+1}^{n+1}} - \underset{(i-1)}{p_i^{n+1}}) = \underset{(-)}{F_+^n} \qquad (5.7)$$

Substituting the two momentum equations (for the - and + cell boundaries) into the mass equation for cell (i) results in:

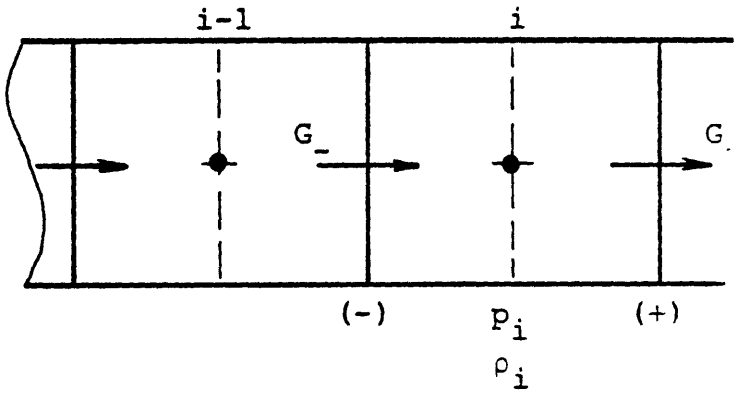

Figure 5.1 Staggerred mesh for the momentum equations.

$$\frac{1}{\Delta t^2}(\rho_i^{n+1} - \rho_i^n) + \frac{1}{\Delta t \Delta x}(G_+^n - G_-^n) - \frac{1}{\Delta x^2}(p_{i+1}^{n+1} - 2p_i^{n+1} + p_{i-1}^{n+1})$$

$$= \frac{1}{\Delta x}(conv_+^n - conv_-^n) - \frac{1}{\Delta x}(F_+^n - F_-^n) \qquad (5.8)$$

Writing equation (5.6) for the n-th time level gives:

$$\frac{1}{\Delta t}(\rho_i^n - \rho_i^{n-1}) = -\frac{1}{\Delta x}(G_+^n - G_-^n) \qquad (5.9)$$

Substituting eq.(5.9) into eq.(5.8) finally yields:

$$\frac{1}{\Delta t^2}(\rho_i^{n+1} - 2\rho_i^n + \rho_i^{n-1}) - \frac{1}{\Delta x^2}(p_{i+1}^{n+1} - 2p_i^{n+1} + p_{i-1}^{n+1})$$

$$= \frac{1}{\Delta x}(conv_+^n - conv_-^n) - \frac{1}{\Delta x}(F_+^n - F_-^n) \qquad (5.10)$$

The perfect equivalence between eq.(5.10) and eq.(5.5) is easily noted.

Density appears in eq.(5.10) at three time levels. To avoid storing quantities at three time levels one actually uses eq.(5.8). It is in this latter form that we cast our pressure field problem.

To continue our discussion let us eliminate the density in favor of the pressure, using the equation of state in the

form:

$$\rho_i^{n+1} - \rho_i^n = \frac{1}{c^2}(p_i^{n+1} - p_i^n) \tag{5.11}$$

Substitute eq.(5.11) into eq.(5.8):

$$(\Delta t^2/\Delta x^2)\{-p_{i-1}^{n+1} + [2+(\Delta x/c\Delta t)^2] - p_{i+1}^{n+1}\} = (1/c^2)p_i^n$$

$$-(\Delta t/\Delta x)(G_+^n - G_-^n) + (\Delta t^2/\Delta x)[(conv_+^n - conv_-^n)$$

$$-(F_+^n - F_-^n)] \tag{5.12}$$

The right-hand-side of the above equation contains only old-time quantities; we have indeed an equation for the new pressure.

It is interesting to note the dependency of the right-hand-side of the pressure equation on the time step. Indeed the right-hand-side varies parabolically with Δt. Thus while the variation is continuous, it is not monotonic. This has an important effect on our non-linear solution. At times, in order to achieve convergence, the "solution" must be brought closer to the guess. This, in principle, is achieved by a reduction of the time step. In the limit of $\Delta t \to 0$, it is easily seen that eq.(5.12) reduces to

$$p_i^{n+1} = p_i^n$$

provided c is finite. However, an initial reduction in time step may lead to an increase in the right-hand-side. To accomplish a reduction in the right-hand-side a rather significant reduction in time step may sometimes be necessary. We have actually noted this behavior in our two-phase flow calculations. The term responsible for this behavior is the second one in the right-hand side of eq.(5.12). Recalling eq.(5.9), one immediately notes that this term is really a "measure" of compressibility.

For single-phase liquid this term is very small, being rather a measure of mass conservation. For a well-converged pressure field, this term is negligible. In contrast, in two-phase flow, especially at low pressures, the high density variations and the difficulty to conserve mass very tightly combine to make this term dominant.

5.3 Solution of the Pressure Field in Subassembly-like Geometries -- Specific Aspects

The spatial grid associated with a reactor fuel assembly usually features a rather large aspect ratio, that is the mesh spacing in one direction is significantly larger than in the other direction(s). Indeed to provide adequate resolution transversely one chooses a mesh size on the order of the fuel pin pitch. In contrast the mesh spacing in the

axial direction is usually significantly larger (say be a factor of 5 to 20) for reasons of computational cost and/or storage limitation. This situation has an important consequence regarding the application of iterative schemes to the pressure field solution. We shall look at this in detail for the remainder of this section.

Consider again the finite difference representation of the mass and momentum equations (eqs. 5.6 and 5.7). As a refinement let us treat the distributed resistence semi-implicitly (as in the previous chapter) in the form:

$$F^{n+1}_{\substack{+\\(-)}} = -K^{n}_{\substack{+\\(-)}}\, G^{n+1}_{\substack{+\\(-)}} \tag{5.13}$$

where $K^n = fn(G^n,...)$.

From (5.7) and (5.13) one then obtains an expression for the advanced mass flux, G^{n+1}, in terms of the advanced pressures and other old time quantities:

$$G^{n+1}_{\substack{+\\(-)}} = G^{n}_{\substack{+\\(-)}} - \frac{\Delta t}{\Delta x(1+\Delta t K)} \left(p^{n+1}_{\substack{i+1\\(i)}} - p^{n+1}_{\substack{i\\(i-1)}}\right) - \frac{\Delta t}{1+\Delta t K}\, conv^{n}_{\substack{+\\(-)}} \tag{5.14}$$

Substituting eq.(5.14) into eq.(5.6) and using (eq.5.11) results in an equation similar to eq.(5.12):

$$\frac{\Delta t^2}{\Delta x^2}\left\{ -\frac{1}{1+\Delta tK} p_{i-1}^{n+1} + \left[\frac{2}{1+\Delta tK} + \left(\frac{\Delta x}{c\Delta t}\right)^2\right] p_i^{n+1} - \frac{1}{1+\Delta tK} p_{i+1}^{n+1} \right\}$$

$$= \frac{1}{c^2} p_i^n - \frac{\Delta t}{\Delta x}(G_+^n - G_-^n) + \frac{\Delta t^2}{\Delta x(1+\Delta tK)}(conv_+^n - conv_-^n) \qquad (5.15)$$

The off-diagonal elements in the matrix corresponding to the pressure equation are therefore

$$a_{\substack{ij \\ (j\neq i)}} = -\frac{\Delta t^2}{\Delta x^2(1+\Delta tK)}$$

Thus for a given time step, a_{ij} is inversely proportional to the square of the mesh spacing.

Our derivation of the pressure equation (5.15) can be very easily extended to two- and three-dimensions. Consider a two-dimensional problem with Δz and Δx the axial and the transverse mesh spacings, respectively. In this case, the off-diagonal elements of the matrix associated with the pressure problem are

$$a_{iz} = -\frac{\Delta t^2}{\Delta z^2(1+\Delta tK_z)} \text{ and } a_{ix} = -\frac{\Delta t^2}{\Delta x^2(1+\Delta tK_x)}$$

Their ratio is then:

$$\frac{a_{ix}}{a_{iz}} = \frac{\Delta z^2}{\Delta x^2} \cdot \frac{1+\Delta t K_z}{1+\Delta t K_x} \qquad (5.16)$$

Assume for the moment $K_z \cong K_x$; then for an aspect ratio $\Delta z/\Delta x$ of, say, 10, the ratio of the off-diagonal elements is equal to 100. We note thus a much stronger transverse "coupling". But this is not the whole story. Assuming a Blassius-type expression for the friction coefficient, i.e., $f = aRe^b$ (with $b \cong -0.2$) it is easy to see that $K \sim G^{1-b}$. Thus for the usual values of b, K varies almost linearly with G. Now in assembly-like geometries the axial velocities are much larger than the radial ones, therefore in general K_z is significantly larger than K_x. This additional effect further increases the ratio a_{ix}/a_{iz}.

The conclusion is that for assembly-like geometries and usual spatial grid selection, the transverse pressure coupling is much stronger than the axial one. In other words a pressure perturbation in a transverse neighbor will have a much greater effect than a similar perturbation occurring in an axial neighbor. The recognition of this aspect of the pressure field problem is crucial to constructing an efficient iterative scheme.

5.4 Direct Methods

In recent years the direct methods of solution for simultaneous linear algebraic equations have reached a very

high level of maturity. The technical commumity has now at its disposal a number of highly sophisticated mathematical software packages [1,2,3,4] containing extensive capabilities in linear algebra. Indeed the user will find a wide availability of algorithms from which he has to judiciously select those best suited to his problem. More specifically the subprograms he chooses must perform optimally with regard to economy and reliability as modules in the overall computational scheme.

That today we have highly reliable direct linear equation solvers is due to no small extent to Wilkinson's seminal work on rounding errors [5]. Excellent discussions of modern schemes are given in [6] and [7]. Additional theoretical background can be found in [8,9,10]. All these works are only a few from a very rich field.

The relevance of the direct methods to our pressure problem is two-fold. First they can be used for moderately sized problems as complete solvers for the pressure field. Second a direct method can be used as a part of an overall block iterative scheme, for large problems. Of course what is moderately sized and what is large is somewhat arbitrary depending to a great extent on the particular computing environment. Later in this chapter we shall provide additional comments regarding the choice of direct vs. iterative methods for the pressure field solution.

5.4.1 General Band Matrices

In the previous chapter we showed that if the convective terms in both the mass and energy equations are treated semi-implicitly, the resulting matrix for the pressure problem is non-symmetric but still diagonally dominant (for some time step size). In our scheme each cell is spatially coupled to at the most six neighbors, therefore the matrix has a seven-stripe structure. Such matrix is called a band matrix. Let 2m+1 be the band width; then $a_{ij} = 0$ if $|i-j| > m$. Let the rank of the matrix be n. The concept of a band matrix is useful only if m is appreciably smaller than n. By taking advantage of the band structure a linear equation solver can save both time and storage. Space is saved because only the elements between the leftmost and the rightmost stripes are stored. Note that space must be provided even for the zero elements located in between these outermost stripes. This is because of the "fill-in" process typical of the Gauss elimination. Fortunately for irreducibly diagonally dominant matrices row interchanges [i.e., pivoting] are not necessary [6]. Consequently the "fill-in" is limited to within the outermost stripes and the resulting LU decomposition will have the same bandwith as the original matrix. As a result the storage requirement is (2m+1)n locations, compared with n for a full matrix.

Using the band structure of L and U saves time also. The purpose of Gaussian elimination is to reduce the number

of unknowns in each equation. For a band matrix, the number of unknows in each equation is small to begin with, and therefore the reduction to triangular form takes less time. In fact, the decomposition involves roughly nm^2 multiplications, compared with $n^3/3$ for a full matrix.

To illustrate these concepts consider the following 5x20 grid (Fig. 5.2). In this example n=100 and m=5. (Note that if instead of row-by-row ordering one chose ordering by columns, m would be 20; clearly that ordering which leads to the minimum band width must be chosen.) Storing the matrix in band form requires (2x5+1)x100 = 1100 locations compared with $100^2 = 10^4$ for a full matrix. As far as the time is concerned, the decomposition for this band matrix involves approximately $100 \times 11^2 = 10^4$ multiplictions versus $100^3/3 = 10^6/3$ if full. Clearly the savings in both time and space are substantial. Note that in one-dimensional cases m=1 and the matrix becomes tridiagonal. In this case the direct solution is very economical, requiring only 3n locations of storage and involving a number of operations on the order of n.

5.4.2 Positive Definite Band Matrices

When the convective terms in the energy equation are treated explicitly we have shown that the resulting matrix for the pressure problem is a Stieltjes matrix (i.e., symmetric, positive definite and with non-positive

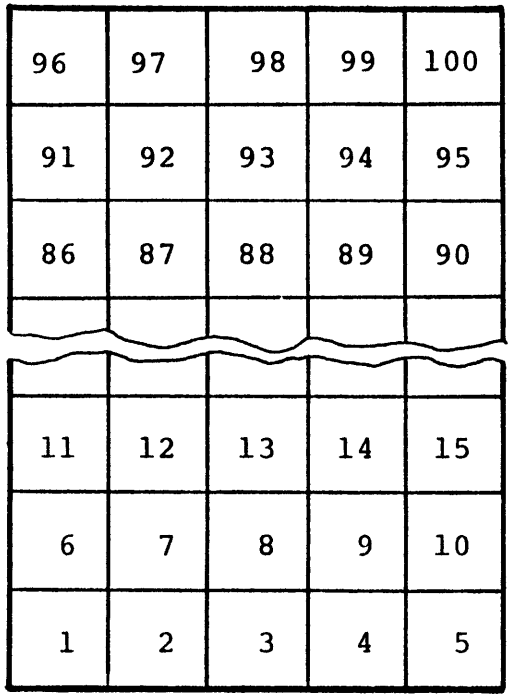

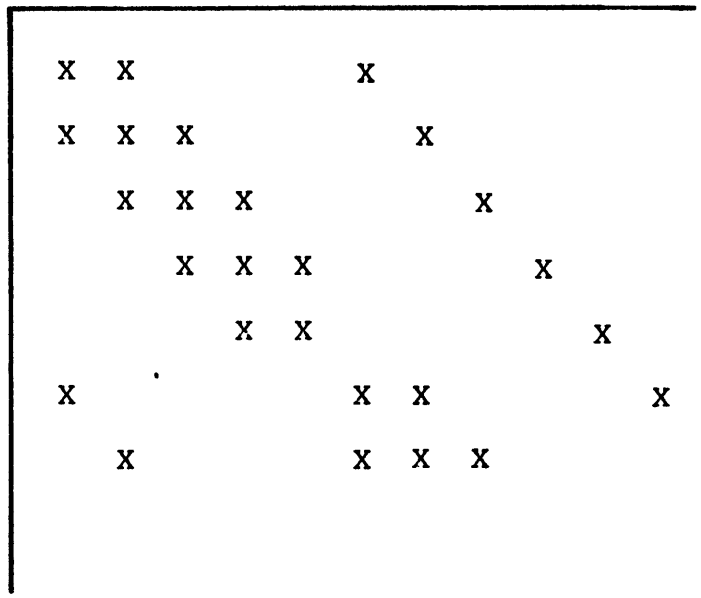

Figure 5.2 Two-dimensional grid and associated matrix structure.

off-diagonal entries [12]). For symmetric positive definite matrices there exists a modification of the Gauss elimination which preserves symmetry (see [6], [8], [11]). This algorithm is called Cholesky's method (Fadeev and Fadeeva [9] call it the square root method). The method consists of a special decomposition, of the form:

$$A = LL^T.$$

The main virtues of this algorithm are:

- no necessity for pivoting,
- only slightly over half of the matrix must be stored (i.e., (m+1)n) due to symmetry.

Its only disadvantage (small on modern computers) is the necessity of calculating n square roots. Overall, for positive definite symmetric matrices this is the algorithm of choice. Its efficiency and economy of storage make possible its use in fairly large problems.

5.5 Iterative Methods

The discretization of a wide range of problems in physics and engineering leads to large systems of linear algebraic equations characterized by very sparse matrices. By limiting the spatial coupling for a cell to only its immediate neighbors, the usual low order finite difference approximations produce only a few non-zero entries in each row of the resulting matrix. Indeed this is one major factor favoring low order approximations over higher order

ones, the latter yielding potentially greater accuracy but at the some time unacceptable cost of "filling in" the matrix by adding non-zero entries.

In the previous section we described how this sparseness is taken advantage of in dealing with band versus full matrices. We have also noted that the elimination process leads inherently to a certain amount of "fill-in". This is true even without the necessity for pivoting. Let 2s+1 be the number of stripes (i.e., the maximum number of non-zero entries in a row), 2m+1 be the band width and n be the rank of the matrix . Then if s<<m the additional storage required by the "fill-in" process is very substantial. Consider for illustration the following example. Let n_x, n_y and n be the number of grid points in the x-, y- and z-direction, respectively. Assume $n_x = 5$, $n_y = 6$, $n_z = 40$ and ordering by horizontal plane. In this case n = 1200, m = 30 and s = 3. The initial matrix requires (2s+1)n = 8,400 locations of storage. To provide for the fill-in during the elimination process the storage would have to be (2m+1)n = 73,200, thus an increase by a factor of about 9. For large three-dimensional problems this factor is about m/3.5. Note also that the number of operations involved increases rapidly.

From the foregoing it is clear that an optimum method would be one which preserves matrix sparseness and involves a relatively small total amount of operations. The

iterative methods automatically satisfy the first requirement, necessitating only relatively modest storage. To answer the second requirement is much more difficult. While it is true that due to sparseness, the number of operations per iteration is small, the number of iterations may be prohibitively large (for some acceptable level of accuracy), thus rendering the total operation count and therefore the computing time unacceptable. Indeed the challenge of the iterative methods in practical applications is to find adequate means of accelerating the basic scheme.

In this section we shall present a number of methods we have investigated as potential pressure field solvers for large problems.

5.5.1 Successive Block Overrelaxation (SBOR)

Relaxation methods are probably the best known and the most widely used among iterative methods. Indeed their use preceded the appearance of automatic computing machines. A summary of some of these methods especially as applied to manual computing can be found in [13]. However the impetus for extensive research was provided by the advent of digital computers. There exists a vast literature devoted to this subject. References will be made to more widely known works which through their approach and coverage have maintained their relevance. Excellent expositions of the subject are given by Varga [12], Forsythe and Wasow [14], Young [15],

and Wachspress [16], among others.

5.5.1.1 General considerations

We are seeking the solution of the matrix equation Ax = b, where A is a given non-singular nxn matrix. Following Varga [12], we consider expressing the matrix A in the form

$$A = M - N$$

where M and N are also nxn matrices. If M is non-singular, this represents a splitting of the matrix A and associated with it there is an iterative method

$$Mx^{(m+1)} = Nx^{(m)} + b, \quad m \geq 0 \tag{5.17}$$

or equivalently

$$x^{(m+1)} = M^{-1}Nx^{(m)} + M^{-1}b, \quad m \geq 0 \tag{5.17'}$$

If $M^{-1} \geq 0$ and $N \geq 0$ then $A = M - N$ is a regular splitting. Expressing now A as a matrix sum we have

$$A = D - L - U$$

where D is a diagonal (or block-diagonal) matrix and L and U are respectively strictly lower and upper triangular nxn matrices. If one chooses the following forms for M and N:

$$M = \frac{1}{\omega}(D-\omega L); \quad N = \frac{1}{\omega}[\omega U + (1-\omega)D]$$

then (5.17) gives the successive overrelaxation iterative method. The method is a "point" or a "block" method according to whether D is diagonal or block-diagonal. As shown in the previous chapter, A is a real, irreducibly di-

agonally dominant nxn matrix with $a_{ij} \leq 0$ for all $i \neq j$ and $a_{ii} > 0$ for all $1 < i < n$. It can be proved (Varga [12]) that if these requirements are met, then $A^{-1} > 0$. Therefore we can indeed construct the regular splitting mentioned above.

To fully construct the method, one has to decide on the actual splitting and to define a scheme for evaluating the optimum overrelaxation parameter. These aspects will now be addressed.

5.5.1.2 Choice of splitting

Considering a general three-dimensional case, the A matrix can be expressed in our case as a sum of one-stripe matrices:

$$A = - L_z - L_x - L_y + D_o - U_y - U_x - U_z$$

Here L_x and U_x, L_y and U_y, and L_z and U_z represent the spatial coupling in the x-, y- and z-direction, respectively and D_o is a diagonal matrix. We can now examine a few splitting schemes.

a) Point SOR

This scheme is obtained when

$$D = D_o; \; L = L_x + L_y + L_z; \; U = U_x + U_y + U_z$$

For our marginally diagonally dominant matrices (indeed for single-phase liquid, practically the diagonal dominance is

provided only by the pressure boundary condition, as shown later in this chapter), this method is much too slow. As shown in [12], going from a point to a block overrelaxation for two regular splittings of the same matrix leads to a higher convergence rate. This choice is successful if the increased convergence rate more than counterbalances the inherent increase in computational work per iteration.

b) Line SOR

For a very modest increase in computational effort but no additional storage, the line-SOR displays a greater convergence rate than (a). A natural choice for "lines" are the vertical (z) channels, especially so if the x-y domain is not rectangular (i.e., the boundaries in the x- or y- direction are irregular). The z-line SOR is obtained when

$$D = -L_z + D_o - U_z;\ L = L_x + L_y;\ U = U_x + U_y$$

As shown earlier in this chapter, the matrix entries corresponding to the z-direction are generally substantially smaller than those corresponding to the other two directions. As a result the convergence of this scheme proved to be unacceptably slow. The error decay curves for a number of ω's are shown in Fig. 5.3. The problem considered consisted of a 5x5x20 domain, single-phase liquid, with an aspect ratio $\Delta z/\Delta x$ of about 6 and $\Delta y \cong \Delta x$. The boundary conditions were inlet velocity - outlet pressure. As one can see, the asymptotic rate of convergence is very low, a

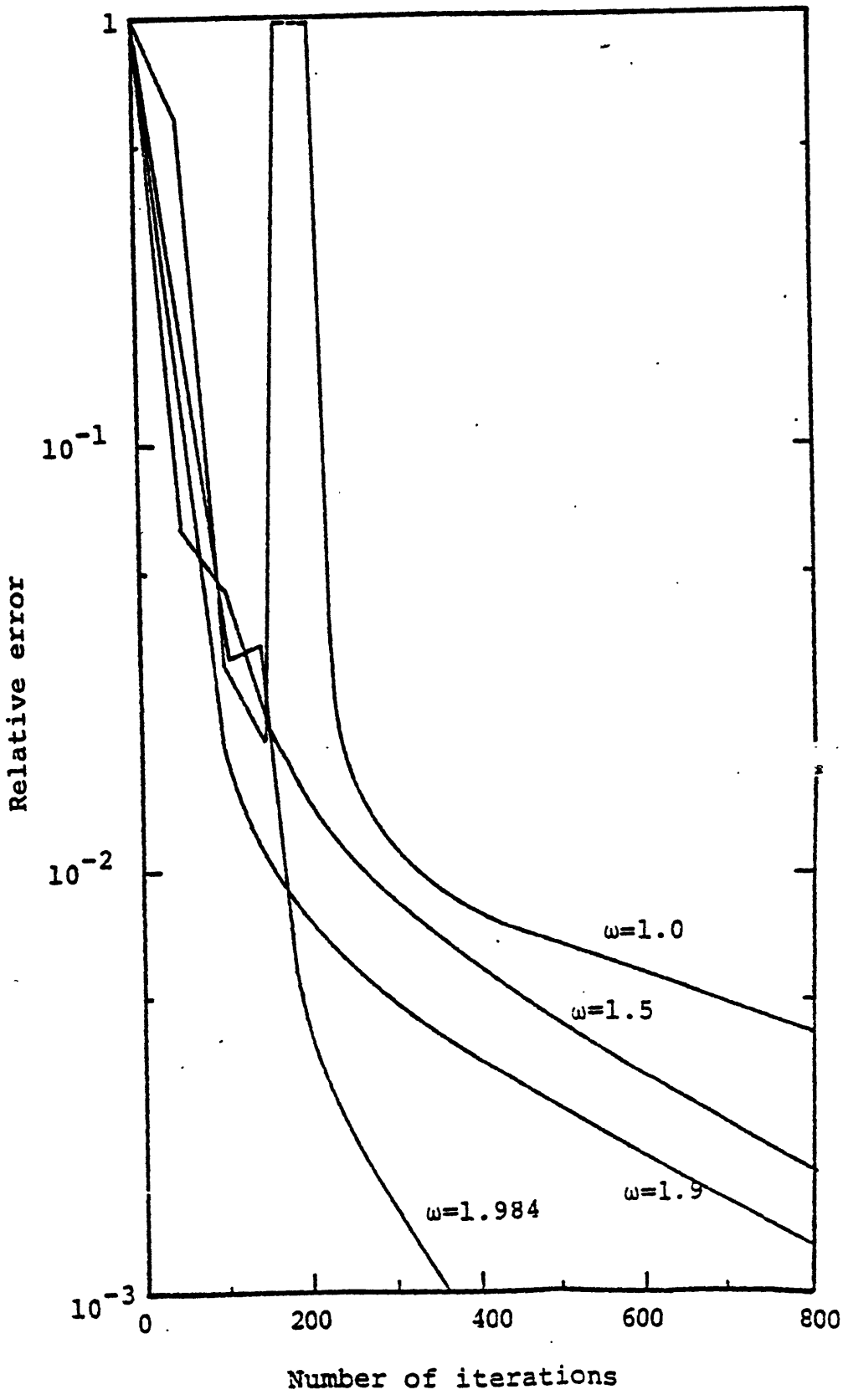

Figure 5.3 Comparison of Error Decay Rates for successive line over-relaxation.

great many iterations being required for adequate accuracy. (For the pressure problem a reasonable convergence criterion is $10^{-6} - 10^{-5}$.)

We should mention that while for our particular 3-D applications the line-SOR has not proved useful, the scheme may be entirely adequate for other problems. (Indeed we have successfully used the x-line SOR in 2-D problems.) We also note that we have tried a x-line SOR and a y-line SOR variant, with only marginal improvement over the z-line SOR.

c) Plane SOR

As indicated earlier, the matrix entries corresponding to the x- and y- directions are significantly greater than those corresponding to the z- direction (associated with the main flow). The strong pressure coupling in the horizontal (x-y) plane points therefore towards another splitting:

$$D = - L_x - L_y + D_o - U_y - U_x; \; L = L_z; \; U = U_z$$

In this scheme a direct inversion is performed for each horizontal plane successively as the three-dimensional grid is swept in the z-direction. A significant improvement in convergence rate over (b) is achieved (see Fig. 5.4). This gain however comes at the price of increased computational effort and storage. These aspects necessitate a more detailed examination.

Consider first the situation where the storage is at premium. The minimum storage requirement is 7n (for a

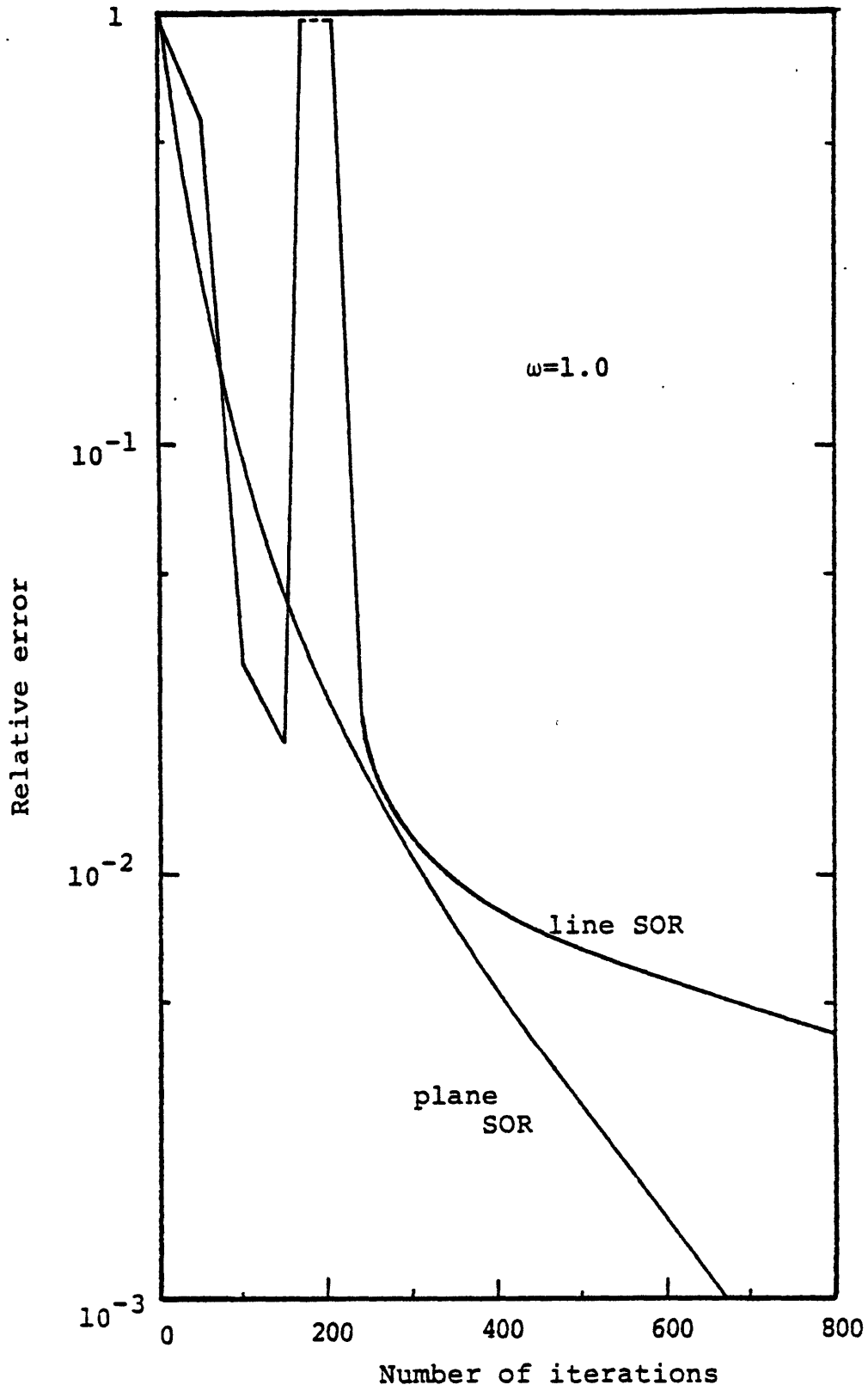

Figure 5.4 Comparison of Error Decay Rates for Line and Plane successive over-relaxation (unaccelerated).

seven-stripe matrix). The point and line SOR do not require any additional storage. The plane SOR however needs some extra storage, required by the direct solution in the x-y plane. The matrices corresponding to each plane are of five-stripe type. Assume $n_x < n_y$. To minimize the band width of these matrices one chooses an ordering scheme by row. The band width of these five-stripe matrices is then $2n_x+1$ and their rank is $n_x n_y$. Then each of these matrices require $(2n_x+1)n_x n_y$ locations. If we try to save on storage, then this amount of locations must be provided as "scratch pad" space. Relative to the base (i.e., $7n_x n_y n_z$) storage, the additional storage represents a fractional increase of $(2n_x+1)/7n_z$. For the example given at the beginning of this section (i.e., $n_x = 5$, $n_z = 40$) this additional storage is less than 4% of the base storage. For this very modest increase in storage a high price is paid in terms of computing work. What happens is that since we are providing storage for one "plane" matrix only, the LU decomposition must be performed over and over during each iteration. Even though the number of iterations required for a given accuracy is significantly reduced compared to that required by the line SOR, the large increase in computational work per iteration render any reduction in the total computing time marginal. Nevertheless, it must be said that this conclusion is based on our specific application. The performance of this storage saving implementation

of the plane SOR may be entirely satisfactory in other problems.

In our situation the main concern was the computing time. A very significant reduction in computing effort is achieved if storage is provided for all "plane" matrices. In this case the LU decomposition is performed only once, during the first iterative cycle and the L and U matrices are stored in place. During all the subsequent iterations, only a back-substitution is necessary. For the generally narrow bandwidths encountered in our problems, this back-substitution requires a computational effort not much greater than the corresponding process in the line SOR (note that in the line SOR implementation, this stored-in-place LU decomposition for the tridiagonal matrices involved was used).

In this implementation space must be provided for all "x-y" matrices and also, obviously, for the entries corresponding to the z-direction. The storage requirement is therefore $(2+(2n_x+1))n_x n_y n_z$. Compared to the base storage, this constitutes an increase by a factor of $(2+(2n_x+1))/7$. In our example (i.e., for $n_x = 5$) this factor is about 2. Taking into account that the base storage for the pressure matrix constitutes less than 10% of the total storage required by our numerical scheme, this increase in storage is quite modest.

It may be of interest to assess the storage requirement

for a fully direct solution. In our applications n_z is greater than both n_x and n_y. The minimum band width is achieved by a plane-by-plane numbering scheme, where a plane is composed of all the mesh cells at a certain z-level. In this case the band width is $(2n_xn_y+1)$ and the storage required is $(2n_xn_y+1)n_xn_yn_z$, representing an increase by a factor of $(2n_xn_y+1)/7$. In our example (i.e., $n_x = 5$, $n_y = 6$) this factor would be about 9. This is a very substantial increase, which nonetheless might be accomodated for a small problem. Again, "small" or "large" are characteristics very much dependent on the particular computing environment.

To conclude, our implementation of the plane SOR has proven very satisfactory in our applications.

5.5.1.3 Determination of the optimum overrelaxation parameter

In slowly converging problems finding a reliable and efficient accelerating scheme is evidently of primary importance. Perhaps the best known technique of increasing the convergence of an iterative scheme is the overrelaxation. The effectiveness of this technique is tied directly to the determination of the optimum overrelaxation parameter (ω).

If the eigenvalues of the associated Jacobi (i.e., simultaneous displacement) iterative matrix are real, then a theoretical foundation exists regarding the evaluation of this parameter. If the matrix involved is symmetric it can be shown [18] that this is indeed the case. For one variant

of our numerical scheme the resulting pressure matrix is not symmetric, therefore there is no certainty that the associated Jacobi iterative matrix will have real eigenvalues. Still we did apply the same technique for finding the accelerating parameter, the only justification being its success in our experience. It would probably be interesting to actually study the eigenvalue spectrum in this case, but this is no trivial task for the large matrices involved.

In general the methods of estimating the overrelaxation parameter fall into two categories:

a) a priori methods, with the objective of finding the spectral radius of the associated Jacobi or SOR iteration matrices, before actually starting the iteration process. These methods are very reliable, making possible a very accurate determination of the parameter. Their only and, unfortunately, major drawback is they are not economical. First, being iterative but usually not accelerated (such as Jacobi or Gauss-Seidel), they are slow, requiring a large number of iterations. Second, these iterations are performed (usually) with null right-hand-side, in which case they are "wasted" in as far as the solution to the actual matrix equation is concerned.

b) a posteriori methods, in which one starts the SOR iterations with some $\omega < \omega_{opt}$ and then obtains new estimates for ω based on the actual numerical results. The problem

here is that if at some point $\omega > \omega_{opt}$, the algorithm for further refining ω is no longer valid, because the eigenvalues of the SOR iteration matrix become complex.

Detailed discussions of some of these methods are given in [12,14,15,16]. In the following we will describe the scheme that we implemented for accelerating the SOR iteration.

The eigenvalues μ of the SOR matrix are related to those (λ) of the corresponding Jacobi matrix by

$$(\lambda + \omega - 1)^2 = \lambda\omega^2\mu^2 \qquad (5.18)$$

The optimum overrelaxation parameter (i.e., for which the spectral radius of the SOR matrix is minimum) is given by

$$\omega_{opt} = 2/\{1 + [1-\rho^2(B)]^{1/2}\} \qquad (5.19)$$

where $\rho(B)$ is the spectral radius of the associated Jacobi matrix. If one obtains an estimate for the spectral radius of the SOR matrix $\rho(L_\omega)$, then for some value of ω one can calculate $\rho(B)$ from eq.(5.18). To calculate the spectral radius one can use the displacement vector, i.e., the difference between the results of successive iterations:

$$d^{(m)} = x^{(m)} - x^{(m-1)}$$

Let $||d^{(m)}||$ be any norm. Then it can be shown that

$$\|d^{(m+1)}\|/\|d^{(m)}\| \underset{m\to\infty}{} \rho(L_\omega)$$

We have used the 1-norm, i.e., the sum of the absolute value of the components, due to its computing ease. Thus we estimate $\rho(L_\omega)$ from:

$$\rho(L_\omega) \approx \|d^{(m+1)}\|_1/\|d^{(m)}\|_1 \qquad (5.20)$$

This estimate and the associated ω update are performed every k iterations. The ω-updating algorithm is given below:

1) Start iterations with $\omega < \omega_{opt}$; if no better estimate is available $\omega = 1$ is used;
2) Every k iterations, obtain $\rho(L_\omega)$ from eq.(5.29), $\rho(B)$ from eq.(5.18) and a new ω from eq.(5.19);
3) Continue iterating with the new ω for another k iterations and then repeat step (2);
4) Stop the iterations when either the desired convergence or the maximum allowed number of iterations has been reached.

The only "degree of freedom" in the above procedure is the frequency of updating the overrelaxation parameter. Too seldom an update will lead to slow convergence. On the other hand, too frequent an update will yield a poor estimate for $\rho(L_\omega)$ by not allowing the higher harmonics to decay enough. It is very difficult to give general guidelines as to how to achieve the best compromise between these extremes. Usually some numerical experimentation will point

towards an adequate choice.

5.5.2 Alternating Direction Implicit (ADI)

In the mid-1950s, Peaceman and Rachford [18] and, shortly after, Douglas and Rachford [19] introduced a new method for the solution of parabolic equations. Given the analogy between an iterative process and a transient problem (extensively discussed in [12]), this new method was almost immediately applied to the iterative solution of elliptic equations. The ADI scheme belongs to the larger class of fractional step (or operator splitting) methods, a review of which is given by Yanenko [20]. A succinct but insightful discussion of the ADI method is presented in [21].

5.5.2.1 General considerations

Given the matrix equation $Ax = b$ one can construct an associated time-dependent problem

$$C\frac{dx}{dt} = - Ax + b \qquad (5.21)$$

where C is an arbitrary positive diagonal matrix. In the following we will consider $C = I$. One could then construct an implicit time-stepping scheme

$$\frac{x^{n+1} - x^{n}}{\tau} = - Ax^{n+1} + b \qquad (5.22)$$

With fixed boundary conditions and source, the steady-state solution of the above is just the solution of our original

equation. Note however that the solution of (5.22) involves a matrix inversion at every step. For three-dimensional problems A is a large seven-stripe matrix whose inversion is not trivial. The A matrix can be expressed as the sum of three matrices

$$A = A_x + A_y + A_z$$

each being associated with one spatial direction. After suitable permutations, each of these matrices is tridiagonal. If a scheme could be devised such that the time advancement be carried out in sub-steps, each involving only the inversion of a tridiagonal matrix, the result would be a potentially very efficient solution method. If in addition the time step could be viewed as an acceleration parameter and an optimum τ(or sequence of τ's) could be determined, we would have at our disposal a very powerful method, both in terms of computational effort per step as well as regarding the convergence rate. For the model problem (i.e., Laplace's equation on the unit square, with uniform mesh spacings and homogeneous boundary conditions), a number of ADI schemes, with optimal acceleration parameters, have been devised which display enormous gains in convergence over the SOR. Their theoretical analysis however generally imposes a very severe constraint, requiring that the spatial operators be commutative. The method has been applied nonetheless heuristically to more general

two-dimensional problems with mixed results [12].

5.5.2.2 Three-dimensional ADI iteration

The technical literature on ADI, while quite abundant on 2-D applications, is very scarce when dealing with 3-D problems. One reason for this is the fact that some ADI schemes cannot be properly extended from 2-D to 3-D applications, as they lose their unconditional stability and/or consistency [20]. Nevertheless there are a few 3-D ADI schemes and we chose Douglas' variant [22] for further investigation.

As applied to eq.(5.21), this scheme is:

$$\frac{1}{\tau}(x^{n+1/3} - x^n) = -\frac{1}{2}A_x(x^{n+1/3} + x^n) - A_y x^n - A_z x^n + b \qquad (5.23a)$$

$$\frac{1}{\tau}(x^{n+2/3} - x^n) = -\frac{1}{2}A_x(x^{n+1/3} + x^n) - \frac{1}{2}A_y(x^{n+2/3} + x^n) - A_z x^n + b \qquad (5.23b)$$

$$\frac{1}{\tau}(x^{n+1} - x^n) = -\frac{1}{2}A_x(x^{n+1/3} + x^n) - \frac{1}{2}A_y(x^{n+2/3} + x^n) - \frac{1}{2}A_z(x^{n+1} + x^n) + b \qquad (5.23c)$$

After eliminating the intermediate steps, the scheme reduces to

$$\frac{1}{\tau}(x^{n+1} - x^n) = \frac{1}{2}A(x^{n+1} + x^n) + b - O(\tau^2) \qquad (5.24)$$

Thus up to a term of the same order of magnitude as the truncation error (in time), this scheme is analogous to the well-known Crank-Nicholson's scheme.

The scheme (5.23) can be re-arranged for computational ease. Let

$$B_i = I + \frac{\tau}{2} A_i, \quad i = x,y \text{ or } z.$$

$$u^{n+\ell/3} = x^{n+\ell/3} - x^n, \quad \ell = 1,2,3.$$

Note that $x^{n+\ell/3} + x^n = u^{n+\ell/3} + 2x^n$. Eq.(5.23) can now be re-written as:

$$B_x u^{n+1/3} = -\tau A x^n + \tau b \qquad (5.25a)$$

$$B_y u^{n+2/3} = u^{n+1/3} \qquad (5.25b)$$

$$B_z u^{n+1} = u^{n+2/3} \qquad (5.25c)$$

$$x^{n+1} = u^{n+1} + x^n \qquad (5.25d)$$

Obviously in this form the scheme is much more economical. To reduce the computational work per iteration, the B

matrices must be decomposed and stored. In principle A can be reconstructed every time from the B's. If the B's are already decomposed that would involve a substantial computational effort. Thus for efficiency one would have to store A also, in its original form. Additional storage is required for the vector u. As expected, computational savings come at some cost in storage.

We have implemented the ADI scheme in the form of eq.(5.25) and used it as an iterative pressure solver. A sensitivity study using τ as an acceleration parameter was performed. The results generally display a behavior much like the line SOR (for varying ω).

Overall our experience with the ADI scheme has been disappointing. Its convergence rate was strongly dependent on the choice of τ, but even for the optimum (determined by trial and error) it was no better than the line SOR with optimum ω. Note also that the computational work per iteration, even in our highly optimized implementation, is still greater than for the line SOR. Because of the above reasons (and, to a lesser extent, the increased storage) our conclusion was that the 3-D ADI was not a viable candidate as an iterative pressure problem solver for our applications.

5.5.3 Coarse Mesh Rebalancing (CMR)

The methods belonging to this class are of more recent vintage, their use having become more widespread in the late

60s and during the 70s. Some of the ideas involved can be found however in earlier works, for example Kellogg and Noderer [23] and Kopp [26]. Wachspress [16] described such a scheme calling it "variational acceleration." Nakamura [17] applied a CMR method to a variety of problems in reactor physics, fluid mechanics and structural analysis and studied some of its theoretical aspects. Brandt [25] has also used and analyzed a CMR method extensively.

As it will be later seen, this class of methods belongs to a larger category known as the weighted residual methods (WRM). What one basically does when solving a problem by such a method is attempt to find a "weaker" solution. For example, instead of finding a solution satisfying a certain equation in a pointwise sense, a solution is sought that satisfies that equation in an integral sense.

The CMR methods are used to find corrections to a solution obtained by some other means in order to accelerate an iterative process or, at times, to improve the conservation of a physical quantity (for instance, mass) within some (relatively) large subdomain.

5.5.3.1 General considerations

Basically, one can divide the CMR methods according to the type of corrections they yield, namely:

- multiplicative, or
- additive.

In the following we shall briefly introduce both approaches,

later focusing on the multiplicative corrections, which in our numerical experiments proved superior. The discussion is partly adapted from [17].

a) multiplicative corrections.

In a coarse-mesh-rebalanced iterative scheme, the iteration process is interrupted periodically, say, every n iterations. The approximations obtained after these n-iteration cycles are called prebalanced vectors. Let us denote one such vector by x_o. The result of the coarse mesh rebalancing is called a rebalanced vector, denoted by x, which then becomes the initial guess for the next n-iteration cycle. A prebalanced vector and a rebalanced vector are related by:

$$x = (\sum_{k=1}^{K} \phi_k P_k) x_o \qquad (5.26)$$

wnere:

P_k = partitioning matrices;

ϕ_k = arbitrary coefficients, to be determined via the weighted residual method;

K = number of coarse mesh regions.

The residual vector r is given by:

$$r = Ax - b = A(\sum_{k=1}^{K} \phi_k P_k) x_o - b \qquad (5.27)$$

The K arbitrary coefficients are determined by introducing K

independent weighting vectors, w_k, and requiring, according to the weighted residual methods, that the residual be orthogonal to each weighting vector:

$$\langle w_\ell, r\rangle = 0$$

or

$$\sum_{k=1}^{K} \langle w_\ell, AP_k x_o\rangle \phi_k = \langle w_\ell, b\rangle, \quad \ell=1,\ldots,K \qquad (5.28)$$

Eqs.(5.28) form a set of K equations from which the K coefficients (multiplicative corrections) are obtained.

There are various choices for w_k's and for P_k's. Two types of partitioning are widely used. The first type is called disjunctive partitioning. In this case P_k is a diagonal matrix, containing zero elements except for those elements corresponding to the subdomain D_k, which are unity. For example, consider a domain containing N = 6 mesh cells and a coarse mesh partitioning into K = 3 subdomains. Assume that the second subregion (k=2) contains the third and the fourth mesh cells. In this case we have

$$P_2 = \text{diag}\ (0\ 0\ 1\ 1\ 0\ 0)$$

The second type of partitioning is called pyramid partitioning. It is similar to the first one, except that instead of unity, the elements corresponding to the subdomain D_k become interpolating functions, achieving a "smoother" transition between the fine and the coarse grids.

Even more choices exist regarding the weighting vectors. In the context of the CMR used as an acceleration method, the two probably most often used weighting methods are:

- Galerkin's:

$$w_\ell = P_\ell x_o$$

- Region balancing:

$$w_\ell = P_\ell \underline{1}$$

(where $\underline{1}$ = col (1 1 1 1 ... 1), i.e., a vector with all elements equal to unity).

b) additive corrections

In this approach the relationship between the prebalanced and rebalanced vectors is:

$$x = x_o + \left(\sum_{k=1}^{K} \phi_k u_k \right) \tag{5.29}$$

Here u_k is a vector to be prescribed. As before we form the residual vector and impose that it be orthogonal to K weighting vectors. One obtains:

$$\sum_{k=1}^{K} \langle w_\ell, A u_k \rangle \phi_k = \langle w_\ell, b - Ax_o \rangle, \ \ell=1,\ldots K \tag{5.30}$$

from which the K coefficients can be determined. One common choice for u_k is $u_k = P_k \underline{1}$.

5.5.3.2 CMR with multiplicative corrections, applied to assembly-type geometries.

We now present our specific implementation of this method. Our basic iterative scheme is the successive plane overrelaxation (SPOR). In our applications a natural choice for coarse mesh subdomains are the horizontal planes. Consequently we have decided to use disjunctive partitioning and region balance weighting. This choice leads to a relatively simple algorithm which can be programmed in such a way as to add only a small amount of computational work to the basic iterative scheme. We note that this combination of partitioning and weighting was reported very successful by Nakamura and Esposito [26].

Consider a row in our matrix equation Ax = b:

$$a^{zL}_{i,j,k}x_{i,j,k-1} + a^{xL}_{i,j,k}x_{i-1,j,k} + a^{yL}_{i,j,k}x_{i,j-1,k} + a_{i,j,k}x_{i,j,k}$$

$$+ a^{yU}_{i,j,k}x_{i,j+1,k} + a^{xU}_{i,j,k}x_{i+1,j,k} + a^{zU}_{i,j,k}x_{i,j,k+1} = b_{i,j,k} \qquad (5.31)$$

where i,j,k are the mesh indices in the x-, y-, and z-direction, respectively. The other notations are then self-explanatory.

The coarse mesh equations can now be obtained from eqs.(5.28):

$$C_k^L \phi_{k-1} + C_k^o \phi_k + C_k^U \phi_{k+1} = S_k, \quad k=1,\ldots,K \tag{5.32}$$

where:

$$C_k^{L(U)} = \sum_{ij} a_{i,j,k}^{zL(U)} x_{i,j,k_{(+)}1}$$

$$C_k^o = \sum_{i,j} (a_{i,j,k}^{xL} x_{i-1,j,k} + a_{i,j,k}^{yL} x_{i,j-1,k} + a_{i,j,k}^{o} x_{i,j,k}$$

$$+ a_{i,j,k}^{yU} x_{i,j+1,k} + a_{i,j,k}^{xU} x_{i+1,j,k})$$

$$S_k = \sum_{i,j} b_{i,j,k}$$

Eqs.(5.32) form a tridiagonal system whose solution is very simply accomplished, yielding the multiplicative corrections ϕ_k's. Actually more computational work is generally required by the construction of the matrix C and the vector S.

Two remarks are in order in regard to the solution of

$$C\phi = S$$

First, a slight saving in computational time can be accomplished by calculating the vector S (i.e., the coarse mesh right hand side) only once and storing it for the duration of the iteration. The price in additional storage is quite negligible. Second, particular attention must be paid when

constructing the elements of the C matrix near the boundaries. As the pressure on the boundary is known, the corresponding ϕ must preserve it. Therefore

$$\phi_o = \phi_{k+1} = 1$$

The scheme described so far was implemented as a means of accelerating our basic iterative scheme.

Our experience with this method has been mixed. In some instances, the accelerating effect was dramatic, in some others, the acceleration was marginal. In some (albeit few) cases the iteration was actually destroyed, the CMR preventing convergence or even leading to divergence. We have experimented extensively with the choice of rebalancing frequency. Unfortunately no systematic effect was noticed. One interesting observation has been that when the right hand side b contained fairly large components (typically occurring in the early Newton iterations), the CMR was generally more effective than when the b_{ijk}'s were small and not displaying any systematic trend. This latter situation occurs almost always in later Newton iterations. We were unable to draw more precise, quantitative conclusions that would have reduced the almost totally heuristic character of the application of this accelerating technique. Recently Brandt et al. [27] reported an application of an additive correction CMR (described in detail in [25]) to accelerating the pressure solution in SOLA-ICE [28]. Their resuls, which pertain to a 2-D problem, indicate a certain accelerating

effect, but far from spectacular.

Our experience with the CMR method indicate that much more work would be necessary to use its potential. Other combinations of partitioning and weighting may prove more effective, different choices for the coarse mesh grid may be advantageous. Extensive numerical experimentation would be needed, as the non-linear character of this iterative acceleration practically precludes any rigorous analysis.

5.6 Boundary Conditions

In chapter 4, we have discussed the boundary conditions associated with our numerical method. That discussion was actually more general in character, being based on the partial differential equations describing the two-phase flow model. Here we present some complementary aspects, in particular the manner in which the boundary conditions are treated in and affect the pressure field solution.

5.6.1 Pressure Boundary Condition

Consider for simplicity a one-dimensional incompressible flow. It is easy to see that in this situation eq.(5.12) reduces to:

$$- p_{i-1}^{n+1} + 2p_i^{n+1} - p_{i+1}^{n+1} = - \Delta x(F_+^n - F_-^n) \qquad (5.34)$$

Let us look at, say, the inlet boundary (Fig. 5.5). The inlet pressure is prescribed in a "fictitious" cell, in this

case cell "0". This pressure will now alter the right-hand-side of the pressure equation (5.34) written for the first real cell, i.e., i=1:

$$2p_1^{n+1} - p_2^{n+1} = -\Delta x(F_+^n - F_-^n)_1 + p_o^{n+1} \qquad (5.35)$$

The pressure coefficients display strict diagonal dominance. In fact this finding is more general. Indeed it is the pressure boundary conditions that assure (for incompressible fluids) the strict diagonal dominance of the pressure coefficient matrix. At least one such boundary condition (mathematically equivalent to the Dirichlet-type boundary) is needed if the resulting matrix is to be irreducibly diagonally dominant, thus rendering the problem solvable.

While it is true that in our treatment some liquid compressibility is assumed, its very small value still makes the pressure boundary condition practically responsible for strict diagonal dominance.

5.6.2 Velocity Boundary Condition

Consider the same situation as before, but in this case assume that the velocity is specified at the inlet. In this case the momentum equation written for the "edge" 1/2 becomes unnecessary. It can be easily shown that the pressure equation for cell 1 becomes:

$$p_1^{n+1} - p_2^{n+1} = -\Delta x\, F_{3/2}^n - \frac{\Delta x}{\Delta t} G_{3/2}^n + \frac{\Delta x}{\Delta t} G_{1/2}^{n+1} \qquad (5.36)$$

Clearly this type of boundary does not provide diagonal dominance. Mathematically it is equivalent to the Neumann-type boundary condition, i.e., the normal derivative of pressure is specified. Noteworthy that when the fluid is incompressible and only velocity boundary conditions are specified, the pressure coefficient matrix becomes singular. Physically this implies that for an incompressible fluid mass cannot be added or extracted at arbitrary rates.

Actually there is more to be said about this latter situation. Consider the steady-state flow of an incompressible but viscous fluid and impose velocity boundary conditions at both ends of the pipe. In particular the mass flux is obviously uniform and so is the velocity (if the duct area is constant). The pressure drops can be obtained directly from the momentum equations:

$$\Delta p_{i+1/2} = p_i - p_{i+1} = - F_{i+1/2} \tag{5.37}$$

What one cannot determine however are the absolute pressures! In order to determine them, the absolute pressure must be specified for one cell, say i^*. This amounts to breaking up the domain into two subdomains, $i = 1$ to $i = i^*$ and $i = i^*$ to $i = I$. Now each of these two subproblems are perfectly solvable, each being characterized by a velocity/pressure or pressure/velocity set of boundary conditions. Mathematically we removed the i^*-th equation

from the system, rendering the rank of the associated matrix one less than its order.

5.6.3 Total Inlet Flow Rate Boundary Condition

Often the simulation of an experiment requires a prescribed mass flow rate at the inlet to the domain. While in one-dimensional (single-channel) representations this can be easily achieved through an inlet velocity boundary condition, simulations of multiple inter-connected channels are significantly more difficult with this constraint.

One "easy" way to specify a given inlet mass flow rate would be to prescribe the velocity of the inlet of all channels. However one does not know a priori the flow splits. Even for geometrically similar channels, large changes in properties would cause differences in hydraulic behavior. This is especially true for two-phase flows. Thus a more or less arbitrary inlet flow distribution would generally create nonphysical cross-flows persisting for some distance downstream from the inlet. Depending on the problem under consideration, the predictions will be negatively affected.

There are schemes that allow the specification of the total inlet flow rate (see [28] and [29]). Their major drawback is an additional "layer" of iterations, at a significant computational cost. Moreover, these schemes are associated with "marching" methods and it is not clear whether their adaptation to truly boundary-value solution

schemes is possible.

We have developed a method which makes possible the specification of the inlet mass flow rate in a manner intrinsically connected to the pressure field solution. This method will now be described. Condider the situation depicted in Fig. 5.6. Here we have four channels fed from a common "plenum." The plenum pressure, p , will be determined together with the pressures inside the domain such that a given total mass flow rate is achieved.

In the previous chapter we have seen that in our numerical method, the momentum equations yield relations between new time velocities and pressures. Written for the inlet "edge", these relations are:

$$u_{li}^{k} = a_{li}^{k} (p_{li} - p_{o}) + b_{li}^{k} \qquad (5.38)$$

where superscript k refers to vapor (v) and liquid (l), "i" is the channel index, and a and b contain only old time quantities. The flow rate for phase k into channel i is

$$W_{li}^{k} = A_{li}(\alpha^{k}\rho^{k})_{li}^{*} u_{li}^{k} \qquad (5.39)$$

where A_{li} is the i-th channel inlet area and the "macroscopic" densities $(\alpha^{k}\rho^{k})^{*}$ are evaluated exactly as in the mass equation (see previous chapter). The mixture mass flow rate into the i-th channel

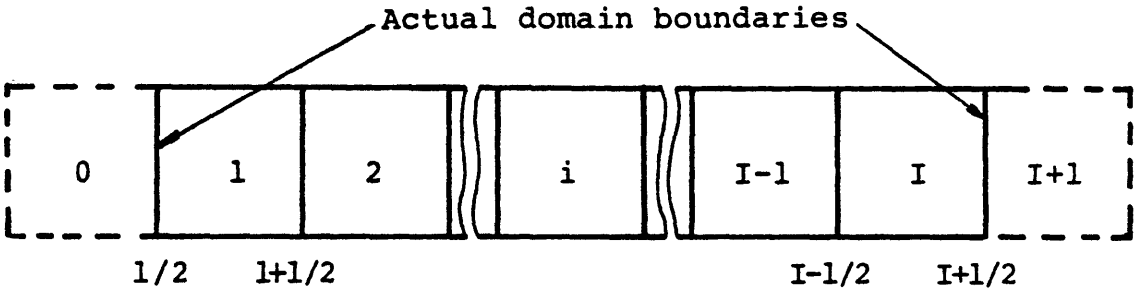

Figure 5.5 One-dimensional grid with fictitious boundary cell.

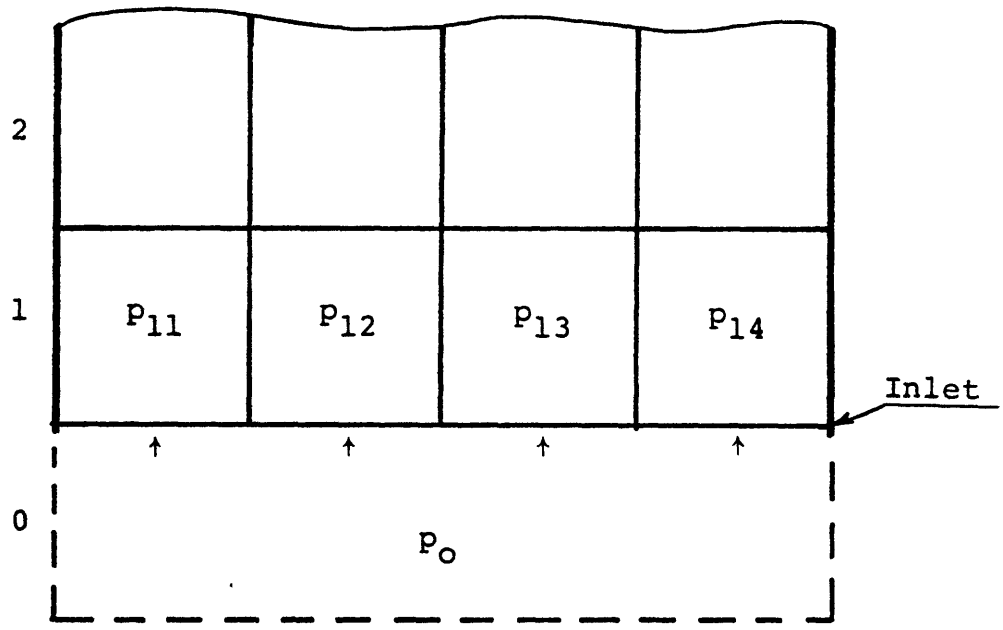

Figure 5.6 Inlet mass flow rate boundary condition (cell numbering).

$$W_{1i} = W_{1i}^{v} + W_{1i}^{\ell} \tag{5.40}$$

can then be written, by combining eqs.(5.38), (5.39) and (5.40) as:

$$W_{1i} = a'_{1i}(p_{1i}-p_o) + b'_{1i} \tag{5.41}$$

where:

$$a'_{1i} = A_{1i}[(\alpha^v\rho^v)^*_{1i}a^v_{1i} + (\alpha^\ell\rho^\ell)^*_{1i}a^\ell_{1i}] \tag{5.42}$$

$$b'_{1i} = A_{1i}[(\alpha^v\rho^v)^*_{1i}b^v_{1i} + (\alpha^\ell\rho^\ell)^*_{1i}b^\ell_{1i}] \tag{5.43}$$

The total inlet mass flow rate is

$$W_1 = \sum_i W_{1i} \tag{5.44}$$

Substitution of (5.41) into (5.44) yields an additional equation for pressures:

$$(\sum_i a'_{1i})p_o - \sum_i a'_{1i}p_{1i} = \sum_i b'_{1i} - W_1 \tag{5.45}$$

In terms of pressure corrections the above equation leads to:

$$(\sum_i a'_{1i})\delta p_o - \sum_i a'_{1i}\,\delta p_{1i} = 0 \tag{5.46}$$

The steps required to implement this boundary condition are then the following:

- evaluate coefficients a'_{1i} and b'_{1i}, for all i;
- based on the current guess for pressures inside the domain and the specified total mass flow rate, a consistent guess for the plenum pressure, p_o, is obtained from eq.(5.45);
- eq.(5.46) is then solved as a part of the pressure field solution;
- the resulting correction, δp_o, is used to update the pressure p_o in the plenum, just as all the other pressure corrections are used to update the pressures inside the domain.

The crucial point to emphasize is the perfect integration of the additional pressure equation into the overall pressure field solution. The extra computational work and storage required are virtually insignificant. Basically we add one unknown and one equation to our system, increasing the order and the rank of the coefficient matrix by one. The left upper corner of the matrix corresponding to the domain illustrated in Fig. 5.6 is shown in Fig. 5.7. The (X) indicate entries due to the additional equation. The dashed lines evidence the block structure of this matrix, each block corresponding to a layer of cells (in our case a row of four cells). As can be seen, the band width of the ma-

FIGURE 5.7

MATRIX MODIFICATION DUE TO THE INLET MASS FLOW RATE BOUNDARY CONDITION

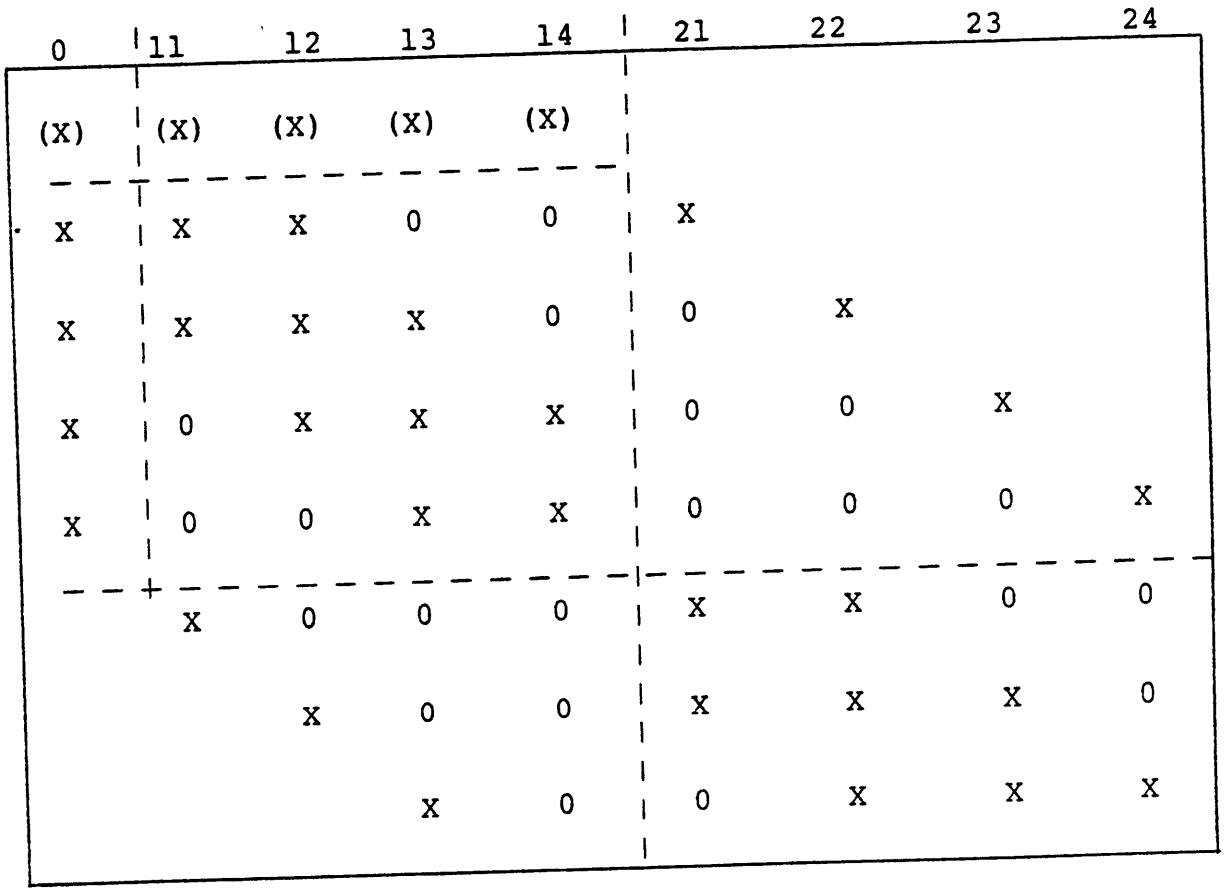

trix (in our case 4 + 1 + 4 = 9) remains unchanged. This again supports our contention about the ease of implementation of this new boundary condition capability in our various pressure solvers.

5.7 Integration of the Pressure Field Solution into the Overall Computing Scheme

After discussing in detail various aspects of the pressure field solution, it is appropriate to conclude the chapter with some considerations on the incorporation of this computing stage into the overall numerical scheme, with the objective of minimizing the total computing effort.

5.7.1 Selection of Pressure Solvers

The major factor influencing the choice of a particular pressure solver is the dimensionality of the problem. While it is perfectly feasible to construct a pressure solver applicable to all spatial representation, in many instances it is substantially more effective computationally to "tailor" to some extent a pressure solver to a certain problem type. This has been our approach and Table 5.1 indicate the availability of various "customized" pressure solvers. Note that a second factor has been taken into account, namely the symmetry (or lack of it) of the pressure coefficient matrix.

We remark that generally our higher dimensionality pressure solvers will "collapse" properly when used in a problem of lower dimensionality. The specific information as to when this is so is more appropriately provided in the

TABLE 5.1

PRESSURE SOLVER - PROBLEM TYPE MATCHING

	1-D		2-D		3-D	
	S	N/S	S	N/S	S	N/S
LU-tridiagonal	x	x				
LU-5-stripe banded			x	x		
SLOR-radial blocks			x	x		
SLOR-axial blocks					x	x
SPOR-planar blocks					x	x
LL^T-7-stripe banded	x		x		x	

Legend:

n-D = n-dimensional domain

S = symmetric

N/S = non-symmetric

code user's guide.

5.7.2 Accuracy of Pressure Solution

At this point the reader should recall that the pressure field solution is really an "inner" step of a non-linear solution, the latter being intrinsically iterative. That is, each non-linear iteration provides an improved guess for the next iteration, which then provides a further improvement and so on. The question that one may raise is the following: since each pressure field solution basically constitutes only an intermediate step towards attaining the final solution to the non-linear problem, how accurate must the former be? While this is a legitimate question, its answer is unfortunately quite difficult and the following comments are offered as guidance only.

With respect to the direct methods we can state practically with no hesitation that for the diagonally dominant matrices involved, the solution is very accurate and there is no need for iterative refinement.

In the case of the iterative methods one must actually choose the convergence criterion. Based on the previous remarks the conclusion may be reached that a rather loose convergence criterion would speed up the overall computation. Unfortunately often this is not so. Indeed a poorly converged pressure field solution may substantially slow down or even destroy the non-linear iteration. Probably a safe rule to follow is to impose a convergence criterion for

the presssure field one to two orders of magnitude tighter (i.e., smaller) than its counterpart for the non-linear iteration. In any case, numerical experimentation must be used for further guidance.

5.7.3 Non-linear Solution Type

Fundamental to our non-linear solution scheme is the construction of the Jacobian matrix, which in turn generates the pressure coefficient matrix. If this Jacobian is updated every non-linear iteration, then each time the pressure field solution must be started from "square one." This is the case if Newton's or the secant methods are used. While they might provide faster convergence, a fairly large computational effort is required for every iteration.

In contrast, if the parallel-chord method is used, the Jacobian is calculated only once and all the LU decompositions can be performed during the first non-linear iteration. Subsequent iterations then require only "back-substitutions", at great savings in computations. The drawback is that the convergence of the parallel-chord method is generally lower than that of the other two methods. In only mildly non-linear problems such as those encountered in single-phase liquid flows, there is no incentive to update the Jacobian, thus the choice points clearly towards the parallel-chord method. In two-phase flows the strong non-linearities would make however this method much less effective. The optimum in terms of overall computational ef-

fort would be to update the Jacobian periodically, thus achieving both an adequate convergence rate and at the same time a relatively low average computing work per iteration. Once again numerical experimentation is needed to find a near optimum frequency for the Jacobian update.

5.8 References

1. IMSL Library Reference Manual, Edition 8, 1981.

2. LINPACK Users' Guide, SIAM, 1979.

3. NAG Fortran Library Manual, Mark 8, 1981.

4. Harwell Subroutine Library, AERE-R9185, 1978.

5. Wilkinson, J.H., Rounding errors in Algebraic Processes, Prentice - Hall, (1963).

6. Forsythe, G.E. and Moller, C.B., Computer Solution of Linear Algebraic Systems, Prentice - Hall, (1967).

7. Forsythe, E.G., Malcolm, M.A. and Moller, C.B., Computer Methods for Mathematical Computation, Prentice - Hall, (1977).

8. Householder, A.S., The Theory of Matrices in Numerical Analysis, Blaisdell, (1964).

9. Faddeev, D.K. and Fadeeva, V.N., Computational Methods of Linear Algebra, W.H. Freeman, (1963).

10. Dahlquist, G. and Bjorck, A., Numerical Methods, Prentice - Hall, (1974).

11. Schwarz, H.R., Rutishauser, H. and Steifel, E., Numerical Analysis of Symmetric Matrices, Prentice - Hall, (1973).

12. Varga, R.S., Matrix Iterative Analysis, Prentice Hall, (1962).

13. Southwell, R.V., Relaxation Methods in Theoretical Physics, Clarendon, (1946).

14. Forsythe, G.E. and Wasow, W.R., Finite Difference Methods for Partial Differential Equations, Wiley, (1960).

15. Young, D.M., Iterative Solution of Large Linear Systems, Academic, (1971).

16. Wachspress, E.L., Iterative Solution of Ellyptic Systems and Applications to the Neutron Diffusion Equations of Reactor Physics, Prentice - Hall, (1966).

17. Nakamura, S., Computational Methods in Engineering and Science, with Application to Fluid Dynamics and Nuclear

Systems, Wiley, (1977).

18. Peaceman, D.W. and Rachford, H.H., The Numerical Solution of Parabolic and Elliptic Differential Equations, J. Soc. Indust. Appl. Math., 3 (1955).

19. Douglas, J. and Rachford, H., On the numerical solution of heat conduction problems in two and three space variables, Trans. Amer. Math. Soc.,82 (1956).

20. Yanenko, N.N., The Method of Fractional Steps, Springer - Verlag, (1971).

21. Birkhoff, G., The Numerical Solution of Elliptic Equations, SIAM, (1972).

22. Douglas, J., Alternating direction method for three space variables, Num. Math., 4 (1962).

23. Kellog, R.B. and Noderer, L.C., Scaled iterations and linear equations, J. Soc.Industr. Appl. Math. Vol. 8, no. 4, (1960).

24. Kopp, H.J., Synthetic Method Solution of the Transport Equation, Nuc. Sci. Eng. 17 (1963).

25. Brandt, A., Math. Comp. 31 (1977).

26. Nakamura, S. and Esposito, V.J., Coarse mesh rebalancing applied to hydraulic analysis, CONF-7030414, NTIS (1973).

27. Brandt, A., J.E. Dendy and Ruppel, H., J. Comp. Phys. 34 (1980).

28. Sha, W.T., An overview of rod-bundle thermal hydraulic analysis, ANL-79-10 (1980).

29. Wolf, L., Kelly, J.E. and Schor, A.L., Review of iterative solution methods for pressure-drop forced BWR core analysis, MIT, Dept. of Nucl. Eng. (1977).

CHAPTER 6. STABILITY AND CHARACTERISTIC ANALYSIS

6.1 Introduction

As already mentioned in Chapter 4, the stability of a numerical scheme is an absolute necessity if a converged solution to a well-posed initial boundary value problem is to be obtained. Since our numerical scheme for this work is not fully implicit, it is only conditionally stable, i.e., there are some time step limits which must be satisfied. In the section of Chapter 4 addressing the time step control strategy, we have indicated without proof what these limits are and how they are used to ensure a stable calculation. In this chapter, we will attempt to substantiate these time step criteria. We should note that although conceptually possible, a complete and rigorous stability analysis is algebraically prohibitive. Consequently, we have taken a simplified approach for this presentation which we believe is quite adequate in bringing out the salient points. It should be also noted that in the last analysis, stability is ascertained through extensive numerical experimentation.

Above, we have associated a converged solution to a well-posed initial boundary condition. The time-dependent single-phase fluid dynamics equations are hyperbolic in character, in that small perturbations propagate with real finite characteristic velocities. Clearly, one would ex-

pect this to be also true in the case of two-phase flow equations. Unfortunately, it has been known for some years now that the common two-phase flow equation sets with unequal velocities display a peculiar trait, namely they have some complex characteristics. Therefore, they are not hyperbolic and consequently, they do not represent a well-posed initial value problem. The implications of this finding are important from both a theoretical and practical point of view, having definitely an impact on the physical soundness of the model as well as on any numerical solution of it. A brief analysis of this aspect, applied to our two-phase model, forms the object of the second major section of this chapter.

6.2 Stability Analysis

We recall from Chapter 4 that the numerical scheme we selected for this work treats two phenomena, convection and diffusion, in an explicit manner. Generally, an explicit treatment leads to conditional stability, i.e., there will be upper limits to the size of the time step. The object of this section is to find these limits, thus substantiating the time step control strategy we implemented in this work.

6.2.1 Convection

6.2.1.1 A Semi-Implicit Numerical Scheme for Fluid Dynamics

For simplicity we shall consider a one-dimensional inviscid adiabatic flow. The equations describing this kind of flow are the continuity and momentum equations, given below:

$$\frac{\partial \rho}{\partial t} + \rho\frac{\partial U}{\partial x} + U\frac{\partial \rho}{\partial x} = 0 \qquad (6.1a)$$

$$\frac{\partial U}{\partial t} + U\frac{\partial U}{\partial x} + \frac{1}{\rho}\frac{\partial p}{\partial x} = 0 \qquad (6.1b)$$

$$\rho = \rho(p) \qquad (6.1c)$$

Using a staggered mesh, treating the terms related to sonic propagation (see Chapter 4) implicitly and the convective terms explicitly, we have

$$\rho_j^{n+1} - \rho_j^n + r\rho_j^n(U_{j+1/2}^{n+1} - U_{j-1/2}^{n+1}) + rU_{j-1/2}^{n+1}(\rho_j^n - \rho_{j-1}^n) = 0 \qquad (6.2)$$

$$U_{j+1/2}^{n+1} - U_{j+1/2}^n + rU_{j+1/2}^n(U_{j+1/2}^n - U_{j-1/2}^n) + (r/\rho_{j+1/2}^n)(p_{j+1}^{n+1} - p_j^{n+1}) = 0 \qquad (6.3)$$

where $r = \Delta t/\Delta x$.

Above, a donor cell logic (assuming flow in the direction of increasing x) was used for the spatial derivatives of the density (in the mass equation) and of the velocity (in the momentum equation). The reader may easily verify that the last two terms in the mass equations are equivalent to the form used in Chapter 4, i.e.,

$$\Delta\rho U \rightarrow \rho^n_j U^{n+1}_{j+1/2} - \rho^n_{j-1} U^{n+1}_{j-1/2} \tag{6.4}$$

Next we eliminate the density differences in favor of the pressure differences:

$$\Delta\rho = a^{-2}\Delta p \tag{6.5}$$

where $a^2 = (dp/d\rho)_s$ and treat the quantities multiplying the differences as constant coefficients. We can now apply the standard von Neumann linear stability analysis ([1]) by considering a Fourier component of p and U, namely

$$p^n_j = \hat{p}^n e^{ij\theta} \quad \text{and} \quad U^n_j = \hat{U}^n e^{ij\theta} \tag{6.6}$$

where $\theta = k\Delta x$ (k is the wave number, related to the wave length, Λ, through the relation $k = 2\pi/\Lambda$). The amplitudes

of these components then satisfy the equation:

$$V^{n+1} = GV^n \tag{6.7}$$

where $V = \mathrm{col}(\hat{p},\hat{U})$. The eigenvalues of the amplification matrix, G, are given by:

$$\det\begin{vmatrix} \lambda - c & 2i\lambda r\rho a^2 \sin(\theta/2) \\ 2i\lambda(r/\rho)\sin(\theta/2) & \lambda - c \end{vmatrix} = 0 \tag{6.8}$$

where $c = 1 - rU(1 - e^{-i\theta})$

From Eq. (6.8), one immediately finds that λ's are given by

$$\lambda = \frac{c}{1+4r^2a^2\sin^2(\theta/2)} (1 \pm 2ira \sin \theta/2) \tag{6.9}$$

For stability, the eigenvalues must satisfy the condition:

$$|\lambda| \leq 1 \tag{6.10}$$

which leads, after some algebraic manipulation, to:

$$- rU(1-rU) \leq r^2a^2 \tag{6.11}$$

For positive velocity, a sufficient condition to satisfy (6.11) is

$$rU \leq 1$$

that is,

$$\Delta t \leq \Delta x/U \tag{6.12}$$

Therefore, the discretization (6.2, 6.3) leads to the standard time step limitation for explicit upwind convection.

6.2.1.2 Multi-Dimensional Explicit Convection

In light of (6.12), one might conclude that the extension to a multidimensional flow would consist simply of obtaining an equivalent condition for each direction and then taking the most restrictive one. We shall see, however, that this is not the case.

Consider the "model" two-dimensional convection equation ([2]):

$$\frac{\partial \phi}{\partial t} + U_x \frac{\partial \phi}{\partial x} + U_y \frac{\partial \phi}{\partial y} = 0 \tag{6.13}$$

The finite difference equivalent of this equation, using

donor-cell differencing (with $U_x > 0$, $U_y > 0$), is:

$$\phi^{n+1}_{j,\ell} - \phi^{n}_{j,\ell} + C_x(\phi^{n}_{j,\ell} - \phi^{n}_{j-1,\ell}) + C_y(\phi^{n}_{j,\ell} - \phi^{n}_{j,\ell-1}) = 0 \qquad (6.14)$$

where:

$$C_x = U_x\Delta t/\Delta x \quad \text{and} \quad C_y = U_y\Delta t/\Delta y$$

Extending the von Neumann analysis to two dimensions, we consider

$$\phi^{n}_{j\ell} = \hat{\phi}^{n} e^{ij\theta_x} e^{i\ell\theta_y} \qquad (6.15)$$

Substituting (6.15) into (6.14) we find

$$\hat{\phi}^{n+1} = \lambda\hat{\phi}^{n} \qquad (6.16)$$

where the amplification factor, λ, is given by:

$$\lambda = 1 - C_x - C_y + C_x e^{-i\theta_x} + C_y e^{-\theta_y} \qquad (6.17)$$

For stability, the condition $|\lambda| \leq 1$ must be satisfied. After some re-grouping, one obtains:

$$|\lambda|^2 = (1 - C_x - C_y)^2 + 2(1 - C_x - C_y)(C_x \cos\theta_x + C_y \cos\theta_y) + C_x^2 + C_y^2 + 2C_x C_y \cos(\theta_x - \theta_y) \tag{6.18}$$

Since some terms (namely the "squares") are always positive, $|\lambda|^2$ will attain its maximum value when all the terms are positive and maximum in magnitude. Assuming $1 - C_x - C_y \geq 0$, this happens when $\theta_x = \theta_y = 0$ (since $\cos\theta \leq 1$). In this case:

$$\max_{(\text{for all } \theta_x, \theta_y)} |\lambda|^2 = 1$$

Therefore, for stability we must have:

$$C_x + C_y \leq 1$$

or

$$\Delta t \leq (U_x/\Delta x + U_y/\Delta y)^{-1} \tag{6.19}$$

In an entirely similar manner, one can extend the analysis to three-dimensional flows, yielding:

$$\Delta t \leq (U_x/\Delta x + U_y/\Delta y + U_z/\Delta z)^{-1} \qquad (6.20)$$

Clearly, conditions (6.19) and (6.20) are more stringent than (6.12). For example, considering $U_x = U_y = U_z$, the limitations represented by (6.19) and (6.20) constitute 1/2 and 1/3, respectively, of the limit given by (6.12).

6.2.1.3 Effect of Complex Characteristics on Stability

This effect can best be illustrated by reviewing a simple, but insightful example containing the basic features of interest in an algebraically tractable form. Following Stewart ([3]), let us consider the equation:

$$\partial\phi/\partial t + U(1 + \varepsilon i)\partial\phi/\partial x + K\phi = 0 \qquad (6.21)$$

Assume U and K are non-negative constants. This equation represents the convective transport of a quantity ϕ with a complex velocity, including a damping term.

A finite difference equivalent, treating explicitly the convection and implicitly the (local) damping, is

$$\phi_j^{n+1} - \phi_j^n + rU(1 + \varepsilon i)(\phi_j^n - \phi_{j-1}^n) + (\Delta t)K\phi_j^{n+1} = 0 \qquad (6.22)$$

where $r = \Delta t/\Delta x$.

Note that donor cell differencing is used for the convective term. As before, let

$$\phi_j^n = \hat{\phi}^n \, e^{ij\theta}$$

where $\theta = k\Delta x$ and $k = \pi/\ell\Delta x$, $\ell = 1,2,\ldots,L$ (L = total number of spatial intervals). The amplification factor is found to be:

$$\lambda = (1 + K\Delta t)^{-1} \, [1-rU(1 + \varepsilon i)(1 - e^{-i\theta})] \quad (6.23)$$

For stability, the condition $|\lambda| \leq 1$ must be met, i.e., the locus of $\lambda(\theta)$ must lie inside the unit circle.

It is easy to see that:

$$\text{-for } \theta \to 0 \qquad \lambda \to (1 + K\Delta t)^{-1} \quad (6.24a)$$

$$\text{-for } \theta = \pi \qquad \lambda \to (1 + K\Delta t)^{-1}[1-2ru(1+i\varepsilon)] \quad (6.24b)$$

Equation (6.23) represents, in the complex plane, a circle with a radius R given by

$$R = (1 + K\Delta t)^{-1} \, (1 + \varepsilon^2)^{1/2} \, rU \quad (6.25)$$

and passing through the point $[(1 + K\Delta t)^{-1}, 0]$. In other

words the damping term provides a contraction, while the complex velocity produces a dilation. In addition, the complex velocity leads to a rotation by an angle arctan ε. This geometrical representation is illustrated in Fig. 6.1 (for $\varepsilon > 0$). Note that the locus of λ is actually only the bottom half of this circle.

A few remarks can now be made. First let us consider the case $K = \varepsilon = 0$, i.e., real characteristic with no damping. This is the standard convection problem. The locus of λ will pass through the point (1,0) and the radius will be just rU; the center of the circle is on the real axis. Clearly, when $rU < 1$, the condition $|\lambda| \leq 1$ is met. Note that the points corresponding to the long wavelength (i.e., large ℓ) components are the closest to the unit circle.

When $\varepsilon = 0$ but $K > 0$, there will be a contraction of the locus of λ (as already noted) which may allow for an rU in excess of unity.

Now if $K = 0$ but $\varepsilon \neq 0$, the locus of λ passes through the point (1,0) and is tilted by an angle arctan ε. Clearly, the situation raising concern is that for $\varepsilon > 0$ (it should be noted that when complex characteristics occur, they do so in conjugate pairs, therefore, there is always an $\varepsilon > 0$). In this case, for some ℓ large enough,

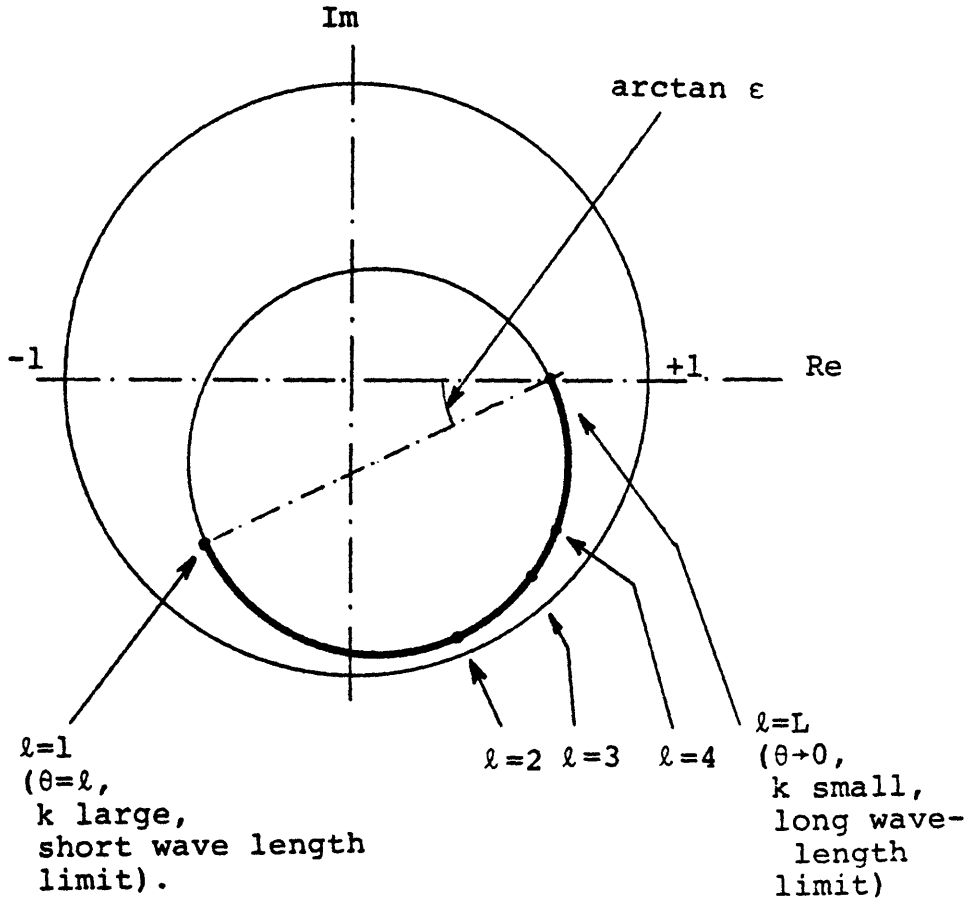

FIGURE 6.1 Locus of λ - Eq. (6.23)

the locus of λ will be outside the unit circle. We note that a smaller Δt leads to a larger "threshold" ℓ. In principle, if there are only a few nodes, the numerical solution may still be stable.

Finally, if $K > 0$ and $\varepsilon > 0$, the above locus undergoes a contraction and passes through the point $[(1 + K\Delta t)^{-1}, 0]$. The rotation due to ε now leads to a situation in which we find points corresponding to some relatively short wavelength components close to (or possibly outside) the unit circle, whereas the very long wavelength components (with ℓ near L) may be perfectly stable. This point, we feel, has not been sufficiently emphasized in [3]. In other words, it appears that the very short wavelength modes are stabilized by the donor cell differencing, the very long wavelength modes are stabilized by the damping term, but the intermediate wavelength components may be unstable due to the complex characteristic velocity.

For this last case, it is interesting to note the effect of the time step reduction for a <u>fixed</u> mesh size. Recalling the expression of the radius R, it is evident that for $\Delta t \to 0$, R will decrease linearly with Δt, thus compensating for the intercept with the real axis moving toward the point (1,0). For any finite mesh size, hence finite L,

one could always find some time step which would render all the Fourier modes stable.

Reference [3] contains an interesting stability analysis applied to an isothermal unequal velocity two-phase flow model. It is shown there that stability of the very short wavelength components is assured by the donor cell differencing, while the long wavelength modes are stabilized by the interfacial momentum exchange. However, the concern over the intermediate wavelength modes is left unanswered.

To conclude this subsection on a positive note, we should state that a very large body of numerical experience substantiate the fact that successful computations can be made even with ill-posed models (i.e., models having complex characteristics) for reasonable mesh sizes and physically meaningful wall and interfacial momentum exchange terms.

6.2.2 Locally Implicit Diffusion Equation

In Chapter 4, it was stated that the fully explicit radial liquid conduction imposes a time step limitation of the form (for $\Delta x = \Delta y$):

$$\Delta t \leq \frac{\Delta x^2}{4\alpha} \tag{6.26}$$

where α = thermal diffusivity. This limitation of the

explicit treatment of the diffusion transport is well-known (see, for example, [1], [2], [4]) and will not be proved here. In that same chapter, however, we introduced an alternate scheme, locally implicit, which displays unconditional stability. The analysis of this scheme is presented below.

For simplicity, let us consider a one dimensional diffusion equation without source:

$$\partial T/\partial t = \alpha \partial^2 T/\partial x^2 \tag{6.27}$$

The corresponding locally implicit difference equation is:

$$T_j^{n+1} - T_j^n = d(T_{j-1}^n - 2T_j^{n+1} + T_{j+1}^n) \tag{6.28}$$

where

$$d = \alpha \Delta t/\Delta x^2.$$

The obvious advantage of this scheme is the lack of spatial coupling at the new time, which means that computationally this scheme requires essentially the same effort as the explicit scheme.

To assess its stability, consider as before a Fourier component:

$$T_j^n = \hat{T}^n e^{ij\theta}$$

The resulting amplification factor λ is given by:

$$\lambda = \frac{2d\cos\theta+1}{2d + 1} \tag{6.29}$$

For stability $|\lambda| \leq 1$, or $-1 \leq \lambda \leq 1$, for any θ:
The first inequality leads to

$$0 < 2d\ (1 + \cos\theta) + 2$$

which is always satisfied (note that $1 + \cos\theta \geq 0$). The other inequality simply yields

$$\cos\theta \leq 1$$

which is obviously true. Therefore, the scheme (6.28) is unconditionally stable. Unfortunately, its use is not without some drawbacks.

First, we recall from Chapter 4 that this scheme is not conservative, and consequently the recommendation was to use it mostly for steady-state simulations, although its cautious application to some slow transients was not ruled out.

There is another, more subtle flaw associated with this scheme even when used to reach a steady-state through

a transient. Let us re-write Eq. (6.28) in a modified form:

$$T_j^{n+1} - T_j^n = d(T_{j-1}^n - 2T_j^n + T_{j+1}^n + 2T_j^n - 2T_j^{n+1})$$

$$= d(T_{j-1}^n - 2T_j^n + T_{j+1}^n) - 2d(T_j^{n+1} - T_j^n) \quad (6.30)$$

or after re-grouping:

$$(1 + 2d)(T_j^{n+1} - T_j^n) = d\ (T_{j-1}^n - 2T_j^n + T_{j+1}^n) \quad (6.31)$$

Equation (6.31) clearly looks just like the explicit scheme, but with an increased thermal inertia! The effect of this somewhat surprising feature is to slow down changes in T_j. Therefore, although we may take larger time steps (limited, in our case, only by the explicit treatment of the convective transport), the increased apparent thermal inertia may slow down the establishment of steady-state. It is practically impossible to say a priori what would be more advantageous (i.e., computationally more economical): a fully explicit treatment with some shorter time steps or a locally implicit scheme with longer time steps but with the difficulty noted above. Therefore, numerical experimentation must be used for guidance.

6.3 Characteristics Analysis

6.3.1 Background

As it was stated in the introductory section of this Chapter, it has been known for the last several years that many commonly used two-phase flow systems of equations possess complex characteristics. It appears that a significant incentive for further research of this aspect was provided by a round table discussion at the Fifth International Heat Transfer Conference in 1974 ([5]). Indeed in the years following it, there have been numerous papers dealing directly or indirectly with this subject (for example [6] - [10], to quote some of the more representative ones). It seems that there is even somewhat earlier work documenting the existence of complex characteristics ([11], [12]). Currently, there is no consensus as to the implications of the complex characteristics, but it is generally agreed that the equations are ill-posed as an initial value (or Cauchy) problem ([13]).

The general one-dimensional system of first-order partial differential equations can be written as:

$$A(\phi)\ \frac{\partial \phi}{\partial t} + B(\phi)\ \frac{\partial \phi}{\partial x} + C(\phi) = 0 \qquad (6.32)$$

where

ϕ = vector of dependent variables,

A,B = coefficient matrices,

C = source (sink) vector.

The characteristics (or characteristic speeds), λ, are defined by the equation:

$$\det (A\lambda - B) = 0 \tag{6.33}$$

Mathematically, the characteristics may separate discontinuities in the solution, thus constituting trajectories along which discontinuities may propagate ([14]) in the x-t plane. In the limit of very short wavelength, the characteristics are just the speeds at which small perturbations propagate ([9]). If all the characteristics are real and distinct, the problem defined by Eq. (6.32) is of hyperbolic type. By analogy to the time-dependent, one-dimensional, single-phase compressible flow, whose governing equations are always hyperbolic (see, for example, [15]), it is reasonable to expect that the governing equations of its two-phase counterpart should also be hyperbolic. As already mentioned, many two-phase flow models exhibit, however, complex characteristics.

We do not purport to have solved this current con-

troversy surrounding two-phase flow modeling. Instead, our purpose for the remainder of this chapter is to provide some insight and understanding into this problem, particularly as it applies to our four-equation two-phase flow model.

6.3.2 General Formulation

Let us rewrite the governing equations, presented in Chapter 2 in one-dimensional form:

$$\frac{\partial \rho_m}{\partial t} + \frac{\partial}{\partial x}\left[\alpha \rho_v U_v + (1-\alpha)\rho_\ell U_\ell\right] = 0 \tag{6.34.a}$$

$$\frac{\partial}{\partial t}\left(\rho_m e_m\right) + \frac{\partial}{\partial x}\left[\alpha \rho_v e_v U_v + (1-\alpha)\rho_\ell e_\ell U_\ell\right] + p\frac{\partial}{\partial x}\left[\alpha U_v + (1-\alpha)U_\ell\right] = Q \tag{6.34.b}$$

$$\alpha \rho_v \frac{\partial U_v}{\partial t} + \alpha \rho_v U_v \frac{\partial U_v}{\partial x} + \alpha \frac{\partial p}{\partial x} = F_v \tag{6.34.c}$$

$$(1-\alpha)\rho_\ell \frac{\partial U_\ell}{\partial t} + (1-\alpha)\rho_\ell U_\ell \frac{\partial U_\ell}{\partial x} + (1-\alpha)\frac{\partial p}{\partial x} = F_\ell \tag{6.34.d}$$

where F_v and F_ℓ denote the total forces acting on the vapor and liquid, respectively. We can select as main dependent variables p, α, U_v and U_ℓ. Note that the choice of α

as an "energy" variable leads to somewhat simpler algebraic expressions.

Recalling the definitions of ρ_m and e_m, using the appropriate equations of state and considering, for the moment, that F_v and F_ℓ do not contain differential terms, Eqs. (6.34) can be recast in the form (6.32). The corresponding coefficient matrices are given below:

$$A = \begin{vmatrix} a_p^m & -\Delta\rho & 0 & 0 \\ a_p^e & -\Delta(\rho e) & 0 & 0 \\ 0 & 0 & \alpha\rho_v & 0 \\ 0 & 0 & 0 & (1-\alpha)\rho_\ell \end{vmatrix} \qquad (6.35.a)$$

$$B = \begin{vmatrix} b_p^m & -\Delta(\rho U) & \alpha\rho_v & (1-\alpha)\rho_\ell \\ b_p^e & -\Delta(\rho h U) & \alpha\rho_v h_v & (1-\alpha)\rho_\ell h_\ell \\ \alpha & 0 & \alpha\rho_v U_v & 0 \\ (1-\alpha) & 0 & 0 & (1-\alpha)\rho_\ell U_\ell \end{vmatrix} \qquad (6.35.b)$$

where:

$$a_p^m = \alpha\rho_{v,p} + (1 - \alpha)\rho_{\ell,p}$$

$$a_p^e = \alpha(e_v\rho_{v,p} + \rho_v e_{v,p}) + (1 - \alpha)(e_\ell\rho_{\ell,p} + \rho_\ell e_{\ell,p})$$

$$\Delta\rho = \rho_\ell - \rho_v$$

$$\Delta(\rho e) = \rho_\ell e_\ell - \rho_v e_v$$

$$b_p^m = \alpha U_v\rho_{v,p} + (1-\alpha)\ U_\ell\rho_{\ell,p}$$

$$b_p^e = \alpha U_v\ (e_v\rho_{v,p} + \rho_v e_{v,p}) + (1-\alpha)U_\ell(e_\ell\rho_{\ell,p} + \rho_\ell e_{\ell,p})$$

$$\Delta\rho U = \rho_\ell U_\ell - \rho_v U_v$$

$$\Delta(\rho hU) = \rho_\ell h_\ell U_\ell - \rho_v h_v U_v$$

$$(h_v = e_v + p/\rho_v,\quad h_\ell = e_\ell + p/\rho_\ell,$$

$$\rho_{v,p} = d\rho_v/dp,\ \rho_{\ell,p} = d\rho_\ell/dp,$$

$$e_{v,p} = de_v/dp,\ e_{\ell,p} = de_\ell/dp)$$

The specific structure of the coefficient matrices generates, through (6.33), a fourth order algebraic equation in λ. Unfortunately, it appears that this equation cannot be factored. Therefore, we resorted to a numerical evaluation of the eigenvalues λ. We used as parameters:

- the pressure,
- the void fraction, .
- the total mass flux, G, i.e.,

$$G = [\alpha\rho_v U_v + (1-\alpha)\rho_\ell U_\ell]/[\alpha\rho_v + (1-\alpha)\rho_\ell],$$

- the slip ratio, S, i.e.,

$$S = U_v/U_\ell$$

Generally, the results indicate the existence of two real characteristics of large magnitude and two complex conjugate characteristics of a magnitude on the order of transport velocities. Except for relatively large slip ratios, the magnitude of the imaginary part is substantially smaller than that of the real part of the complex characteristics. At very small void fractions (i.e., $\alpha \cong 0.001$) all four characteristics become complex, whereas at very high void fractions (i.e., $\alpha \cong 0.999$), they are all real, for the entire range of slip ratios studied ($1<S\leq 100$).

To gain some insight into the actual functional dependencies involved, a simplified analysis was performed under the assumption that the phase properties are constant, that is, the phases are incompressible. With this assumption

$$a_p^m = a_p^e = b_p^m = b_p^e = 0$$

The resulting modified matrices, when substituted into Eq. (6.33) generate a second order algebraic equation, much more amenable to analysis. The results of this analysis constitute the object of the following subsections.

6.3.3 Characteristics for the Four-Equation Incompressible Flow Model

The characteristic equation (6.33) becomes in this case:

$$\det \begin{vmatrix} 0 & (\rho_v\eta_v - \rho_\ell\eta_\ell) & -\alpha & -(1-\alpha) \\ 0 & (\rho_v h_v\eta_v - \rho_\ell h_\ell\eta_\ell) & -\alpha h_v & -(1-\alpha)h_\ell \\ -1 & 0 & \eta_v & 0 \\ -1 & 0 & 0 & \eta_\ell \end{vmatrix} = 0 \qquad (6.36)$$

where:

$$\eta_v = \lambda - U_v \quad \text{and} \quad \eta_\ell = \lambda - U_\ell$$

Expanding the determinant, we get:

$$\alpha\eta_\ell \cdot \det \begin{vmatrix} (\rho_v\eta_v - \rho_\ell\eta_\ell) & -1 \\ (\rho_v h_v \eta_v - \rho_\ell h_\ell \eta_\ell) & -h_v \end{vmatrix} + (1-\alpha)\eta_v \cdot \det \begin{vmatrix} (\rho_v\eta_v - \rho_\ell\eta_\ell) & -1 \\ (\rho_v h_v \eta_v - \rho_\ell h_\ell \eta_\ell) & -h_\ell \end{vmatrix} = 0$$

or

$$\alpha\rho_\ell \, \eta_\ell^2 + (1-\alpha)\rho_v \, \eta_v^2 = 0 \qquad (6.37)$$

Denoting $\beta^2 = \alpha\rho_\ell/(1-\alpha)\rho_v$, Eq. (6.37) leads to

$$\beta\eta_\ell = \pm i\eta_v \qquad (6.37')$$

Recalling the definitions of η_v and η_ℓ, we finally obtain:

$$\lambda = \left[\frac{\beta^2 + S}{\beta^2 + 1} \pm i \, \frac{\beta(S-1)}{\beta^2 + 1}\right] U_\ell \qquad (6.38)$$

Except for very small α's, an approximate expression can be obtained for λ, considering $\beta^2 >> 1$ and $\beta^2 >> S$:

$$\lambda \cong (1 \pm i \frac{S-1}{\beta}) U_{\ell} \qquad (6.39)$$

Therefore, the "slow" characteristics of the incompressible, four-equation two-phase flow model are always complex. (The other two characteristics are infinite, due to the assumption of incompressibility).

A remarkable finding is that the "slow" characteristics of the compressible model are extremely close to the values predicted by Eq. (6.38) or (6.39), except very near the extremes of the void fraction range. Consequently, it appears quite reasonble to extend the results of the incompressible flow analysis to the actual, compressible flow.

6.3.4 Effect of the Mass Exchange Rate on the Characteristics of the Incompressible Flow Model

Up to now, it has been assumed that F_v and F_{ℓ} (see Eqs. (6.34c,d)) contain only algebraic terms. The components of these "forces" are the wall friction,the interfacial momentum exchange and the body force. While the first and the last of these components, being generally purely algebraic, do not affect the characteristics, the momentum exchange term, in the context of our four-equation model raises a question in this respect. Indeed, as we

recall from the material presented in Chapters 2 and 3, the momentum exchange term includes the contribution of the mass exchange rate, which, under the assumption of thermal equilibrium at saturation, can be obtained from one of the phasic mass conservation equations. Therefore, the mass exchange rate is given by a differential equation and one could expect some effect on the characteristics.

From Eqs. (3.44), it follows that the additional terms to be added to the left-hand-side of the phasic momentum equations are:

- for vapor: $\eta \Gamma U_r$ (6.40.a)

- for liquid: $(1-\eta)\ \Gamma U_r$ (6.40.b)

For symmetry let us use the vapor mass equation in the vapor momentum equation and the liquid mass equation in the liquid momentum equation. Assuming also incompressibility, the terms (6.40) then become:

- vapor:

$$\eta U_r \rho_v \frac{\partial \alpha}{\partial t} + \eta U_r \rho_v U_v \frac{\partial \alpha}{\partial x} + \eta U_r \rho_v \alpha \frac{\partial U_v}{\partial x} \qquad (6.41.a)$$

- liquid:

$$(1-\eta)U_r\rho_\ell \frac{\partial\alpha}{\partial t} + (1-\eta)U_r\rho_\ell U_\ell \frac{\partial\alpha}{\partial x} - (1-\eta)U_r\rho_\ell(1-\alpha) \frac{\partial U_\ell}{\partial x} \qquad (6.41.b)$$

The last two lines of the coefficient matrices will be altered as shown below:

$$A = \begin{vmatrix} - & - & - & - \\ - & - & - & - \\ 0 & \eta U_r\rho_v & \alpha\rho_v & 0 \\ 0 & (1-\eta)U_r\rho_\ell & 0 & (1-\alpha)\rho_\ell \end{vmatrix} \qquad (6.42.a)$$

$$B = \begin{vmatrix} - & - & - & - \\ - & - & - & - \\ \alpha & \eta U_r\rho_v U_v & \alpha\rho_v(U_v+\eta U_r) & 0 \\ (1-\alpha) & (1-\eta)U_r\rho_\ell U_\ell & 0 & (1-\alpha)\rho_\ell[U_\ell-(1-\eta)U_r] \end{vmatrix} \qquad (6.42.b)$$

These changes will in turn modify the characteristic equation, which now becomes:

$$\det \begin{vmatrix} 0 & (\rho_v \eta_v - \rho_\ell \eta_\ell) & -1 & -1 \\ 0 & (\rho_v h_v \eta_v - \rho_\ell h_\ell \eta_\ell) & -h_v & -h_\ell \\ -\alpha & \eta U_r \rho_v \eta_v & (\eta_v - \eta U_r) & 0 \\ -(1-\alpha) & (1-\eta) U_r \rho_\ell \eta_\ell & 0 & [\eta_\ell + (1-\eta) U_r] \end{vmatrix} = 0 \qquad (6.43)$$

Expanding this determinant, it turns out that all the terms generated by the mass exchange (i.e., the terms in U_r) cancel each other! We thus have the interesting and surprising result that the inclusion of the mass exchange rate, given by a differential equation, into the momentum exchange terms has no effect on the characteristics of the incompressible flow model. In fact, we found this to be true for the compressible flow model as well.

To our knowledge, this fact has not been proved or noted elsewhere. It indicates the existence of differential constitutive equations which do not affect the characteristics. Further investigation of this aspect is needed to elucidate its implications.

6.4 REFERENCES

1. R.D. Richtmeyer and K.W. Morton, "Difference Methods for Initial Value Problems", "Interscience Publishers, (1967).

2. P.J. Roache, "Computational Fluid Dynamics," Hermosa Publishers,(1976).

3. H.B. Stewart, "Stability of Two-Phase Flow Calculations Using Two-Fluid Models," Journal of Computational Physics 33, 1979).

4. B. Carnahan, H.A. Luther and J.O. Wilkes, "Applied Numerical Methods," John Wiley & Sons, (1969).

5. D. Gidaspow, "Introduction to Modeling of Two-Phase Flow," Round Table Discussion, Proc.5th Int. Heat Transfer Conf., Tokyo, Japan (1974).

6. R.W. Lyczkowski, D. Gidaspow, C.W. Solbrig and E.D. Hughes, "Characteristics and Stability Analyses of Transient One-Dimensional Two-Phase Flow Equations and Their Finite Difference Approximations," ASME Paper No. 75-WA/HT-23; see also Nucl. Sci. Eng., 66, (1978).

7. W.M. Bryce, "Determination of the Hyperbolic Regime of the Hydrodynamic Equations Modelled in the LOCA Code RELAP-UK," Proc. OECD/NEA Specialists' Mtg., Transient Two-Phase Flow, Toronto, Canada (1976).

8. J.A. Bouré and A. Latrobe, "On Well-Posedness of Two-Phase Flow Problems", Paper No. 76-CSME/CSChE-9,(1976).

9. J.D. Ramshaw and J.A. Trapp, "Characteristics, Stability and Short-Wavelength Phenomena in Two-Phase Flow Equation Systems", Nucl. Sci. Eng., 66,(1978).

10. R.T. Lahey, Jr., L.Y. Cheng, D.A. Drew and J.E. Flaherty, "The Effect of Virtual Mass on the Numerical Stability of Accelerating Two-Phase Flows," Int. J. Multiphase Flow, 6, (1980).

11. E.R. Siegmann, "Theoretical Study of Transient Sodium Boiling in Reactor Coolant Channels Utilizing a Compressible Flow Model," Argonne National Laboratory Report No. ANL-7842,(1971).

12. J.A. Bouré, "Dynamique des Ecoulements Diphasique: Propagation de Petites Perturbations," Centre d'Etudes Nucleaires, Grenoble, Report No. CEA-R-4456,(1973).

13. J. Hadamard, "Lectures on Cauchy's Problem on Linear Partial Differential Equations, "Yale University Press, (1923).

14. P.R. Garabedian, "Partial Differential Equations," John Wiley,(1964).

15. A.H. Shapiro, "The Dynamics and Thermodynamics of Compressible Fluid Flow," Ronald Press,(1953).

CHAPTER 7. EXPERIMENT SIMULATION

7.1 Introduction

The model and the methods described in the previous chapters have been implemented into the computer code THERMIT-4E.

During the process of assemblying a large and complex computational framework, one becomes acutely aware of various sources of uncertainty:

- physical models are used sometimes extrapolatively;
- simplifications are made which may appear valid if considered individually, but whose combined effect is not clear;
- implementation of various models almost always involves some arbitrary, though seemingly reasonable, decisions;
- numerical methods are, after all, only approximate means of solution.

Consequently, the ultimate justification for a specific choice lies in the capability of the overall model to simulate and display reasonable agreement with experiments.

We would like to emphasize that all our

calculations have been run on a best estimate basis, without any "fine tuning", to assess the truly predictive capabilities of our model.

The code has been exercised in one-, two- and three-dimensional configurations, to check and prove its geometrical versatility.

Two experiment series were selected for simulation.

7.2 EB19GR Experiments

This is a 19-pin, electrically heated, steady-state test series performed on the CFNa loop at Grenoble, France [1]. Table 7.1 presents the significant design data of the test section.

The flow rate in the experiments was gradually reduced from 2.25Kg/s to about 0.26 Kg/s. The last flow rate corresponds to the sodium temperature reaching the saturation line at the end of the heated section, based on a heat balance.

The tests have been simulated in both one- and three-dimensional configurations.

7.2.1 One-Dimensional Simulations

One-dimensional simulations have been performed to provide a check and, at the same time, a proof of

TABLE 7.1

Design Data for the GR19 Experiment

Number of Pins	19
Clad OD (m)	8.65×10^{-3}
Heated Length (m)	0.6
Downstream Unheated Length (m)	0.494
Upstream Unheated Length (m)	0.12
Wire Wrap OD (m)	1.28×10^{-3}
Wire Wrap Lead (m)	0.18
Flat to Flat (m)	4.58×10^{-2}
Inlet Temperature (°C)	400
Power (kw)	170 (axially uniform)

capability. A quarter of the bundle is collapsed into a flow channel of uniform cross-section.

Figure 7.2 displays the axial temperature distribution for various flow rates. In single-phase, the fluid temperature in the adiabatic section downstream of the heated zone remains constant. In two-phase flow conditions, the fluid temperature, equal to the saturation temperature, decreases slightly due to the drop in pressure.

The following three figures illustrate the profound effect of the phase slip on the major flow characteristics. The void fraction for the case of homogeneous flow attains substantially greater values (Fig. 7.3). As can be seen from Fig. 7.4, the slip has a strong effect on the pressure drop. It is interesting to note the appearance of a small inflexion in the upper curve in this figure. The effect is a manifestation of the fact that the friction and acceleration pressure drops, on the one hand, and the gravitational pressure drop, on the other, vary with void fraction in opposite directions. Finally, Figure 7.5 shows the axial distribution of the velocity, with and without slip.

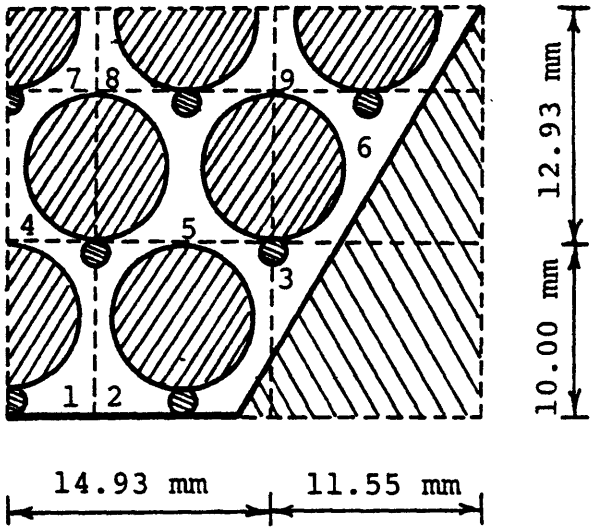

Figure 7.1 Geometrical Configuration for the GR.19 Eb Experiment

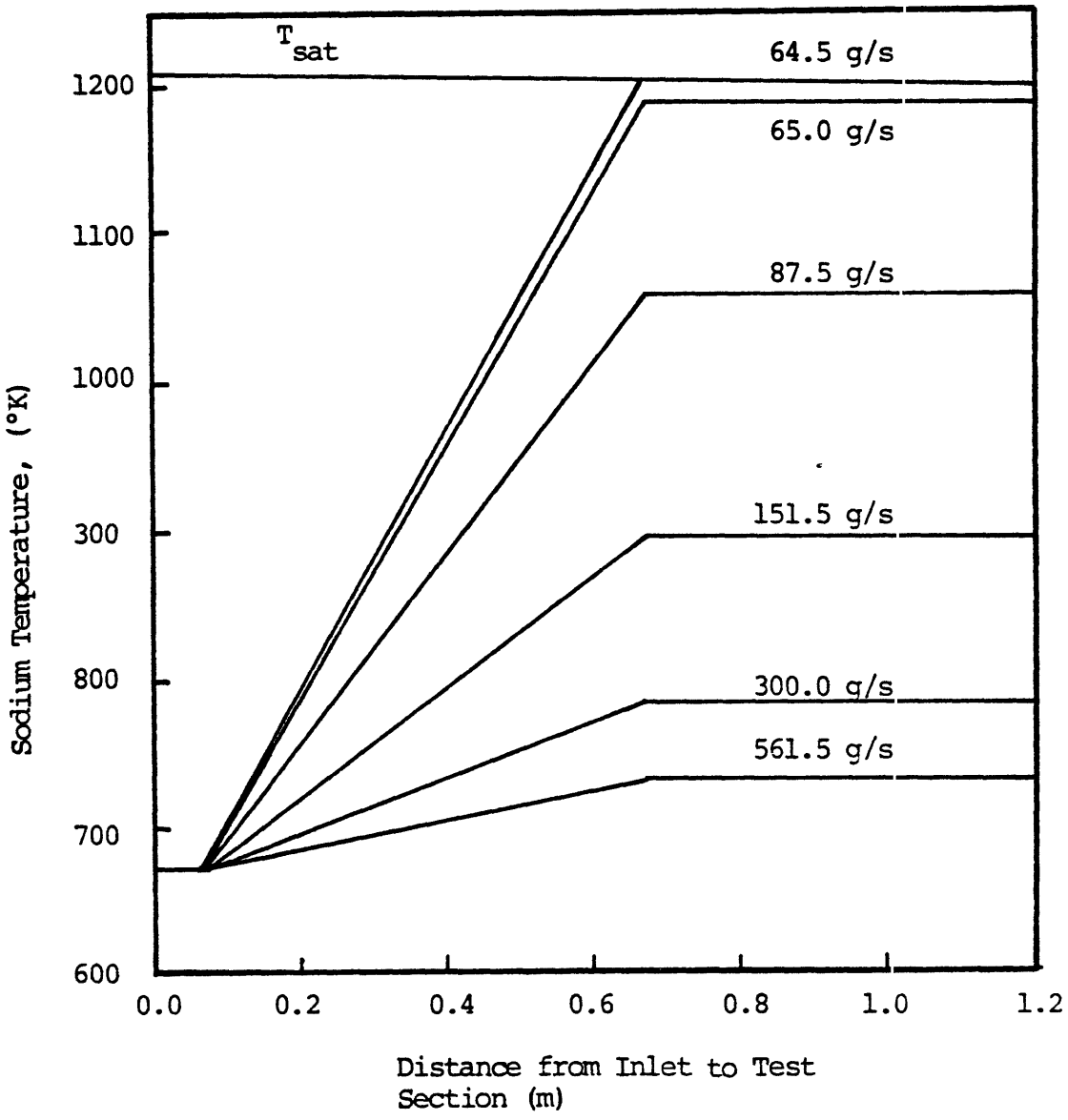

Figure 7.2 Axial Sodium Temperature Distribution, One-Dimensional Representation

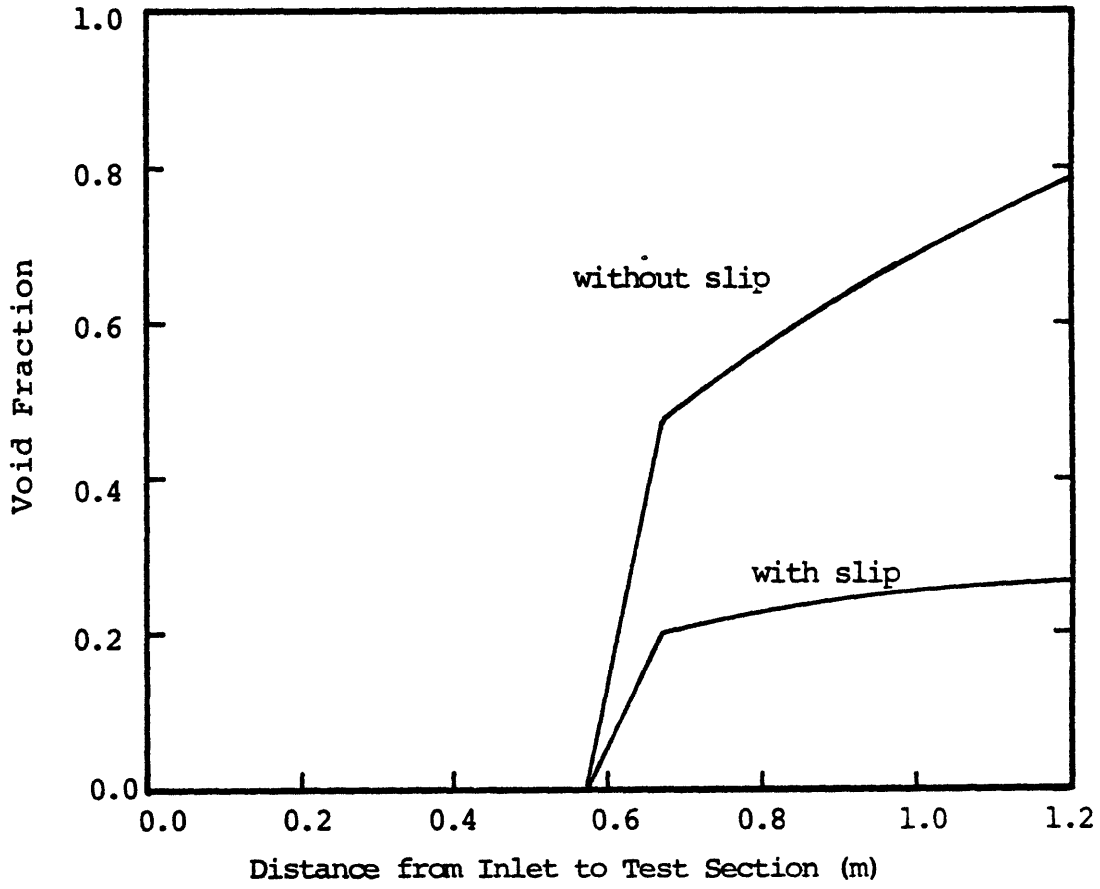

Figure 7.3 Axial Void Distribution, One-Dimensional Representation

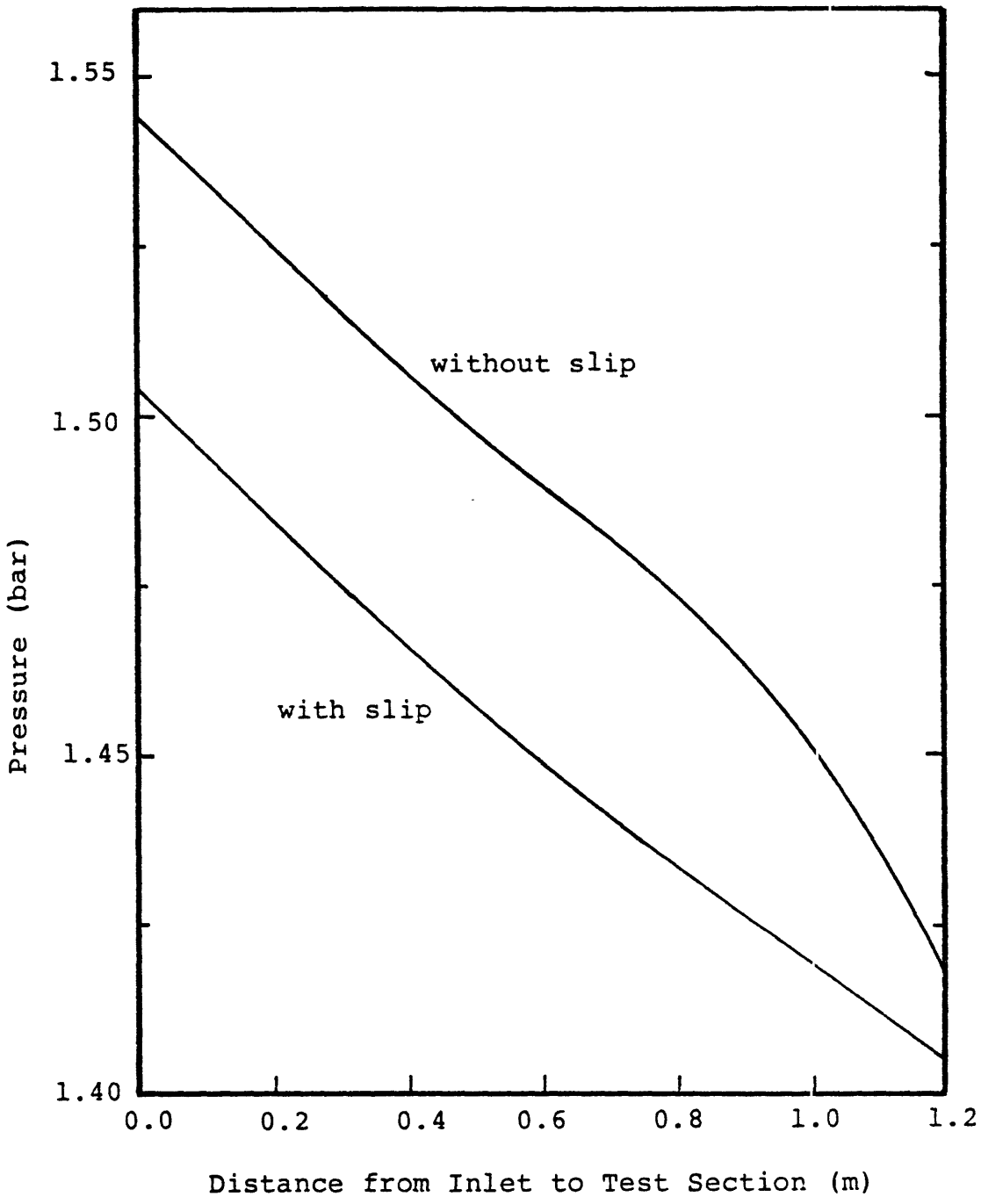

Figure 7.4 Axial Pressure Distribution, One-Dimensional Representation

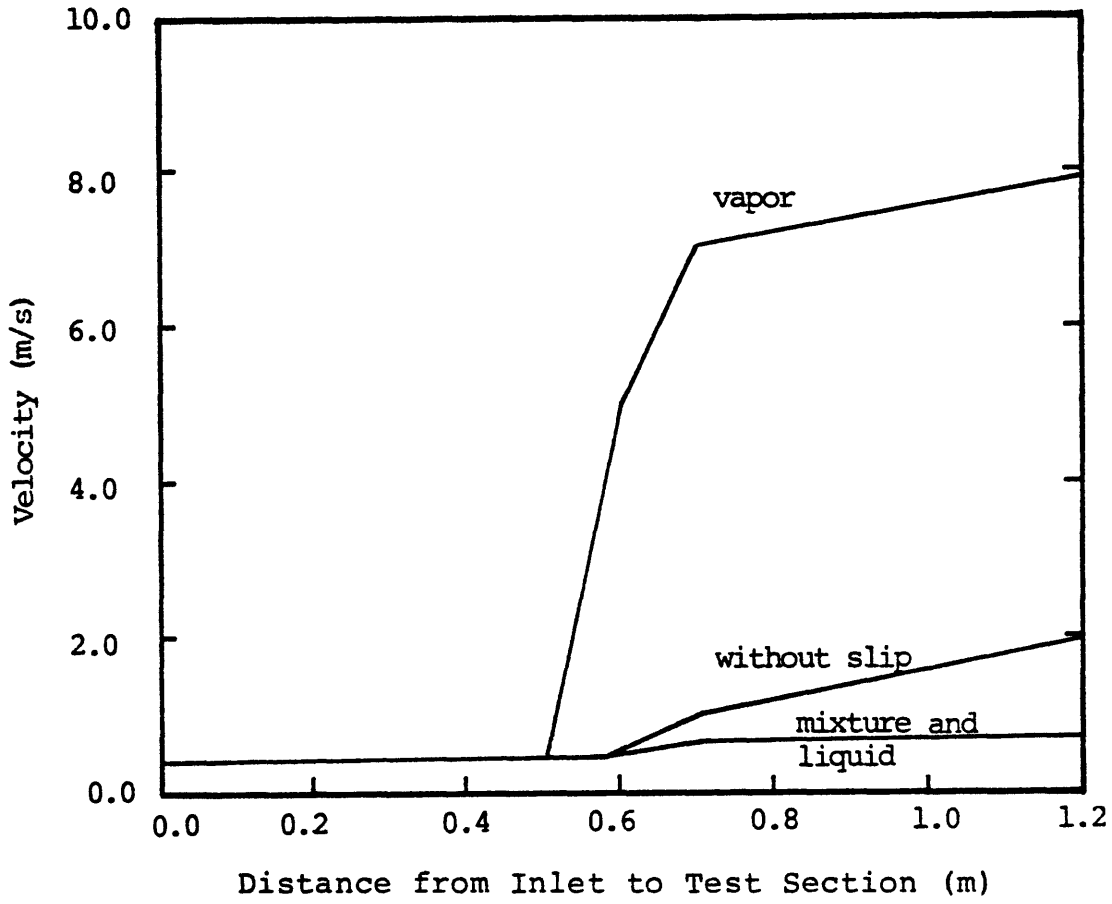

Figure 7.5 Axial Velocity Distribution,
One-Dimensional Representation

It is apparent that the slip between phases has a dramatic effect on the flow, hence an unequal velocity two-phase flow model becomes a necessity for sodium boiling simulations.

7.2.2 Three-Dimensional Simulations

The geometric configuration used in our simulation is a quarter of the bundle as shown in Fig. 7.1. One notes the mesh layout in which a triangular lattice is represented by a cartesian grid. This representation is obviously made possible by our porous body approach.

To test our model for the enhanced liquid conduction (see Chapter 3, Section 3.3.4), we performed a number of single-phase calculations at various flow rates. The radial temperature distributions at three flow rates (2.25 Kg/s, 0.606 Kg/s and 0.350 Kg/s), at the end of the heated zone and at the end of the test section, are shown in Figs. 7.6-7.11. The difference between the maximum and the mean sodium temperatures is plotted in Fig. 7.12 as a function of flow rate. The agreement with the reported experimental results is very good. Figure 7.13 displays the axial

temperature distribution, for each channel, for the highest flow, illustrating the attenuation of the radial temperature gradient in the adiabatic zone due to liquid conduction.

It is interesting to remark that even for the lowest flow in the experiment a true steady-state is not reached. Actually a pulsating behavior is encountered, with the outlet flow rate oscillating about the fixed inlet flow rate. Figure 7.14 illustrates the void fraction distribution at a point in time at which the outlet mass flow rate is nearly the same as that at the inlet. It can be seen that an appreciable portion of the assembly is voided, with some upstream progression occurring in the center channel (i.e., channel no. 7 in Fig. 7.1).

The reported experimental results concerning the boiling regime are only of qualitative nature, with the authors also mentioning chugging at the outlet.

7.3 SLSF-W1 Experiments

The SLSF-W1 Experiment [2] was designed to help resolve fast breeder reactor safety development questions in areas of:

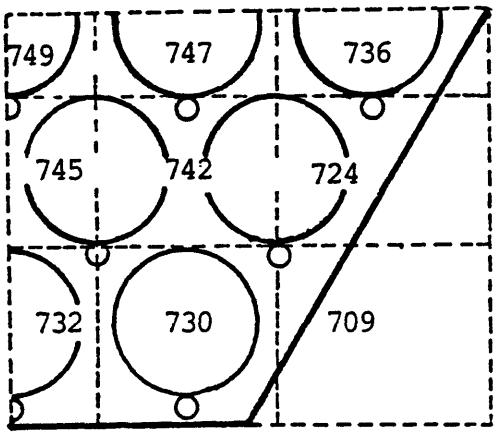

Figure 7.6 GR.19 Radial Sodium Temperature Distribution--
High Flow--End of Heated Zone.

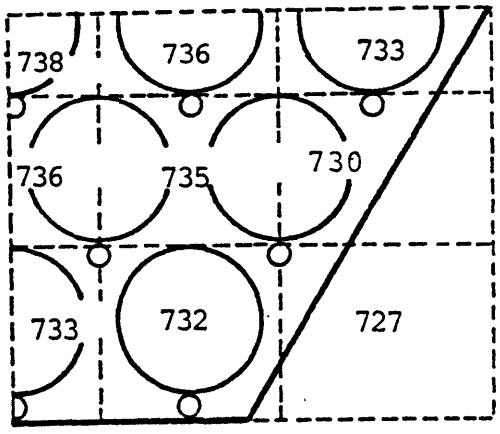

Figure 7.7 GR.19 Radial Sodium Temperature Distribution--
High Flow--End of Test Section.

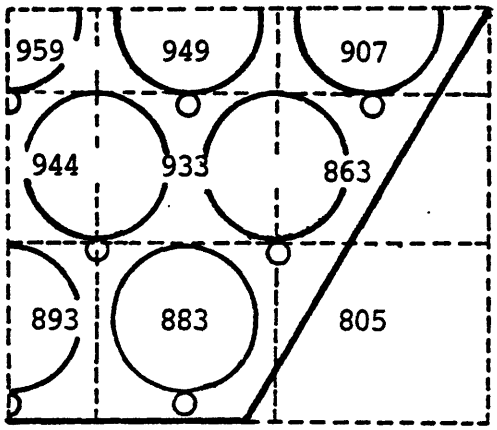

Figure 7.8 GR.19 Radial Sodium Temperature Distribution--Medium Flow--End of Heated Zone.

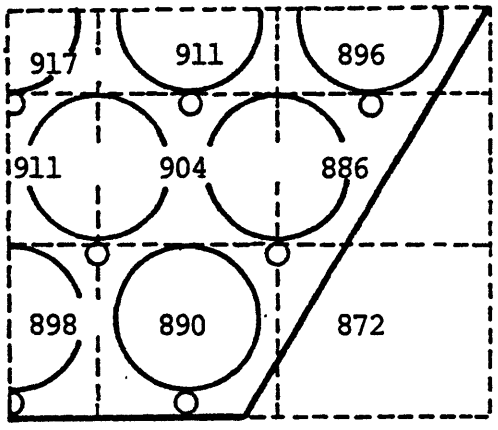

Figure 7.9 GR.19 Radial Sodium Temperature Distribution--Medium Flow--End of Test Section.

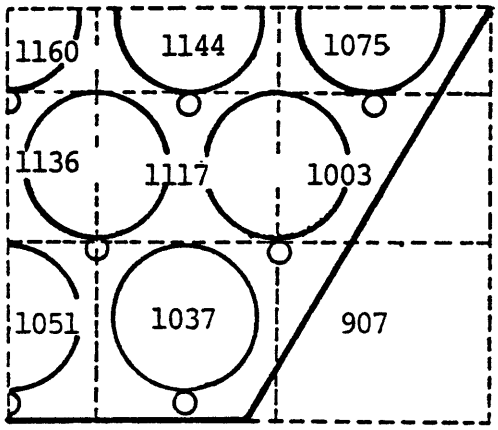

Figure 7.10 GR.19 Radial Sodium Temperature Distribution--Low Flow--End of Heated Zone.

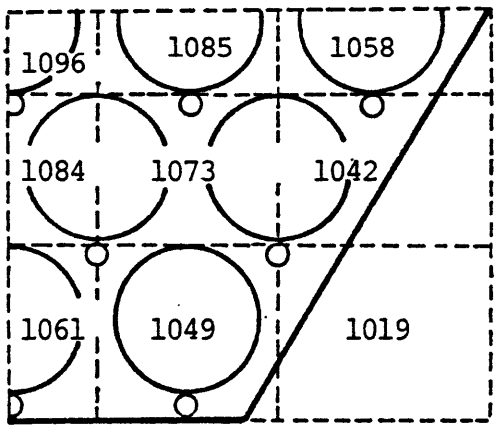

Figure 7.11 GR.19 Radial Sodium Temperature Distribution--Low Flow--End of Test Section.

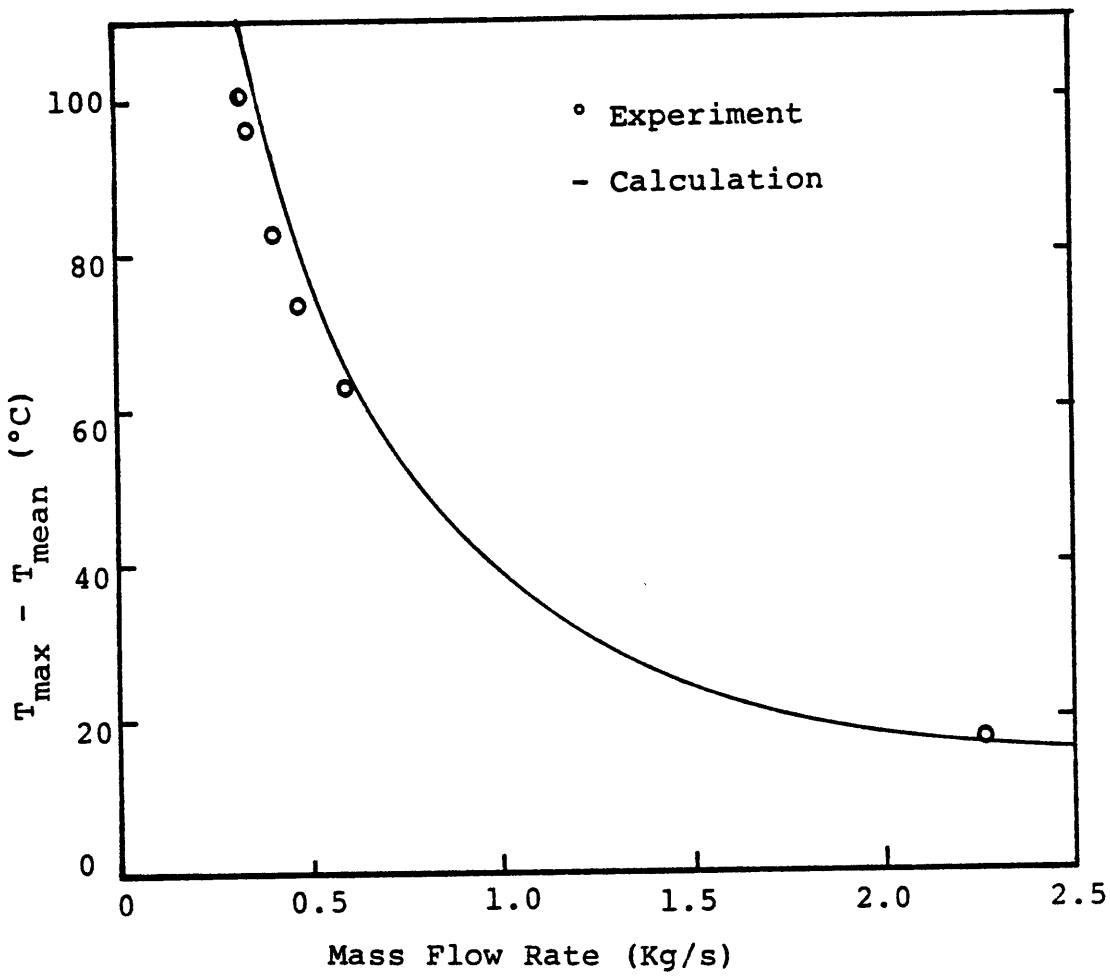

Figure 7.12 GR.19 $T_{max} - T_{mean}$ versus Mass Flow Rate (End of Heated Zone).

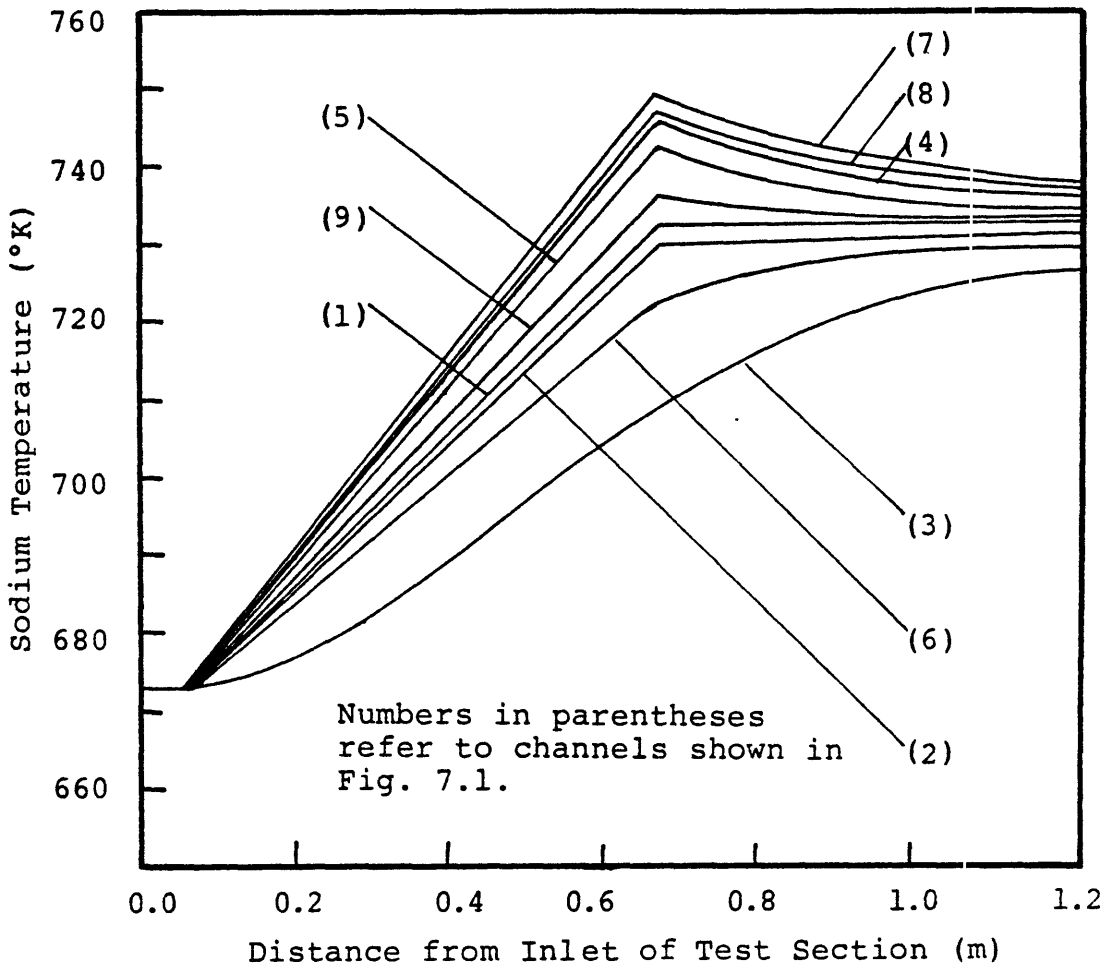

Figure 7.13 GR.19 Axial Sodium Temperature Distribution--High Flow,Three-Dimensional Representation.

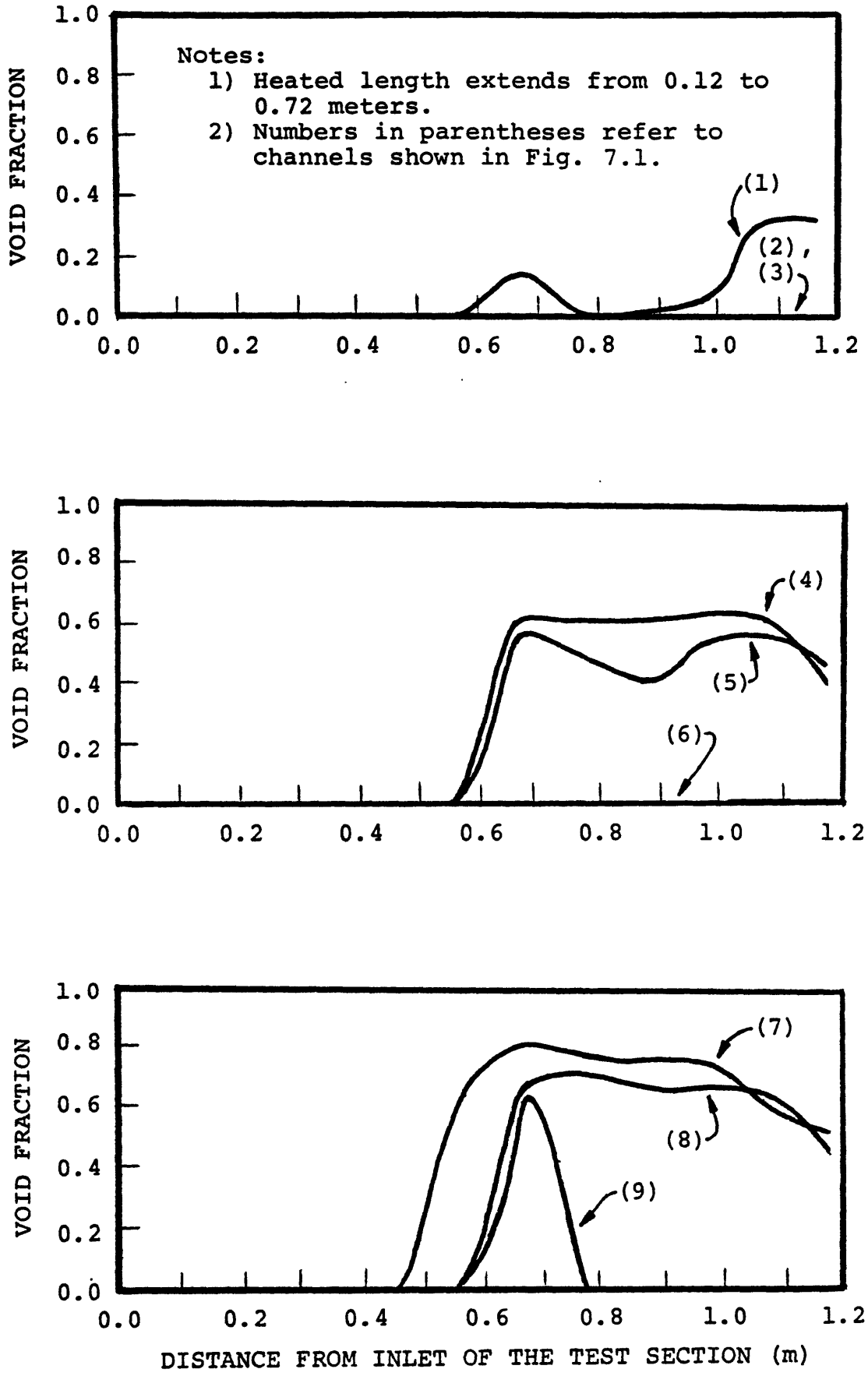

Figure 7.14 GR.19 Axial Void Distribution--Three-Dimensional Representation.

- heat release characteristics of FBR fuel pins during loss-of-piping integrity accident conditions;
- sodium boiling and void characteristics;
- coolant boiling conditions required to produce incipient fuel pin failure.

The SLSF in-pile loop was operated in the Engineering Test Reactor of Idaho National Engineering Laboratory. The principal design data of the test section are given in Table 7.2.

Two series of experiments have been performed. The objective of the LOPI tests was to investigate the fuel pin heat release characteristics for a protected loss-of-piping integrity (LOPI) accident. The other series, the boiling window tests (BWT), was designed to determine if there is a regime beyond the onset of boiling that persists and does not immediately lead to dryout and fuel pin failure. This regime of boiling in the bundle is characterized as "stable" boiling ("boiling window") even though it really pertains to a transient phenomenon.

The 19-pin bundle was designed to allow a good approximation of the behavior of the coolant in

TABLE 7.2

Design Data for the SLSF W1 Experiment

Number of Pins	19
Fuel Pellet OD (m)	4.94×10^{-3}
Clad OD (m)	5.842×10^{-3}
Clad ID (m)	5.030×10^{-3}
Wire Wrap OD (m)	
inner pins	1.422×10^{-3}
outer pins	7.11×10^{-4}
Wire Wrap Lead (m)	.3048
Flat to Flat (m)	3.26×10^{-2}
Duct Wall Thickness (m)	1.016×10^{-3}
Length of Fuel (m)	.9144
Inlet to Bottom of Fuel (m)	.2794
Top of Fuel to End of Pins (m)	1.270
Fill Gas	Helium-Neon (10%), 1.7 bar at 68°F
Fuel	Uranium-Plutonium mixed oxide, Pu 25% of total mass.
Inlet Temperature (°C)	388

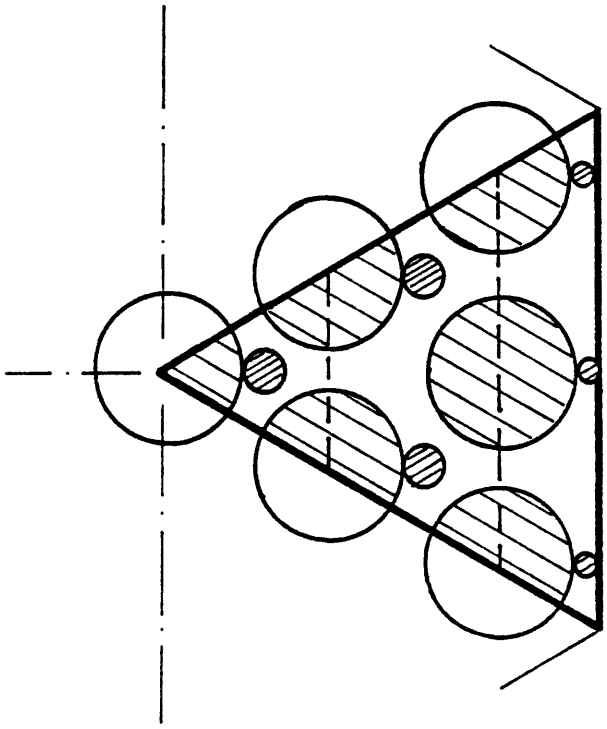

Figure 7.15 Geometrical Configuration for the SLSF W1 Experiment.

a full size fuel bundle: the diameter of the wire wrap spacer for the outer pins was half of that used for the inner pins, thus reducing the amount of flow in the peripheral region; at the same time, through appropriate enrichment selection, an almost flat radial power profile was achieved. The axial power distribution was cosine-shaped.

For simulations, we chose tests from each series. Given the azimuthal symmetry of the test bundle, a two-dimensional (r-z) representation (Fig. 7.15) using three radial channels, was deemed adequate. The measured total inlet mass flow rate was used as inlet boundary condition.

7.3.1 LOPI Tests

Each LOPI test was initiated from steady-state full power, full flow conditions. Over the first 0.5 seconds of the transient, the inlet flow was rapidly decreased. At 0.65 seconds into the transient, the reactor was scrammed. At approximately 3.0 seconds, flow recovery started.

Two of the LOPI tests were selected for simulation. The first, LOPI 2A, started from a power of 668 kW (test bundle power) and a mass flow rate of 1.95 Kg/s. The flow decay curve is shown in Fig. 7.16. There was no indicaton of boiling in this test, and our calculations confirmed it. The reason for choosing

this non-boiling test was a desire to check our overall model, under single-phase conditions, insofar as heat release characteristics are concerned: thermal inertia of fuel and clad, stored energy, and heat transfer to coolant.

The experimental results and our predictions are compared in Figs. 7.17-7.19. The agreement is quite good, especially so if one bears in mind that the measurements are point readings, whereas the predictions represent average mesh cell temperatures. The axial distribution of the bundle-averaged sodium temperature is plotted in Fig. 7.20 at different times into the transients. One notes that early in the transient (say up to about 2.3s), the large thermal inertia of the fuel pins almost totally obscure the fact that the scram occurred earlier. As a result the maximum temperature changes only slightly, while the "peak" broadens. Later, the fuel cools down and so does the sodium.

The second test selected from this series was LOPI 4. We note that originally the tests in this series were to be different only with respect to the fuel condition prior to the accident. However, the failure of one of the thermocouples used for test section power

calculation lead to running of the experiment at approximately 5% over power (specifically 705.3kW). The inlet mass flow rate, shown in Fig. 7.21 was almost identical to the previous one.

Our results and the experimental data are displayed in Figs. 7.22-7.24. The sodium temperature measurements at the end of the heated zone in the central and middle channels are well matched by our calculations. Our results indicate a somewhat higher temperature than the data taken near the midpoint of the heated length, at the center of the assembly. The factors that may account for this difference are local temperature distribution, thermocouple lag and magnitude of radial coolant mixing. Unfortunately, the assembly was too sparsely instrumented at this axial level, thus preventing the inference of a radial temperature distribution, which might have helped in making a more precise assessment.

As in the experiment, our calculation predicted about 0.5 seconds of boiling (Fig.7.22). Noteworthy that the voided region was limited to the central channel and it extended only a small distance (on the order of 5 cm) above and below the end of the heated section. The test results indirectly confirm this void evolution in that only the centrally located thermocouples display

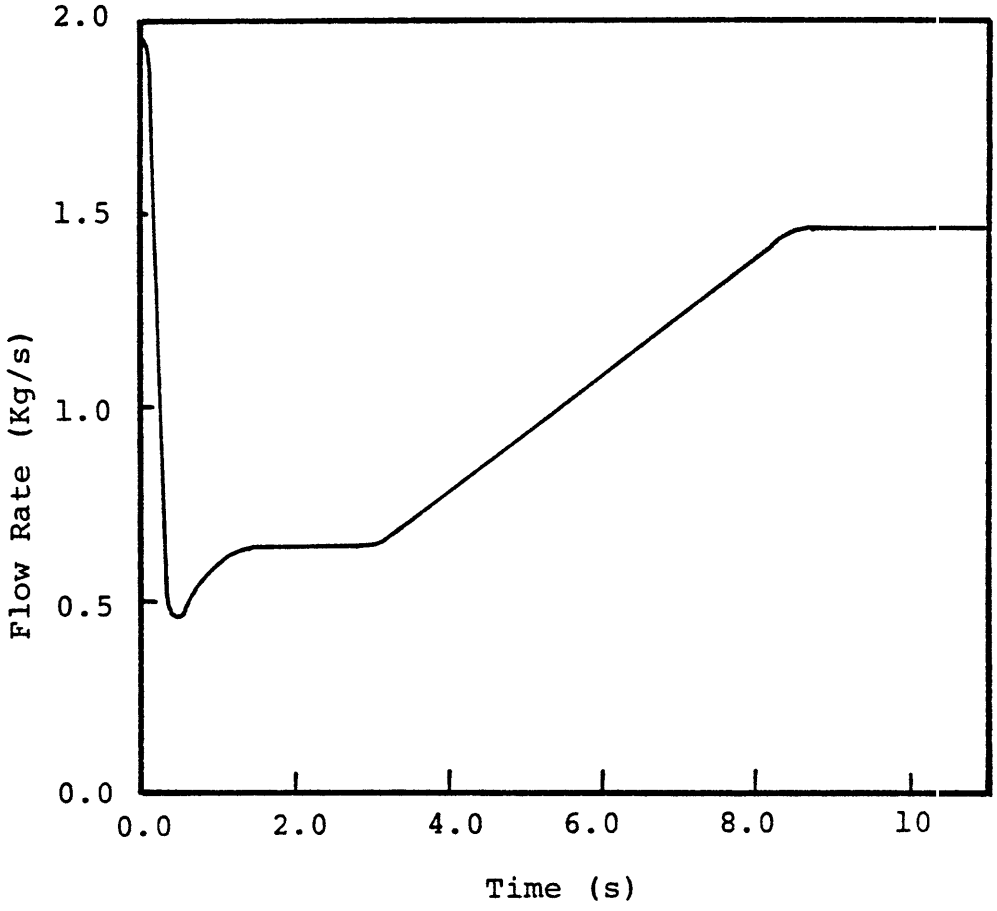

Figure 7.16 SLSF-LOPI 2A Inlet Mass Flow Rate.

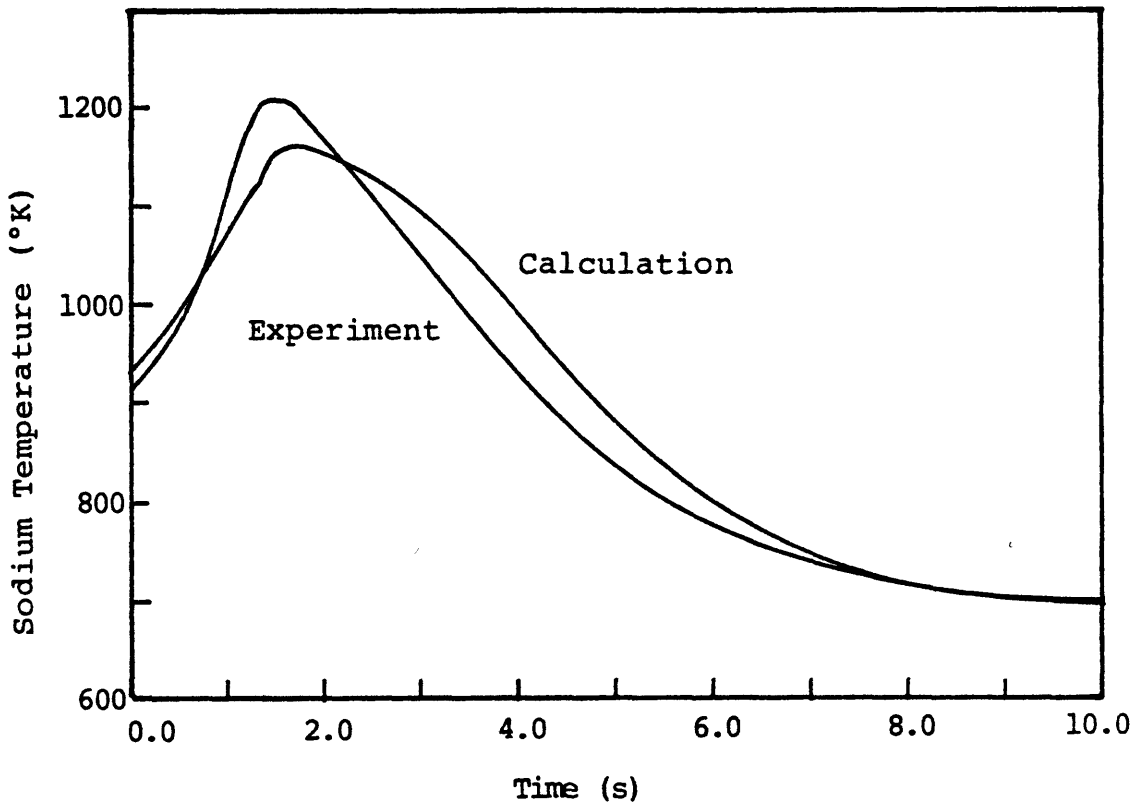

Figure 7.17 SLSF LOPI2A Sodium Temperature in Central Channel, at .94m above Bottom of Fuel (End of Heated Zone)

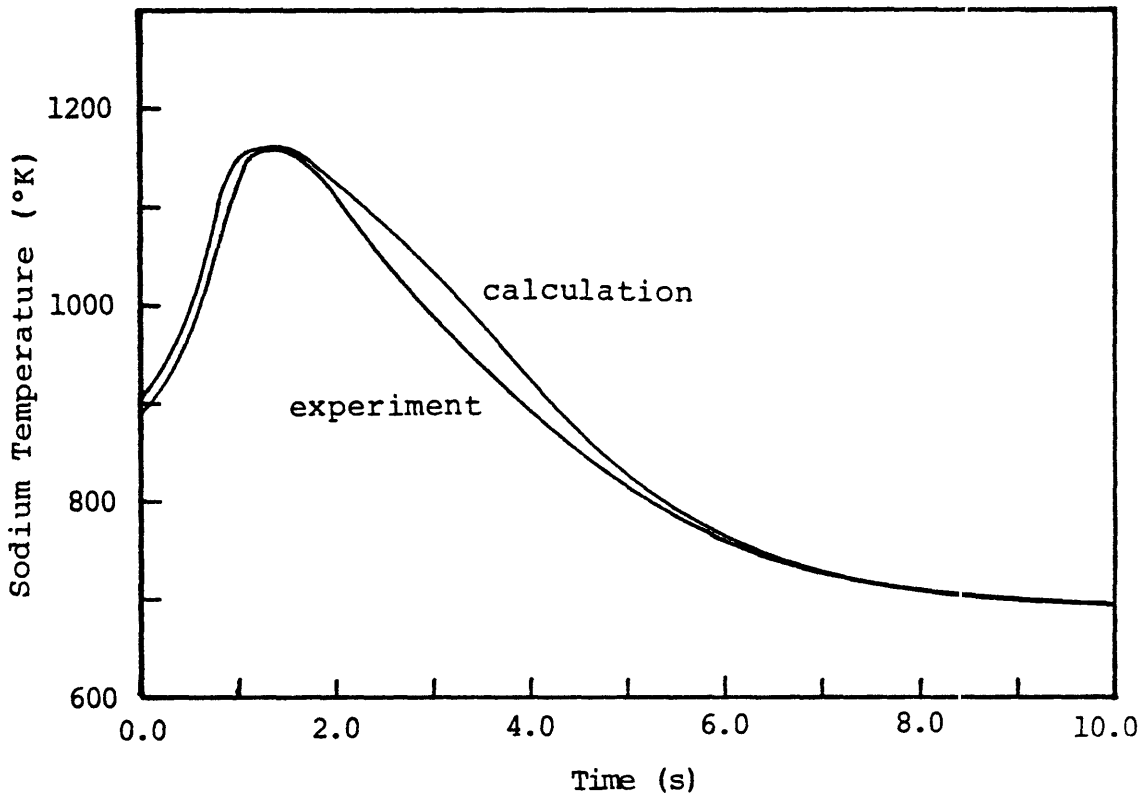

Figure 7.18 SLSF LOPI2A Sodium Temperature in Central Channel, at .74m above Bottom of Fuel.

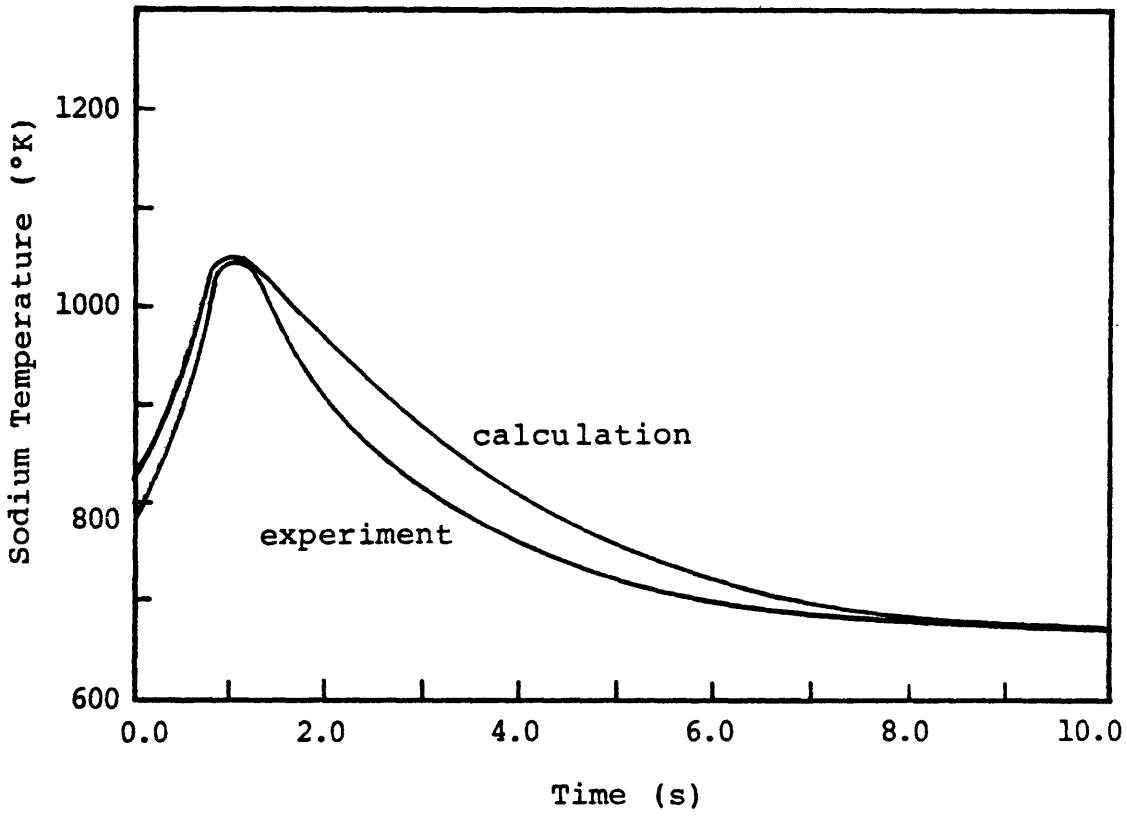

Figure 7.19 SLSF LOPI2A Sodium Temperature in Central Channel, at .46m above Bottom of Fuel (Middle of Heated Zone).

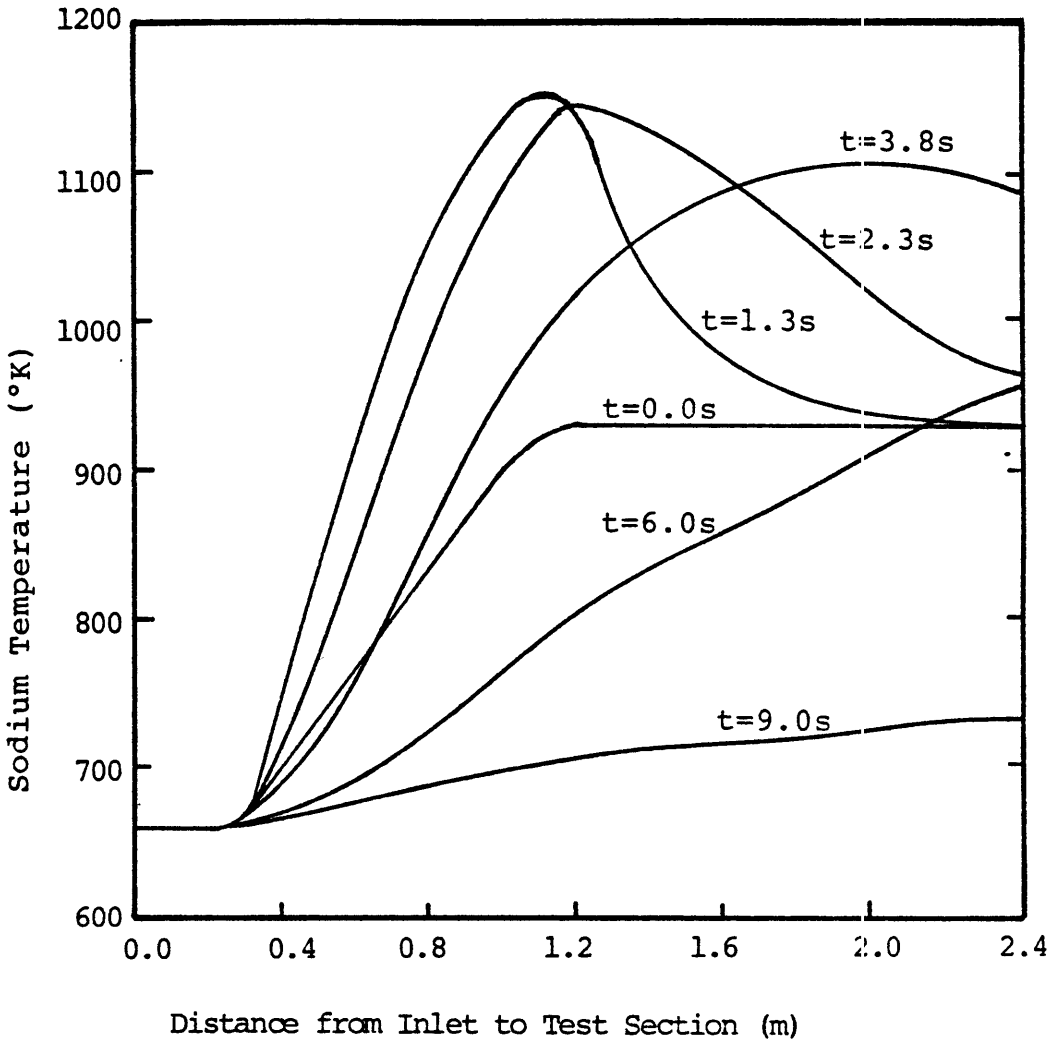

Figure 7.20 SLSF LOPI2A Axial Bundle-Average Sodium Temperature Distribution.

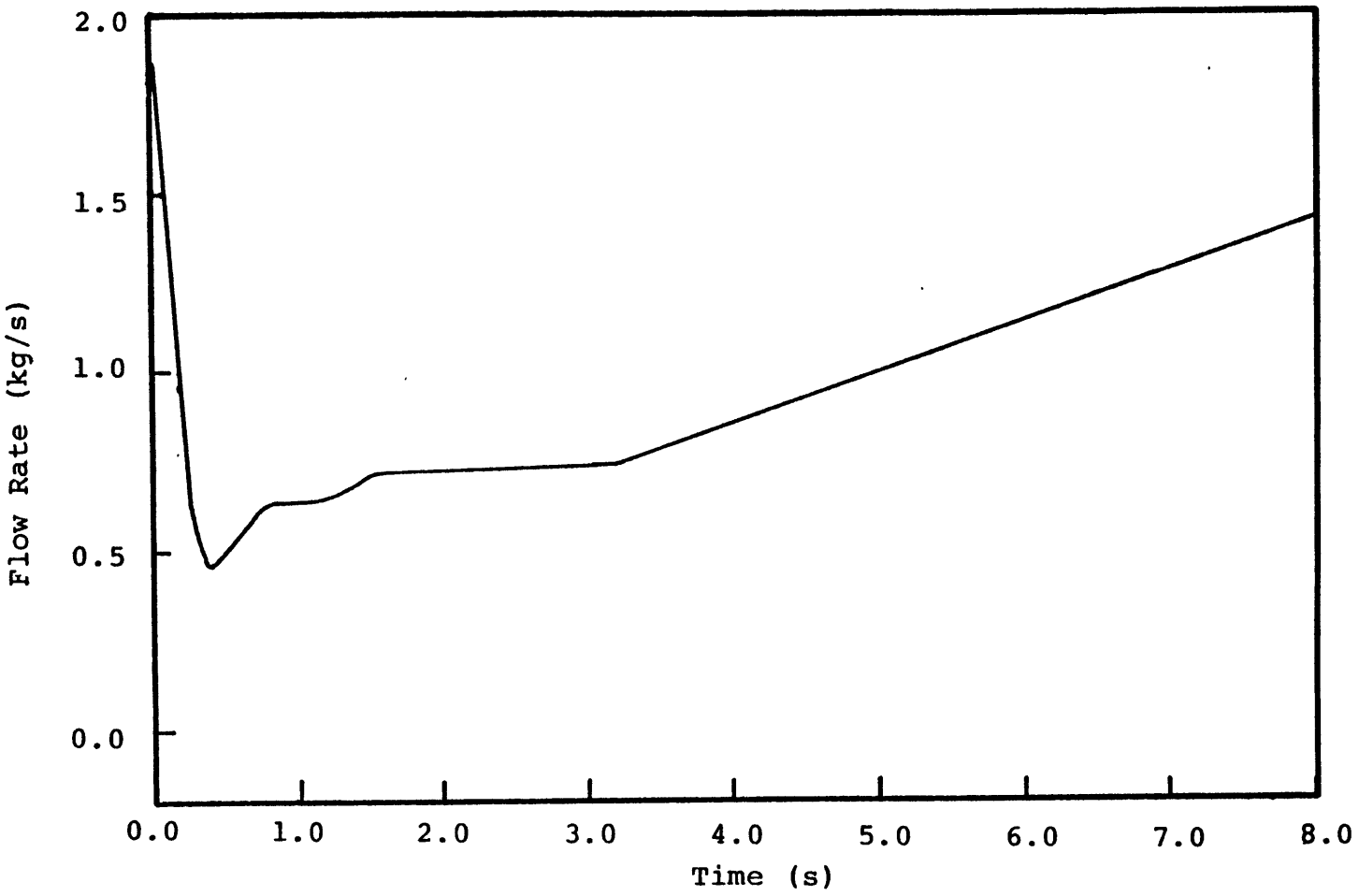

Figure 7.21 SLSF-LOPI 4 Inlet Mass Flow Rate.

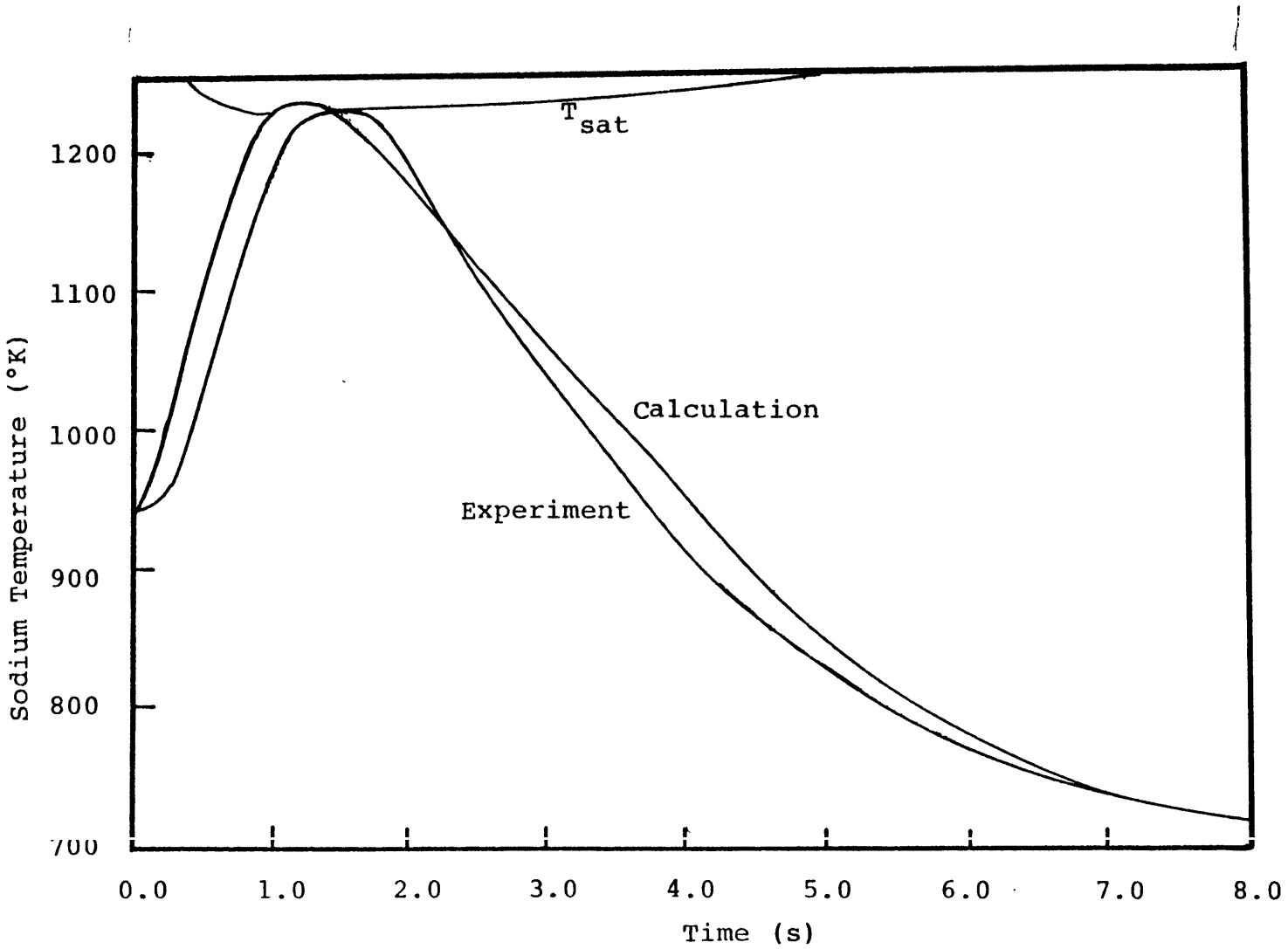

Figure 7.22 SLSF-LOPI 4 Sodium Temperature in Central Channel, End of Heated Zone.

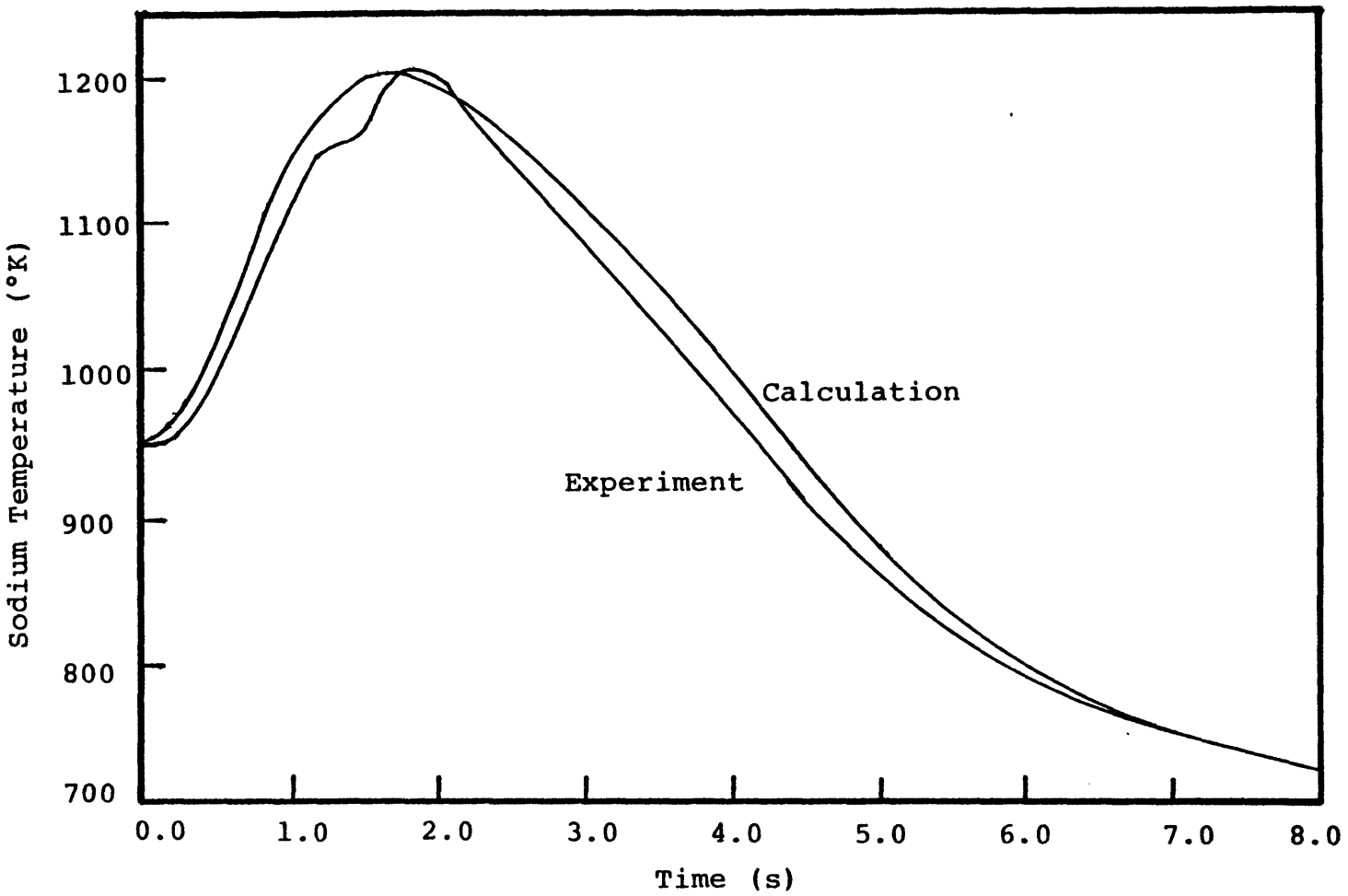

Figure 7.23 SLSF-LOPI 4 Sodium Temperature in Middle Channel, End of Heated Zone.

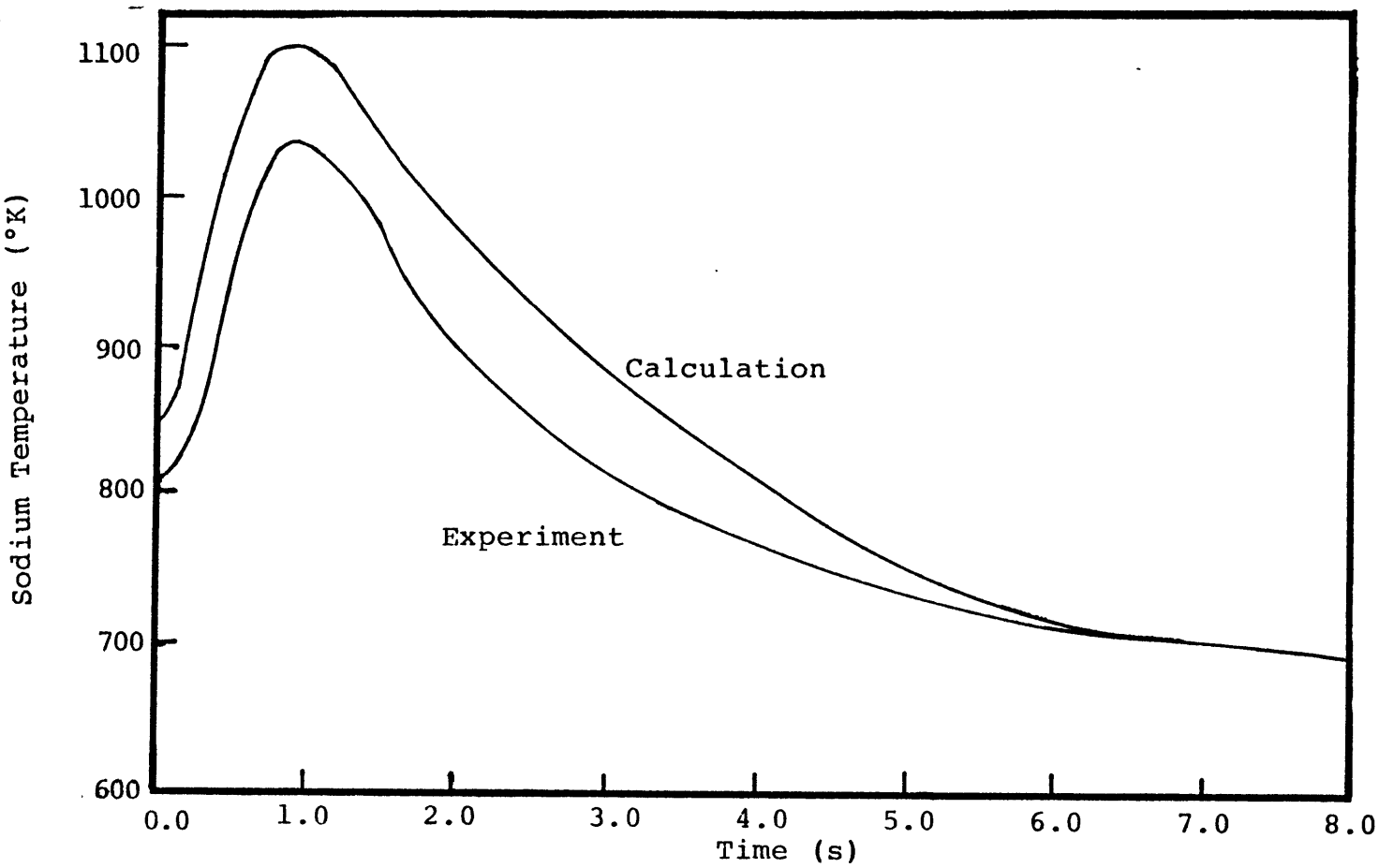

Figure 7.24 SLSF-LOPI 4 Sodium Temperature in Central Channel, Middle of Heated Zone.

the almost flat traces indicative of the saturation temperature being reached.

7.3.2 BWT Tests

In these tests, the bundle power is maintained constant, while the inlet flow rate is rapidly decreased to its "low flow" value, in 0.5 seconds, kept there for a specified period of time and then finally returned to its initial value in 0.5 seconds. The objective of these tests was to determine stable boiling limits as a function of fuel pin power and bundle flow rate.

The last test in this series, BWT 7B', was chosen for simulation. This test was the most severe, resulting in clad dryout and fuel failure. It was felt that this test, being characterized by the highest power-to-flow ratio in this series, would provide a proof of capability, since none of the "milder" tests were expected to create essentially new situations in as far as our methods were concerned.

The power in this test was maintained fixed at 668 kW until 3.5 seconds into the transient, at which time indications of severe dryout lead to the decision to scram the reactor. The measured inlet flow rate is shown in Fig. 7.25. Boiling initiation at about 1.7 seconds caused an increasingly rapid inlet flow

decay, leading to flow reversal at about 2.8 seconds, followed by flow oscillations.

Our simulation focused on the first 3 seconds of the transient, i.e, the pre-dryout period.

Our results are shown together with the experimental data in Figs. 7.26-7.28. We match quite well the temperature in the central channel, at the end of the heated zone. As in the experiment, boiling also started at about 1.7 seconds into the transient. Our calculations indicate a higher temperature at the mid-plane of the heated zone just as in the case of LOPI 4. The comments already made there also pertain to this experiment. We do not have, at this point, a clear explanation for this discrepancy.

The axial and radial boiling front propagation is illustrated in Figs. 7.29 - 7.31. One notes about 0.6 seconds delay between the boiling inception times in the central and peripheral channels (1.7 vs 2.3 sec). The pronounced two-dimensional character of the void evolution in the early part of the transient is evident.

The existence of a stable boiling period prior to dryout is an indication of the overly conservative nature of the modeling of coolant boiling and cladding

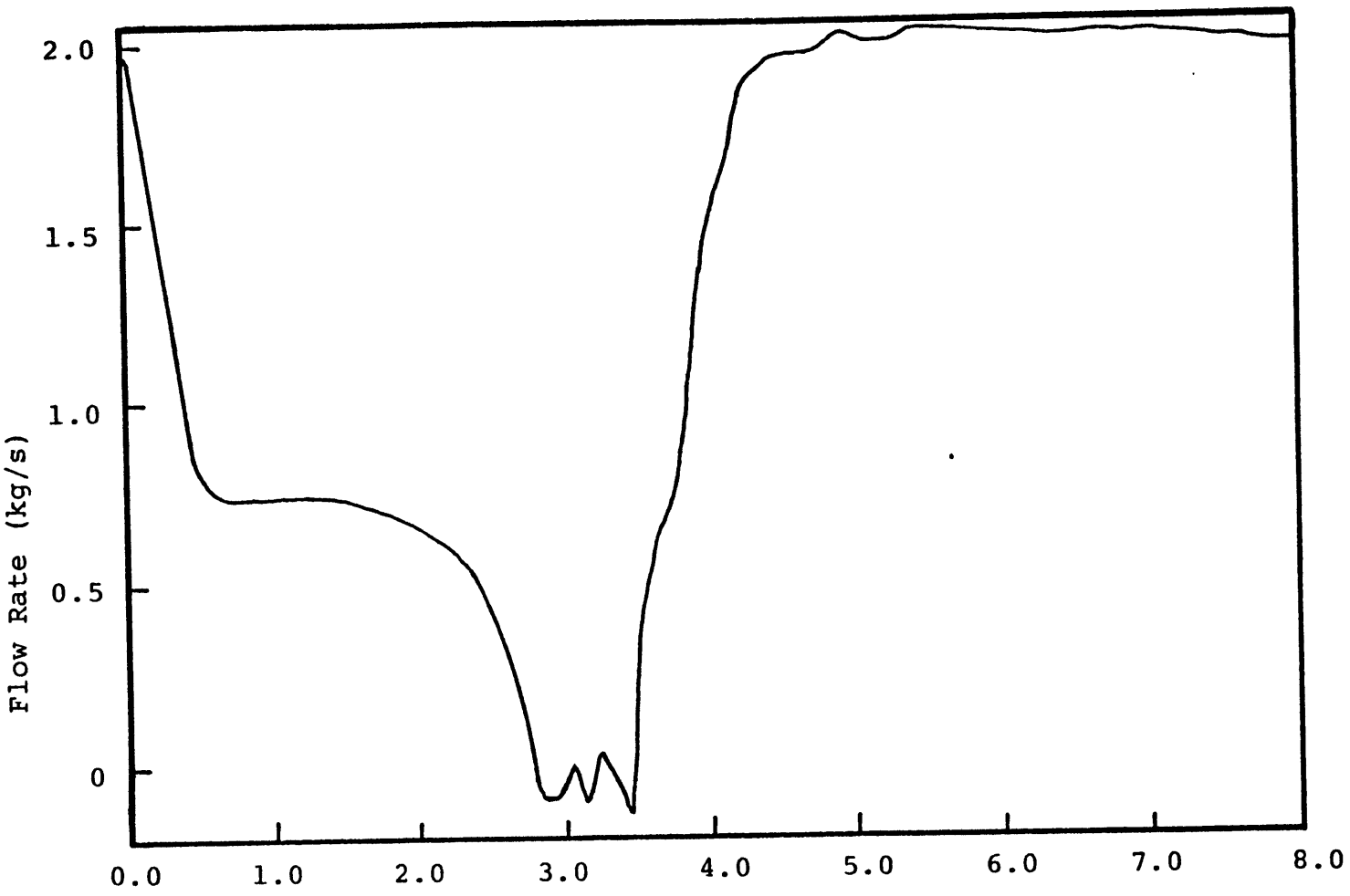

Figure 7.25 SLSF--BWT 7B' Inlet Mass Flow Rate

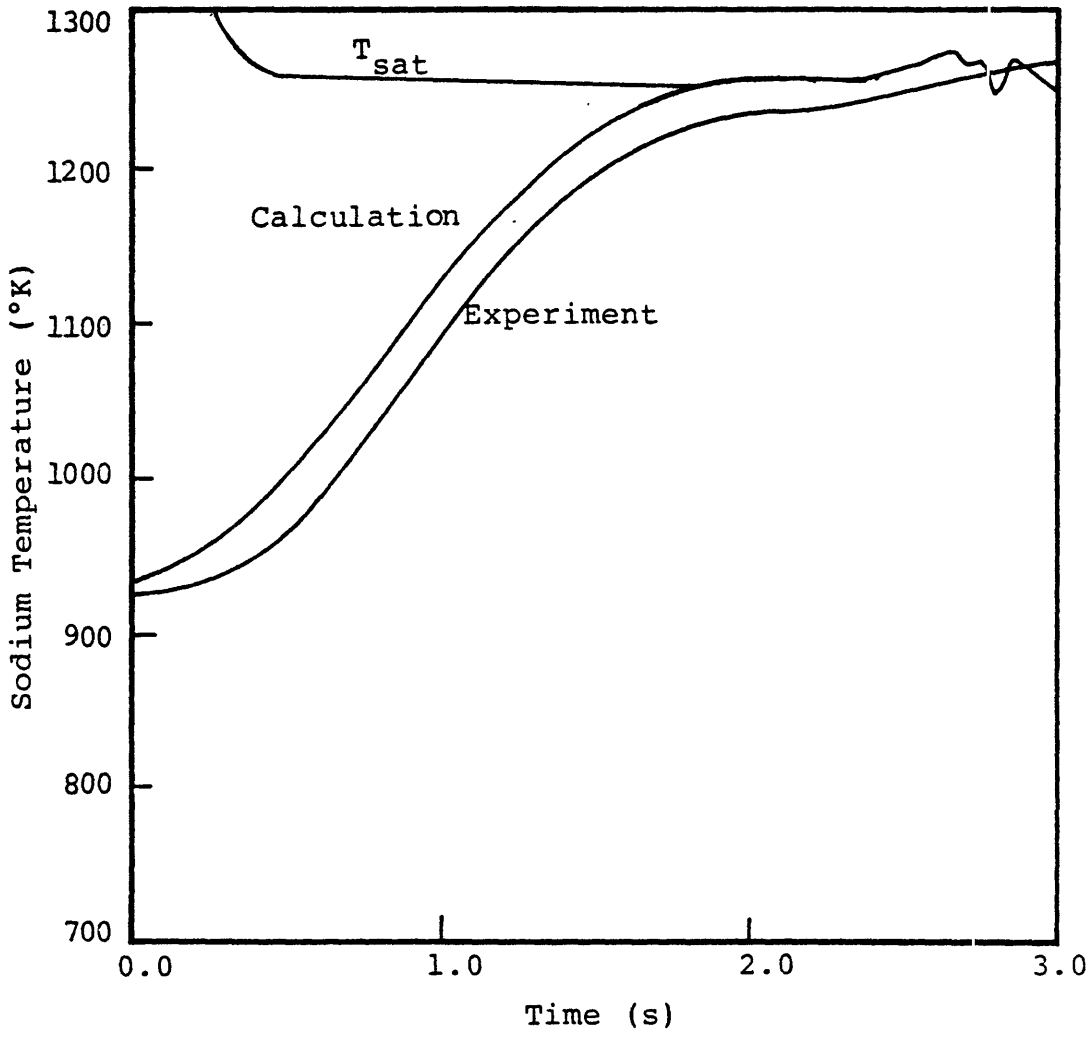

Figure 7.26 SLSF BWT 7B' Sodium Temperature in Central Channel, End of Heated Zone.

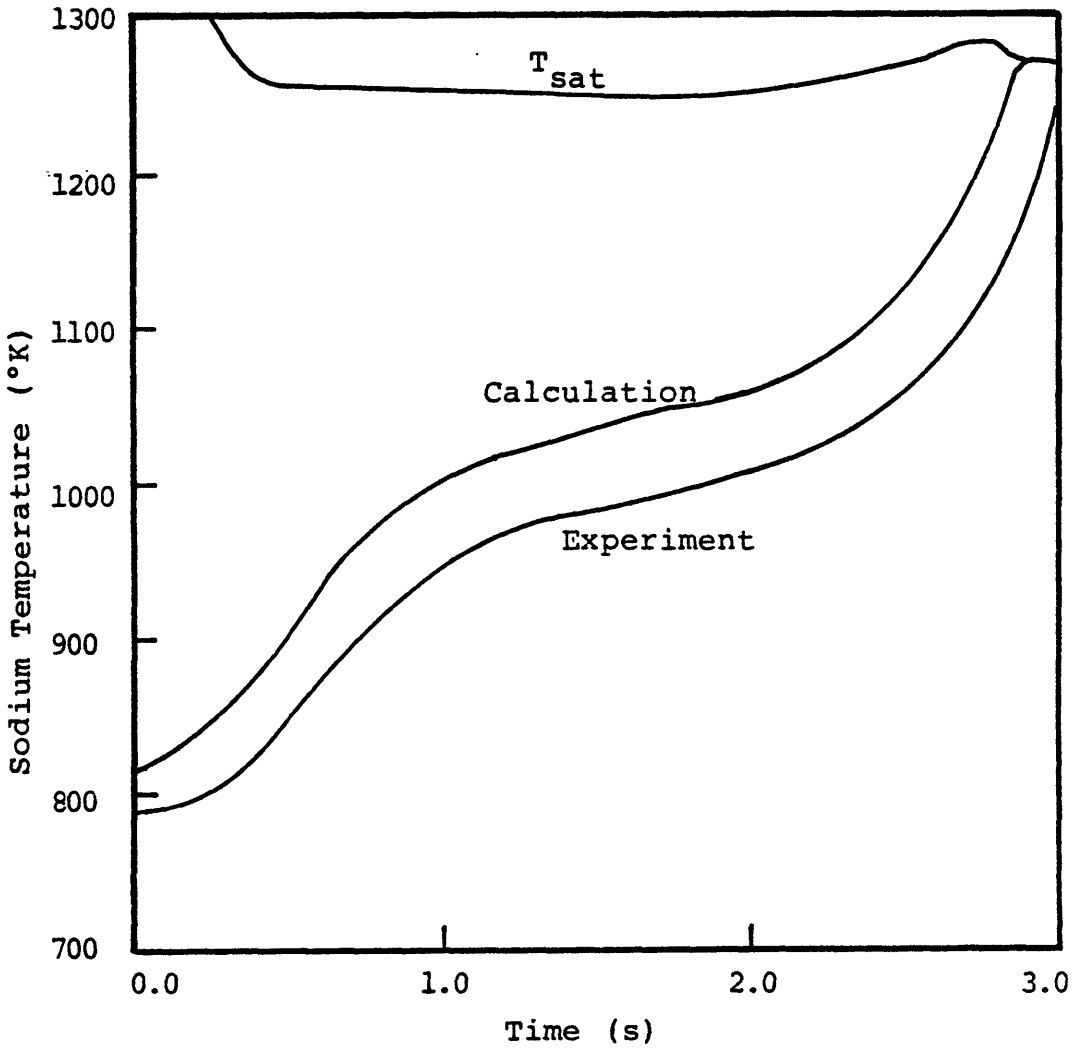

Figure 7.27 SLSF-BWT 7B' Sodium Temperature in Central Channel, Middle of Heated Zone.

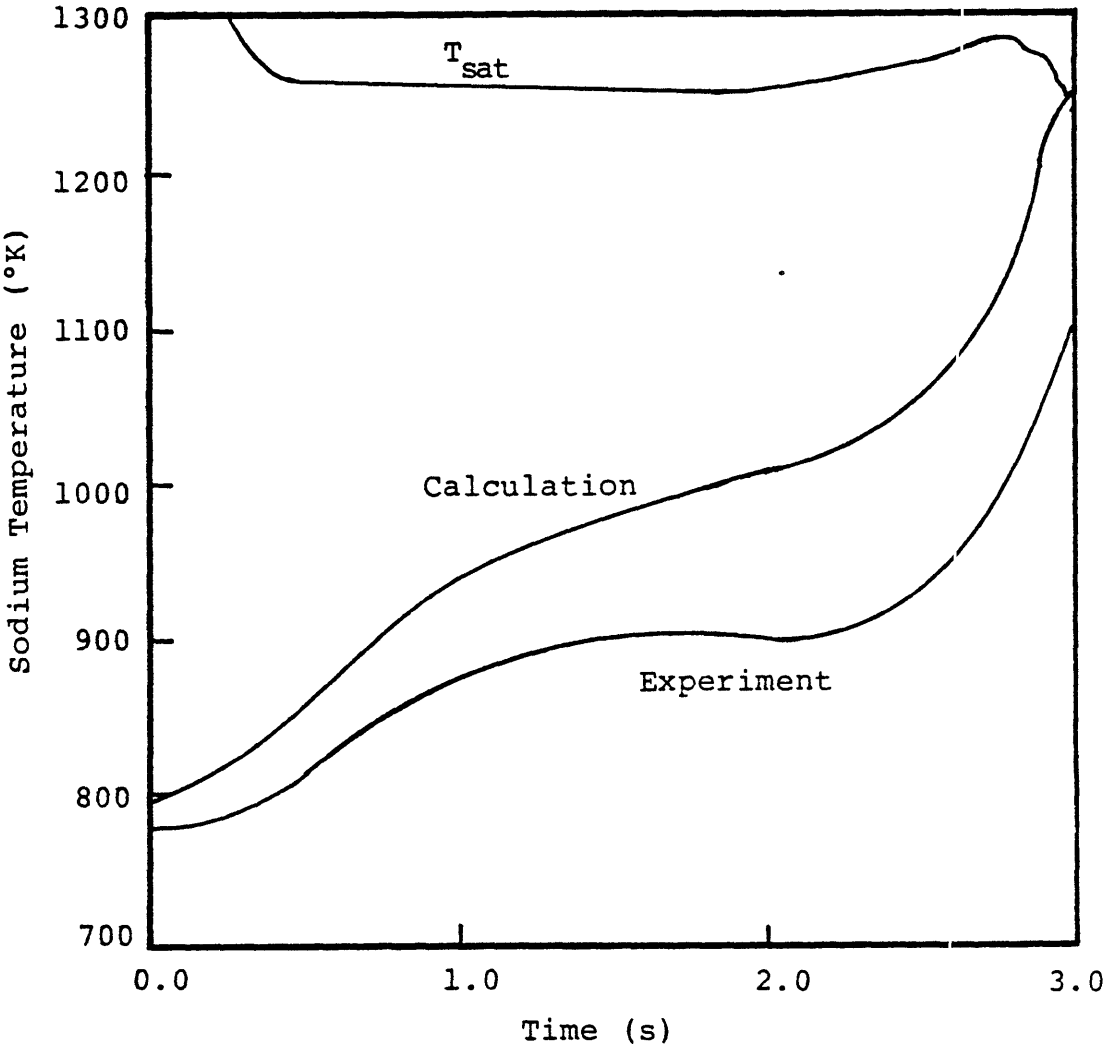

Figure 7.28 SLSF-BWT 7B' Sodium Temperature in Peripheral Channel, Middle of Heated Zone.

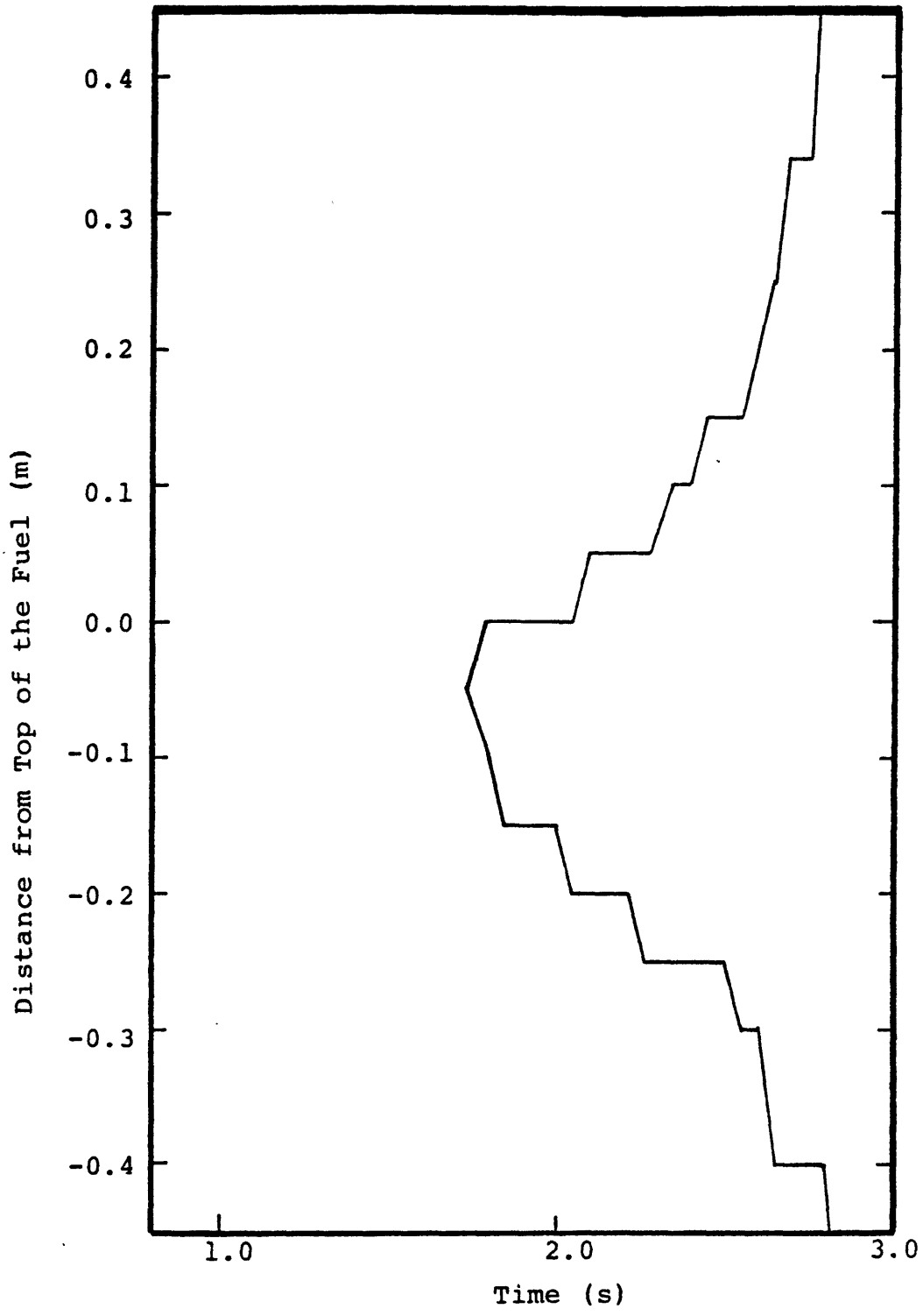

Figure 7.29 SLSF-BWT 7B' Map of Boiling Region--Central Channel.

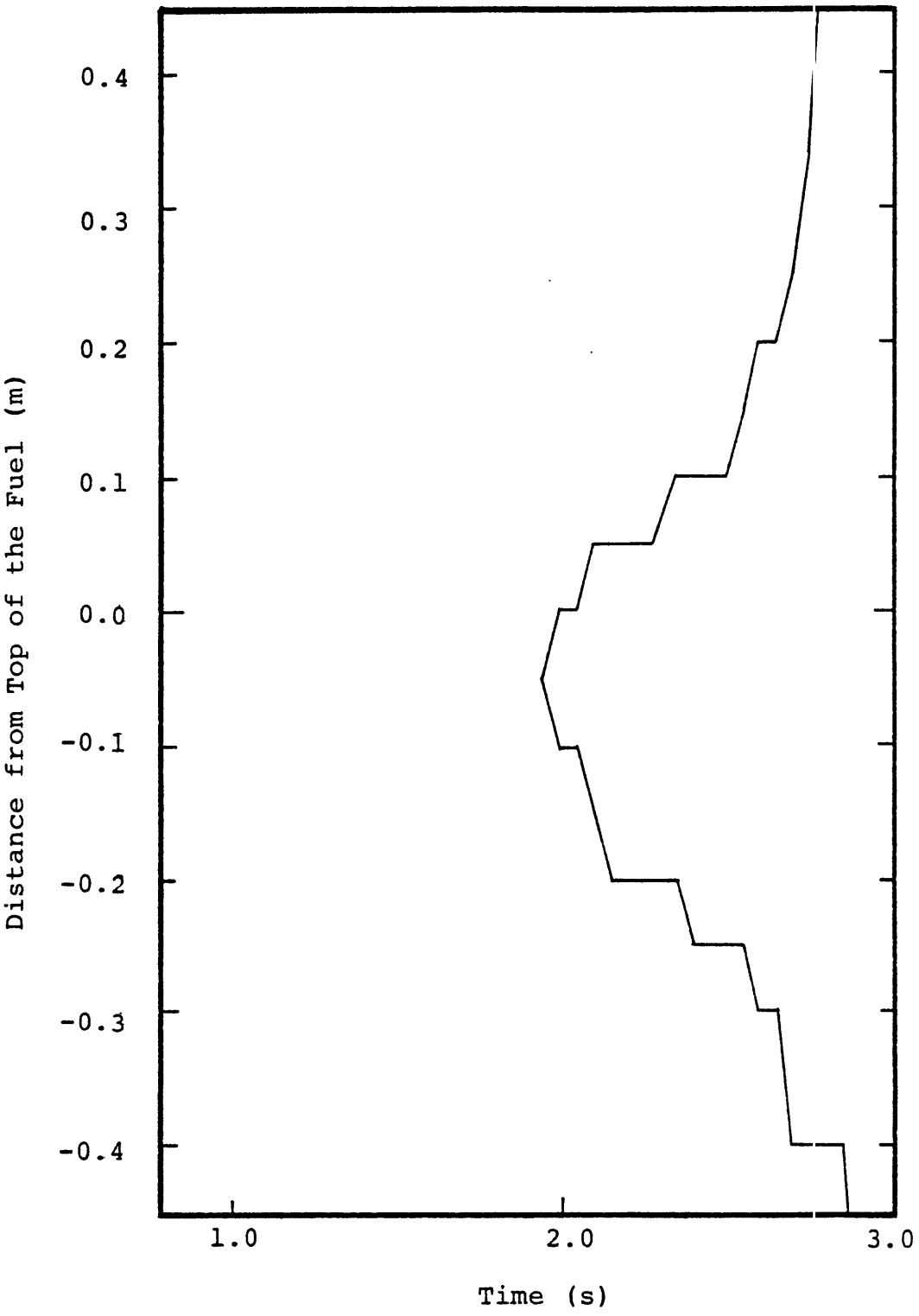

Figure 7.30 SLSF-BWT 7B' Map of Boiling Region--Middle Channel.

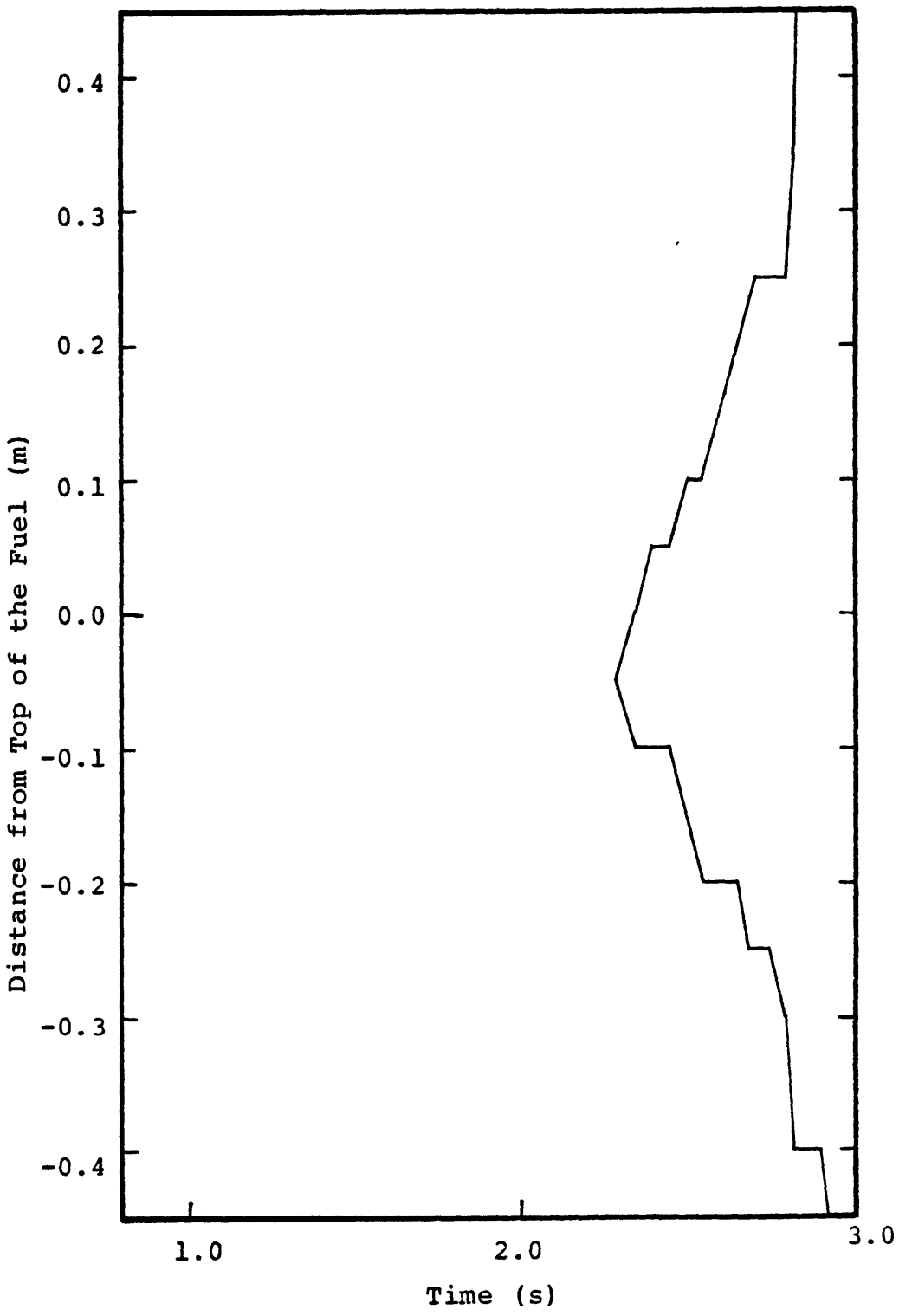

Figure 7.31 SLSF-BWT 7B' Map of Boiling Region--
Peripheral Channel.

dryout in current safety codes.

It is probably worth noting that while fuel pin cladding breach was detected (by the Cover Gas Sampling System), the fuel bundle damage appeared to be minimal, with no indication of coolant flow blockage.

7.4 References

1. G. Basque, D. Grand, B. Menant, "Theoretical Analysis and Experimental Evidence of Three Types of Thermohydraulic Incoherency in Undisturbed Cluster Geometry", IAEA Specialists' Meeting on Thermodynamics of Fast Breeder Reactor Fuel Sub-Assemblies under Nominal and Non-Nominal Operating Conditions, Karlsruhe, Germany (1979).

2. R.B. Rothrock and J.M. Henderson, Description and Results of the W-1 SLSF Experiment-Fuel Pin Heat Release Characteristics and Sodium Boiling Stability," Hanford Engineering Laboratory Report No. HEDL-TC-1497, (1979).

CHAPTER 8. CONCLUSIONS AND RECOMMENDATIONS

8.1 Conclusions

A three-dimensional numerical model for the simulation of sodium boiling transients has been developed. The model uses mixture mass and energy equations, while employing a separate momentum equation for each phase. Thermal equilibrium on the saturation line between coexisting phases is assumed.

The set of equations governing the evolution of the two-phase flow has been rigourously derived, starting from the local-instantaneous form of the field equations. The assumptions made in obtaining the final "working" set of equations have been clearly identified, facilitating further refinements wherever warranted by the particular application.

The four governing equations are supplemented by a number of constitutive relations, addressing the interphase and intraphase exchanges, as well as the fluid-solid interactions. Here our efforts have been directed mainly towards establishing a consistent framework, followed by a careful selection and implementation of models. It should be noted that our four-equation two-phase flow model requires only one interfacial relation, i.e., the momentum exchange, compared to the six-equation model

which needs two additional relations, describing the mass and energy exchanges. Consequently, the relatively high degree of uncertainty currently associated with the interfacial exchange phenomena is considerably reduced.

From a numerical point of view, our basic approach is a semi-implicit method, in which pressure pulse propagation and local effects characterized by short characteristic times are treated implicitly, while convective transport and diffusion heat transfer phenomena, associated with longer time constants, are handled explicitly. The method remains tractable and efficient in multidimensional applications. The temporal and spatial discretization process generates a set of non-linear equations, solved by Newton's method, in its regular form or in one of its related version, the secant and the parallel-chord schemes, which under some circumstances, may become more advantageous. The fluid-to-heat source coupling is handled in a highly implicit manner, avoiding stability problems related to some of the rather short time constants involved.

A very detailed discussion of the numerical methods involved has been presented, attempting as much as possible to justify the choice of various schemes, to reveal and

explain some subtleties, in order to provide a firm basis for future work.

The particular discretization and linearization scheme chosen leads to a large system of linear equations for pressures. The pressure field incorporates both the spatial coupling (due to fluxes of mass, momentum and energy) and, through a reduction process, the local coupling. Consequently, the efficient and accurate solution of the pressure field is fundamental to our method. A number of solution schemes, both direct and iterative, have been investigated.

Our conclusion is that for the small to moderately-sized problems we have dealt with, the direct solutions are superior in as far as the computing effort is concerned, for a given level of accuracy. We emphasize that this conclusion has been reached for a particular computing environment. For larger problems or, in general, in circumstances where the storage requirements become the limiting factor, we found the successive Block Over-relaxation (using as "blocks" planes of cells in the direction(s) characterized by small mesh sizes), with adaptive optimum relaxation parameter search, to be a very suitable scheme.

A large flexibility is provided regarding the choice of boundary condition. In addition to allowing

the more customary velocity and pressure boundary conditions, a method enabling the specification of the total inlet mass flow rate was devised. Noteworthy is the fact that the method is perfectly integrated into the pressure field solution, does not call for another layer of iterations, and does not add significantly to the total computational work and storage requirement.

A detailed stability and characteristic analysis has been performed. The main conclusion of the stability analysis was that stable solution may be obtained even for apparently ill-posed problems. However, we showed that while the very short and the very long wavelength components are stabilized by the donor cell differencing and the damping terms respectively, the intermediate wavelength components may be limiting from a stability point of view.

The characteristic analysis confirmed the existence of complex characteristics for a wide range of two-phase flow conditions. We found that an approximate (analytical) analysis assuming incompressible phases was in very good agreement with the exact (numerical) analysis except very near the limits of the void fraction range. Another interesting and somewhat surprising finding was that apparently there are differential constitutive relations which do not affect the characteristics.

Simulation of a number of experiments has yielded very encouraging results. The numerical method and the constitutive relations have performed quite well, especially so in light of the extreme severity of the conditions involving sodium boiling. The major conclusions, drawn from our calculational experience are:

a) For single-phase conditions, the variant of our method treating the convection terms in the energy equation explicitly gives excellent results and it is advantageous computationally because the coefficient matrix of the pressure field becomes symmetric and positive definite;

b) For two-phase flows, the semi-implicit treatment of the convection in both mass and energy equations has proved generally superior;

c) In some circumstances, especially at phase transitions, Newton's method (or its variations) required very short time steps for convergence;

d) A modified strategy has been found to perform quite robustly in our applications: instead of a full non-linear iteration, the

linearization is performed only about the old time step and then the mass and energy residuals are kept below acceptable limits through adequate time step control.

We would like to emphasize that all our calculations have been run on a best estimate basis, without any fine tuning. In light of the above, the performance of the constitutive relation package is quite remarkable.

Nonetheless, based on our work of selecting, modifying and adapting various models, we certainly feel that further work in a number of areas, mentioned in the next section of this chapter, is needed. Only a systematic sensitivity analysis would point areas in which refinement or replacement of constitutive models would be most beneficial. Obviously, such an analysis would alsc greatly increase the confidence in our model's predictive capabilities.

8.2 Recommendations

The research performed during the development and application of the four-equation sodium boiling model has enabled us to identify areas in which further work would be highly advisable. Such additional investigation would address both physical and numerical modeling questions.

To begin, work is needed with regard to the treatment of two-phase flow pressure losses in LMFBR rod bundles using wire-spacers. The complex flow pattern and the inability to quantitatively identify two-phase flow regimes combine to inject a significant dose of uncertainty into any modeling attempt. The degree of uncertainty would be greatly reduced only by the availability of reliable and detailed experimental results. However, the difficulty of obtaining such results for the geometries and flow conditions of interest should not be underestimated.

A closely related aspect, the interfacial momentum exchange, requires further attention. Local pressure distribution effects, i.e., virtual mass, may have to be included and generally the local flow topology may be given increased importance. Once again the difficult geometry constitutes a major impediment in removing the rather speculative character of various hypotheses.

The fluid-solid heat transfer needs further investigation. While the single-phase and saturated boiling regimes seem to be adequately modeled, additional work is needed to correctly complete the boiling curve. In particular, the disruption of the liquid film, leading eventually to

dryout requires careful consideration, given its effect on the rate of progression of some transients.

The steady-state single-phase liquid energy diffusion appears correctly accounted for. Further work is needed to assess transient effects, as well as to model the conduction and mixing of a two-phase mixture.

Our applications have dealt with azimuthally uniform configurations. In situations displaying a significant departure from azimuthal symmetry, such as power skew and flow blockages, the peripheral swirl flow, neglected in our work, must be incorporated. In such situations, a more detailed representation of the hex can may also be called for.

Given the tight and complex nature of the coupling of various phenomena in two-phase flow, it is almost impossible to predict the impact of a change in a particular model on the results. It is thus imperative that a systematic sensitivity analysis be undertaken to identify those constitutive models which have the strongest effect on the overall results.

Regarding the numerical method, we feel that a concentrated effort must be devoted to further study non-linear solution schemes. Given the extremely severe non-linearities associated with the numerical simulation

of sodium boiling and the fact that often the limitation on the time step size was due to difficulty in obtaining a converged solution, the need for further work in this area cannot be overstated.

On a longer term basis, the possibility of higher degrees of implicitness should be investigated. Indeed at very high void fractions, the large vapor velocities may lead to rather short time steps, for the mesh size of interest, if the convection is treated explicitly, as in our method. However, in light of the previous observation, the impact of a longer time step on the non-linear solution must be assessed.

The severe nature of the sodium boiling transients can generate pressure and flow oscillations and in some instances even temporary total flow reversals. In such situations, the flow dynamics of the test section and of the rest of the loop are essentially inseparable. If one simulates only the test section, providing adequate boundary conditions often becomes a trial-and-error exercise. To achieve a truly predictive capability, we strongly recommend that a significant effort be devoted to incorporate the rest of the loop into the calculational framework.

Appendix A

Volume-Averaged Two-Phase Flow Conservation Equations

A.1 Introduction

The derivation of a tractable set of equations describing the evolution of the two-phase flow consists of applying an averaging procedure to the local instantaneous conservation equations, followed by various simplifying assumptions aimed at reducing the number of unknowns and the constitutive relations.

The averaging procedure may involve various operators:

- instantaneous volume- and area-averaging operators,
- local time-averaging operators,
- statistical averaging operators,
- combined averaging operators (e.g., space/time or time/space).

Detailed discussions of various averaging procedures are given by Delhaye and Achard [1] and Ishii [2].

The objective of this appendix is to provide a rigorous derivation of the equations governing the two-phase flow, attempting to elucidate the meaning of the terms appearing in these equations and the implications of various assumptions and approximations. For our purpose, we chose the volume-averaging procedure which we believe is quite adequate for presenting the salient aspects of such a derivation, without undue complications. The derivation generally

follows and extends the methodology presented in [1]. A similar approach is taken by Banerjee and Hancox in [3] and by Banerjee and Chan in [4].

A.2 Mathematical Preliminaries

Consider the situation depicted in figure A.1 (for simplicity, only a two-dimensional configuration is shown). Let V_a be the volume of phase a, A_i the interfacial area and A_{wa} the contact area between phase a and the solid structure (referred to as "the wall" in the following). A_{wa} is considered fixed and impermeable. Let V be the total fluid volume, i.e., $V = \sum_a V_a$. We will use net fluid flow areas and volumes, thus implicitly accounting for the presence of the solids. Alternately, one could use total volumes and areas and define porosities (as in [5]), thus virtually treating the solid as a third phase. Obviously these variations in geometrical treatment are fully equivalent.

Special forms of the Leibnitz and Gauss theorems ([1]) will be availed of:

(a) The Leibnitz rule: transforms the time rate-of-change of a volume integral into the sum of a volume integral and a surface integral:

$$\frac{\partial}{\partial t}\int_{V_a(t)} f(x,y,z,t)\,dV = \int_{V_a(t)} \frac{\partial f}{\partial t}\,dV + \int_{A_i(t)} \vec{U}_i\cdot\vec{n}_a\,dA \qquad (A.1)$$

Note that this theorem considers a volume bounded by a

moving boundary. In our case, only A_i represents a moving surface, the other surfaces bounding the volume V_a, i.e., A_{wa}, A_{y+}, A_{y-}, A_{z-} and A_{z+}, being fixed.

(b) The Gauss theorem: transforms the volume integral of a spatial derivative into the spatial derivative of a volume integral plus a surface integral:

$$\int_{V_a(t)} \nabla\cdot\vec{B}\, dV = \nabla\cdot\int_{V_a(t)} \vec{B}\, dV + \int_{A_i(t)+A_{wa}} \vec{n}_a\cdot\vec{B}\, dA \tag{A.2}$$

We will define the volume average as:

$$\langle f_a\rangle = \frac{1}{V_a}\int_{V_a} f_a\, dV = \frac{1}{\alpha_a V}\int_{V_a} f_a\, dV \tag{A.3}$$

where $\alpha_a = V_a / V$.

Note that the total fluid volume is constant.

A.3 Local Instantaneous General Conservation Equation

The local instantaneous form of the general conservation equation, for phase a, is (Truesdell and Toupin in [6]):

$$\frac{\partial}{\partial t}\rho_a\psi_a + \nabla\cdot(\rho_a\psi_a\vec{U}_a) + \nabla\cdot\vec{J}_a - \rho_a\phi_a = 0 \tag{A.4}$$

The conserved quantity per unit mass, ψ_a, the flux term $\vec{J}_a$, and the source per unit mass, ϕ_a, are defined in Table A.1,

where $\vec{U}_a$ = velocity vector

$\overline{\overline{\pi}}_a$ = total stress tensor

$\vec{F}$ = body force per unit mass

$\vec{e}_a$ = internal energy per unit mass

$\vec{q}_a$ = heat flux

Equation (A.4) is valid within each phase, at every point, and must be supplemented by a jump condition at the interface. This equation constitutes the starting point in the derivation.

A.4 Volume-Averaged Equations

A.4.1 General conservation equation

Integrate Eq. (A.4) over the volume V_a, using Eqs. (A.1) and (A.2) as follows:

$$\int_{V_a} \frac{\partial}{\partial t} \rho_a \psi_a \, dV = \frac{\partial}{\partial t} \int_{V_a} \rho_a \psi_a \, dV - \int_{A_i} \rho_a \psi_a \vec{U}_i \cdot \vec{n}_a \, dA$$

$$\int_{V_a} \nabla \cdot (\rho_a \psi_a \vec{U}_a + \vec{J}_a) \, dV = \nabla \cdot \int_{V_a} (\rho_a \psi_a \vec{U}_a + \vec{J}_a) \, dV + \int_{A_i + A_{wa}} \vec{n}_a \cdot (\rho_a \psi_a \vec{U}_a + \vec{J}_a) \, dA$$

Then the general volume-averaged conservation equation for phase a is (using definition (A.3)):

$$V \frac{\partial}{\partial t} \alpha_a \langle \rho_a \psi_a \rangle + V \nabla \cdot \alpha_a \langle \alpha_a \psi_a \vec{U}_a + \vec{J}_a \rangle - V \alpha_a \langle \rho_a \phi_a \rangle = - \int_{A_i} [\rho_a \psi_a (\vec{U}_a - \vec{U}_i) + \vec{J}_a] \cdot \vec{n}_a \, dA - \int_{A_{wa}} \vec{J}_a \cdot \vec{n}_a \, dA \qquad (A.5)$$

Let $\dot{m}_a$ be the interphase mass flux, i.e.,

$$\dot{m}_a = \rho_a(\vec{U}_a - \vec{U}_i)\cdot\vec{n}_a \tag{A.6}$$

We can finally write:

$$\frac{\partial}{\partial t}\alpha_a\langle\rho_a\psi_a\rangle + \nabla\cdot\alpha_a\langle\rho_a\psi_a\vec{U}_a + \vec{J}_a\rangle - \alpha_a\langle\rho_a\phi_a\rangle$$

$$= -\frac{1}{V}\int_{A_i}(\dot{m}_a\psi_a + \vec{J}_a\cdot\vec{n}_a)\,dA - \frac{1}{V}\int_{A_{wa}}\vec{J}_a\cdot\vec{n}_a\,dA \tag{A.7}$$

The conservation equation for each quantity (mass, momentum and energy) for each phase may now be derived.

A.4.2 Mass equation

In this case, $\psi_a = 1$, $\vec{J}_a = 0$, $\phi_a = 0$. We have:

$$\frac{\partial}{\partial t}\alpha_a\langle\rho_a\rangle + \nabla\cdot\alpha_a\langle\rho_a\vec{U}_a\rangle = -\frac{1}{V}\int_{A_i}\dot{m}_a\,dA = \Gamma_{ia} \tag{A.8}$$

Generally the interfacial mass transfer rate, Γ_{ia}, is not known "a priori" and an "extraneous" correlation (that is, a constitutive relation) must be supplied.

A.4.3 Momentum equation

In this case, $\psi_a = \vec{U}_a$, $\vec{J}_a = -\bar{\bar{\pi}}_a = p_a\bar{\bar{I}} - \bar{\bar{\tau}}_a$ (where p_a is the pressure, $\bar{\bar{\tau}}_a$ the shear stress tensor and $\bar{\bar{I}}$ the unit tensor), $\phi_a = \vec{F}$. We have:

$$\frac{\partial}{\partial t}\alpha_a\langle\rho_a\vec{U}_a\rangle + \nabla\cdot\alpha_a\langle\rho_a\vec{U}_a\vec{U}_a + p_a\bar{\bar{I}} - \bar{\bar{\tau}}_a\rangle - \alpha_a\langle\rho_a\vec{F}\rangle$$

$$= -\frac{1}{V}\int_{A_i}(\dot{m}_a\vec{U}_a + p_a\bar{\bar{I}}\cdot\vec{n}_a - \bar{\bar{\tau}}_a\cdot\vec{n}_a)\,dA$$

$$-\frac{1}{V}\int_{A_{wa}}(p_a\bar{\bar{I}} - \bar{\bar{\tau}}_a)\cdot\vec{n}_a\,dA \qquad (A.9)$$

As in [3], let us express the pressure on the bounding surfaces A_i and A_{wa} as:

$$p_a\big|_{i(w)} = \langle p_a\rangle + \Delta p_a \qquad (A.10)$$

We note that Δp_a can be split into two components ([4]), one representing the difference between the average interfacial (or wall) pressure and the volume-averaged phase pressure, the other the difference between the local and the average interfacial (or wall) pressures. Generally, however, the form (A.10) is adequate. The reason for expressing the local interfacial and wall pressures as above will immediately become apparent.

The terms in the right-hand side of (A.9) containing pressures can be combined into:

$$\frac{1}{V}\int_{A_i+A_{wa}}(\langle p_a\rangle + \Delta p_a)\,\bar{\bar{I}}\cdot\vec{n}_a\,dA$$

$$= \frac{1}{V}\langle p_a\rangle\int_{A_i+A_{wa}}\bar{\bar{I}}\cdot\vec{n}_a\,dA + \frac{1}{V}\int_{A_i+A_{wa}}\Delta p_a\bar{\bar{I}}\cdot\vec{n}_a\,dA \qquad (A.11)$$

Using Gauss' theorem, Eq. (A.2), for $\vec{B} = \bar{\bar{I}}$ yields:

$$\int_{V_a} \nabla\cdot\bar{\bar{I}}\, dV = 0 = \nabla\cdot\bar{\bar{I}}\int_{V_a} dV + \int_{A_i+A_{wa}} \vec{n}_a\cdot\bar{\bar{I}}\, dA \qquad (A.12)$$

Therefore the first term in the right-hand side of (A.11) can be written as:

$$\frac{1}{V}\langle p_a\rangle\int_{A_i+A_{wa}} \bar{\bar{I}}\cdot\vec{n}_a\, dA = -\langle p_a\rangle\nabla\alpha_a \qquad (A.13)$$

(One notes that this term is similar to that appearing in the derivations for single-phase flows for control volumes with sloping walls.) This term may be combined with the pressure term in the left-hand side of (A.9), finally yielding:

$$\frac{\partial}{\partial t}\alpha_a\langle\rho_a\vec{U}_a\rangle + \nabla\cdot\alpha_a\langle\rho_a\vec{U}_a\vec{U}_a\rangle + \alpha_a\nabla\langle p_a\rangle$$

$$- \nabla\cdot\alpha_a\langle\bar{\bar{\tau}}_a\rangle - \alpha_a\langle\rho_a\vec{F}\rangle = -\vec{F}_{ia} - \vec{F}_{wa} \qquad (A.14)$$

where $$\vec{F}_{ia} = \frac{1}{V}\int_{A_i} (\dot{m}_a\vec{U}_a + \Delta p_a\vec{n}_a - \bar{\bar{\tau}}_a\cdot\vec{n}_a)\, dA \qquad (A.15)$$

and $$\vec{F}_{wa} = \frac{1}{V}\int_{A_{wa}} (\Delta p_a\vec{n} - \bar{\bar{\tau}}_a\cdot\vec{n}_a)\, dA \qquad (A.16)$$

Generally, correlations must be provided for the total interfacial momentum exchange ($\vec{F}_{ia}$) and the total wall drag ($\vec{F}_{wa}$).

A.4.4 Total energy equation

In this case, $\psi_a = e_a + U_a^2/2$, $\vec{J}_a = \vec{q}_a - \bar{\bar{\pi}}_a\cdot\vec{U}_a =$

$\vec{q}_a + (p_a\bar{\bar{I}} - \bar{\bar{\tau}}_a)\cdot\vec{U}_a$, $\phi_a = \vec{F}\cdot\vec{U}_a$ (neglecting volumetric heat generation). We have

$$\frac{\partial}{\partial t}\alpha_a\langle\rho_a(e_a + U_a{}^2/2)\rangle + \nabla\cdot\alpha_a\langle\rho_a(e_a + U_a{}^2/2)\vec{U}_a\rangle$$

$$+ \nabla\cdot\alpha_a\langle\vec{q}_a\rangle + \nabla\cdot\alpha_a\langle p_a\vec{U}_a\rangle$$

$$- \nabla\cdot\alpha_a\langle\bar{\bar{\tau}}_a\cdot\vec{U}_a\rangle - \alpha_a\langle\rho_a\vec{F}\cdot\vec{U}_a\rangle$$

$$= -\frac{1}{V}\int_{A_i}[\dot{m}_a(e_a + U_a{}^2/2) + \vec{q}_a\cdot\vec{n}_a + p_a\vec{U}_a\cdot\vec{n}_a$$

$$- (\bar{\bar{\tau}}_a\cdot\vec{U}_a)\cdot\vec{n}_a]\,dA$$

$$-\frac{1}{V}\int_{A_{wa}}\vec{q}_a\cdot\vec{n}_a\,dA \qquad (A.17)$$

where again the "wall" was assumed impermeable (i.e., $\vec{U}_a\big|_w = 0$) and fixed ($\vec{U}_w = 0$).

Note that, using (A.6), we have:

$$p_a\vec{U}_a\cdot\vec{n}_a = p_a\vec{U}_a\cdot\vec{n}_a - p_a\vec{U}_i\cdot\vec{n}_a + p_a\vec{U}_i\cdot\vec{n}_a$$

$$= \frac{p_a}{\rho_a}\dot{m}_a + p_a\vec{U}_i\cdot\vec{n}_a \qquad (A.18)$$

As previously discussed, $p_a\big|_i = \langle p_a\rangle + \Delta p_a$, hence

$$\frac{1}{V}\int_{A_i}p_a\vec{U}_i\cdot\vec{n}_a\,dA = \frac{1}{V}\langle p_a\rangle\int_{A_i}\vec{U}_i\cdot\vec{n}_a\,dA + \frac{1}{V}\int_{A_i}\Delta p_a\vec{U}_i\cdot\vec{n}_a\,dA \qquad (A.19)$$

Applying Liebnitz' rule for f = 1 gives:

$$\frac{\partial}{\partial t}\int_{V_a} dV = V\frac{\partial \alpha_a}{\partial t} = 0 + \int_{A_i} \vec{U}_i\cdot\vec{n}_a\, dA \qquad (A.20)$$

Therefore, Eq. (A.19) becomes:

$$\frac{1}{V}\int_{A_i} p_a\vec{U}_i\cdot\vec{n}_a\, dA = \langle p_a\rangle \frac{\partial \alpha_a}{\partial t} + \frac{1}{V}\int_{A_i} \Delta p_a\vec{U}_i\cdot\vec{n}_a\, dA \qquad (A.21)$$

Substituting Eqs. (A.21) and (A.18) into Eq. (A.17) and introducing the phase enthalpy, $h_a = e_a + p_a/\rho_a$, we obtain the equation for the total energy conservation in the form shown below:

$$\frac{\partial}{\partial t}\alpha_a\langle\rho_a(e_a + U_a{}^2/2)\rangle + \nabla\cdot\alpha_a\langle\rho_a(e_a + U_a{}^2/2)\vec{U}_a\rangle$$

$$+ \nabla\cdot\alpha_a\langle\vec{q}_a\rangle + \langle p_a\rangle\frac{\partial \alpha_a}{\partial t} + \nabla\cdot\alpha_a\langle p_a\vec{U}_a\rangle$$

$$- \nabla\cdot\alpha_a\langle\overline{\overline{\tau}}_a\cdot\vec{U}_a\rangle - \alpha_a\langle\rho_a\vec{F}\cdot\vec{U}_a\rangle$$

$$= Q_{ia} + Q_{wa} \qquad (A.22)$$

where

$$Q_{ia} = -\frac{1}{V}\int_{A_i}[\dot{m}_a(h_a + U_a{}^2/2) + \vec{q}_a\cdot\vec{n}_a + \Delta p_a\vec{U}_i\cdot\vec{n}_a$$

$$- (\overline{\overline{\tau}}_a\cdot\vec{U}_a)\cdot\vec{n}_a]\, dA \qquad (A.23)$$

and

$$Q_{wa} = -\frac{1}{V}\int_{A_{wa}} \vec{q}_a\cdot\vec{n}_a\, dA \qquad (A.24)$$

Once again, correlations must be supplied for the total interfacial energy exchange (Q_{ia}) and the wall heat source (Q_{wa}).

A.5 Local Instantaneous General Interface Jump Condition

The local instantaneous conservation equations for each phase, Eq. (A.7), must be supplemented by a "jump" condition, i.e., a conservation equation governing the interfacial exchanges.

Treating the interface as a contact discontinuity, the generalized conservation equation across the interface can be derived as follows. Consider a small "pillbox" control volume constructed at the interface A_i, as in figure A.2, containing both phases. The general equation of conservation for this volume is obtained by summing up the volume-averaged phase equations (i.e., the phase equations integrated over their respective subvolume, e.g., (A.7)) and taking the limit of V (i.e., volume occupied by both phases) becoming vanishingly small. Note that in the limit, the control volume under consideration does not contain any portion of the wall surface. Note also that this limit of V is understood to occur through a vanishing thickness, while the area into which it collapses remains finite. We then obtain:

$$\sum_{a=1}^{a=2} \int_{\Delta A_i} (\dot{m}_a \psi_a + \vec{J}_a \cdot \vec{n}_a)\, dA = 0 \qquad (A.25)$$

The requirement that Eq. (A.25) be valid for any arbitrary ΔA_i leads to the local jump condition:

$$\sum_{a=1}^{a=2} (\dot{m}_a \psi_a + \vec{J}_a \cdot \vec{n}_a) = 0 \qquad (A.26)$$

A.6 Interface Area-Averaged Jump Conditions

A.6.1 General interface jump condition

Define another averaging operation, over the interfacial area separating the two-phases:

$$\langle f_a \rangle_i = \frac{1}{V} \int_{A_i} f_a \, dA$$

Then we integrate the local instantaneous jump condition, Eq. (A.26) over the entire A_i to obtain:

$$\frac{1}{V} \int_{A_i} \left\{ \sum_{a=1}^{a=2} (\dot{m}_a \psi_a + \vec{J}_a \cdot \vec{n}_a) \right\} dA$$

$$= \sum_{a=1}^{a=2} \frac{1}{V} \int_{A_i} (\dot{m}_a \psi_a + \vec{J}_a \cdot \vec{n}_a) \, dA$$

$$= \sum_{a=1}^{a=2} (\langle \dot{m}_a \psi_a \rangle_i + \langle \vec{J}_a \cdot \vec{n}_a \rangle_i) \qquad (A.27)$$

The interface jump conditions for mass, momentum and energy can now be readily derived, using Table A.1.

A.6.2 Mass jump condition

$$\sum_{a=1}^{a=2} \langle \dot{m}_a \rangle_i = 0$$

or $$\langle \dot{m}_1 \rangle_i = - \langle \dot{m}_2 \rangle_i = \langle \dot{m} \rangle_i \qquad (A.28)$$

Using this result and the fact that $\vec{n}_1 = -\vec{n}_2 = \vec{n}$ on the interface, we can re-write the general jump condition as

$$\langle \dot{m}(\psi_1 - \psi_2) \rangle_i + \langle (\vec{J}_1 - \vec{J}_2) \cdot \vec{n} \rangle_i = 0 \qquad (A.29)$$

We will use this form in the following.

A.6.3 Momentum jump condition

$$\langle \dot{m}(\vec{U}_1 - \vec{U}_2) \rangle_i + \langle (p_1 - p_2) \bar{\bar{I}} \cdot \vec{n} \rangle_i - \langle (\bar{\bar{\tau}}_1 - \bar{\bar{\tau}}_2) \cdot \vec{n} \rangle_i = 0 \qquad (A.30)$$

Expressing the pressure on the interface as in Eq. (A.10) and using Gauss' theorem, we have (as in section A.4.3):

$$\begin{aligned} \langle (p_1 - p_2) \bar{\bar{I}} \cdot \vec{n} \rangle_i &= \langle p_1 \rangle \langle \bar{\bar{I}} \cdot \vec{n}_1 \rangle_i + \langle p_2 \rangle \langle \bar{\bar{I}} \cdot \vec{n}_2 \rangle_i \\ &\quad + \langle (\Delta p_1 - \Delta p_2) \vec{n} \rangle_i \\ &= - \langle p_1 \rangle \nabla \alpha_1 - \langle p_2 \rangle \nabla \alpha_2 + \langle (\Delta p_1 - \Delta p_2) \vec{n} \rangle_i \\ &= - (\langle p_1 \rangle - \langle p_2 \rangle) \nabla \alpha + \langle (\Delta p_1 - \Delta p_2) \vec{n} \rangle_i \end{aligned} \qquad (A.31)$$

where $\alpha = \alpha_1 = 1 - \alpha_2$.

The jump condition for momentum becomes:

$$(\langle p_1\rangle - \langle p_2\rangle)\nabla\alpha = \langle \dot{m}(\vec{U}_1 - \vec{U}_2)\rangle_i + \langle(\Delta p_1 - \Delta p_2)\vec{n}\rangle_i$$

$$- \langle(\bar{\bar{\tau}}_1 - \bar{\bar{\tau}}_2)\cdot\vec{n}\rangle_i \qquad (A.32)$$

A.6.4 Total energy jump condition

$$\langle \dot{m}[(e_1 + U_1^2/2) - (e_2 + U_2^2/2)]\rangle_i + \langle(p_1\vec{U}_1 - p_2\vec{U}_2)\cdot\vec{n}\rangle_i$$

$$+ \langle(\vec{q}_1 - \vec{q}_2)\cdot\vec{n}\rangle_i - \langle(\bar{\bar{\tau}}_1\cdot\vec{U}_1 - \bar{\bar{\tau}}_2\cdot\vec{U}_2)\cdot\vec{n}\rangle_i = 0 \qquad (A.33)$$

Proceeding similarly to section A.4.4, the pressure terms above can be further re-arranged:

$$\langle(p_1\vec{U}_1 - p_2\vec{U}_2)\cdot\vec{n}\rangle_i = \langle(\frac{p_1}{\rho_1} - \frac{p_2}{\rho_2})\dot{m}\rangle_i + \langle p_1\rangle\langle\vec{U}_i\cdot\vec{n}_1\rangle_i$$

$$+ \langle p_2\rangle\langle\vec{U}_i\cdot\vec{n}_2\rangle_i + \langle(\Delta p_1 - \Delta p_2)\vec{U}_i\cdot\vec{n}\rangle_i$$

$$= \langle\dot{m}(\frac{p_1}{\rho_1} - \frac{p_2}{\rho_2})\rangle_i + (\langle p_1\rangle - \langle p_2\rangle)\frac{\partial\alpha}{\partial t}$$

$$+ \langle(\Delta p_1 - \Delta p_2)\vec{U}_i\cdot\vec{n}\rangle_i \qquad (A.34)$$

The jump condition for total energy, using the previously defined phase enthalpy, becomes:

$$(\langle p_1\rangle - \langle p_2\rangle)\frac{\partial\alpha}{\partial t} = -\langle\dot{m}[(h_1 + U_1^2/2) - (h_2 + U_2^2/2)]\rangle_i$$

$$- \langle(\Delta p_1 - \Delta p_2)\vec{U}_i\cdot\vec{n}\rangle_i - \langle(\vec{q}_1 - \vec{q}_2)\vec{n}\rangle_i$$

$$+ \langle(\bar{\bar{\tau}}_1 \cdot \vec{U}_1 - \bar{\bar{\tau}}_2 \cdot \vec{U}_2) \cdot \vec{n}\rangle_i \qquad (A.35)$$

A.7 Working Equations

The results obtained thus far are collected and displayed in Tables A.2 through A.4. The derived conservation equations for each bulk fluid phase and for the interface are in spatially-averaged instantaneous form. These equations may now be time- or ensemble-averaged. However, in transient flows, the period over which the time averaging must be taken cannot be generally defined. This is especially true for rapid transients because of the frequency spectrum of the phenomena involved and also because of the temporal resolution of the measuring devices ([1]). A statistical averaging of the instantaneous space-averaged equations is therefore recommended.

The time- or ensemble-averaged equations remain in the same form. For example, terms like $\partial\alpha_a\langle\rho_a\psi_a\rangle/\partial t$ become $\overline{\partial\alpha_a\langle\rho_a\psi_a\rangle}/\partial t$, where the overbar indicates temporal or statistical averaging. As demonstrated in [1], the spatial and the temporal (statistical) averaging operators are commutative.

The bulk and interphase conservation equations just derived are exact, in that starting from the complete local instantaneous equations we have applied a rigorous mathematical procedure to obtain a set of averaged equations. The original problem, intractable for all practical purposes due to its need to track a hopelessly complicated moving boundary configuration, has been transformed into a simpler formulation.

However, information is lost in the averaging process and must now be supplied as auxiliary relationships. Indeed, as can be seen, the averaged equations contain far more unknowns than there are equations. To get a practical working model, further simplifications and assumptions must be made.

Regarding the auxiliary (or constitutive) relationships, one can distinguish a few types:

(a) relationships required by the original local instantaneous equations (e.g., shear stress, heat flux); obviously the need for them is not a result of the averaging.

(b) relationships for interfacial and wall transfer of mass, momentum and energy.

(c) relationships for intraphase distribution of the dependent variables, made necessary by the spatial averaging.

(d) relationships for terms containing temporal or statistical fluctuations; such terms are a results of the time or ensemble averaging.

A few comments on the last two types of constitutive relationships are in order. First let us consider the effects of spatial averaging. The volume-averaged conservation equations (see Table A.2) contain averages of various products of the dependent variables. Generally we wish to solve the equations so that averages of each dependent variable are obtained. Two equivalent approaches can be formally used:

(a) define distribution coefficients, i.e., multiplicative corrections:

$$\langle fg \rangle = C \langle f \rangle \langle g \rangle$$

(b) define "covariant" terms, i.e., additive corrections:

$$\langle fg \rangle = \langle f \rangle \langle g \rangle + \Delta$$

Either approach requires the knowledge or the assumption of a spatial distribution. For our working equations, we will assume flat profiles, leading to $C = 1$ or $\Delta = 0$, with the understanding that other distributions may be easily incorporated if needed or warranted in certain situations.

The effects introduced by the temporal (or statistical) averaging are formally quite similar. Traditionally, the approach (b) above has been taken with regard to this type of averaging, by expressing each dependent variable as a sum of an average ("the signal") and a fluctuation ("the noise"). For our equations, the direct application of this procedure leads to a fairly large number of additional terms. The problem that immediately arises is that of interpreting these terms, that is, of identifying some specific phenomenon with a term (or combination thereof). Such an exercise, especially when combined with spatial distribution effects, is generally futile. For the purpose of arriving at a tractable working

set of equations, the temporal or statistical fluctuations are accounted for through an enhancement of some of the already defined transport terms, again with the understanding that additional terms may be necessary in certain situations.

With the previous discussion in mind, we shall drop the symbols for the averaging operations ($< >$ and $\overline{\quad}$) and consider all dependent variables volume- and time- (or ensemble-) averaged.

At this point it is instructive to perform a count of unknowns and equations:

20 unknowns:

- 10 dependent variables (α_a, ρ_a, p_a, e_a, $\vec{U}_a$; $a = 1,2$),
- 4 wall exchange terms ($\vec{F}_{wa}$, Q_{wa}; $a = 1,2$),
- 6 interfacial exchange terms (Γ_{ia}, $\vec{F}_{ia}$, Q_{ia}; $a = 1,2$).

12 equations:

- 6 conservation equations,
- 2 equations of state ($\rho_a = \rho_a(p_a, e_a)$; $a = 1,2$),
- 1 constraint ($\alpha_1 + \alpha_2 = 1$),
- 3 interface jump conditions.

Therefore eight additional relationships are needed for closure.

We shall now make the usual assumption of equal bulk phase pressures, i.e.,

$$p_1 = p_2 \tag{A.36}$$

With this assumption, the momentum and energy jump conditions (see Table A.4) reduce to:

Momentum:

$$\vec{F}_{i1} + \vec{F}_{i2} = 0 \tag{A.37}$$

Total energy:

$$Q_{i1} + Q_{i2} = 0 \tag{A.38}$$

Let us now introduce the following notations:

$$\left.\begin{aligned} p &= p_1 = p_2 \\ \alpha &= \alpha_1 = 1 - \alpha_2 \\ \Gamma &= \Gamma_{i1} = -\Gamma_{i2} \\ \vec{F}_i &= \vec{F}_{i1} = -\vec{F}_{i2} \\ Q_i &= Q_{i1} = -Q_{12} \end{aligned}\right\} \tag{A.39}$$

These notations can then be substituted into the conservation equations (Table A.2). We now have:

15 unknowns:

8 dependent variables (p, α; ρ_a, e_a, $\vec{U}_a$; $a = 1,2$),

4 wall exchange terms ($\vec{F}_{wa}$, Q_{wa}; $a = 1,2$),

3 interfacial exchange terms (Γ, $\vec{F}_i$, Q_i).

8 equations:

6 conservation equations

2 equations of state ($\rho_a = \rho_a(p, e_a)$; $a = 1, 2$).

Thus the seven wall and interface exchange terms must be supplied as constitutive relationships.

To summarize, we obtained a working model describing the evolution of a two-phase flow. This was achieved by first rigorously deriving a set of averaged conservation equations for the bulk fluid phase and for the interface, after which additional assumptions were introduced to arrive at a working set of equations. The value of this exercise is that it points out clearly the nature of these assumptions, while at the same time providing the framework within which some of these assumptions may be eliminated or replaced by less severe ones. The final set of equations is quite general and can be used for a broad range of applications dealing with two-phase flow. Careful consideration of phenomena involved in some of these applications may lead to further simplifications, making the working equations even more tractable, while still adequate for describing the essential features of the flow.

A.8 References

1. J. M. Delhaye and J. L. Achard, "On the Averaging Operators Introduced in Two-Phase Flow Modeling," OECD Specialists' Meeting on Transient Two-Phase Flow, Toronto, Canada, August 1976.

2. M. Ishii, "Termo-Fluid Dynamic Theory of Two-Phase Flow," Eyrolles, Paris (1975).

3. S. Banerjee and W. T. Hancox, "Transient Thermohydraulics Analysis for Nuclear Reactors," Proc. Sixth International Heat Transfer Conference, Toronto, August 1978.

4. S. Banerjee and A. M. C. Chan, "Separated Flow Models-I: Analysis of the Averaged and Local Instantaneous Formulations," Int. Journal of Multiphase Flow, 6, 1 (1980).

5. W. T. Sha and B. T. Chao, "Conservation Equations for Finite Control Volumes Containing Single-Phase Fluid with Fixed, Dispersed Heat Generating (or Absorbing) Solids," ANL-CT-79-42, July 1979.

6. C. A. Truesdell and R. A. Toupin, "The Classical Field Theories," Encyclopedia of Physics, Vol. 3, Part 1, Springer Verlag (1960).

Table A.1

Quantities Used in the General Conservation Equation

Conservation Equation	ψ_a	J_a	ϕ_a
Mass	1	0	0
Momentum	$\vec{U}_a$	$-\bar{\bar{\pi}}_a$	$\vec{F}$
Total Energy	$e_a + \frac{1}{2}U_a^2$	$\vec{q}_a - \bar{\bar{\pi}}_a \cdot \vec{U}_a$	$\vec{F} \cdot \vec{U}_a$

Table A.2

Volume-Averaged Conservation Equations

Conserved Quantity	Volume-averaged conservation equation for phase "a" (a = 1,2)
Mass	$\frac{\partial}{\partial t}\alpha_a<\rho_a> + \nabla\cdot\alpha_a<\rho_a\vec{U}_a> = \Gamma_{ia}$
Momentum	$\frac{\partial}{\partial t}\alpha_a<\rho_a\vec{U}_a> + \nabla\cdot\alpha_a<\rho_a\vec{U}_a\vec{U}_a> + \alpha_a\nabla<p_a> - \nabla\cdot\alpha_a<\bar{\bar{\tau}}_a> - \alpha_a<\rho_a\vec{F}>$ $= -\vec{F}_{ia} - \vec{F}_{wa}$
Total Energy	$\frac{\partial}{\partial t}\alpha_a<\rho_a(e_a + U_a^2/2)> + \nabla\cdot\alpha_a<\rho_a(e_a + U_a^2/2)\vec{U}_a> + \nabla\cdot\alpha_a<\vec{q}_a> + <p_a>\frac{\partial}{\partial t}\alpha_a$ $+ \nabla\cdot\alpha_a<p_a\vec{U}_a> - \nabla\cdot\alpha_a<\bar{\bar{\tau}}_a\cdot\vec{U}_a> - \alpha_a<\rho\vec{F}_a\cdot\vec{U}_a>$ $= Q_{ia} + Q_{wa}$

Table A.3

Definition of the Exchange Terms in the Volume-Averaged Conservation Equations

Equation	Interfacial Exchange Terms	Wall Exchange Terms
Mass	$\Gamma_{ia} = -\langle \dot{m}_a \rangle_i$	—
Momentum	$\vec{F}_{ia} = \langle \dot{m}_a \vec{U}_a + \Delta p_a \vec{n}_a - \bar{\bar{\tau}}_a \cdot \vec{n}_a \rangle_i$	$\vec{F}_{wa} = \langle \Delta p_a \vec{n}_a - \bar{\bar{\tau}}_a \cdot \vec{n}_a \rangle_{wa}$
Total Energy	$Q_{ia} = -\langle \dot{m}_a (h_a + U_a^2/2) + \vec{q}_a \cdot \vec{n}_a + \Delta p_a \vec{U}_i \cdot \vec{n}_a + (\bar{\bar{\tau}}_a \cdot \vec{U}_a) \cdot \vec{n}_a \rangle_i$	$Q_{wa} = -\langle \vec{q}_a \cdot \vec{n}_a \rangle_{wa}$

Note: The average over the wall surface area is defined as $\langle f_a \rangle_{wa} = \frac{1}{V} \int_{A_{wa}} f_a dA$.

Table A.4

Interfacial Jump Conditions

Conserved Quantity	Area-averaged interfacial jump conditions
Mass	$\Gamma_{i1} + \Gamma_{i2} = 0$
Momentum	$\vec{F}_{i1} + \vec{F}_{i2} - (\langle p_1 \rangle \nabla\alpha_1 + \langle p_2 \rangle \nabla\alpha_2) = 0$
Total Energy	$Q_{i1} + Q_{i2} + (\langle p_1 \rangle \frac{\partial\alpha_1}{\partial t} + \langle p_2 \rangle \frac{\partial\alpha_2}{\partial t}) = 0$

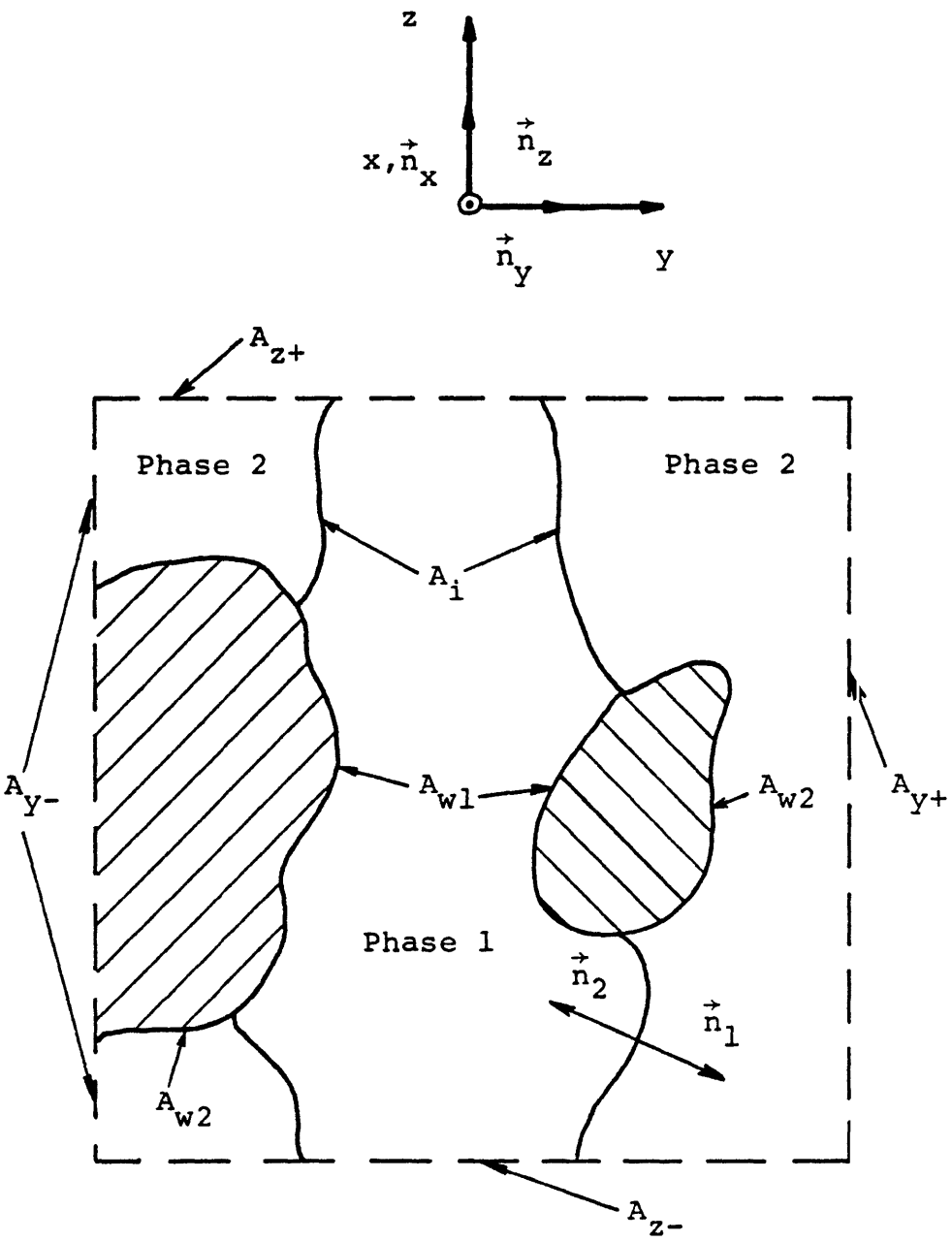

Figure A.1 Definition of geometry for volume averaging

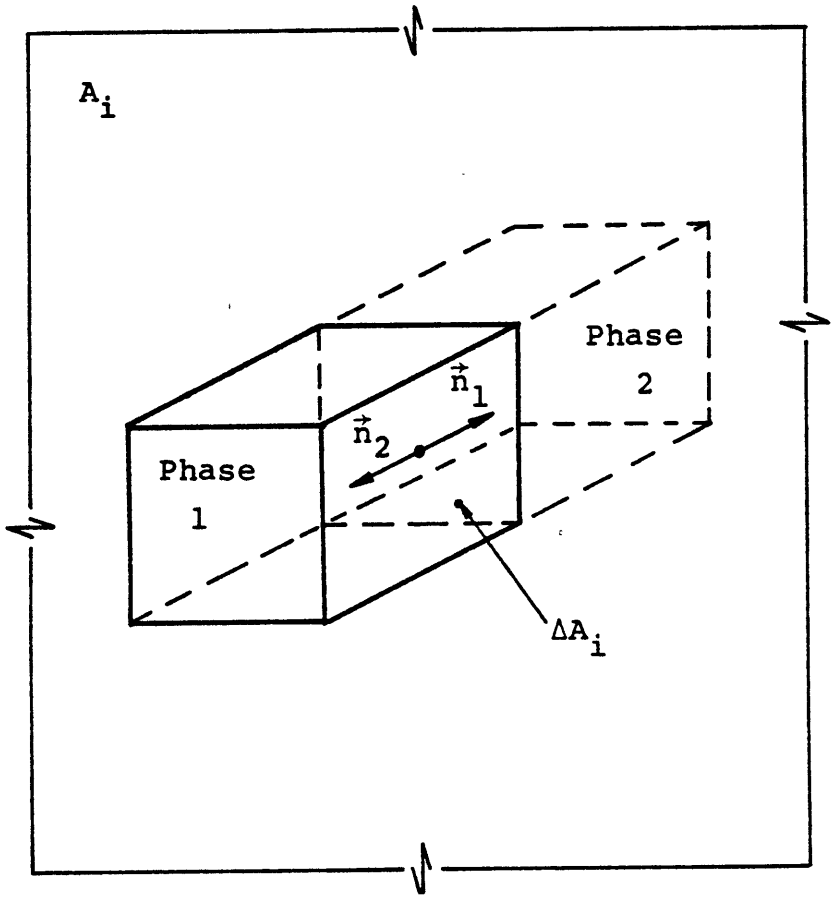

Figure A.2 Definition of geometry for interfacial jump conditions

Appendix B

Sodium Thermo-Physical Properties*

B.1 Thermodynamic Properties

1. Saturation Temperature (°K)

$$T_{sat} = \frac{A_1}{A_2 + \sqrt{A_3 + A_4 \ln(p)}}$$

where: $A_1 = 6.8354 \times 10^5$

$A_2 = -1.1485 \times 10^4$

$A_3 = 1.6156 \times 10^8$

$A_4 = -1.3671 \times 10^6$

Range of validity: $550 < T < 2270$°K

Source: Ref. 1

2. Liquid Density (kg/m^3)

$$\rho_\ell = A_5 + A_6 T + A_7 T^2 + c_\ell^{-2}(p - p_{ref})^{\dagger}$$

where: $A_5 = 1.0042 \times 10^3$

$A_6 = -2.1390 \times 10^{-1}$

$A_7 = -1.1046 \times 10^{-5}$

$c_\ell^{-2} = 2.0 \times 10^{-7}$

$p_{ref} = 1.5 \times 10^5$

Range of Validity: $550 < T < 2270$°K

Source: Ref. 1

---

*T is in °K and p is in MPa in all correlations given in this Appendix.

†See subsection B.3

3. Vapor Density (kg/m^3)

$$\rho_v = \left(\frac{A_8}{T} + A_9 + A_{10}T + A_{11}T^2 + A_{12}T^3 + A_{13}T^4\right) p \times 10^{-6}$$

where: $A_8 = 4.1444 \times 10^3$

$A_9 = -7.4461$

$A_{10} = 1.3768 \times 10^{-2}$

$A_{11} = -1.0834 \times 10^{-5}$

$A_{12} = 3.8903 \times 10^{-9}$

$A_{13} = -4.922 \times 10^{-3}$

Range of Validity: $550 < T < 2270°K$

Source: Ref. 1

4. Liquid Enthalpy (J/kg)

$$h_\ell = A_{14} + A_{15}T + A_{16}T^2 + A_{17}T^3$$

where: $A_{14} = -6.7508 \times 10^4$

$A_{15} = 1.6301 \times 10^3$

$A_{16} = -4.1672 \times 10^{-1}$

$A_{17} = 1.5427 \times 10^{-4}$

Range of Validity: $360 < T < 1644°K$

Source: Ref. 2

5. Vapor Enthalpy (J/kg)

$$h_v = A_{18} + A_{19}T + A_{20}T^2 + A_{21}T^3$$

where: $A_{18} = 5.2464 \times 10^6$

$A_{19} = -3.9950 \times 10^2$

$A_{20} = 6.4578 \times 10^{-1}$

$$A_{21} = 4.8590 \times 10^{-4}$$

Range of Validity: $550 < T < 1644°K$

Source: Refs. 1 and 2*

B.2 Transport Properties

1. Liquid Conductivity (w/m°K)

$$k_\ell = B_1 + B_2T + B_3T^2 + B_4T^3$$

where: $B_1 = 1.1045 \times 10^{2}$

$B_2 = -6.5112 \times 10^{-2}$

$B_3 = 1.543 \times 10^{-5}$

$B_4 = -2.4617 \times 10^{-9}$

Range of Validity: $550 < T < 2270°K$

Source: Ref. 1

2. Vapor Conductivity (w/m°K)

$$k_v = B_5 + B_6T_s + B_7T_s^2$$

where: $T_s = 1.8\,T - 459.7$

$B_5 = 2.8366 \times 10^{-3}$

$B_6 = 6.8830 \times 10^{-5}$

$B_7 = -1.6783 \times 10^{-8}$

Range of Validity: $360 < T < 1644°K$

Source: Ref. 2

---

*Obtained by combining the fits for liquid enthalpy from [1] and of the heat of vaporization from [2].

3. Liquid Viscosity (Pa sec)

$$\mu_\ell = B_8 + \frac{B_9}{T} + \frac{B_{10}}{T^2} + \frac{B_{11}}{T^3}$$

where: $B_8 = 3.6522 \times 10^{-5}$

$B_9 = 1.6626 \times 10^{-1}$

$B_{10} = -4.5688 \times 10^{1}$

$B_{11} = 2.8733 \times 10^{4}$

Range of Validity: $550 < T < 2270°K$

Source: Ref. 1

4. Vapor Viscosity (Pa sec)

$$\mu_v = B_{12} + B_{13}T$$

where: $B_{12} = 1.261 \times 10^{-5}$

$B_{13} = 6.085 \times 10^{-9}$

Range of Validity: $360 < T < 1644°K$

Source: Ref. 2

5. Liquid Surface Tension (N/m)

$$\sigma = B_{14} + B_{15}(T - B_{16})$$

where: $B_{14} = 2.067 \times 10^{-1}$

$B_{15} = -1.0 \times 10^{-4}$

$B_{16} = 2.7314 \times 10^{2}$

Range of Validity: $360 < T < 1644°K$

Source: Ref. 2

B.3 Remarks

The derivatives of the state properties, needed in the

linearization process, were obtained by directly differentiating the fits shown above. Regarding the liquid compressibility, we used an average sonic velocity which yielded $c_\ell^{-2} = \partial\rho/\partial p \simeq 0.2 \times 10^{-6}$ kg m^{-3}Pa. This constant compressibility renders the liquid density dependency on pressure linear, thus numerically very advantageous. Then we provided for consistency a correction to the liquid density of the form previously shown, i.e., $\Delta\rho = c_\ell^{-2}\Delta p$ (a typical pressure, say $p = 1.5 \times 10^5$ Pa, was considered as "reference" pressure). One should note that this approximate treatment is perfectly adequate, as this correction represents about 0.001% of the liquid density, thus well below the accuracy of the fit ($\sim 1.5\%$).

A second remark pertains to the fact that our numerical scheme uses the internal energy as primary variable, therefore the temperature (for single-phase liquid or vapor) must be inferred. While inverse fits can be obtained (i.e., $T = fn(p,e)$) we decided on a different approach. The drawback with such a fit is that it may not generally assure continuity across the saturation line. The reason is this: when we have a two-phase mixture, the pressure determines the (saturation) temperature, which in turn is used to calculate, among other quantities, the internal energies, using the direct fit, i.e., $e_k = h_k - p/\rho_k = fn(p,T)$, with $k = v$ or ℓ. In contrast, when dealing with single-phase flow situations, the temperature would be inferred from the inverse fit. At the saturation line crossover, there

would generally be a discrepancy which cannot be tolerated, as it may lead to lack of convergence of the nonlinear iterations. Consequently we decided to determine the single-phase temperatures using also the direct fit, through an interative procedure. Specifically Newton's method is used. The relatively mild nonlinearity of the direct fit results in only 2 or 3 iterations being needed to attain a more than adequate accuracy, therefore exacting only a very modest (almost negligible in the overall scheme) computational penalty.

A final remark is made in connection to the calculation of liquid internal energy. We found the term p/ρ_ℓ to represent less than 0.01% of the enthalpy for the entire range of validity, thus significantly below the stated accuracy of the fits ($\sim$ 1.5%). Therefore, the assumption $e_\ell = h_\ell$ appeared completely justifiable and it was adopted.

B.4 References

1. Argonne National Laboratory Reactor Development Program Quarterly Progress Report, ANL-RDP-78, December 1978.

2. H.G. Golden and J.V. Tokar, "Thermophysical Properties of Sodium," ANL-7323, August 1967.

APPENDIX C

REVIEW OF NUMERICAL METHODS FOR TWO-PHASE FLOWS

The numerical modeling of two-phase flow has been the object of intense research over the last decade. It is instructive to review some of the methods used in this area, in order to gain a perspective on the evolution and current status of this field. We do not attempt to be exhaustive in this review, but our intention is rather to present the more representative methods that in some way can be considered milestones in this field, spawning new research or constituting the backbone of some of the major computer codes currently in use.

It is appropriate to begin with the ICE technique [1], which has been the starting point, through its basic ideas, for the development of the majority of the numerical fluid dynamics methods currently used in nuclear engineering. It is a semi-implicit method, treating implicitly the pressure pulse propagation, thus no longer restricted by the full Courant criterion. The method employs the now almost universally used staggered mesh, placing the scalar quantities (pressure, density, energy, etc.) at the center of the mesh cell and the velocities (or mass fluxes) at the cell faces. The equation of state is linearized about the old time values. The total energy

equation is advanced explicitly. The mass and momentum equations are combined, resulting in a Poisson equation for pressure. The density is obtained from the linearized equation of state, thus the actual (non-linear) equation of state is never truly satisfied.

The FLASH method [2] is roughly of the same vintage as the previous one. It has been widely used for system codes (RELAP [3], RETRAN [4]). The method is semi-implicit, as ICE, and it also uses a staggered variable placement. Unlike ICE, however, it treats the energy equation in the same manner as the mass equation, thus providing an improved coupling. The equation of state, relating the pressure in a control volume to the fluid mass and energy in that control volume, is linearized about the old time values. It is then used in the momentum equation to eliminate the pressures in favor of the masses and energies of the relevant volumes. Finally, the use of the mass and energy equations leads to a system of linear equations for mass fluxes (or velocities). In this method, the mass and energy equations are linear, thus mass and energy are automatically conserved (within the computing round-off error). Non-linearities are, therefore, "assigned" to the momentum equations.

The marching method has been used extensively in

subchannel codes, such as the widely used codes in the COBRA series [5]. The method generally assumes that the density is independent of pressure, but still dependent of enthalpy. From the point of view of time discretization, the method is fully implicit. The solution proceeds from the inlet, where the flow rate and fluid pressure and enthalpy are normally given. If the outlet pressure is given as a boundary condition, then the appropriate inlet flow rate is determined through an iterative process. At each axial level, the mass and momentum equations are used to obtain a system of equations for cross-flows. These nonlinear equations are solved via a successive substitution procedure. The method is unable to treat local axial flow reversals and the solution generally breaks down under severe conditions leading to relatively large cross-flows. Nonetheless, this method is quite effective for many design calculations and for the analysis of relatively mild transients.

The modified ICE method [6,7,8,9] has been very successfully used in the last few years to simulate a very wide range of transients of interest in reactor safety analysis. It builds on the strengths of the first two methods previously described (ICE and FLASH). As in FLASH, the mass and energy equations are treated in a consistent manner. However, instead of obtaining a sys-

tem of equations for velocities, the modified ICE method uses a different reduction process resulting in a system of equations for pressures, analogous to the original ICE. It should be noted that in two- or three-dimensional problems, the matrix associated with the system of equations for pressure has a significantly simpler structure and is sparser than the matrix corresponding to a system of equations for velocities. The advantage of the "pressure-problem" over the "velocity-problem" increases significantly for multifluid flow treatments. In this method, nonlinearities are handled in two different ways. The linearization may be performed only once, about the old time values, as in [9]. In this case, an acceptable degree of mass and energy conservation is maintained via the time step control. In contrast, the scheme applied in [6,7,8] consists of a full Newton iteration process at every time step. However, in order to achieve convergence within some prescribed criterion, the time step size may be occasionally reduced below its stability limit.

While quite adequate for the analysis of a wide range of transients, the previously described method becomes rather uneconomical in some cases, such as:

- very slow transients, when there is a need to simulate over a long period of time, and
- direct chocked flow simulation, without resorting to special "break" models.

In such cases, the time step size limitation imposed by the explicit treatment of the convective transport may lead to almost prohibitive computing costs. Methods which relax or eliminate this limitation are obviously better suited in such situations, if they offer adequate accuracy and reliability.

The SETS method [10] removes the convective time step limitation through an ingenious series of prediction/corrector steps applied to the basic modified ICE scheme, in one-dimensional configurations. The extension to two- and three-dimensions is not trival, however, and may actually prove uneconomial.

The SIMPLE method [11] attempts to solve the governing equations in a fully implicit manner in up to three-dimensions. The resulting non-linear difference equations are solved via a successive substitution scheme. While this scheme renders a fully implicit method relatively tractable (avoiding the need to construct the complete Jacobian matrix), its convergence is not

always guaranteed. In fact, in some situations, heavy underrelaxation is required to attain a converged solution. In such situations, the convergence is usually very slow, and great many iterations are needed at each time step, to the point of almost cancelling the advantage of a fully implicit scheme. Nevertheless, further work in the area of optimal relaxation strategy may bring this powerful method to its full potential.

The methods described thus far are all based on the finite difference approach. From an accuracy point of view, they are all first order schemes in both time and space. A more novel approach, based on the weighted residual method, shows promise of improved accuracy and efficiency. Such a method has been described by Werner [12]. It is an Asymmetric, Separated Region Weighted Residual (ASWR) method, which apparently yields considerably higher accuracy, for a given mesh size, than finite difference-based methods currently used. In this method, coupling of the regions is restricted to "nearest neighbor", greatly contributing to the efficiency of the solution. In recent applications [13], the method provided for boiling front tracking (in one-dimension) and it is this particular feature which it is probably responsible to a significant extent for its success. In principle, the ASWR may be extended to two- and three-dimensions, but at the

cost of a considerable increase in computational work. Unfortunately, the interface tracking capability is exceedingly more difficult to extend to multidimensional configurations. It still remains to be seen if this method proves a superior alternative in multidimensional analyses. Nonetheless, the potential offered by the mathematical framework of this method must be noted.

Given the interest in and the difficulties inherent to simulating multidimensional multiphase flows, the years to come will certainly bring forth many evolutionary and, hopefully even a few revolutionary numerical methods.

REFERENCES:

1. F.H. Harlow and A.A. Amsden, A Numerical Fluid Dynamics Calculation Method for All Flow Speeds, J. Comp. Phys. 8 (1971).

2. T.A. Porsching, J.H. Murphy and J.A. Redfield, Stable Numerical Integration of Conservation Equations for Hydraulic Networks, Nucl. Sci. Eng., 43 (1971).

3. K.V. Moore and W.H. Rettig, RELAP-A Computer Code for Transient Thermal-Hydraulic Analysis, ANCR-1127 (1973).

4. K.V. Moore, et al, RETRAN-A Program for One-Dimensional Transient Thermal-Hydraulic Analysis of Complex Fluid Flow Systems, EPRI NP-408 (1977).

5. D.S. Rowe, COBRA IIIC-A Digital Computer Program for the Steady-State and Transient Thermal-Hydraulic Analysis of Rod Bundle Nuclear Fuel Elements, BNWL-1695 (1973).

6. D. Liles and W. Reed, A Semi-Implicit Method for Two-Phase Fluid Dynamics, J. Comp. Phys. 26 (1978).

7. TRAC-P1: An Advanced Best Estimate Computer Program for PWR LOCA Analysis, LA-7279-MS (1978).

8. J. Loomis, W.H. Reed, A. Schor, H.B. Stewart, L. Wolf, THERMIT: A Computer Program for Three-Dimensional Thermal-Hydraulic Analysis of Light Water Reactor Cores, EPRI NP-2032 (1981).

9. V.H. Ransom, et al, RELAP5/MOD1 Code Manual, EGG-2070 (1980).

10. J.H. Mahaffy, A Stability Enhancing Two-Step Method for One-Dimensional Two-Phase Flow, LA-7951-MS (1979).

11. S.V. Patankar, Numerical Heat Transfer and Fluid Flow, pp. 113-134, Hemisphere Publ. Corp., McGraw-Hill (1980).

12. W.F. Werner, Higher Order Methods in Fluid Dynamics, Topical Meeting on Computational Methods in Nuclear Engineering, Williamsburg, Virginia, May 1979.

13. W.F. Werner, Weighted Residual Methods for the Solution of Fluid Dynamics Problems, Topical Meeting on Advances in Mathematical Methods for the Solution of Nuclear Engineering Problems, Munich, Germany, April 1981.

APPENDIX D

ON VOLUME AVERAGING

Two remarks are in order concerning the use of volume-averaged equations. First, one recalls from the material presented in Appendix A that the divergence terms in the volume-averaged equations originate from the surface integrals taken over the fixed boundaries of the control volume occupied by each phase. Consequently our discretized scalar equations (i.e., mass and energy) were written with this observation in mind, substituting the divergence terms by difference of fluxes, i.e., (for the x-direction)

$$\nabla\phi\vec{U} \rightarrow \phi AU|_{x+} - \phi AU|_{x-} \qquad (D.1)$$

The second remark refers to the momentum equations. In Chapter 4, a difference scheme was introduced for these equations, which is essentially a direct equivalent of their differential form. This approach was mainly chosen because of the use of a non-conservative form of the momentum equations, particularly advantages for our numerical method. A somewhat subtle constraint implicitly arises, however, in the context of our porous media representation.

For simplicity, let us consider the single-phase momentum equation:

$$\frac{\partial}{\partial t}(\rho\vec{U}) + \nabla(\rho\vec{U}\vec{U}) + \nabla p = \vec{F} \qquad (D.2)$$

Consider now a control volume containing (possibly) dispersed fixed solids and integrate (D.2) over it:

$$\frac{\partial}{\partial t}\int_{V_f}(\rho\vec{U})\,dv + \int_{A_{ff}}\rho\vec{U}\vec{U}d\vec{A} + \int_{A_{ff}} p d\vec{A} = \int_{V_f}\vec{F}'dv \qquad (D.3)$$

In Equation (D.3), Gauss' theorem was applied to the divergence terms. The fluid-only volume, denoted by V_f, is bounded by the surface A_f, which is turn is made up of:

- A_{ff} = net flow area, through which the control volume exchanges mass with the surrounding space, and
- A_{fs} = fluid-solid interface (on which $\vec{U}=0$).

The form drag, i.e., $\int_{A_{fs}} p d\vec{A}$, was included into

the force $\vec{F}'$. Consider now, for facility, a one-dimensional configuration and neglect spatial distribution effects; Eq. (D.3) then becomes:

$$V_f \frac{\partial}{\partial t} (\rho U) + (\rho U^2 A_{ff})_+ - (\rho U^2 A_{ff})_- + (p\, A_{ff})_+ - (p A_{ff})_- = V_f F' \qquad (D.4)$$

If $(A_{ff})_+ = (A_{ff})_- = A^*_{ff} = V_f/\Delta x$, Eq. (D.4) can be written as:

$$\frac{\partial}{\partial t} (\rho U) + \Delta(\rho U^2)/\Delta x + \Delta p/\Delta x = F' \qquad (D.5)$$

which is clearly the form used to construct a finite difference equivalent.

It follows that the velocities in fact correspond to an area A^*_{ff}, which obviously is the volume-averaged area:

$$\text{i.e., } A^*_{ff} = \frac{1}{\Delta x} \int_{\Delta x} A_{ff}(x)\,dx = V_f/\Delta x \qquad (D.6)$$

Therefore, in calculating the fluxes, the significance of the calculated velocity must be kept in mind. Assuming the density changes negligibly over a short distance (on the order of the mesh size), the velocity at some location x can be obtained as:

$$U(x) = U\, A^{*}_{ff} \,/\, A_{ff}(x) \qquad (D.7)$$

Alternately, one can use directly the volume-averaged areas. This latter approach was taken in this work.

In this way, the staggered-mesh (described in Chapter 4) is properly handled.

APPENDIX E

ON THE DIAGONAL DOMINANCE OF THE PRESSURE PROBLEM

We start from Eq. (4.39), Chapter 4, where all the notations used thereafter were introduced:

$$[I + B^{-1} (D_2 A_1^{\sigma} - D_1 A_2^{\sigma})] \delta p = \ldots \qquad (E.1)$$

Let us denote $\tilde{A}_R$ the matrix in brackets above. First, we should ascertain that B is not singular. Recalling the definition of B.

$$B = D_2 A_1^{d} - D_1 A_2^{d} \qquad (E.2)$$

we can show that none of the entries of this diagonal matrix become zero under any circumstances. For simplicity, we shall assume in the following that the heat sources are fixed (or treated explicitly), thus not contributing to the Jacobian matrix. We note that this simplification does not limit the applicability of the following discussion, as the reader may verify. Let t_1 and t_2 be the sum of the off-diagonal entries of A_1 and A_2, respectively (see Eqs. (4.28, 4.29)); also recall that these off-diagonal entries are non-positive, thus t_1 and t_2 are also non-positive. We shall focus on a given row of matrix $\tilde{A}_R$ (and its components) and with this understanding

we will not use any additional indices. The relevant entries for B are

$$
\begin{aligned}
[D_2] &= (V/\Delta t)\ (\partial \rho_m e_m/\partial e_m)_p \\
[D_1] &= (V/\Delta t)\ (\partial \rho_m/\partial e_m)_p \\
[A_1^d] &= (V/\Delta t)\ (\partial \rho_m/\partial p)_e - t_1 \\
[A_2^d] &= (V/\Delta t)\ e_m(\partial \rho_m/\partial p)_{e_m} - t_2
\end{aligned}
\tag{E.3}
$$

Noting that:

$$(\partial \rho_m e_m/\partial e_m)_p = e_m(\partial \rho_m/\partial e_m)_p + \rho_m$$

one obtains after re-grouping:

$$
\begin{aligned}
[B] = {} & (V/\Delta t)\ (t_2 - t_1 e_m)\ (\partial \rho_m/\partial e_m)_p \\
& + (V/\Delta t)^2\ \rho_m(\partial \rho_m/\partial p)_{e_m} \\
& - (V/\Delta t)\ \rho_m t_1
\end{aligned}
\tag{E.4}
$$

The first term may be positive, according to the sign of the factor $(t_2 - t_1 e_m)$, the second and third terms are always positive (recall that $\partial \rho_m/\partial e_m < 0$ and $\partial \rho_m/\partial p > 0$). The probability that the first term, while negative will be <u>exactly</u> equal in magnitude to the sum of the other two is, for all practical purposes, zero.

We proceed to analyzing the diagonal dominance of $\tilde{A}_R$. First rewrite Eq. (E.4) by regrouping in a form we

will find more convenient:

$$[B] = (V/\Delta t)^2 \rho_m \left(\partial \rho_m / \partial p\right)_{e_m} - (V/\Delta t)\left\{\left[\rho_m + e_m\left(\partial \rho_m / \partial e_m\right)_p\right] t_1 - \left(\partial \rho_m / \partial e_m\right)_p t_2\right\} \tag{E.4'}$$

The grouping $(D_2 A_1^{\sigma} - D_1 A_2^{\sigma})$ in (E.1) gives rise to the off-diagonal entries, the sum of which is (for the row under consideration):

$$S = [D_2] t_1 - [D_1]\, t_2 = (V/\Delta t)\left\{\left[\rho_m + e_m\left(\partial \rho_m / \partial e_m\right)_p\right] t_1 - \left(\partial \rho_m / \partial e_m\right)_p t_2\right\} \tag{E.5}$$

Since the diagonal entry of $\tilde{A}_R$ is 1, the condition for diagonal dominance is simply:

$$|C| \leq 1 \tag{E.6}$$

where:

$$C = S/[B] \tag{E.7}$$

Using Eqs. (E.4') and (E.5) we obtain:

$$1/C = \left[(V/\Delta t)^2 \rho_m \left(\partial \rho_m / \partial p\right)_{e_m} / S\right] - 1 \tag{E.8}$$

The condition (E.6) is equivalent to:

$$|1/C| \geq 1 \tag{E.6'}$$

Let us denote the expression in brackets in (E.8) by E; then (E.6') becomes:

$$|1 - E| \geq 1 \tag{E.9}$$

We are interested in maintaining the off-diagonal entries nonpositive, i.e.,

$$E \leq 0 \tag{E.10}$$

Clearly, this is one of the conditions satisfying (E.9) (the other is $E \geq 2$). Let us analyze in detail the expression for E:

$$E = \frac{(V/\Delta t)\rho_m \, (\partial\rho_m/\partial p)e_m}{[\rho_m + e_m \, (\partial\rho_m/\partial e_m)_p] \, t_1 - (\partial\rho_m/\partial e_m)_p t_2} \tag{E.11}$$

Clearly for an incompressible flow E = 0, thus satisfying (E.10). Equation (E.11) can also be written as:

$$E = \frac{V}{\Delta t} \frac{(\partial\rho_m/\partial p)e_m}{(\partial\rho_m/\partial e_m)_p} \rho_m(\beta t_1 - t_2)^{-1} \tag{E.11'}$$

where $\beta = e_m + \rho_m (\partial \rho_m / \partial e_m)_p^{-1}$ (E.12)

In light of the sign of the density derivatives and of the Eq. (E.11), condition (E.10) will be satisfied if

$$F = \beta t_1 - t_2 \geq 0 \tag{E.13}$$

As already mentioned, both t_1 and t_2 are nonpositive, therefore, whenever $\beta \leq 0$, (E.13) is automatically satisfied. If $\beta > 0$, (E.13) may still be satisfied by

$$\beta t_1 \geq t_2 \quad (\text{or } -\beta t_1 \leq -t_2) \tag{E.13'}$$

that is, the relative magnitudes of βt_1 and t_2 will play a role. If spatial variation of properties is neglected, than it is easily seen (from the material in Chapter 4) that $t_2 = e_m t_1$, (neglecting the $p\nabla\vec{U}$ term), therefore:

$$F = (\beta - e_m) t_1 = \rho_m \, (\partial \rho_m / \partial e_m)_p^{-1} \, t_1 > 0$$

that is, in this idealized case, unconditional diagonal dominance can be proved.

In the general case, the analysis becomes considerably more difficult.

In the case of <u>single-phase liquid</u>, it turns out

that always $|\rho_m(\partial\rho_m/\partial e_m)_p^{-1}| > e_m$. Consequently, $\beta_{liquid} < 0$ and condition (E.13) is satisfied.

For the case of single-phase vapor, consider for simplicity a perfect gas. We have:

$$\rho = \frac{p}{RT}$$

$$e = c_v T$$

$$\rho = \frac{p}{(\gamma-1)e} \qquad \text{(E.14)}$$

Then $$\left(\frac{\partial\rho}{\partial e}\right)_p = -\frac{1}{e^2}\frac{p}{(\gamma-1)} = -\frac{\rho}{e}$$

and thus $\beta = 0$; the inequality (E.13) is satisfied.

Let us turn to the case of two-phase flow. From Appendix B we have

$$(\partial\rho_m/\partial e_m)_p = -\rho_m\,\Delta\rho/[e_m\Delta\rho - \Delta\rho e] \qquad \text{(E.15)}$$

where: $\Delta\rho = \rho_\ell - \rho_v > 0$

$$\Delta\rho e = \rho_\ell e_\ell - \rho_v e_v > 0^+$$

Then

$$\beta = e_m - [e_m\Delta\rho - \Delta\rho e]/\Delta\rho$$

$$= \Delta\rho e/\Delta\rho > 0$$

+This is true in spite of $e_\ell < e_v$, because the liquid/vapor density ratio dominates the behavior of this expression.

We cannot ascertain, the diagonal dominance in general. We can make, however, a few additional considerations. At low pressures, characteristic for sodium applications, $\rho_\ell >> \rho_v$, while e_ℓ and e_v are much closer. Approximately, then $\beta \cong e_\ell$. If all neighboring cells are in two-phase and the pressure does not vary much, e_ℓ becomes a lower bound for e_m. Therefore, it is possible to have

$$- e_\ell t_1 \leq - t_2$$

So far, we have used the conservative form of the energy equation, treating implicitly the convective terms. We shall turn our attention to some of its other variants mentioned in Chapter 4.

First let us analyze the effect of a non-conservative treatment. This form of the energy equation is obtained by subtracting the mass equation (multiplied by e_m) from the conservative form. While the various terms originating from the mass equation (i.e., A_1^d, A_1^σ, D_1, t_1) are unchanged, their energy equation counterparts will be modified as follows:

$$[D_2] \rightarrow [D_2'] = (V/\Delta t)\,\rho_m^n$$

$$[A_2^d] \rightarrow [A_d'^d] = -\,t_2' \qquad \text{(E.16)}$$

$$t_2 \rightarrow t_2' = t_2 - e_m^n\, t_1$$

First of all we note that with $A_2'^d = -t_2'$, A_2' is no longer strictly diagonally dominant. If heat sources are treated implicitly, these will be a local contribution to the pressure dependence, i.e., $[A_2'^d] \neq 0$. However, it is not possible to ascertain a priori the diagonal dominance of A_2', because the sign of the off-diagonal terms will depend on the relative magnitude of $[A_1^\sigma]$ and $[A_2^\sigma]$.

In this case, [B], S, C and E change into:

$$[B'] = (V/\Delta t)^2 \rho_m^n\,(\partial\rho_m/\partial p)_{e_m} - (V/\nabla t)\,[\rho_m^n t_1 - (\partial\rho_m/e_m)_p\, t_2'] \qquad \text{(E.17)}$$

$$S' = (V/\Delta t)\,[\rho_m^n\, t_1 - (\partial\rho_m/e_m)_p\, t_2'] \qquad \text{(E.18)}$$

$$1/C' = [B']/S = [(V/\Delta t)^2 \rho_m^n\,(\partial\rho_m/\partial p)_{e_m}/S] - 1 \qquad \text{(E.19)}$$

$$E' = \frac{(V/\Delta t)\,\rho_m^n\,(\partial\rho_m/\partial p)_{e_m}}{\rho_m^n\,t_1 - (\partial\rho_m/\partial e_m)_p\,t_2'} \tag{E.20}$$

Equation (E.20) can also be written as:

$$E' = \frac{V}{\Delta t}\,\frac{(\partial\rho_m/\partial p)_{e_m}}{(\partial\rho_m/\partial e_m)_p}\,\rho_m^n\,(\beta' t_1 - t_2')^{-1} \tag{E.21}$$

$$\text{where } \beta' = \rho_m^n\,(\partial\rho_m/\partial e_m)_p^{-1} \tag{E.22}$$

The counterpart of F then becomes:

$$F' = \beta' t_1 - t_2' = \beta' t_1 - t_2 + e_m^n\,t_1$$

$$= (\beta' + e_m^n)\,t_1 - t_2$$

$$= [e_m^n + \rho_m^n\,(\partial\rho_m/\partial e_m)_p^{-1}]\,t_1 - t_2 \tag{E.23}$$

Therefore, except for the fact that ρ_m and e_m appear at the old time, the results and hence the discussion are identical to those previously obtained and given for the conservative energy equation. For a numerical scheme linearizing about the old time only, even the above exception disappears.

We have also looked at a scheme using the non-conservative form of the energy equation, treating the

convective terms explicitly. In this case the off-diagonal terms in A_2' will vanish, therefore,

$$\begin{aligned} [A_2^{'d}] &\rightarrow [A_2^{"d}] = 0 \\ t_2' &\rightarrow t_2'' = 0 \end{aligned} \tag{E.24}$$

The expression for E in this case is obtained by simply setting $t_2' = 0$ in Eq. (E.20):

$$E'' = (V/\Delta t)\ (\partial \rho_m/\partial p)_{e_m}\ t_1^{-1} \tag{E.25}$$

Recalling that $(\partial \rho_m/\partial p)_{e_m} > 0$ and $t_1 < 0$, it follows that $E'' < 0$ and, therefore, unconditional diagonal dominance (see condition (E.10)) is always maintained.

In closing, we should remark that the inclusion of the effects of the heat sources does not alter the conclusions of the analysis presented herein.